The Dissertation Committee for Younis Khamis Altobi certifies that this is the approved version of the following dissertation:

Milankovitch Orbital Forcing Control on Shallow-Water Carbonate Cyclicity and Early Dolomitization: Insights from the Lower Cretaceous Cupido Platform, NE Mexico

Committee:

Randall Marrett, Supervisor

Daniel J. Lehrmann

Charles Kerans

Jay L. Banner

Steve Laubach

William L. Fisher

Milankovitch Orbital Forcing Control on Shallow-Water Carbonate Cyclicity and Early Dolomitization: Insights from the Lower Cretaceous Cupido Platform, NE Mexico

by

Younis Khamis Altobi, B.S.

Dissertation

Presented to the Faculty of the Graduate School of

The University of Texas at Austin

in Partial Fulfillment

of the Requirements

for the Degree of

Doctor of Philosophy

The University of Texas at Austin

May, 2007

Dedication

إلى علياء

Acknowledgements

First and foremost, I would like to acknowledge and thank my friend, and supervisor, Dr. Robert Goldhammer. His commitment to research and excellent work, dedication to his students, approach to daily life obstacles, praise, hardship, motivation and guidance inspired me to do more than I thought I could accomplish. His passion and energy for the outdoors, fieldwork, and rocks opened my eyes as a geologist and changed me a person.

I would like to thank my friend and advisor Dr. Randy Marrett for his support, direction, and motivation to continue on with this project after Bob's death. His guidance and teaching allowed me to learn and grow both professionally and personally.

I would also like to thank to Dan Lehrmann for his support, time spent listening to me during out long phone conversations, guidance, and critical reviews of this dissertation. I would also like to thank Charlie Kerans, Jay Banner, Steve Laubach and William Fisher for serving on my committee and discussions. A number of people from the Jackson School provided technical support, and shared their ideas and experiences during my time at UT. Thanks are due to: Jerry Lucia for great discussion on dolomitization processes, Robert Folk for critical reviews or portions of this manuscript and discussions regarding dolomite characteristics and dolomitization processes, Larry Mack for his assistance and insights in data preparation, collection and interpretation during laboratory analyses, Kitty Milliken for expertise in carbonate petrology, the use of Scanning Electron Microscope and Cathodoluminescence, and great discussion on dolomitization models, Urshela Hammers for critical reviews of manuscripts and lengthy discussion on sequence stratigraphic concepts, Linda Hinnov for interactive tutorials and discussions on spectral analysis techniques and interpretation, Wan Yang for ideas into statistical analysis

of high-frequency cycles, James Lee Wilson for ideas and critical questioning of Cupido platform sequence stratigraphic framework and evolution, Tina Foster for sharing ideas about facies, depositional model and stratigraphic correlation across the Cupido platform. Special thanks to my field assistants: Matt Davis, Nick Sommer, Dan Lehrmann, and Luis Rivera. Special thanks to Matt for great memories and lengthy field discussion of dolomitization processes and stratigraphy. Thanks are also due to Wayne Wright, Esti Ucar, Beatriz Garcia Fresca, Robert Forkner, Ted Playton, John Hooker, Leonel Gómez, and Dennis Trombatore.

This work was financed by grants from Petroleum Development Oman (PDO), Mesozoic Margins consortium, the Geology Foundation, Society of Economic Paleontologists and Mineralogists, and Gulf Coast Association of Geological Societies.

Special thanks to many friends, Tom, Luis, Esti, Anna, Alka, Justin, Nysha, Jessie, Meghan, Danny, Barbara. Thank you Qamoorah for being there during the hard times.

Lastly, I would like to thank my parents who made tremendous sacrifices to ensure that I accomplished my goals. For their continuing support, love and motivation for the last 10 years, I am forever in debt.

Milankovitch Orbital Forcing Controls on Shallow-Water Carbonate Cyclicity and Early Dolomitization: Insights from the Lower Cretaceous Cupido Platform, NE Mexico

Younis Khamis Altobi, Ph.D

The University of Texas at Austin, 2007

Supervisor: Randall Marrett

High-resolution sequence stratigraphy coupled with understanding of diagenetic processes within carbonate strata improves our understanding of platform evolution controls, facies models, and reservoir quality. The Cupido platform (Barremian to Aptian) exhibits well developed cyclicity and provides unparalleled outcrops to investigate platform morphology, depositional settings, sequence stratigraphic development, origin of high-frequency cycles, and possible climatic controls on early dolomitization across the shelf.

High-frequency cycles stack into twelve depositional sequences (A-L) that correlate across the platform, which, in turn, build into the highstand part of composite sequence I, two complete composite sequences (II and III), and the transgressive based portion of composite sequence IV. Cupido platform interior

cycles show evidence for an allocyclic origin, including (a) symmetric and asymmetric peritidal and subtidal cycles, (b) lateral continuity across facies tracts, and (c) incomplete subtidal cycles.

Spectral analyses of cycle thickness reveal a strong Milankovitch signal when sedimentation rate is assumed constant within cycles and cycles are tuned to orbital precession. High spectral density peaks are present for long and short eccentricity (E) period calculated for the Early Cretaceous times: E1 (264-392 kyr), E2 (89-98 kyr), and E3 (107-126 kyr). Obliquity component with peaks at period (38-59 kyr) are also present. Strong correlation of Milankovitch signals across the platform suggests that the lateral continuity of high-frequency cycles was caused by shelf-wide sea-level fluctuations.

Early dolomitization of the highstand lower Cupido deposits (LCu) possibly occurred in modified seawater within subtidal and supratidal zones, both at high-frequency cycle-scale and depositional sequence-scale. Dolomitization patterns appear to be linked to Milankovitch-induced 4^{th}-order sea-level events. The transgressive portions of depositional sequences are more pervasively or preferentially dolomitized compared to the highstand portions. Thickness and periodicity clusters of completely dolomitized cycles are equivalent to thickness and duration of depositional sequences. The results strengthen arguments for the role of Milankovitch-induced sea-level fluctuations in the development of greenhouse carbonate platforms and its control on early dolomite distribution in specific settings.

TABLE OF CONTENTS

List of Tables

List of Figures

Chapter 1. Introduction

The early Cretaceous was distinguished by globally high sea level, greenhouse climate, and deposition of thick broad tropical carbonate platforms (Figure 1-1). Some of the world's largest hydrocarbon reservoirs exist in these platforms, for example, the Cretaceous platforms of the Gulf of Mexico (GoM) and the Shuaiba Formation in the Middle East. During the Barremian to Albian, thick carbonate platforms developed around the ancestral GoM (Scott, 1990; Wilson and Ward, 1993). The Cupido Formation of northeastern Mexico represents part of this extensive carbonate system (Wilson, 1990; Goldhammer et al., 1991a; Lehmann et al., 1998; Goldhammer, 1999: Figure 1-2). The Lower Cretaceous Cupido platform extends northeastward into Texas and is equivalent to the Sligo platform of the subsurface Texas Gulf Coast (Conklin and Moore, 1977; Wilson and Pialli, 1977; Goldhammer, 1999; Figures 1-2 and 1-3).

The Lower Cretaceous stratigraphy of northeastern Mexico and South Texas is relatively well-known and has been the focus of extensive studies carried out since the mid 1930s. Very few studies (Ortega, 2002), however, have focused on dolomitization of the Cupido Formation and controls on dolomite distribution within coeval strata. Most previous studies have focused on interpreting the sequence stratigraphic framework of the Cupido Formation (Goldhammer et al., 1991a; Goldhammer, 1999; Lehmann et al., 1999; Foster, 2003 and Altobi et al., 2004).

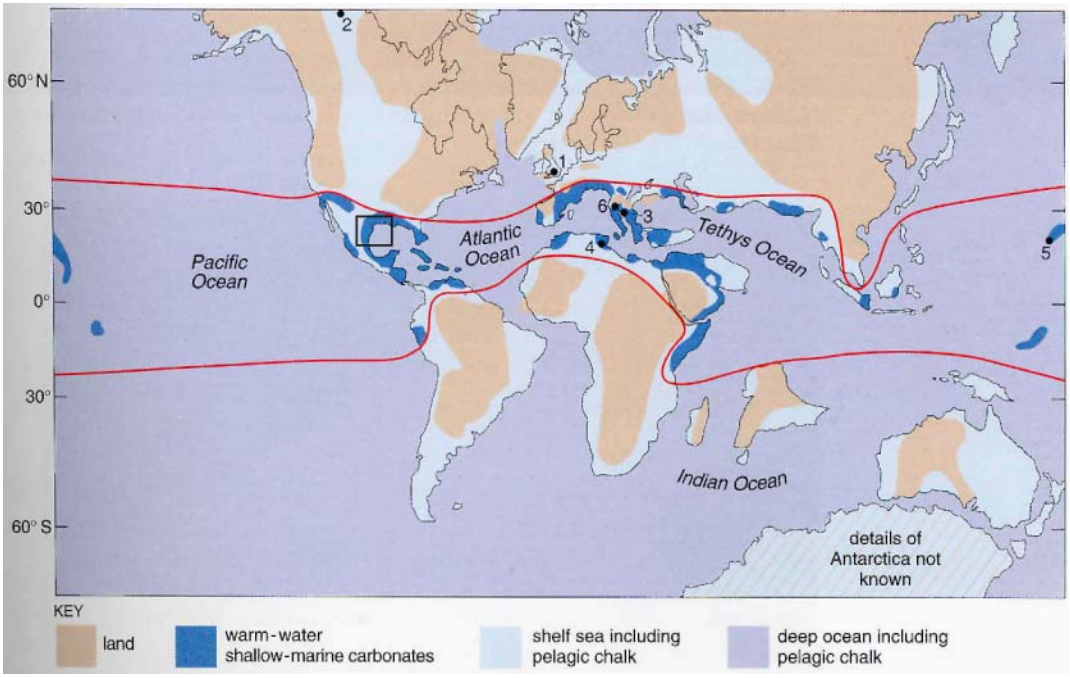

Figure 1-1. Paleogeographic map of the Cretaceous (about 98 Ma).

Map showing approximate reconstruction of the former positions of the continents. The belt of carbonate platform development is shown with red lines (after Skelton, 2003). Black box highlights the approximate location of study area.

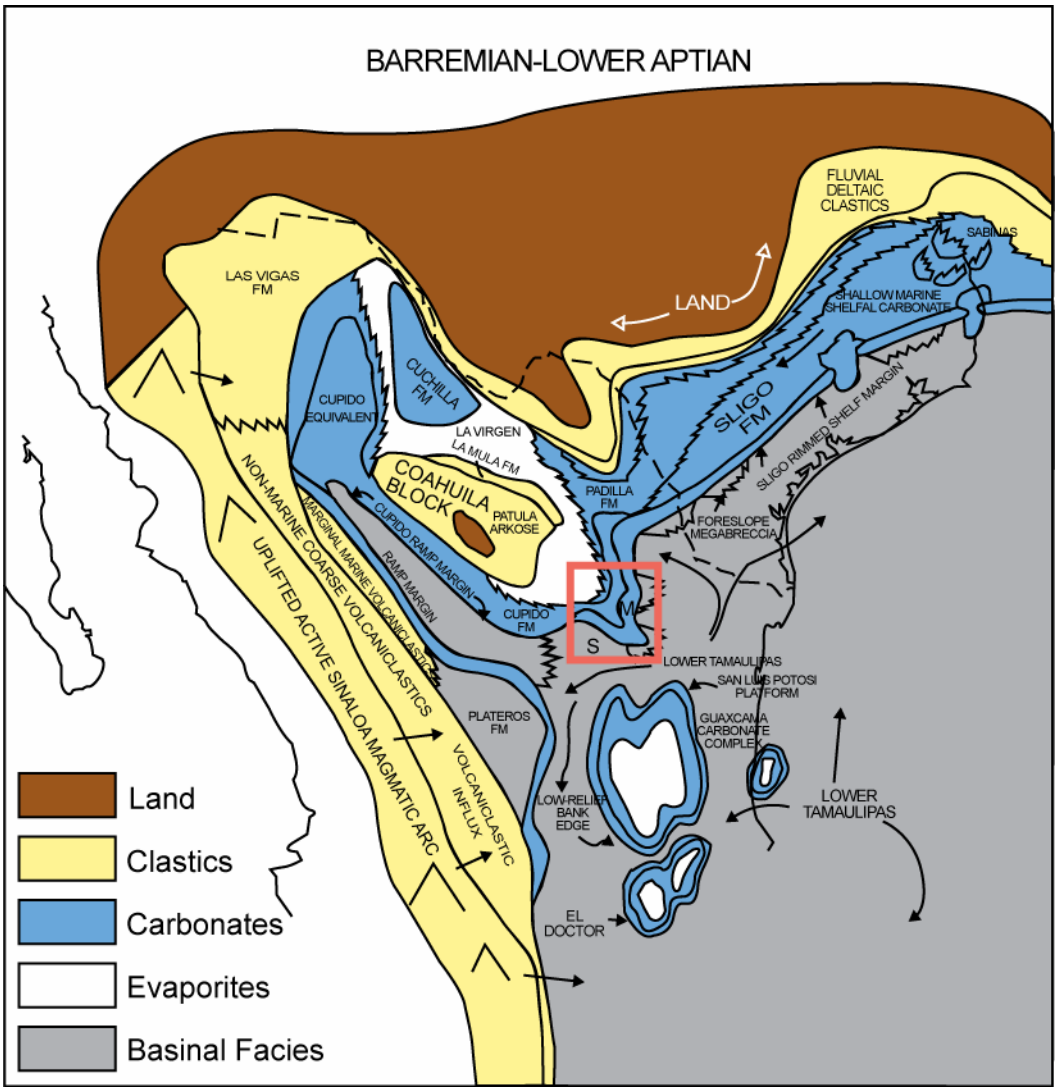

Figure 1-2. Paleogeographic map of Mexico and Texas.

Map of the Barremian to Lower Aptian in the western Gulf of Mexico, modified from Goldhammer (1999). The Cupido and Sligo Platforms are shown in blue. Outline of Mexico and U.S. border is dashed in black. The orange box represents the study area.

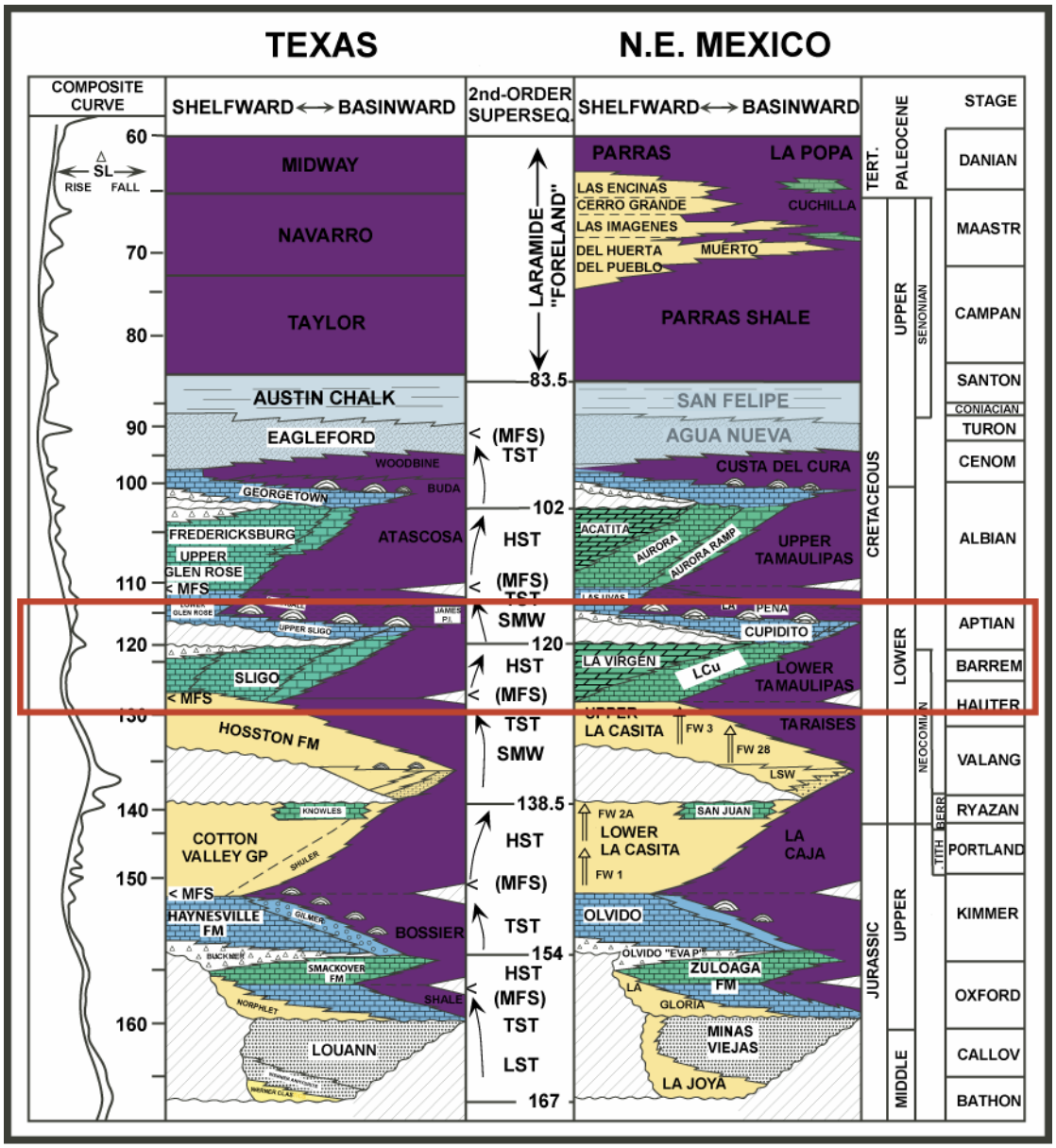

Figure 1-3. Chronostratigraphic chart.

Chart for northeast Mexico and Texas Gulf Coast. The composite eustatic curve is from Haq et al. (1987). Time scale is from Hardenbol et al. (1998) and Gradstein et al. (1995). Second-order sequence boundary ages are approximations in Ma. Abbreviations are: LST-lowstand system tracts, TST-transgressive system tracts, HST-highstand system tracts, LSW-lowstand wedge, SMW-shelf margin wedge, MFS-maximum flooding surface. Lithologies are discussed in text: purple is shale, gray is chalk, yellow is siliciclastic, green is

the regressive portion of carbonates, and blue is the transgressive portion of carbonates. Pinnacle reefs and buildups are shown as small domes. FW1 and FW2 refer to parts of the La Casita Formation defined by Fortunato and Ward (1982). The red box outlines the study interval. Figure modified from Goldhammer (1999).

Thick carbonate successions are commonly characterized by upward shallowing high frequency cycles that are extensively dolomitized (Wilson, 1975; Grotzinger, 1986; Moore, 1989; Koerschner and Read, 1989; Gao and Land, 1991; Montañez and Read, 1992). The type of high-frequency cycles and their stacking pattern can be used to interpret larger scale depositional and composite sequences. Stacked partially to completely dolomitized high-frequency cycles result in partially to massively dolomitized sections. Several conclusions have been made over the years linking overall dolomite distribution and sequence stratigraphy (for example see Harris, 1973; Wilson, 1975; Gorody, 1980; James, 1984; Given and Wilkinson, 1987; Lumsden, 1989; Kerans and Lucia, 1989; Montañez and Read, 1992; Balog, 1999; Smith et al., 2004; Altobi, 2006; Table 1-1).

The Cupido Formation has well developed meter-scale high-frequency cyclicity that has been linked to sea-level changes (Goldhammer et al., 1991a; Lehmann et al., 1999; Altobi et al., 2004). Hence, it provides a good opportunity to evaluate the role of sea-level change on early dolomite distribution in shallow carbonate successions. The excellent outcrops of the Cupido Formation within the Sierra Madre Oriental (SMO) and the Coahuila Marginal Fold Province (CMFP) are the focus of this study. Outcrop-based studies gain advantages over subsurface studies because of the ability to examine and describe rocks and their sedimentary structures directly and to observe lateral and vertical variations

Table 1-1. Previous studies.

Summary of previous conclusions linking dolomite distribution and sea level.

Author	Age	Formation	Conclusions
Harris (1973)	Upper Cambrian and Lower Ordovician	Knox Group	Dolomite is concentrated in shallow water, prograding tidal flats
Gorody (1980)	Lower Ordovician	Mascot Formation	Dolomite is linked to salinity gradient and transition from normal marine to highly saline dolomite facies
Given and Wilkinson (1987)	Phanerozoic Dolostones	A study of dolomitized Phanerozoic Formations	Dolomitization may be enhanced during times of global transgression
Kerans and Lucia (1989)	Lower Ordovician	El Paso Group	Dolomitized tidal flat caps form during third order sea-level fall
Montañez and Read (1992)	Lower Ordovician	Upper Knox Group	Dolomite distribution is linked to third-order eustatic events
Balog (1999)	Late Triassic	Hungarian Carbonates	Cyclic dolomite might be controlled by high frequency by high frequency eustatic changes; Overall vertical distribution is controlled by climate
Smith et al. (2004)	Late Mississippian	Madison Formation	Porous dolomite is common in the trangrssive portions of composite sequences, high frequency sequences and cycles

in rock textures and facies between closely-spaced sections. Large outcrops also provide a two-dimensional view for better correlation.

The first objective of this study is to thoroughly develop the depositional model and describe platform evolution, and sequence stratigraphic framework for the entire Cupido Formation. The conclusions of the first objective will clarify the driving mechanism of meter-scale cyclicity in the Cupido Formation, and the basin-wide extent and correlation of lower order cyclicity with regional or global processes (e.g., sea-level fluctuations). The second objective of this study is to characterize early dolomite types and their distribution across the shallow-water Cupido deposits, to identify possible dolomitization mechanisms and to document any sequence stratigraphic controls on spatial occurrence of early dolomite.

Ensuing this introductionary chapter, the dissertation is divided into three main chapters, which are each formatted for individual publication and a final conclusion chapter. Chapter 2 describes the depositional facies, cycle stacking patterns and the sequence stratigraphic framework of the Cupido Formation. The comparative sedimentology approach (Ginsburg, 1974) is used to interpret depositional environments and facies proportions, in order to determine the paleoenvironmental location of the measured stratigraphic sections and hence build a depositional model for the Cupido Formation. Vertical variations in facies and stacking patterns are used to evaluate sea-level history and changes in the depositional model through time. Chapter 3 addresses the nature and origin of cyclicity observed in the Cupido Formation. Qualitative and quantitative

techniques including Fourier-based spectral analyses (for example, Blackman-Tukey and smoothed periodogram) were used to determine the presence or absence of periodicity. These analyses of cycle types, characteristics, and distributions were used to determine whether cyclicity is due to an allocyclic or autocyclic mechanism. In particular, the role and extent of Milankovitch orbital forcing is evaluated. Chapter 4 specifically describes dolomite distribution within the Cupido Formation and its relationship with the evident cyclicity. Using the high-resolution sequence stratigraphic framework, field and laboratory analyses were carried out to identify trends in vertical and lateral dolomite distribution within the Cupido Formation. The link between dolomite distribution and different orders of cyclicity was investigated to determine the degree to which dolomitization patterns fit into the sequence stratigraphic framework. Finally, Chapter 5 summarizes the conclusions and contributions of the entire study

IMPORTANCE AND SIGNIFICANCE

Dolomite has presented a dilemma since its origin was first considered over one hundred years ago. Several types of studies have attempted to solve the “dolomite problem”. The problem arises from 1) the inability to synthesize dolomite inorganically in the laboratory under standard temperature and pressure (STP, 25 ºC and 1 atm, respectively) despite its widespread occurrence in carbonate rocks of different ages and different depositional environments (Warren, 2000), 2) rarity of dolomite in modern environment compared to ancient

environments. Some argue that widespread dolomite forms mostly in association with near-surface hypersaline brines, others that it can form from schizohaline waters, and still others that the time required to form such large volumes of dolomite means that the process must predominantly occur in the subsurface and perhaps is tied to long-term circulation of seawater through platform sediment (Land, 1985; Hardie, 1987; Warren, 2000). Observations that most modern dolomite is associated with evaporitic settings and the fact that much smaller pore volumes of hypersaline water are required to dolomitize a given volume of limestone (Warren, 1999) has led to the following conclusions: 1) “dolomite is an evaporitic mineral” Friedman (1980), and 2) large-scale dolomite has an origin related to salinity-elevated seawaters (Sun, 1994).

This study is not an attempt to tackle the “dolomite problem”. Instead, the study hopes to contribute to the long term pursuit of solving this problem by understanding the two main objectives: the depositional model and sequence stratigraphic framework for the Cupido Formation, and possible links between early dolomite distribution and sea-level changes. Recognizing links between sequence stratigraphy and early dolomite distribution would help in understanding environmental patterns of dolomite distribution and might highlight the possible role of sea-level changes on dolomite formation. If sea level does play a role in dolomite distribution, then a sequence stratigraphic framework might predict dolomite distribution within specific strata. Linking sea level to

dolomitization would help constrain the current accepted models for dolomite formation and timing.

Carbonate rocks host more than 55% of the world's hydrocarbons with up to 50% in dolomitized carbonate reservoirs. In North America alone, about 80% of hydrocarbon reservoirs are dolomitized carbonate rocks (Warren, 2000). Dolostones also host most Mississippi Valley-type (MVT) deposits of Pb and Zn (Warren, 2000). The economic value of dolomitized carbonate reservoirs is tied closely to reservoir quality, understanding of which can be improved by accurate predictions of dolomite distribution. Understanding the relationship between sequence stratigraphy and dolomitization within the Cupido Formation would have significant practical implications for better modeling and characterization of similar age reservoirs. It would also provide general models useful for carbonate systems of other ages.

The study further emphasizes the value of combining in depth sedimentology, facies identification, comparative sedimentology and logging stratigraphic sections and high resolution sequence stratigraphic tools to: 1) develop a depositional model, 2) interpret platform evolution, 3) build a sequence stratigraphic framework for the entire Cupido Formation, 4) understand genesis of solution-collapse breccia, and 5) define the effect of syndepositional faulting on platform geometry. These data will be useful for hydrocarbon exploration/production studies of similar aged strata in the subsurface Gulf of Mexico.

PREVIOUS WORK

The Cupido Formation was identified initially as the lower member of the La Peña Formation by Imlay (1936) as he mapped the Sierra de Parras of northeastern Mexico. Imlay described this lower member as 427 m thick on average, light to dark gray, thick to medium bedded limestones separated from the Aurora Formation by the shaley upper member of the La Peña Formation. Through fossil identification he also postulated the Barremian-Aptian age of this Unit. He placed the lower member of the La Peña (i.e. Cupido Formation) within the Nuevo Leon Group (Imlay, 1944), which contains some stratigraphic equivalents of the Cupido Formation such as the La Virgen Formation.

Humphrey (1949) measured these strata (Nuevo Leon Group) in the northern area of the Sierra de los Muertos and redefined Imlay's La Peña Formation so that the lower portion became the Cupido Formation. He described the Cupido as "thin to thick bedded and massive limestones, dolomitic limestones, and dolomites with intercalated shales."

Humphrey and later Charleston (1974) restricted the age of Cupido Formation deposition to late Neocomian to early Aptian using ammonites in the La Peña and Taraises formations, above and below the Cupido Formation, respectively. Charleston (1974) was the first to combine field and petrographic studies with statistical analysis of lithofacies characteristics within the Cupido Formation and the surrounding stratigraphic components of Imlay's Nuevo Leon Group (Imlay, 1944).

Ekdale et al. (1976) contributed a numerical analysis of the microfacies in Cupido Formation using Q-mode and R-mode cluster analysis and ordination, another classification technique. Using 16 characteristics determined from petrographic analysis of 100 samples, 15 microfacies were identified through Q-mode and 8 main facies were defined using ordination. They concluded that several facies may develop at the same water depth and assume the same position within a cycle depending on their lateral position on the carbonate platform. As a consequence each upward shoaling cycle might not contain the exact same facies and in the same order. Ekdale et al. (1976) stated that the upper Cupido Formation, measured in Arteaga Canyon, does not contain perfect cyclothems but the cyclicity is indisputable.

Conklin and Moore (1977) recognized the Cupido Formation as a progradational unit in an overall transgressing sea. Using detailed lithologic and paleontologic descriptions they divided the Cupido platform into six units (Figure 1-4). Unit A contains basinal facies, Unit B is fore-reef slope talus facies, Unit C is organic reef facies, Unit D is near-reef shoal facies, Unit E is near-reef tidal flat facies, and Unit F is lagoon, restricted-lagoon and sabkha facies. Unit F is now termed the Cupidito member, the transgressive portion of the Cupido Formation (Wilson and Pialli, 1977). Conklin and Moore (1977) also organized three measured sections, at Potrero Garcia, Potrero Chico, and Potrero Minas Viejas, to illustrate vertical and horizontal facies relationships. These facies were then placed within a stratigraphic framework to develop a progradational platform

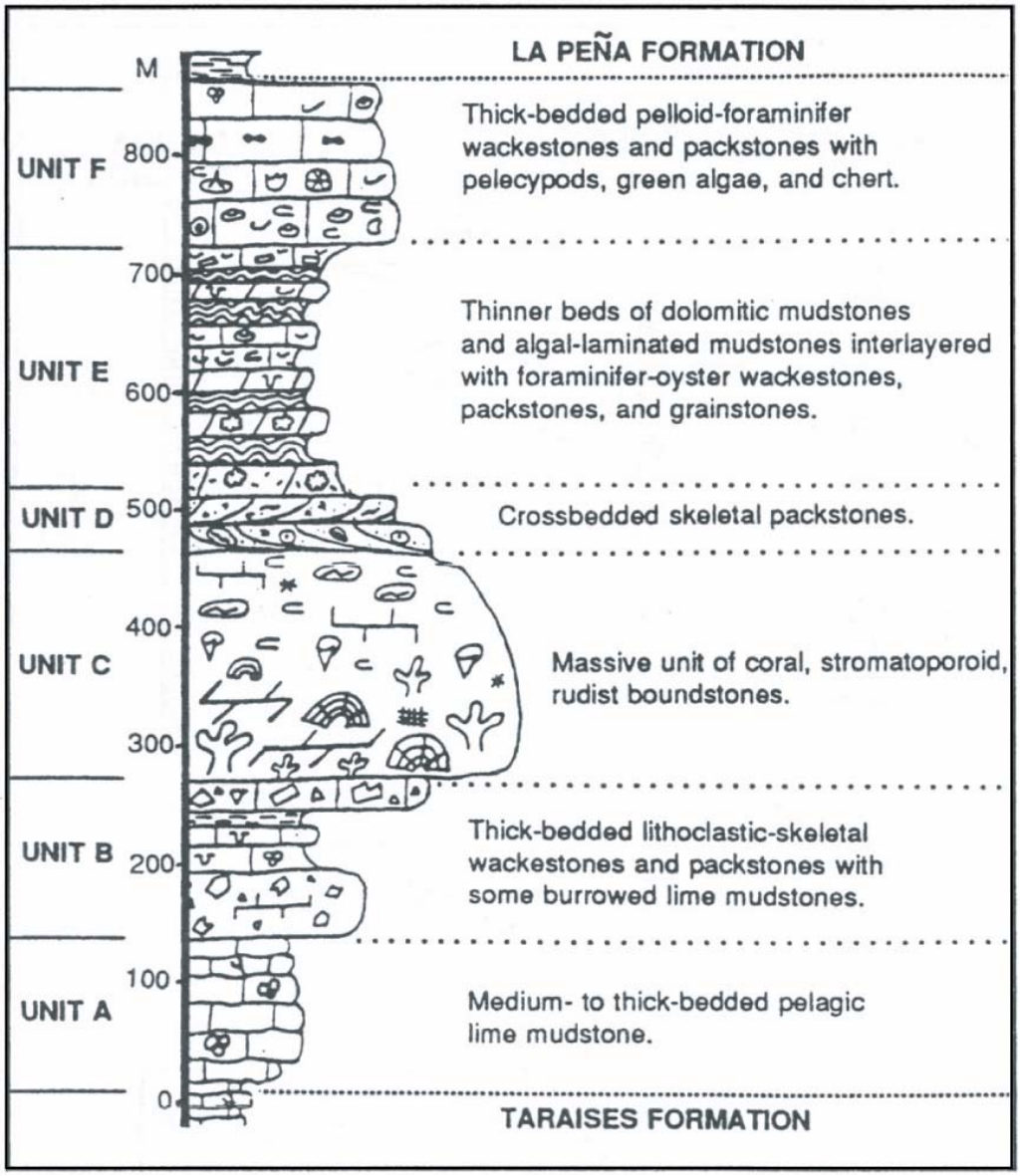

Figure 1-4. Cupido Facies.

Six facies divisions within the Cupido Formation by Conklin and Moore (1977). Unit F has been identified as the Cupidito member and Units A and B are equivalent to the Lower Tamaulipas Formation or the basinal portion of the Cupido Formation.

model and paleogeographic facies/environmental model, later modified by Goldhammer et al. (1991a).

Wilson and Pialli (1977) developed eight detailed facies descriptions of the Cupido Formation and incorporated several microfacies or subfacies of previous workers into their analysis. They presented interpretations of depositional environments for each facies, 3-8 correlating to Conklin and Moore's units A-F, and also focused on the subfacies scale. Wilson and Pialli (1977) were the first to estimate the slope of the shelf margin to be very gentle, 1-2 degrees. They also made several comparisons between Aptian and Albian carbonate platforms and petrographically studied the porosity and diagenesis of the Cupido Formation for the interest of reservoir potential. Wilson and Selvius (1984) compared and combined Conklin and Moore's (1977) facies to Wilson and Pialli's (1977) facies belts. They also expanded the progradational model of the Cupido platform and designated the Cupidito member of the Cupido Formation as facies belt 8 and Unit F of Conklin and Moore (1977). Wilson and Selvius (1984) described the Cupidito member as cyclic lagoonal facies composed of *chondrodonta* wackestones and packstones with other non-skeletal grains and interpreted it as a transgressive deposit in the Upper Aptian placing a subtidal lagoonal environment above tidal flats. Wilson and Ward (1993) described the Cupido and Cupidito facies and rock textures and discussed the higher frequency cycles in the stratigraphic framework to justify a barrier reef depositional model (Figure 1-5).

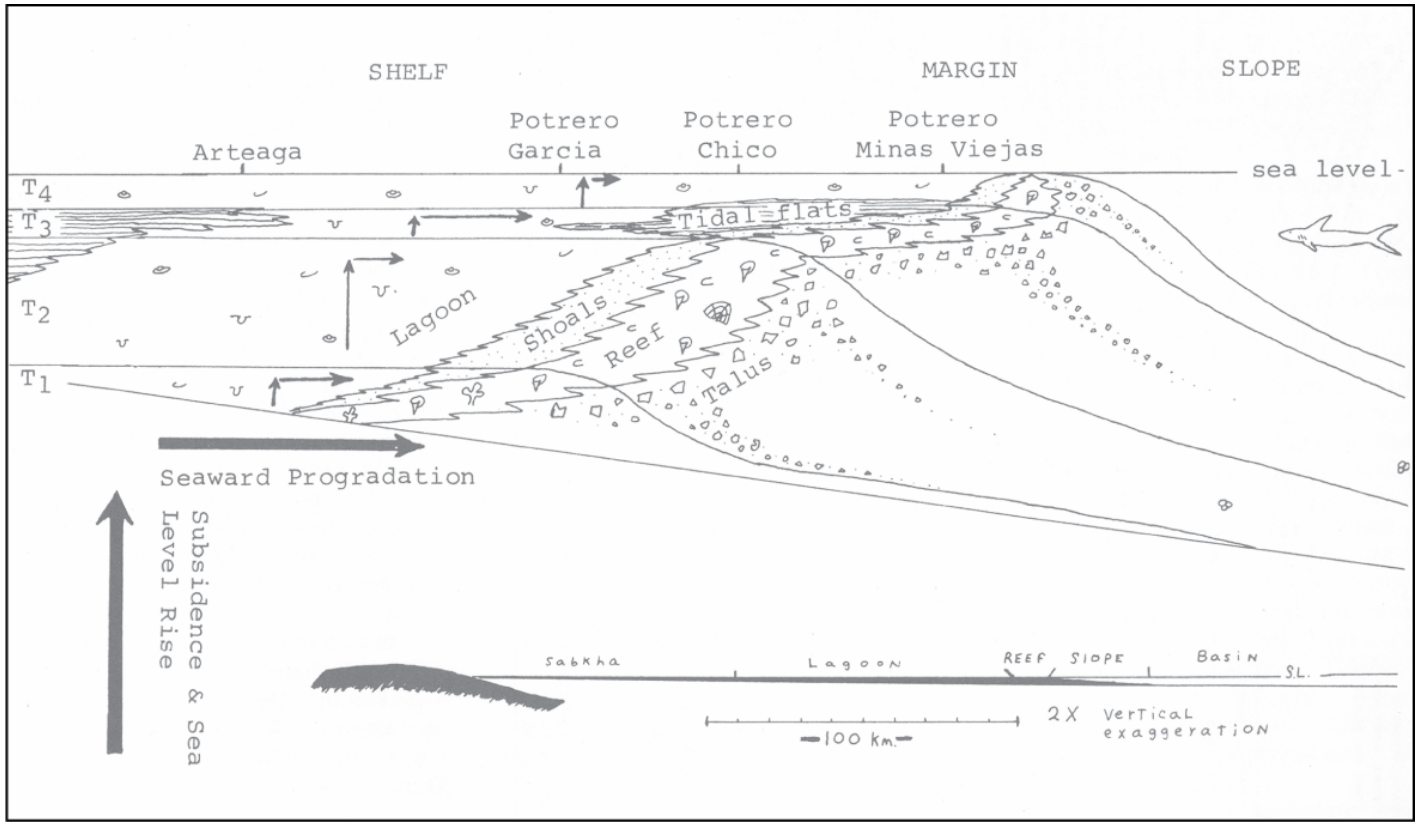

Figure 1-5. Barrier reef model.

Model proposed for the Cupido platform by Wilson and Ward (1993). The model is highly progradational with occasional tidal flats on the reef crest. Note the position of Potreros Garcia, Chico, and Minas Viejas for comparison with the new model proposed in Chapter 2.

McFarlan and Menes (1991) provided descriptions of the Lower Cretaceous stratigraphy of northern Gulf of Mexico, Texas and Louisiana. They made comparisons and correlated the Cupido Formation to the Sligo Formation and the La Peña Formation to the Pearsall Formation. Their discussion, on the stratigraphy of the Gulf of Mexico during the Hauterivian-Aptian, attributed the transgression of the middle Aptian primarily to tectonic activity rather than to sea-level changes.

The detailed stratigraphy of the Mesozoic Gulf of Mexico was compiled by Goldhammer (Goldhammer et al., 1991a; Goldhammer, 1999) using chronostratigraphy in place of lithostratigraphy (Figure 1-3). Second order sequences of the Gulf of Mexico were recognized, compared to the Haq sea-level chart (Haq et al., 1987) and broken down into their component sequences. In his chronostratigraphic and sequence stratigraphic summary, Goldhammer (1999) correlated the Mesozoic formations of the northern and western Gulf of Mexico. Subsidence and accommodation space modeling (Mr Sediment) and Fischer plots were utilized in the analysis of high-frequency cycles to determine low frequency sequence boundaries (Figure 1-6). The high-frequency cycles within the carbonate 2nd-order sequences of the Cupido Formation were studied using autocorrelation analysis and maximum entropy spectral analysis to determine the origin of their apparent cyclicity. Milankovitch allocycles and Ginsburg's autocycles were compared to the data as well as the controlling factors of sedimentation rates and subsidence. No conclusive evidence was

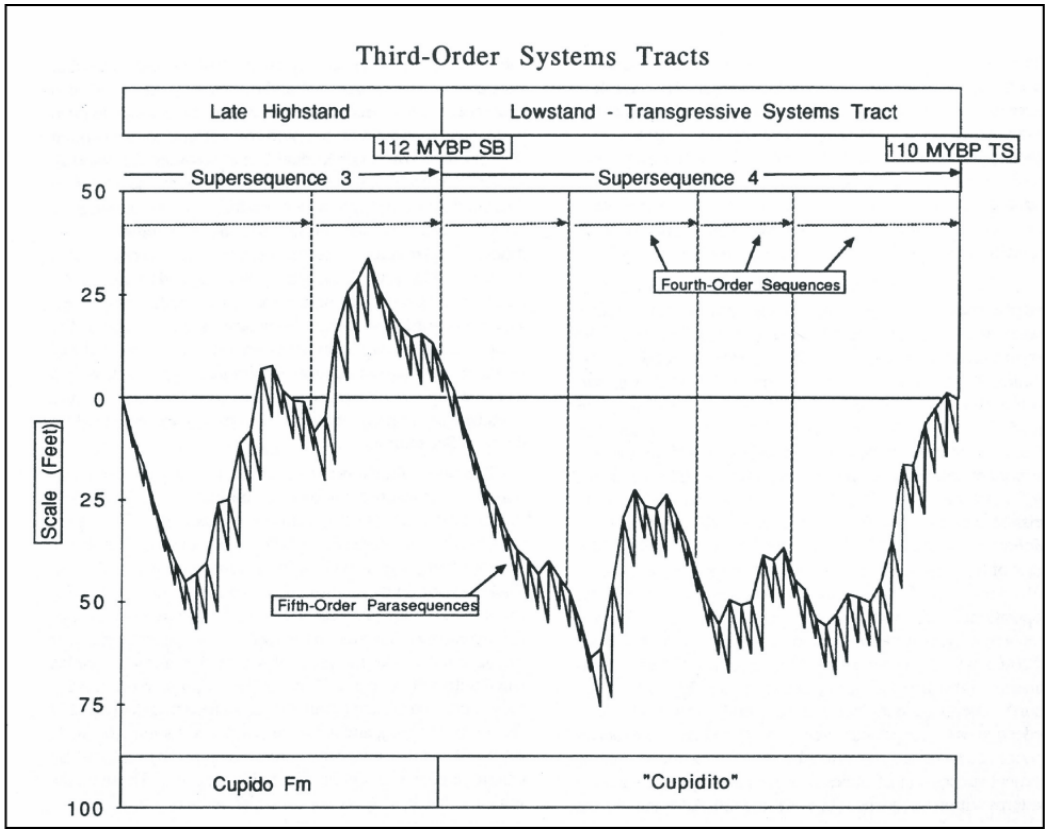

Figure 1-6. Accommodation plot.

Plot of the Cupido Formation by Goldhammer et al. (1991a). Data were taken from a measured section in Potrero Garcia and the analysis illustrates four potential 4th-order depositional sequences within the Cupidito member, the transgressive portion of the Cupido Formation.

found to demonstrate strictly allocyclic Milankovitch origin or strictly random autocyclicity.

Lehmann (Lehmann et al., 1998, 2000) reviewed the main facies types and the evaporitic/tidal flat peritidal cycles of the Cupido Formation. They created a simple facies model and contemplated multiple controls on the sedimentation processes. Lehmann et al. (1998) compiled data from multiple localities for peritidal cycle types in the Cretaceous. A deeper study in the ranges of the Cupido and Aurora formations resulted in minor corrections to previously designated ages, the most significant change being that the Cupido Formation is mid Barremian to late Aptian (Lehmann et al., 1999) as opposed to Lower Barremian to mid Aptian (Imlay, 1936). The map pattern of the Cupido reef margin was constrained using new measured stratigraphic sections (Lehmann et al., 1999) combined with previous work in the Sierra de Parras (Imlay, 1936). Lehmann et al. (2000) later focused on distinguishing composite sequences within the Lower Cretaceous of northeastern Mexico and found five between the Hauterivian and the Albian (Figure 1-7). Herein, the Cupido Formation is divided into two informal parts: thin bedded, progradational lower part known as Cupido, and thick-bedded transgressive part known as Cupidito member. Herein and thereafter, the lower Cupido part is called LCu (Figure 1-8).

Ortega and Marrett (2001) attempted to relate fracture intensity to lithofacies of some Cupido sections and suggested that the degree of dolomitization had the only significant effect on fracture distribution within the

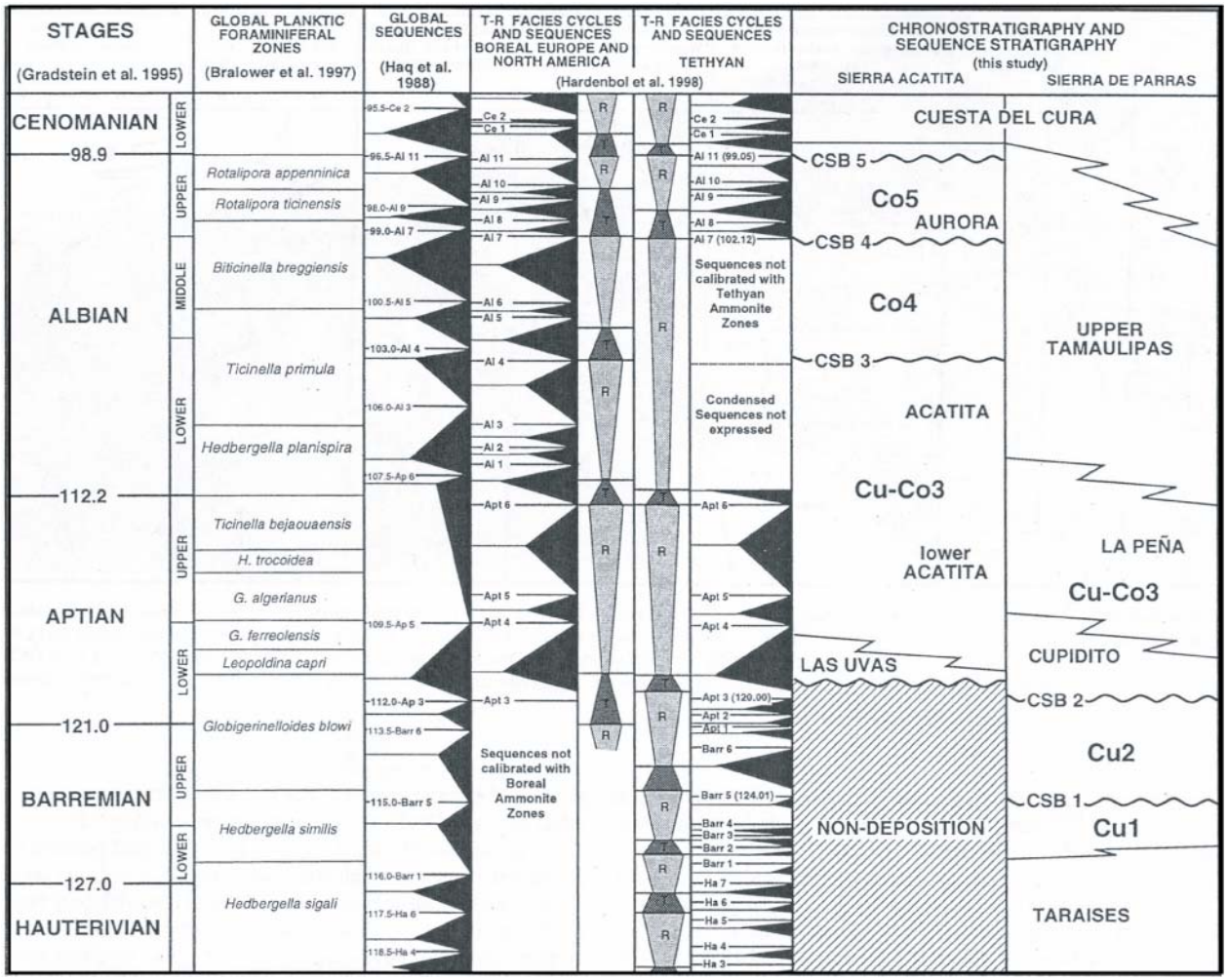

Figure 1-7. Sequence stratigraphic interpretation.

Sequence stratigraphic framework of the Lower Cretaceous as composite sequences with global correlations by Lehmann et al. (2000). Note the number of high-frequency sequences and composite sequences with the new high-resolution sequence stratigraphic framework interpreted in Chapter 2.

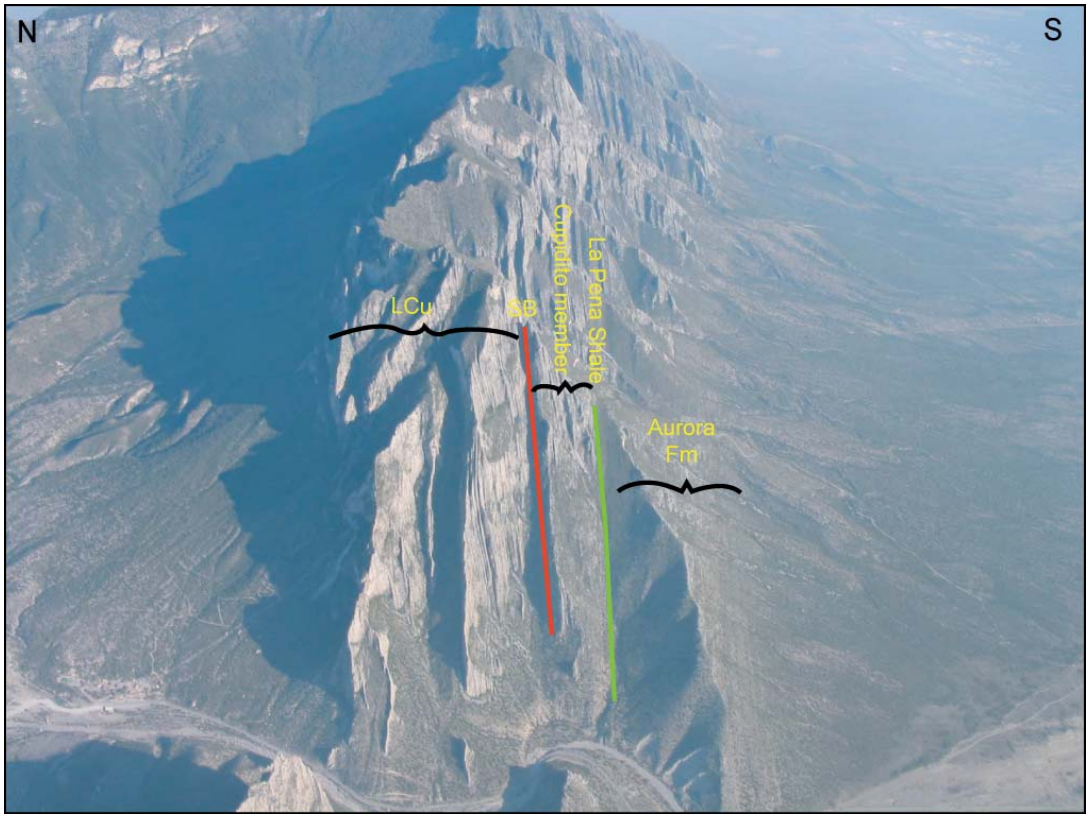

Figure 1-8. Aerial photograph of Potrero Garcia anticline.

Photograph of the southern limb of the Potrero Garcia anticline. Beds are tilted vertically with the stratigraphic younging direction to the right. The green line marks the position of the La Peña Shale and the red line represents the 2nd-order sequence boundary (SB). Photo taken by Goldhammer (2002).

Cupido carbonates. Ortega (2002) briefly documented facies variations and dolomitization patterns within shallowing-upwards cycles.

REGIONAL GEOLOGIC SETTING

Present setting

The Cupido platform is well-exposed between Monterrey and Saltillo, as well as other areas further north and west (Figure 1-9). The study area is located within the uplifted Sierra Madre Oriental fold belt of Mexico as well as north of the fold belt in the form of isolated doubly plunging anticlines (Goldhammer, 1999). From north to south, the anticlines north of the fold belt are Potrero Minas Viejas (PMV), Potrero Chico (PC), and Potrero Garcia (PG; Figure 1-8). Each anticline is breached by a single canyon, which provides the best location for measured stratigraphic sections. Within the Sierra Madre Oriental fold belt (Figure 8), stratigraphic sections were measured at Huasteca Canyon (HC; Figure 1-10A), Cortinas Canyon (CC), and Chorros Canyon (ChC; Figure 1-10B). All sections were measured in isolated locations, where near-vertically dipping beds provide minimal access to describe of lateral continuity of bedding features or the original stratal architecture. Each section was measured through the cyclic platform interior facies, the Cupido Formation, of the Cupido platform.

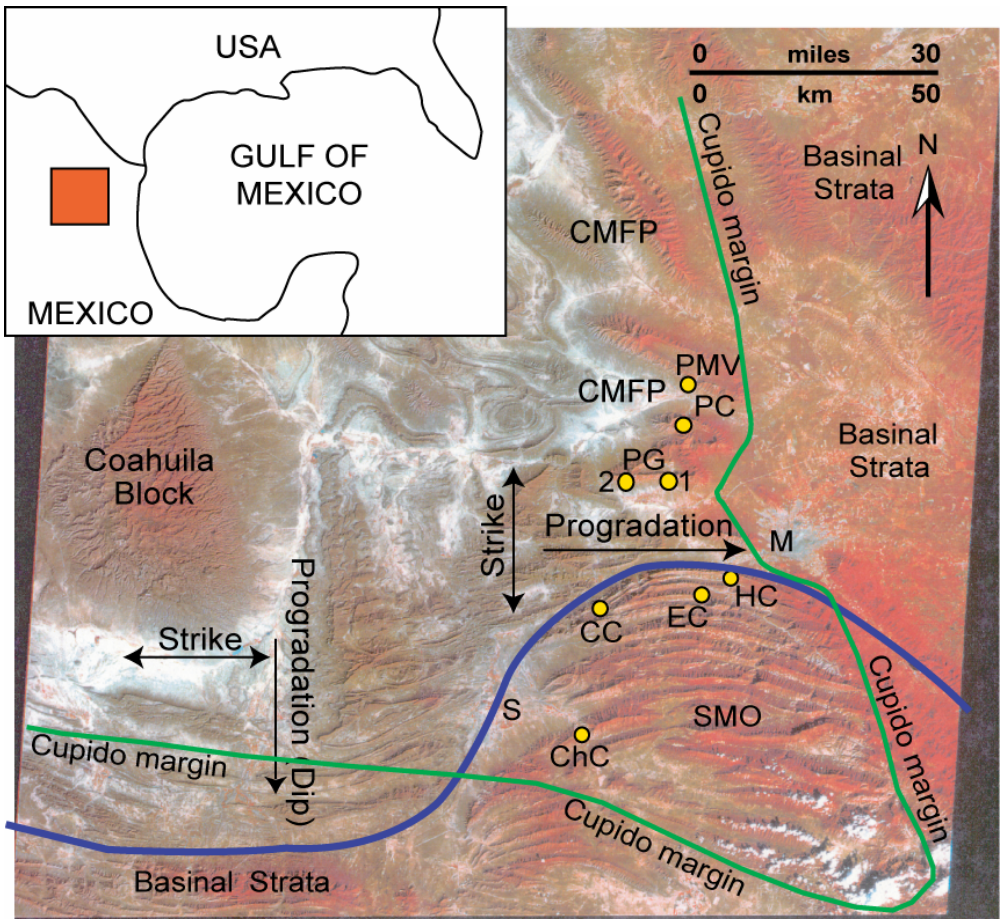

Figure 1-9. Geographic map and Landsat image.

Image illustrating the position of measured sections (yellow circles) relative to the Sierra Madre Oriental (SMO) and the Coahuila block. Monterrey (M) and Saltillo (S) Mexico are shown for orientation. The Coahuila Marginal Fold Province (CMFP) lies northward of the curvilinear thrust front (purple line) of the Sierra Madre Oriental. Anticlines and section names from north to south are Potrero Minas Viejas (PMV), Potrero Chico (PC), Potrero Garcia (PG1 and 2), Huasteca Canyon (HC), Escalera Canyon (EC), Cortinas Canyon (CC), and Chorros Canyon (ChC). The progradation of the Mesozoic passive margin is toward the east, southeast and south away from the Coahuila block. The platform margin trend (green line) is modified from Wilson (1999) and Foster (2003).

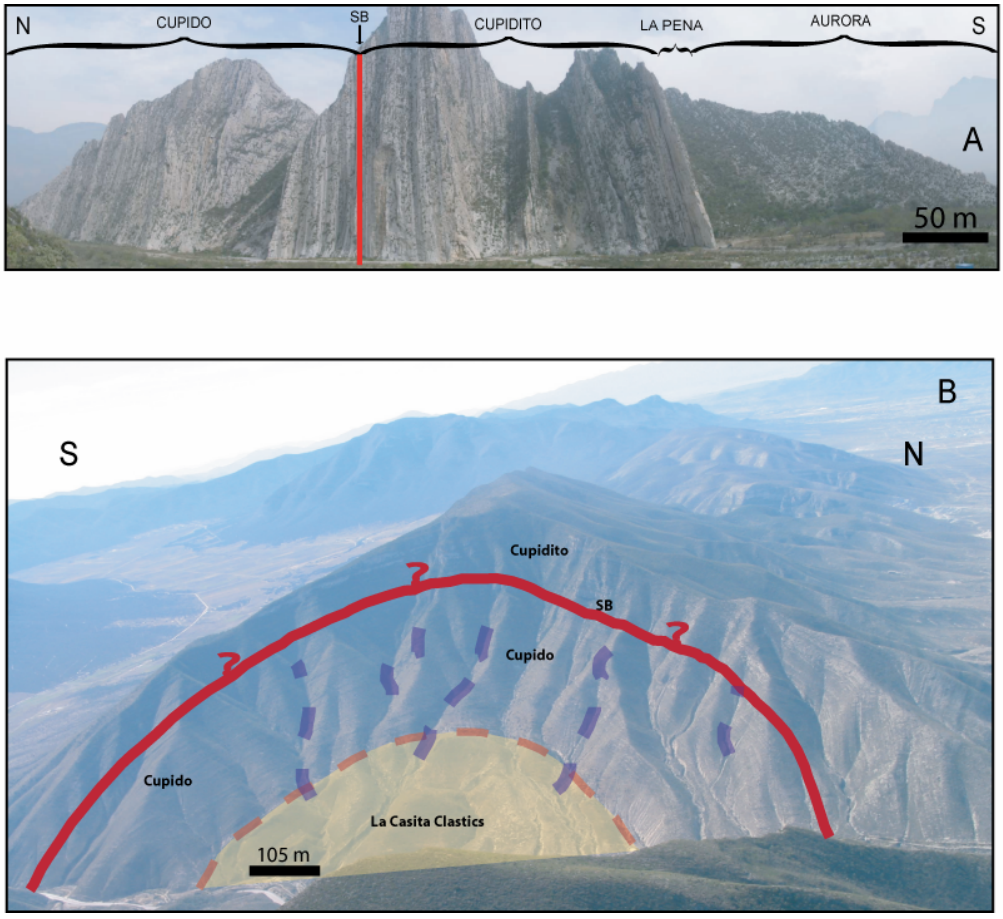

Figure 1-10. Outcrops of the Cupido Formation.

(A) Photo panorama of Huasteca Canyon (HC), SMO near Monterrey. The 2nd-order sequence boundary (SB) is marked in red and separates LCu, regressive, and the Cupidito member, transgressive, parts. Bedding planes are vertical.
(B) Aerial photograph of Chorros Canyon (ChC), SMO near Saltillo, with locations of measured stratigraphic sections (dashed purple lines). The Cupido Formation is a combination of LCu, regressive, and the Cupidito member, transgressive. The Cupidito member transgressive portion is difficult to measure within the anticline and it therefore was measured along the road cut. The solid red line represents the approximate location of the 2nd-order sequence boundary (SB). Photo taken by Goldhammer (2002).

Due to the intense post-depositional deformation in the area related to the Maastrichtian to Eocene Laramide Orogeny, tectonic reconstructions of the anticlines were estimated to determine pre-deformational distances between measured sections at the time of deposition. The estimated distance between Potrero Minas Viejas and Potrero Chico is ~12 km, between Potrero Chico and Potrero Garcia is ~16 km, and between measured sections Garcia 1 and 2 is ~8 km.

Lower Cretaceous paleogeography

The Cupido Formation of the western Gulf of Mexico (GoM) ranges from Middle Barremian to Aptian (126-117 Ma) (Lehmann et al., 2000) in age and is considered equivalent to the Sligo Formation of the northern GoM (Figure 1-3). The Cupido platform, composed of three different formations including the Cupido Formation, has a total thickness of approximately 660-785 m (Wilson and Pialli, 1977; Wilson, 1981; Wilson and Selvius, 1984; Wilson and Ward, 1993; Lehmann et al., 2000). Two thirds of the Cupido platform consists of a regressive, progradational shelf composed of slope, shelf margin, and platform interior facies. The upper third consists of deepening upward transgressive, aggradational-retrogradational platform interior facies, termed the “Cupidito” member by Wilson and Pialli (1977). In the Aptian (115-117 Ma), the Cupido platform was drowned by the La Peña Shale, which is composed of alternating pelagic carbonates and shale (Tinker, 1985). Once carbonate production began

again, the Aurora Formation was deposited as part of the succeeding platform (Figures 1-3, 1-9 and 1-11).

The Cupido platform is currently accepted as being a moderately steep rimmed shelf with a barrier reef system at the shelf crest (Conklin and Moore, 1977; Wilson and Pialli, 1977; Wilson, 1981; Wilson and Selvius, 1984; Wilson and Ward, 1993; Goldhammer, 1999), which is equivalent to the shelf edge (Figure 1-11). The Cupido shelf margin (Figure 1-12) is thought to have trended from Monterrey to the north, where it connects with the reef trend of the Sligo Formation (Figure 1-2), and from Saltillo it assumes a more westerly trend, wrapping around the Coahuila block (Wilson and Pialli, 1977; Wilson, 1981; 1999; Wilson and Selvius, 1984; Wilson and Ward, 1993; Goldhammer et al., 1991a). The Coahuila block is believed to have been the only local subaerial land mass at the time of Cupido deposition, and it had a significant effect on the shape of the platform in northeastern Mexico (Figure 1-2). The reef trend cannot be continually traced at the surface and has been described based on isolated exposures and the concept that it would have surrounded any nearby land mass (Wilson and Pialli, 1977; Wilson, 1999), such as the Coahuila block.

The Coahuila block was surrounded by large basins to the northeast, to the east toward the current position of Monterrey, and to the south (Figure 1-2). These topographic lows provided directions for the progradation of carbonate sediment during the development of the Cupido platform. The basins provide the

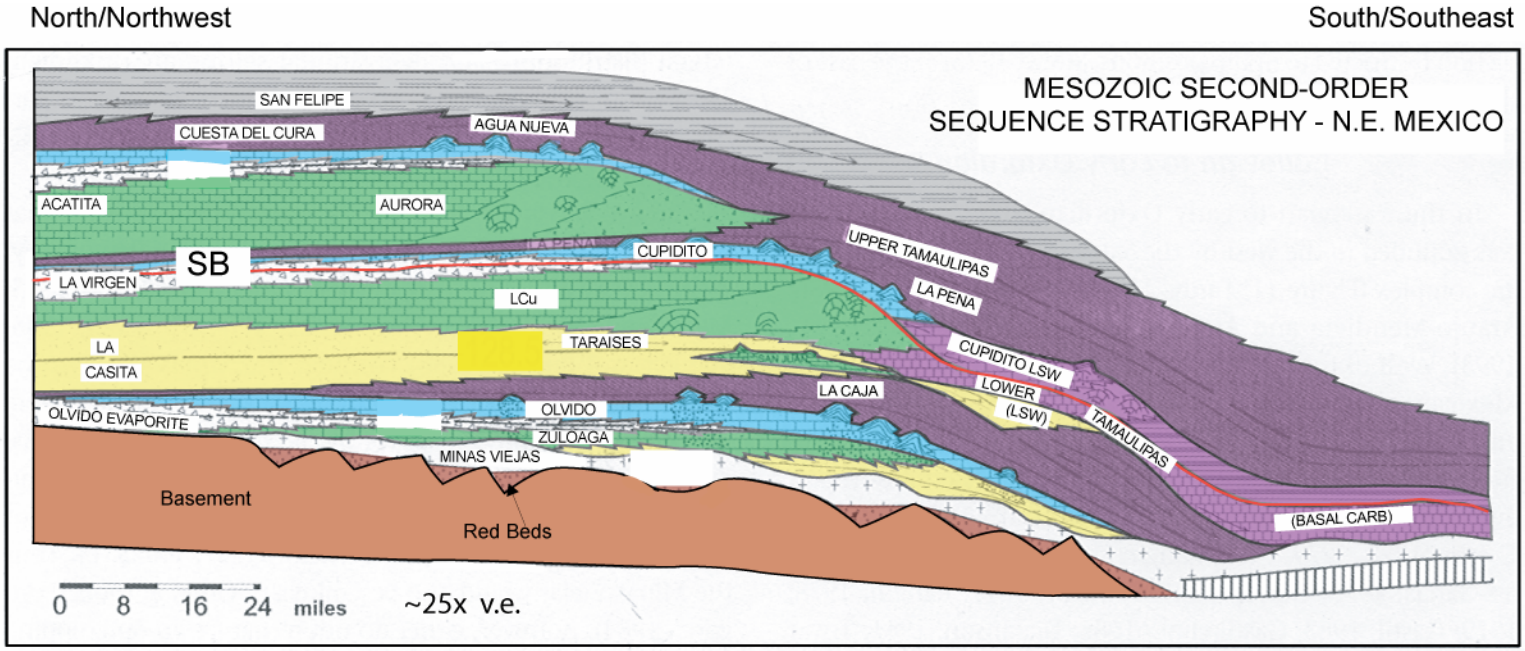

Figure 1-11. Regional cross section.

Restored schematic, dip-oriented regional cross section of the Mesozoic western Gulf of Mexico. North-northwest to south-southeast (left to right) trending in Mexico, reconstructed from south Texas subsurface analogues. Horizontal scale is approximate and vertical exaggeration is ~25 times. Formation lithologies are described in text and the 2nd-order sequence boundary (SB) within the Cupido Formation is shown. Modified from Goldhammer (1999).

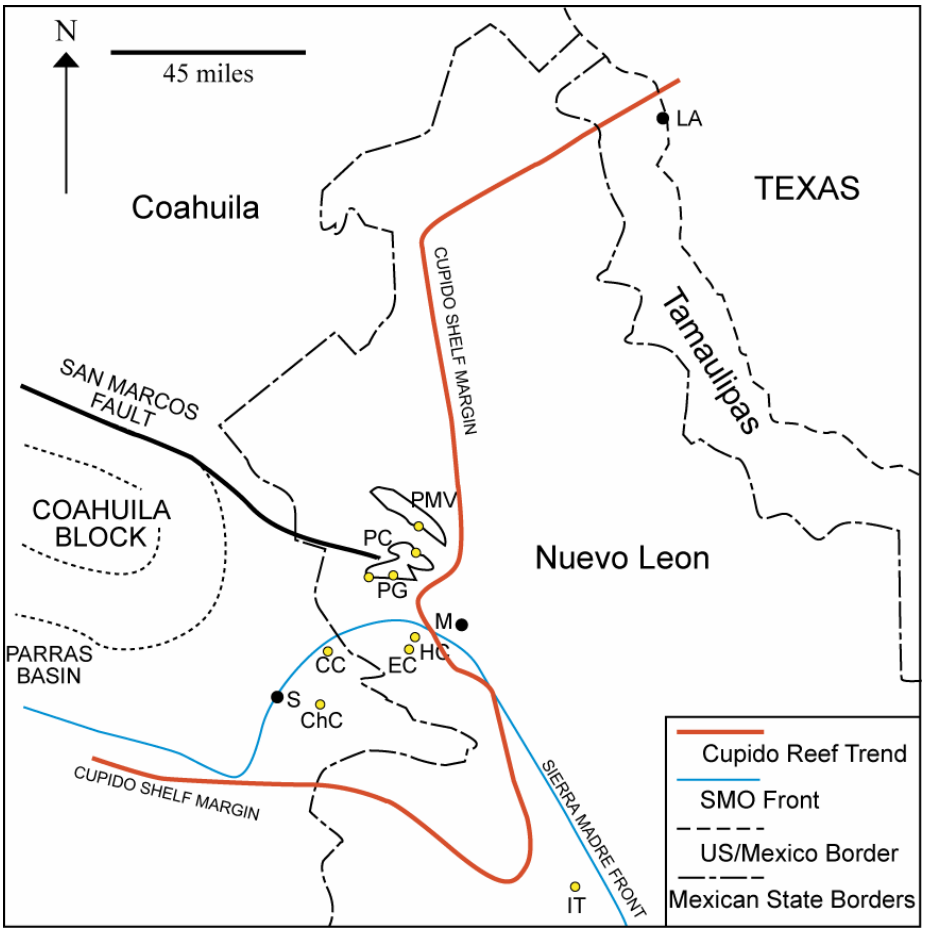

Figure 1-12. Map of reef trend.

Map of northeastern Mexico and south Texas illustrating the currently accepted reef trend, solid red line, relative to the Coahuila block as suggested by Wilson (1999) and modified by Foster (2003). The leading edge of the Sierra Madre Oriental fold belt is also drawn as a blue line; refer to the Landsat image in Figure 8. Yellow circles indicate the positions of measured sections in this study. Anticlines and section names from north to south are Potrero Minas Viejas (PMV), Potrero Chico (PC), Potrero Garcia (PG), Huasteca Canyon (HC), Escalera Canyon (EC), Cortinas Canyon (CC), Chorros Canyon (CC), and Iturbide Canyon (IT). Monterrey (M), Saltillo (S), and Laredo (LA) are marked for reference.

relative position of each measured section on the platform during deposition. Accordingly, strike direction along the platform follows the outline of the Coahuila block and dip direction, perpendicular to the shore line, extends radially away from the Coahuila block to the northeast, east, and south.

Tectonic history

The western Gulf of Mexico has a complex structural and stratigraphic history (Figures 1-13 to 1-20). Several regionally significant events that affected the northeastern portion of present day Mexico are pertinent to this discussion: formation of the Coahuila block; formation of the Sabinas basin and Monterrey trough; deposition of the Minas Viejas Evaporite; passive margin deposition in the Gulf of Mexico; and deformation associated with the Laramide Orogeny (Figures 1-2 and 1-13). The following discussion outlines the complex interplay between tectonism and regional sedimentation.

Coahuila block

Paleozoic plate reconstruction of Scotese (Scotese, 1997) for the Pangea supercontinent places South America, North America, and Yucatan together following a continent-continent collision (Figure 1-14). The convergent margin that preceded the collision produced granite to granodiorite rocks within the

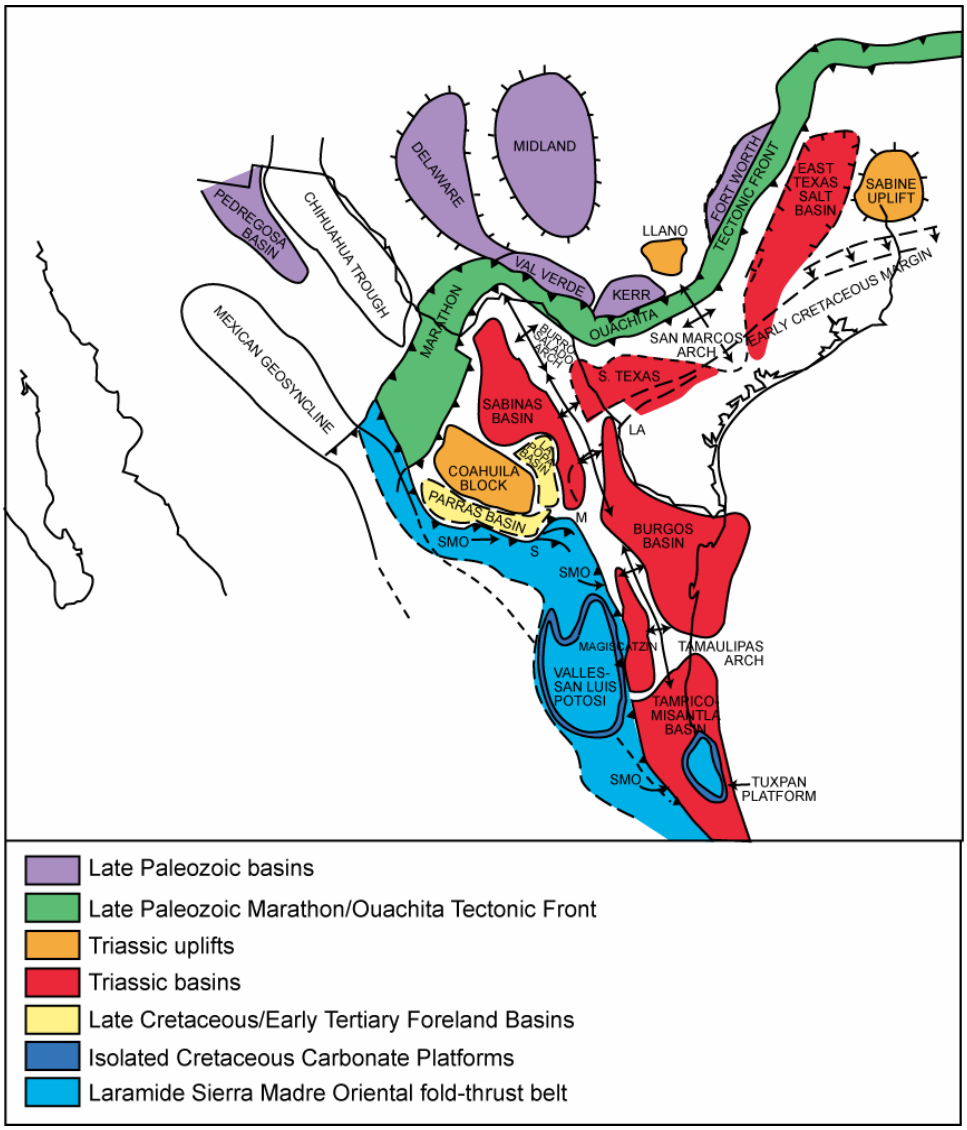

Figure 1-13. Regional tectonic map.

Map for the northwestern portion of the Gulf of Mexico as it appears today. Outlined are the general features that played some role in the development of the Cupido Platform including deformation during the Laramide Orogeny, which formed the Sierra Madre Oriental (SMO). Monterrey (M) and Saltillo (S) Mexico as well as Laredo (LA), and Texas are shown for reference. Modified from Goldhammer (1999).

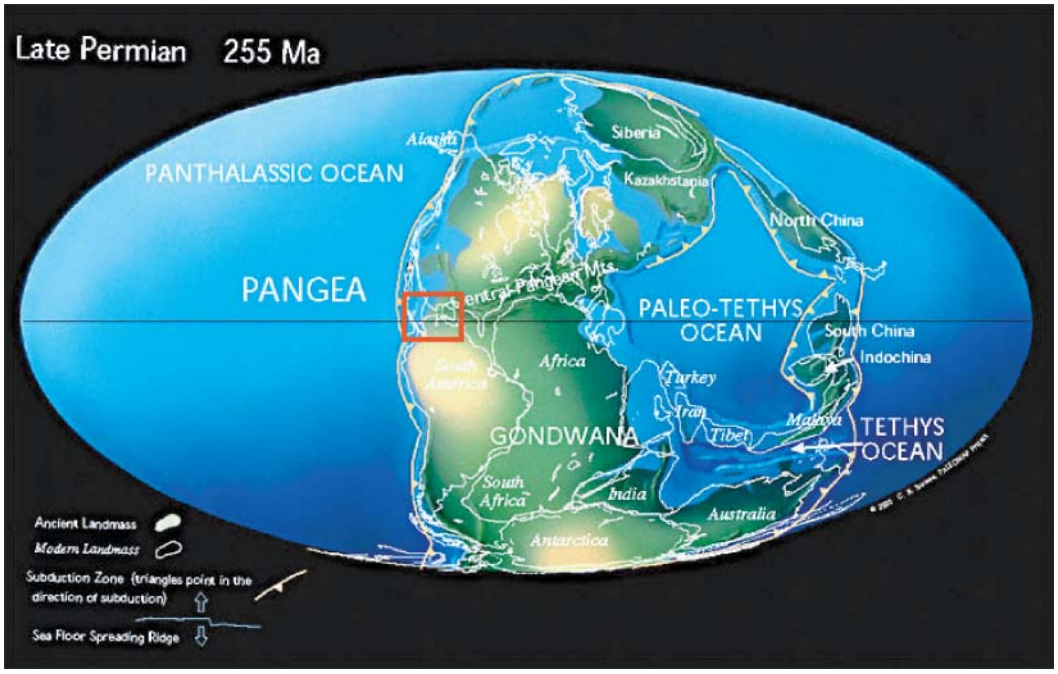

Figure 1-14. Paleogeographic reconstruction.

Reconstruction of the Late Permian, red box encloses study area. Modified from Scotese (1997).

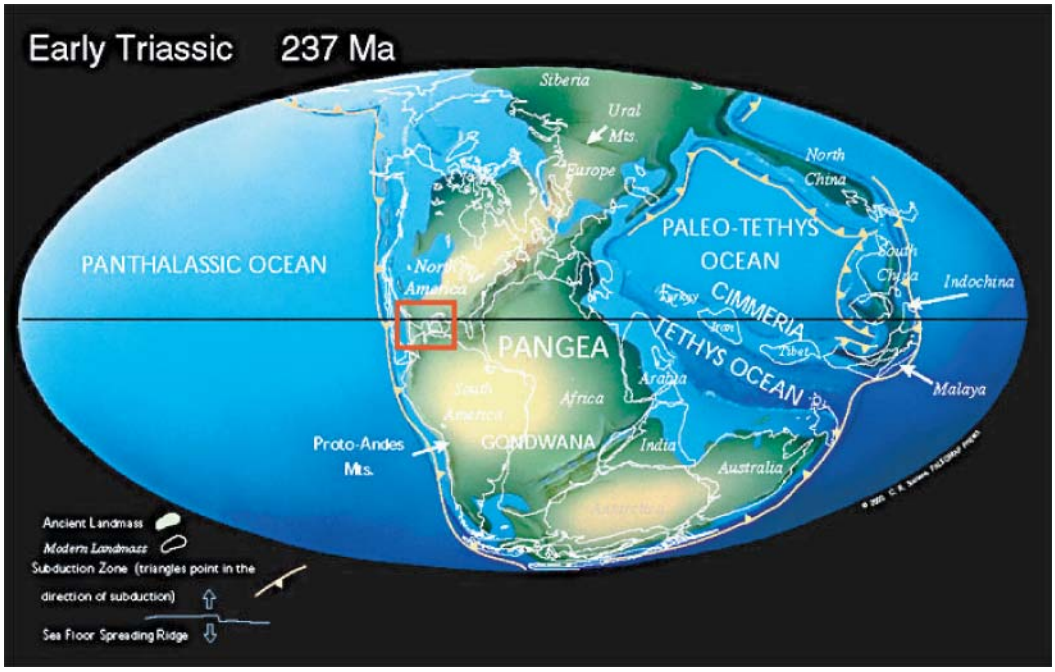

Figure 1-15. Paleogeographic reconstruction.

Reconstruction of the Early Triassic, red box encloses study area. Modified from Scotese (1997).

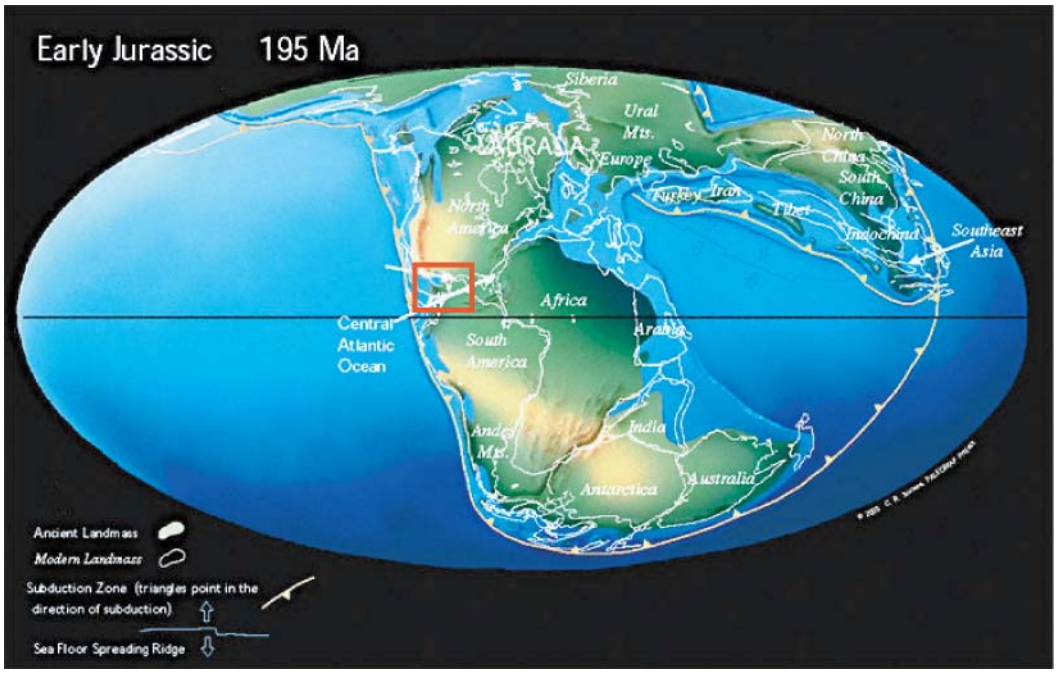

Figure 1-16. Paleogeographic reconstruction.

Reconstruction of the Early Jurassic, red box encloses study area. Modified from Scotese (1997).

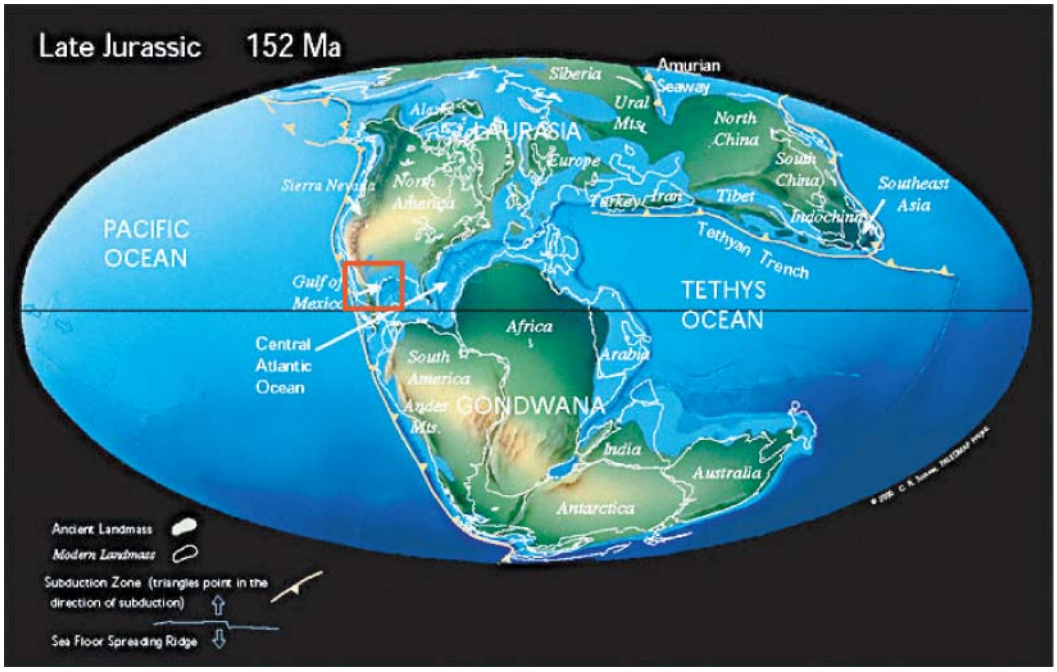

Figure 1-17. Paleogeographic reconstruction.

Reconstruction of the Late Jurassic, red box encloses study area. Modified from Scotese (1997).

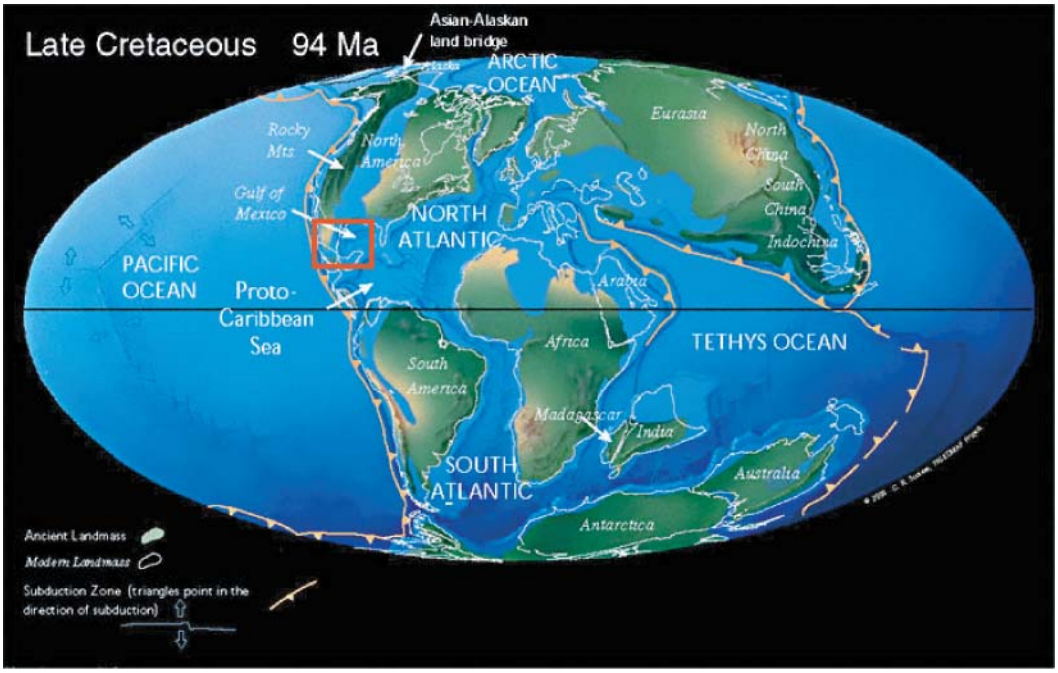

Figure 1-18. Paleogeographic reconstruction.

Reconstruction of the Late Cretaceous, red box encloses study area. Modified from Scotese (1997).

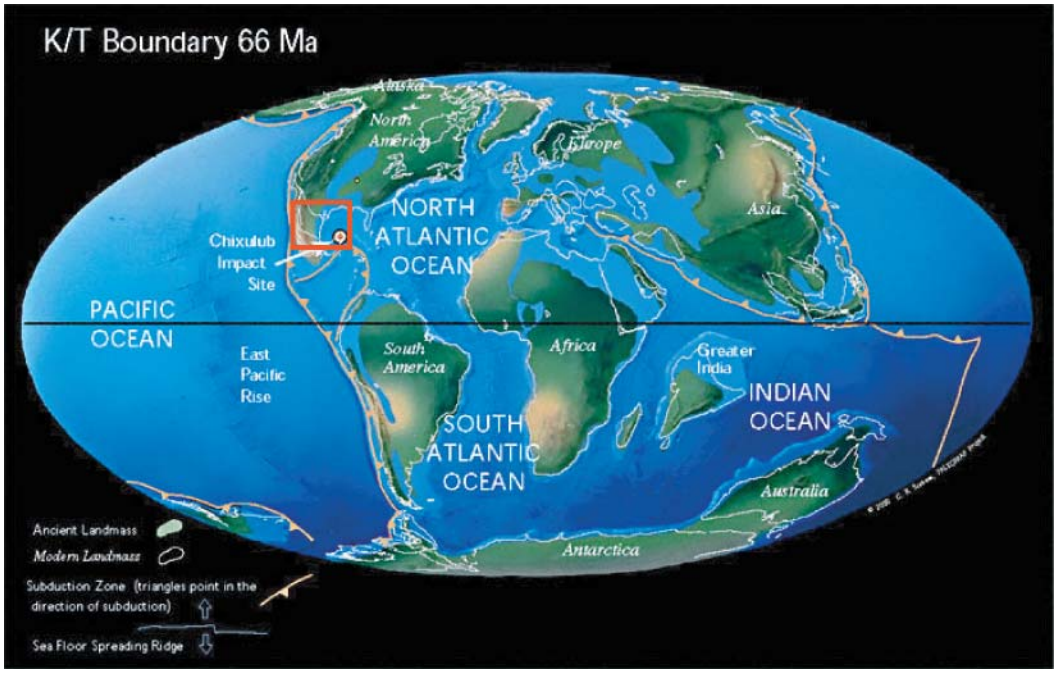

Figure 1-19. Paleogeographic reconstruction.

Reconstruction of the Cretaceous/Tertiary Boundary, red box encloses study area. Modified from Scotese (1997).

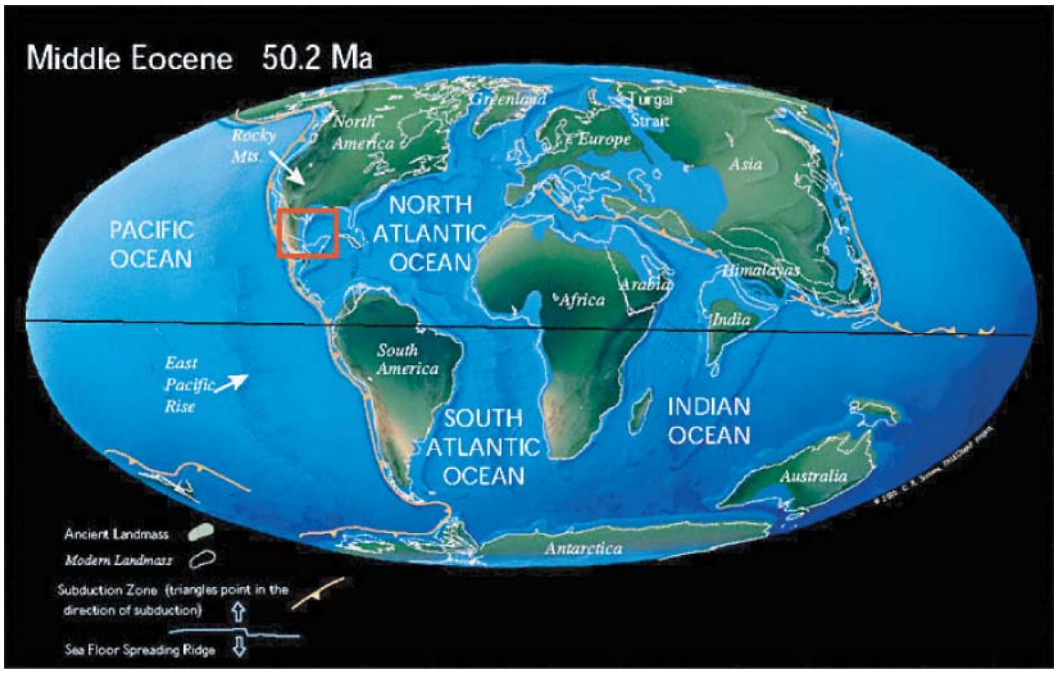

Figure 1-20. Paleogeographic reconstruction.

Reconstruction of the Middle Eocene, red box encloses study area. Modified from Scotese (1997).

Coahuila block, a volcanic arc terrane formed by the subduction of the North American Plate beneath the South American Plate during the Ouachita Orogeny in Late Pennsylvanian to Late Permian times (Pindell, 1985; Wilson, 1990; Figure 1-14). The Late Permian accretion of the Coahuila arc terrane onto the North American Plate also entrained the attached continental rise and slope sediments of the South American Plate and was accompanied by accretion of Middle Paleozoic crystalline basement of the Maya block (Handschy et al., 1987), one of several blocks that later combined to form a part of Central America. The uplifted Coahuila block acted as a local basement high, clastic sediment source, and also controlled the distribution of carbonate deposits throughout Mesozoic and Cenozoic sedimentation in the Gulf of Mexico (Figures 1-21 and 1-22).

Sabinas basin and Monterrey trough

Break-up of the Pangea supercontinent initiated during the Triassic (Figure 1-15) with rifting of South America away from the accreted terranes (Ball and Harrison, 1969; Anderson and Schmidt, 1983; Ross and Scotese, 1988; Pindell, 1985; Bartok, 1993; Goldhammer, 1999). The Sabinas basin and Monterrey trough (Figures 1-13 and 1-21), which surround the Coahuila block to the north and east respectively, were developed as a result of subsidence associated with half-graben formation during Triassic rifting and crustal attenuation. Late Triassic and Early Jurassic (Figure 1-16) deposits within these

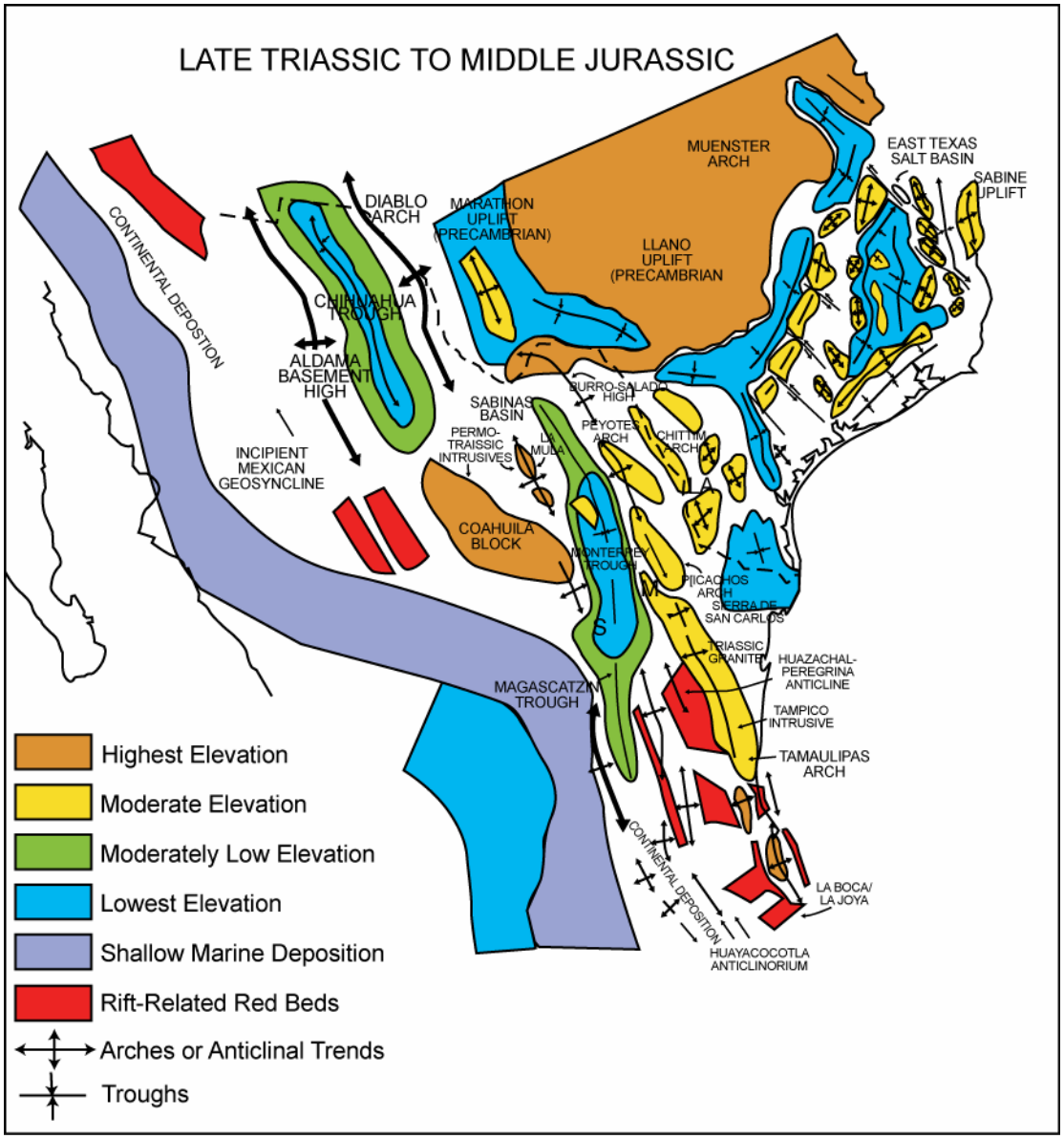

Figure 1-21. Late Triassic and Middle Jurassic paleogeography.

Paleogeography of the western Gulf of Mexico during the Late Triassic and Middle Jurassic. Black dashed line outlines the Texas and Mexico border; Monterrey (M) and Saltillo (S), Mexico are shown for reference. Note that this key is different from the following paleogeographic maps in that it relates to elevations instead of lithologies. Modified from Goldhammer (1999).

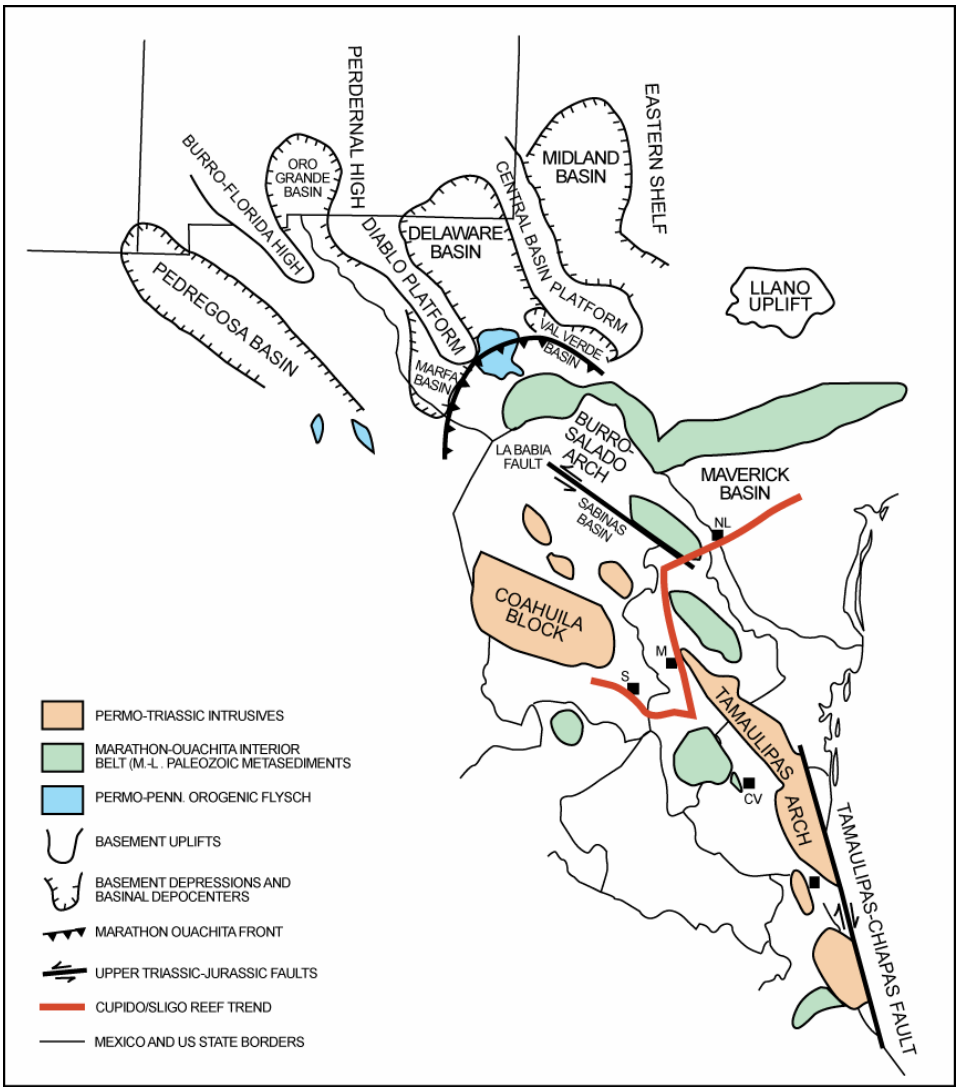

Figure 1-22. Paleotectonic map.

Map of northeastern Mexico, Texas, and New Mexico showing the accreted terranes and compressional deformation associated with the Ouachita Orogeny from the Late Pennsylvanian to Late Permian. Late Triassic granite and granodiorite intrusions are also shown. Mexico cities are abbreviated; Nuevo Laredo (NL), Monterrey (M), Saltillo (S), Ciudad Victoria (CV), Tampico (TA), and Mexican state outlines are dashed. Cupido/Sligo outline is the currently accepted reef trend. Figure is modified from Goldhammer (1999).

basins consisted of 300-1000 m-thick subaerial red beds of the Huizachal Formation (Mixon et al., 1959; Salvador, 1987; Goldhammer, 1999). Deposition of clastic sediments ended in the Middle Jurassic with the first exposure of the ancestral Gulf of Mexico to an open ocean. However, the Sabinas basin and Monterrey trough continued to act as sites for normal-marine sedimentation throughout the Cretaceous.

Minas Viejas evaporite

Late Bathonian to Callovian marine fossils and sediments across western and eastern Mexico suggests that a connection existed between the Pacific Ocean and the proto-Gulf of Mexico in the Early Jurassic (Figures 1-16, 1-23, 1-24, and 1-25). Ephemeral seaways linking the two marine basins most likely developed along the lowest elevations, or the most attenuated crust, and might have only occurred during hurricanes or unusually high tides (Salvador, 1987).

Periodic marine incursions into some of the basins resulted in the deposition of extensive gypsum and halite deposits estimated to be 3-4 km thick (Ross and Scotese, 1988). These evaporites are referred to as the Louann Salt in the United States and the Minas Viejas Evaporite in Mexico (Figures 1-3 and 1-25); other names have been assigned to equivalent deposits along the southern Gulf of Mexico. They are herein suggested to be Callovian in age and,

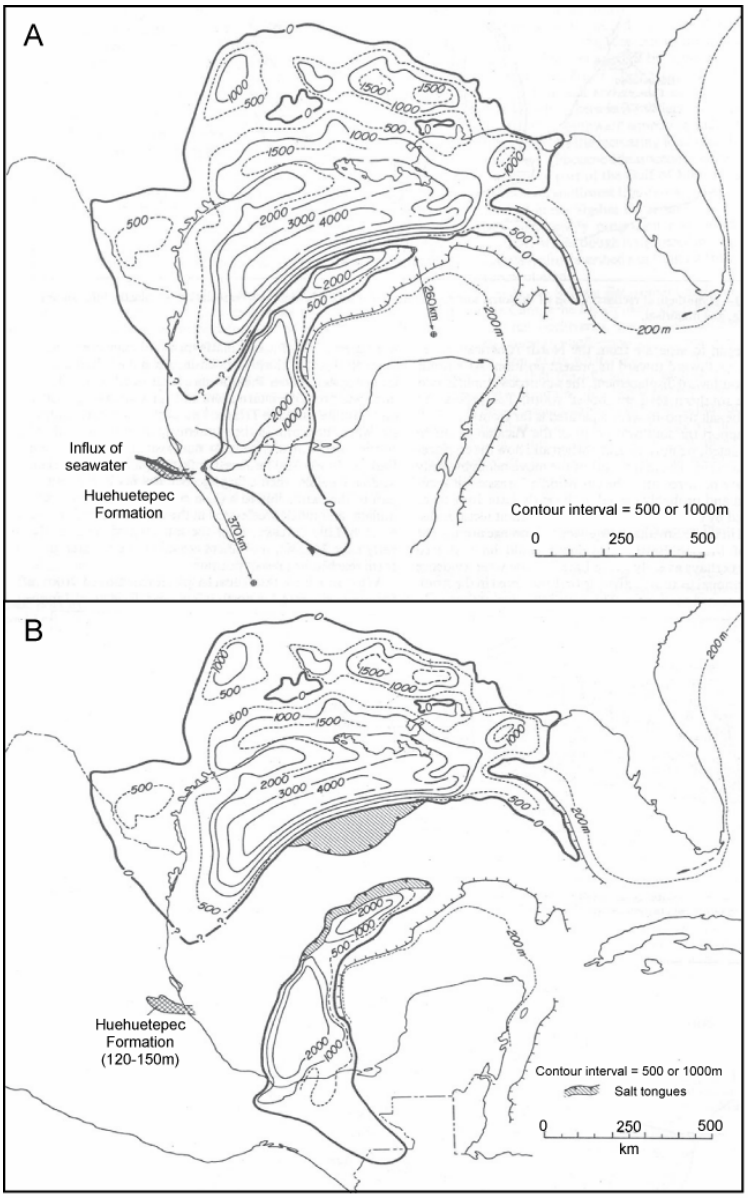

Figure 1-23. Isopach maps of evaporite distribution.

Evaporite distribution in the ancestral Gulf of Mexico during A) Callovian deposition and B) Oxfordian rifting stages. Estimate of original thickness is speculative in most part and is derived from multiple sources (mainly well information and or from reflection seismic profiles). Thickness is measured in meters. Modified from Salvador (1987).

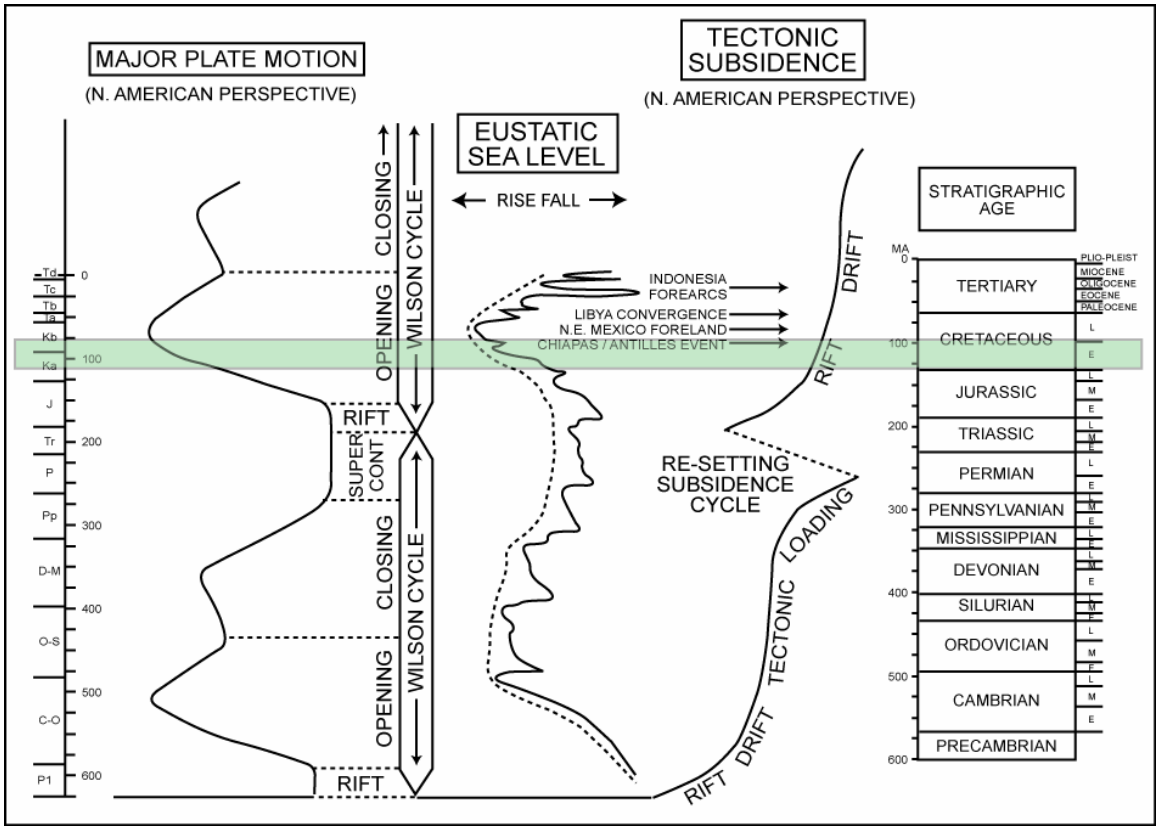

Figure 1-24. Low-order Cyclicity.

First order sequences (>100 m.y. duration) related to the formation and division of supercontinents and Wilson cycles, modified from Goldhammer (2003). Also shown are variations of eustatic sea level and global tectonic subsidence relative to plate motions. Shaded box encloses study interval.

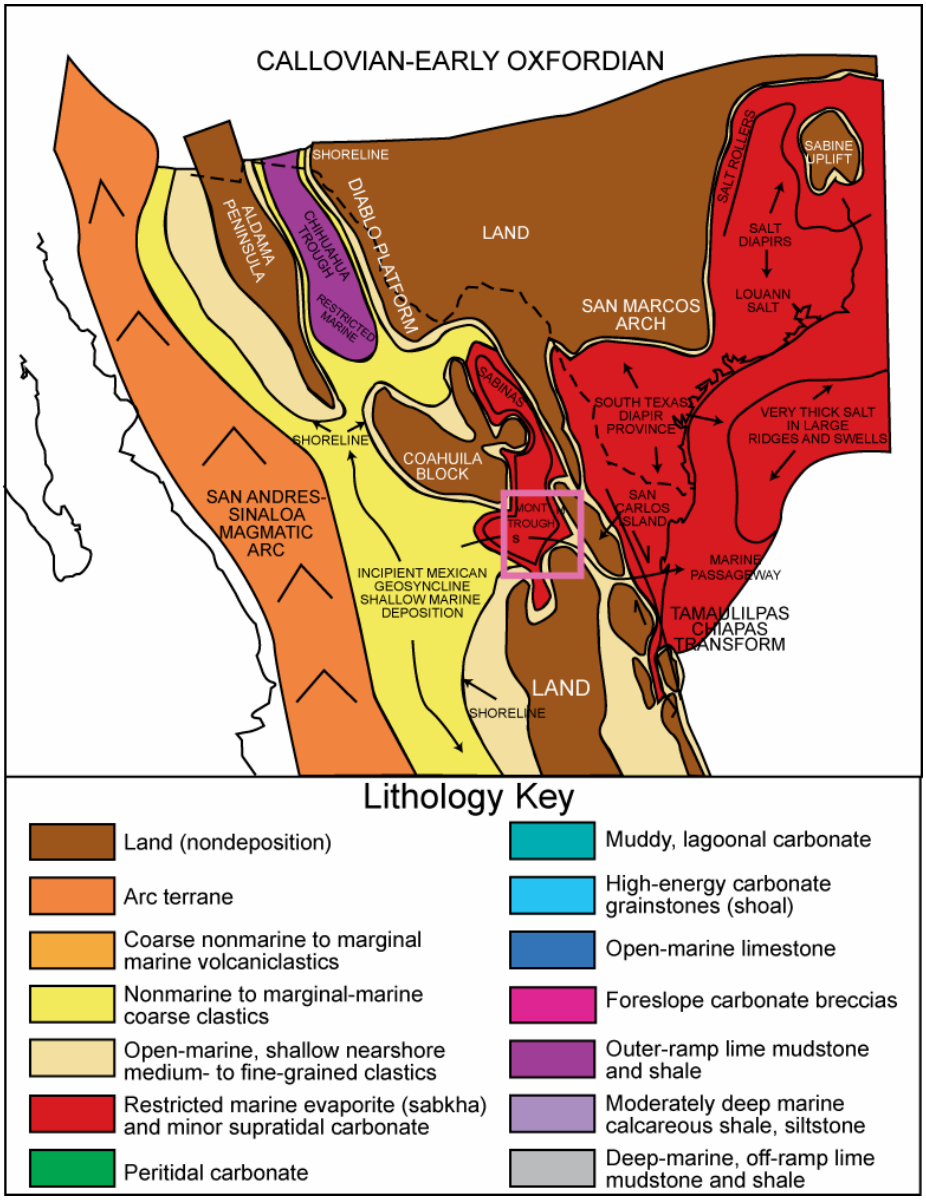

Figure 1-25. Callovian to Early Oxfordian paleogeography.

Paleogeographic map of the Callovian to Early Oxfordian, western Gulf of Mexico and northern Mexico. The Texas and Mexico border is outlined; Monterrey (M) and Saltillo (S), Mexico, are shown for reference. See text for details. This key matches all paleogeographic reconstructions shown in Figures 26-31. Modified from Goldhammer (1999).

equivalent to the Louann Salt (Salvador, 1987; Goldhammer, 1999). The evaporite deposits show considerable variability in thickness, which may be due to onlapping of the evaporites against the submerged antecedent topography of the rapidly subsiding rift graben or deposition within multiple shallow lakes exhibiting different subsidence rates (Salvador, 1987). The thick evaporite sequences subsequently influenced Laramide deformation by acting as decollement during compression.

Passive margin development

A number of regionally significant events occurred during Oxfordian times. The connection between the Pacific Ocean and the proto-Gulf of Mexico closed due to uplift of the Sinaloa arc terrane along the paleo-Pacific coast (Tardy, 1977; Goldhammer, 1999). Movement and active seafloor spreading in the Gulf of Mexico began dividing the Callovian evaporite sequence (Figures 1-23, 1-24, and 1-25). Active spreading also provided a second and permanent connection to an unrestricted marine basin, the Atlantic Ocean (Figure 1-17). This new connection allowed open circulation, dilution to normal sea-water salinity, and a transition to deep water depositional environments in the Gulf of Mexico (Salvador, 1987; Ross and Scotese, 1988). The termination of active seafloor spreading in the Gulf of Mexico during the Berriasian and the continued cooling of the passive margin were associated with a gradual decrease in the rate of tectonic subsidence (Goldhammer et al., 1991a). Passive margin deposition within the

Gulf of Mexico prevailed throughout the rest of the Mesozoic (Figures 1-18 and 1-19).

Laramide orogeny

Deformation associated with the Maastrichtian to Eocene Laramide Orogeny formed the fold-and-thrust belt exposed within the Sierra Madre Oriental and Coahuila Marginal Fold Province (Wall et al., 1961) of northeastern Mexico (Figures 1-8 and 1-13). These belts are divided by the curvilinear shape of the Sierra Madre Oriental front, which is defined by lateral continuity of folded and uplifted carbonates (Figure 1-8). The structural fabric of the Sierra Madre Oriental fold-and-thrust belt within the study area is characterized by east-west-trending, doubly plunging, arcuate, and tight to isoclinal folds. The Coahuila Province contains northwest-southeast-trending, doubly plunging, tight folds exhibiting narrow anticlines and broad synclines.

Stratigraphic history

Deposition of the Late Jurassic to Late Cretaceous sedimentary sequence of the Gulf of Mexico occurred along a passive margin. The Laramide Orogeny created a foreland basin along the western Gulf of Mexico during the Paleogene, which complicates the sequence stratigraphy of the area (Goldhammer, 1999). Following the rifting of Pangea, but prior to the Laramide Orogeny, four 2nd-order (10-100 m.y.) sequences (Figures 1-3 and 1-11) were deposited along the

passive margin of the Gulf of Mexico from Callovian to Santonian times. Second-order sequence boundaries (Figure 1-3) divide the Callovian to Oxfordian Minas Viejas/Zuloaga, the Kimmeridgian to Portlandian Olvido/Lower La Casita, the Neocomian to Lower Aptian Upper La Casita/Cupido, the Upper Aptian to Albian Cupidito/Aurora, and Cenomanian to Santonian Upper Aurora/Indidura Formations (Goldhammer et al., 1991a; Goldhammer, 1999). These sequences represent the second order cyclic rise and fall of sea level in an overall first-order transgression, which is interpreted as the result of the break up of the Pangea supercontinent (Goldhammer, 1999; Figure 1-24). Although recognized as uncertain and subject to change, the time scale of Gradstein et al. (1995) is used for the following chronostratigraphic discussion. Interpretation of the stratigraphic positions of the 2nd-order sequences in northeast Mexico has been complicated by structural deformation during the Laramide Orogeny. However, seismic data from areas that contain equivalent rocks but were not affected by Laramide deformation (e.g. Texas and Louisiana) have enabled the reconstruction of the equivalent stratigraphy in northeastern Mexico (Goldhammer, 1999; Figure 1-11).

The 1000 m-thick evaporites of the Minas Viejas Formation, which unconformably overlies the Early Triassic Huizachal red beds (Mixon et al., 1959; Todd and Mitchum, 1977), record the initial flooding of the Gulf of Mexico by the

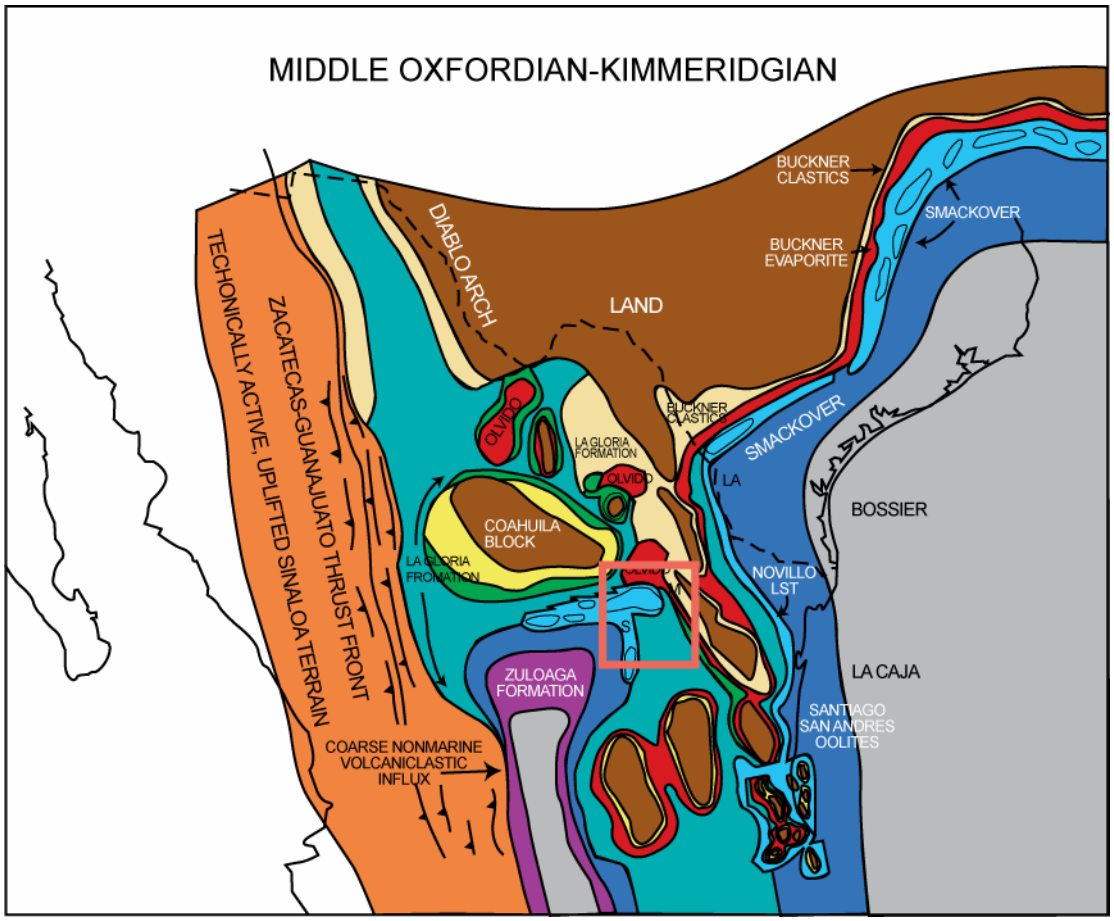

Figure 1-26. Middle Oxfordian to Kimmeridgian paleogeography.

Paleogeographic map of the Middle Oxfordian to Kimmeridgian. Refer to text for details, key is the same as Figure 1-25. Modified after Goldhammer (1999). The box encloses the study area.

Pacific Ocean (Goldhammer, 1999) and were deposited in a restricted environment in initial transgression during the Callovian (Figures 1-3 and 1-25). A transgressive system tract (TST) recorded the initial rise of sea level as contact was made between the GoM and the Atlantic Ocean during the Oxfordian. Near-shore clastics, marine carbonates, and deeper marine shales were deposited along ramp margins nucleated around pre-existing land masses (Goldhammer, 1999). The Early Oxfordian La Gloria Formation, equivalent to the Norphlet Formation of the northern Gulf of Mexico (Figures 1-3 and 1-26), was the first to cover the unconformity above the Minas Viejas Formation and the newly formed oceanic crust, straddling the spreading center in the Gulf of Mexico. Sediments derived from the Coahuila block and Tamaulipas arch contain fine to coarse, feldspathic quartz sandstones 100 m thick (Oivanki, 1974). The depositional environments are interpreted as marginal marine to near-shore shallow-marine grading into ramp interior carbonates.

The Zuloaga Formation is found down dip of the La Gloria Formation and unconformably overlies the Huizachal red beds and Minas Viejas evaporites (Goldhammer, 1999; Oivanki, 1974). The Zuloaga Formation is Oxfordian in age, equivalent to the Smackover Formation in the northern Gulf of Mexico (Figures 1-3 and 1-26), and ranges from 150-500 m thick.

The Olvido Formation was deposited during the transition from highstand to transgression in the Kimmeridgian (Todd and Mitchum, 1977; Salvador, 1987). The Olvido Formation is divided into two sections: the Olvido evaporite and the

Olvido carbonate lime mudstone (Goldhammer et al., 1991a). The Olvido evaporite lies directly above the Zuloaga Formation and conformably below the Olvido carbonate. It correlates with the Buckner Anhydrite (Figure 1-3) and ranges in thickness from 20 to 200 m.

The La Caja Formation is the basinal stratigraphic equivalent of the Olvido lime mudstone in the Kimmeridgian (Figure 1-26), the deeper basinal equivalent of the Lower La Casita Formation from the Tithonian to Portlandian, and correlates with the Bossier Shale of the northern Gulf of Mexico (Figure 1-3).

The La Casita Formation lies conformably above the Olvido Formation and contains the 138.5 Ma 2nd-order sequence boundary (Figure 1-3). It can be stratigraphically divided into a lower (highstand) and an upper (transgressive) section. The Lower La Casita Formation is Tithonian to Berriasian in age and correlates with the Cotton Valley Group of the northern Gulf of Mexico (Figures 1-3 and 1-27). The Upper La Casita Formation is Hauterivian in age and equivalent to the Hosston Formation (Todd and Mitchum, 1977; Salvador, 1987). The total thickness of the La Casita Formation is between 650-800 m.

The basinal, and likewise transgressional, equivalent to the Upper La Casita Formation is the Middle Berriasian to Hauterivian Taraises Formation (Figures 1-3 and 1-27; Fortunato, 1982; Fortunato and Ward, 1982). It conformably overlies the La Caja Formation and has a thickness ranging from 135 to 500 m (Blauser, 1981). The deeper-water facies of the Taraises Formation

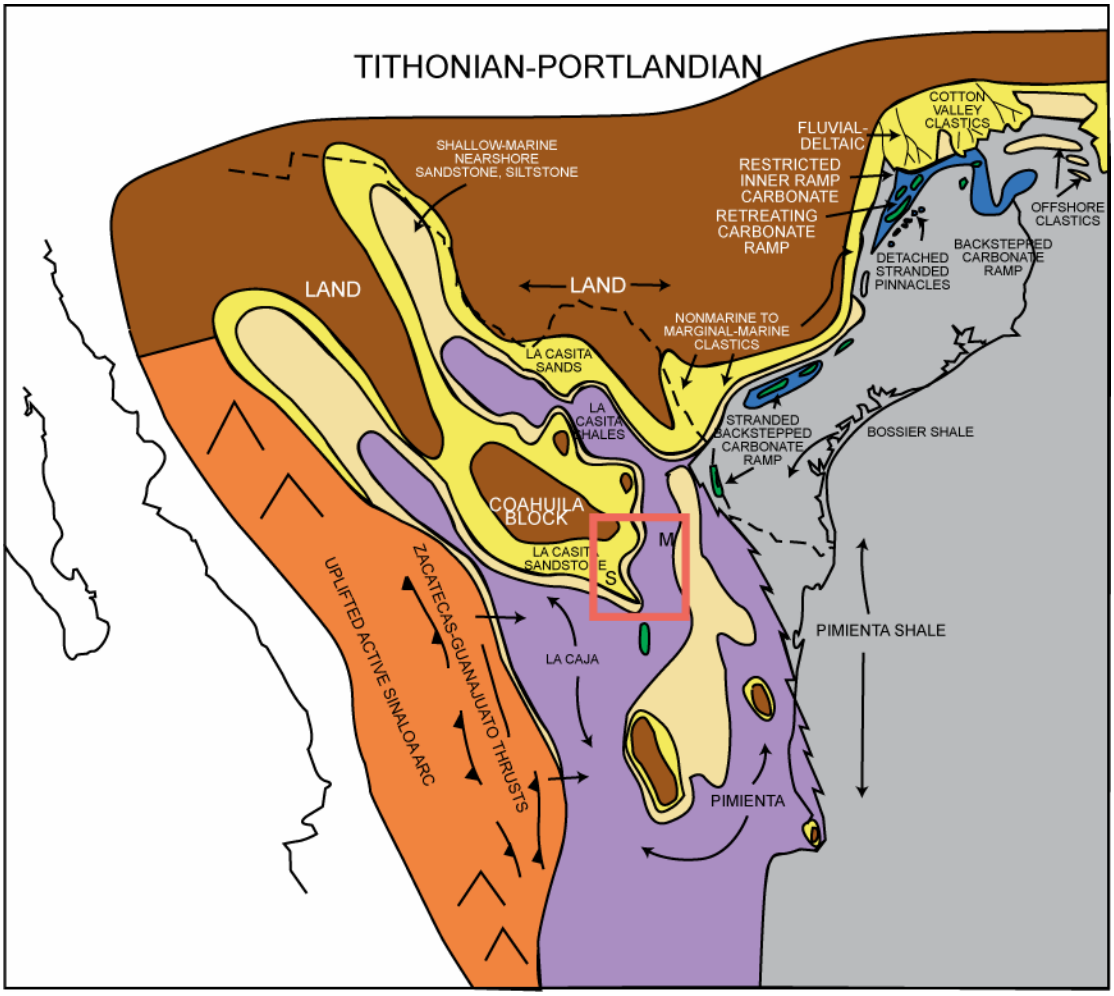

Figure 1-27. Tithonian to Portlandian paleogeography.

Paleogeographic map of the Tithonian to Portlandian. Refer to text for details, key is the same as Figure 1-25. Modified from Goldhammer (1999). The box encloses the study area.

are composed of black, cherty, pelagic lime mudstones and intercalated shales (Blauser, 1981).

The La Virgen Formation represents the beginning of a regression (Figure 1-3), which developed a formation similar to the carbonate-dominated Zuloaga Formation. The La Virgen Formation conformably overlies the La Casita Formation and changes down dip to the Cupido and the Lower Tamaulipas formations (Figure 1-28). The Cupido and La Virgen formations, with a combined thickness of 700-1200 m, make up the low relief, reef-rimmed carbonate platform of the Barremian through the middle Aptian. This platform followed the contours of the Coahuila block. The platform interior contains shallow marine high-energy grainstone shoals, open shelf skeletal lime sands, muddy lagoonal carbonates, and restricted tidal flat facies. It also notably lacks a near-shore clastic facies.

The Cupido Formation lies conformably above both the La Casita and Taraises formations (Figures 1-3 and 1-28) and is situated stratigraphically up dip from the Lower Tamaulipas Formation and down dip from the La Virgen Formation (Goldhammer, 1999). It is divided into lower and upper units. The lower unit is composed dominantly of regressive, progradational lithofacies (more details summarized in the earlier previous work section). The upper unit is interpreted as the transgressive portion above the 2nd-order sequence boundary and has been named the “Cupidito” member (Wilson and Pialli, 1977; Wilson, 1981, Goldhammer, 1999). The transgression that developed the Cupidito member also caused the retrogradation of all carbonate platforms in the Gulf of

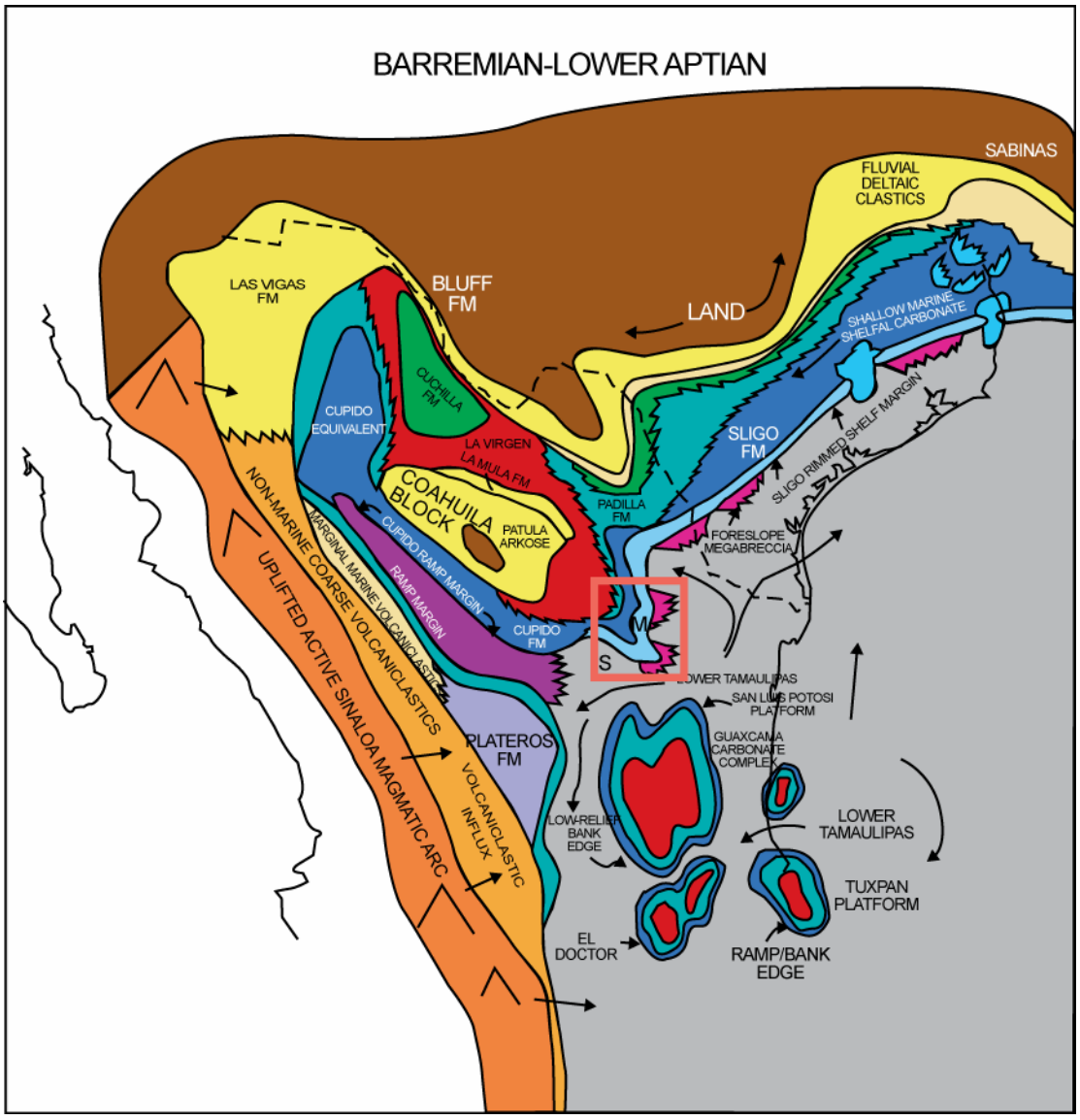

Figure 1-28. Barremian to Lower Aptian paleogeography.

Paleogeographic map of the Barremian to Lower Aptian. Refer to text for details, key is the same as Figure 1-25. Modified from Goldhammer (1999). The box encloses the study area.

Mexico and the growth of subsequent reef build-ups prior to inundation (Bebout and Loucks, 1977; McFarlan and Menes, 1991). The La Peña Formation records this flooding event in the late Aptian (Figure 1-29) and is equivalent to the Pearsall Group of the northern Gulf of Mexico (Tinker, 1985).

The Lower Tamaulipas Formation, the basinal equivalent of the Cupido Formation, conformably sits above the Taraises Formation and is 600 m thick. The LowerTamaulipas Formation contains gray to black, thin- to medium-bedded, cherty basinal lime mudstones and shales (Goldhammer, 1999). Wilson (1969) interpreted the depositional environment of the Lower Tamaulipas Formation as a dysaerobic, quiet basinal setting at depths of 50-150 m. The Lower Tamaulipas, Cupido, and La Virgen formations combined form a single regressive stratigraphic unit equivalent to the Sligo Formation of Texas (Figures 1-2 and 1-28).

The Aurora Formation, which rests conformably above the La Peña Formation, is Albian in age, equivalent to the Glen Rose and Fredericksburg formations of Texas (Goldhammer, 1999), and ranges from 500 to 700 m thick. The Aurora Formation is regressive and forms the highstand system tract below the 102 Ma 2nd-order sequence boundary (Figures 1-3 and 1-30). It forms the second stage of Cretaceous carbonate platform growth in northeastern Mexico (Wilson, 1975; Smith, 1981). Similar to the Cupido Formation, the Aurora developed a low-angle ramp that surrounded part of the Coahuila block (Smith, 1981). The environments of deposition and facies are normal marine lagoonal

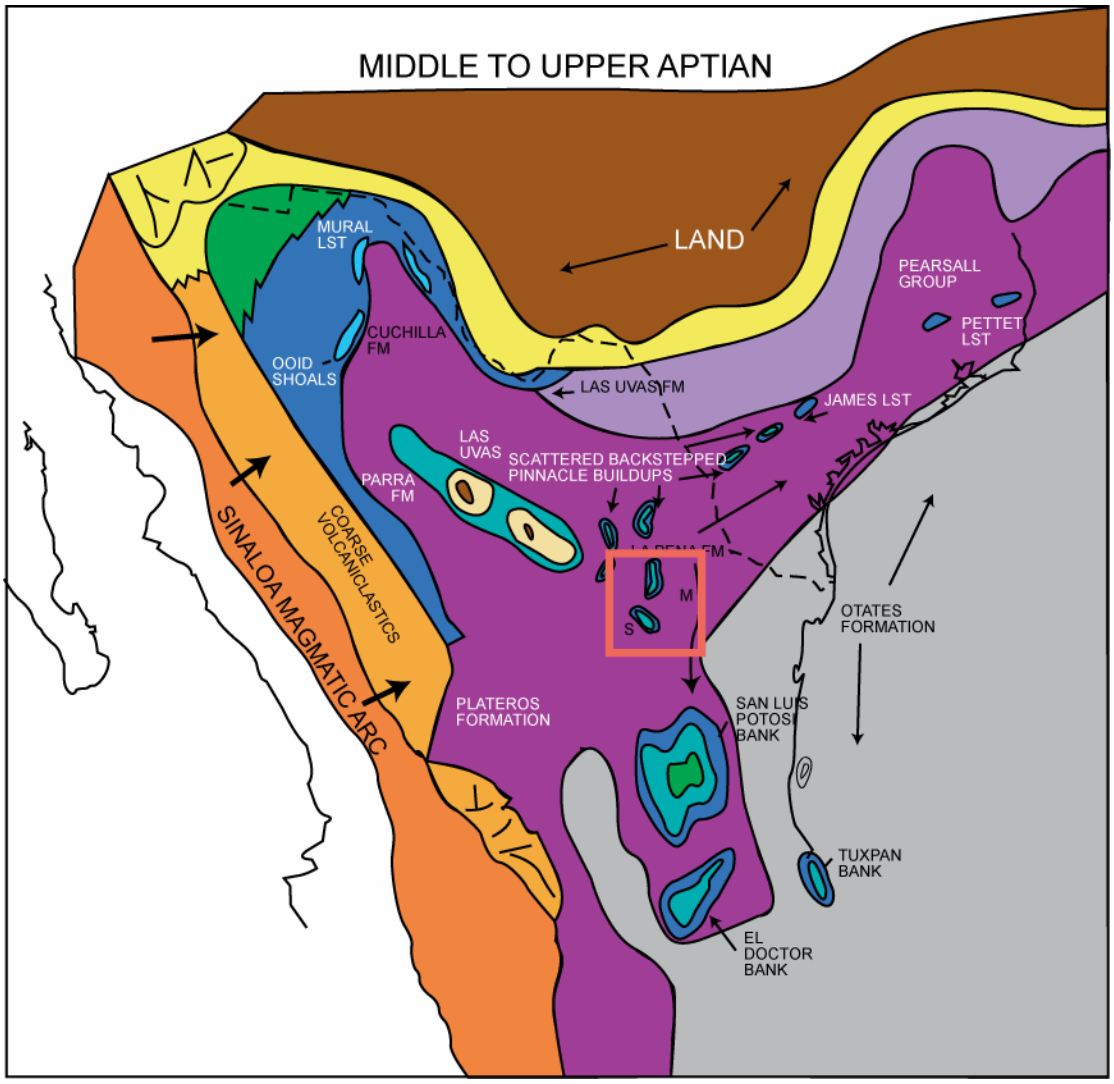

Figure 1-29. Middle to Upper Aptian paleogeography.

Paleogeographic map of the Middle to Upper Aptian. Refer to text for details, key is the same as Figure 1-25. Modified from Goldhammer (1999). The box encloses the study area.

sediments with a rudist bioherm rimmed shelf.

The Albian Upper Tamaulipas Formation conformably overlies the La Peña Formation. It is the basinal stratigraphic equivalent of the Aurora Formation (Figure 1-3 and 1-30) and is equivalent to the Atascosa Formation of southern Texas (Figure 1-3; Smith, 1981). The Upper Tamaulipas Formation thickens basinward to between 100 and 200 m. Its lithology consists of thin- and thick-bedded, cherty, dark pelagic mudstone to wackestone (Ross, 1981) and is interpreted as deep water anaerobic to dysaerobic off-ramp deposits (Goldhammer, 1999).

Above the 102 Ma sequence boundary (Figure 1-3), the Aurora Formation back-stepped due to a large transgressive flooding event, which connected the Gulf of Mexico to the Western Interior Seaway during the Cenomanian and resulted in carbonate build-ups or pinnacle reefs within the Aurora Formation (Goldhammer, 1999). Subsequently, the Aurora Formation was overstepped by the latest Albian to Cenomanian Cuesta del Cura Formation (Smith, 1981). The Cuesta del Cura Formation may disconformably overly the Aurora and Upper Tamaulipas formations, but it is equivalent to the Georgetown-Del Rio-Buda formations of Texas (Figure 1-3). It consists of 60 m of dark, thin- to medium-bedded, laminated lime wackestone to packstones and thin shales (Ice, 1981). The Cuesta del Cura Formation is interpreted as deep-water pelagic carbonates and shales (Goldhammer, 1999). It marks the onset of pelagic deposition for the Gulf of Mexico in the Upper Cretaceous, and is overlain by shales and chalk of

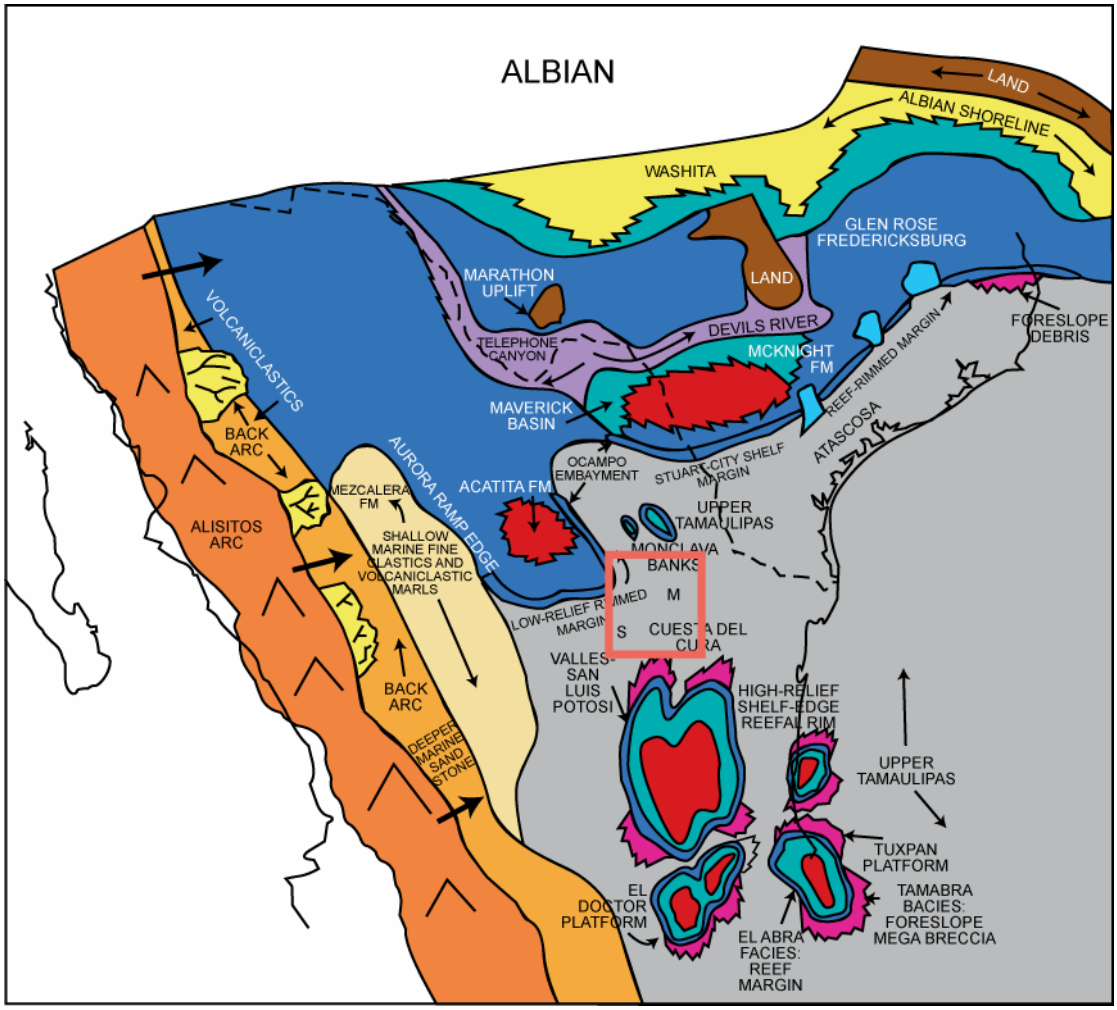

Figure 1-30. Albian paleogeography.

Paleogeographic map of the Albian. Refer to text for details, key is the same as Figure 1-25. Modified after Goldhammer (1999). The box encloses the study area.

the Indidura Formation. The Laramide Orogeny complicates the subsequent stratigraphic history of the western Gulf of Mexico at this time (Figure 1-31).

METHODOLOGY

Fifteen stratigraphic sections through the Cupido Formation were measured and described in detail (Figure 1-9; Appendix A). The sections were measured at Chorros Canyon (ChC; 6 sections), Cortinas Canyon (CC; 1 section), Escalera Canyon (EC; I section), Potrero Garcia (PG; 2 sections), Potrero Chico (PC; 1 section), Potrero Minas Viejas (PMV; 1 section), Huasteca Canyon (HC; 2 sections) and Iturbide Canyon (IC; 1 section). The locations of the measured sections were chosen because of accessibility to the outcrop and exposure of large section of the Cupido Formation. The six sections measured at Chorros Canyon were used for detailed study of lateral and vertical dolomite distribution. All of the field work was carried out during five field seasons (December 2002; April 2003; summer 2003; January 2004; December 2004) totaling 19 weeks. Figure 1-9 shows location of the measured sections relative to Cupido platform margin.

Each section was logged bed-by-bed at cm-scale, documenting thickness, color, grain size, lithofacies, depositional texture, biota, sedimentary structures and any evidence for subaerial exposure. Where possible, beds were traced laterally to determine lateral continuity and overall facies variability. Samples

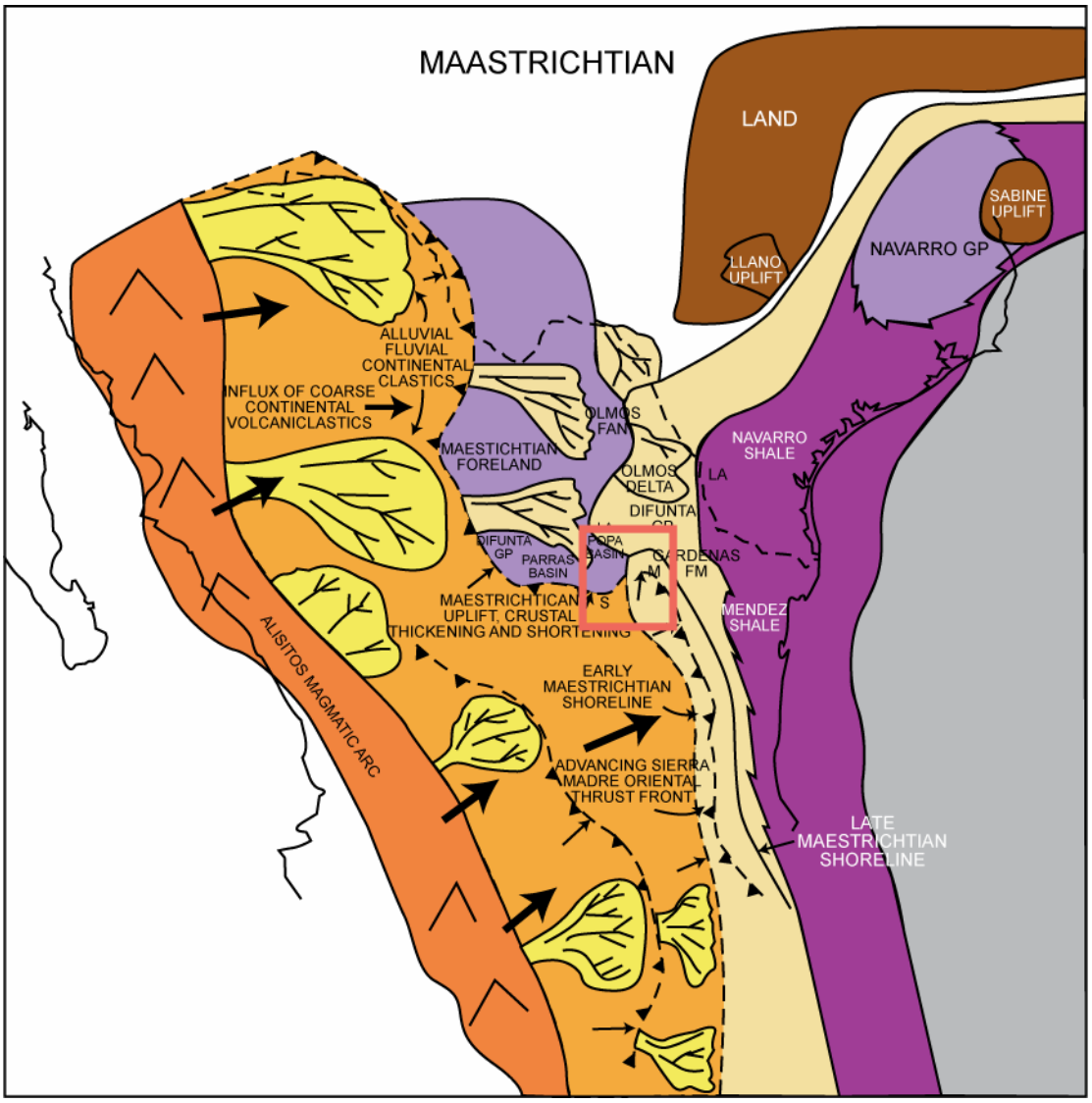

Figure 1-31. Maastrichtian paleogeography.

Paleogeographic map of the Maastrichtian. Refer to text for details, key is the same as Figure 1-25. Modified after Goldhammer (1999). The box encloses the study area.

were collected at each measured section and were slabbed and polished to document depositional features and stratigraphic relationships. Samples were collected at less than 15 m interval depending on facies variability. A total of 482 rock samples were collected from the Cupido Formation, 257 slabbed samples, and 314 thin sections (250 large) were prepared for petrographic analysis. Appendix B contains a list of the samples and thin sections prepared for analysis, digital photos and photomicrographs at a variety of scale of the described lithofacies. Thin sections were stained with Alizarin Red (Dickson, 1965) for petrographic description and to aid in grain identification. Facies were defined on the basis of depositional textures, sedimentary structures and fossil content following Dunham's (1962) classification scheme.

In depth methodology descriptions of the techniques, classification schemes and any statistical analysis used in this study are discussed with the individual chapters (2-4).

Chapter 2. High-resolution sequence stratigraphy, evolution and morphology of the Cupido platform, NE Mexico

ABSTRACT

The Lower Cretaceous (Barremian to Aptian) Cupido platform of northeastern Mexico forms part of an extensive carbonate platform system that surrounded the ancestral Gulf of Mexico. Detailed stratigraphic sections combined with comparative sedimentology analysis provide evidence for a revised depositional model for the Cupido platform. A stable grainstone shoal developed behind a discontinuous rudist coralline algal bank on the margin facing the ancestral Gulf of Mexico to the east. A thick succession of cyclic peritidal and subtidal deposits accumulated on a broad shelf lagoon (~ 100 km) on the lee side of this margin.

The Cupido Formation exhibits meter-scale high-frequency cyclicity which stacks into lower-order depositional and composite sequences that correlate across the platform. High-frequency cycles stack into depositional sequences (43-86 m thick) which in turn stack into lower-order composite sequences (145-168 m thick). A total of 12 depositional sequences (A-L) are interpreted within the Cupido Formation. Depositional sequences (A-F) compose the LCu and stack into partial composite sequence I (highstand part only) and composite sequences II. Overlying this, depositional sequences (G-L) comprise the transgressive Cupidito member which stack into composite sequences III and

partial composite sequence IV (transgressive part only). The 2nd-order sequence boundary is represented by a laterally extensive thick collapse-breccia caused by the dissolution of the underlying bedded evaporites, breakage, and mixing of overlying layered lithofacies.

Two-dimensional correlation of the measured stratigraphic sections revealed two additional depositional sequences landwards of the Cupido platform margin deposited simultaneously with the La Peña Shale deposition as it drowned the shoal complex in the early stages of the 2nd-order transgression. These retrogradational geometries on the Cupido platform are supported by landward thickening in the transgressive portion of the equivalent subsurface Sligo Formation. Near the platform margin, the cyclicity is disturbed by the presence of large-scale syndepositional growth faults. Movement along these faults resulted in thicker depositional sequences in the outer shelf due to the dramatic increase of accommodation space available for sedimentation.

The complete depositional model and high-resolution sequence stratigraphic framework for the Cupido Formation, presented herein, reveal subtle complexities of facies models and their controls, which were not in previous studies. Results serve as practical analogues for the subsurface equivalent Sligo Formation of Texas and can be applied to similar reservoirs for better understanding of facies distribution and models, and their lateral variations.

INTRODUCTION

Previous work on the Lower Cretaceous Cupido Formation exposed in the Sierra Madre Oriental (SMO) in NE Mexico includes surface mapping, biostratigraphic dating and facies description by Imlay (1936 and 1944), Humphrey (1949), Charleston (1974), Ekdale et al. (1976), Conklin and Moore (1977), Wilson and Pialli (1977), Wilson and Selvius (1984), Goldhammer et al., (1991a), Wilson and Ward (1993), Lehmann et al. (1999), and Foster (2003). In northeastern Mexico, the Cupido Formation is divided into two parts, separated by a 2nd-order sequence boundary, thin-bedded progradational LCu deposits and thicker bedded retrogradational Cupidito member (Wilson and Pialli, 1977; Wilson, 1981; Goldhammer, 1999). Construction of a sequence stratigraphic framework for the Cupido was started by Goldhammer et al. (1991a) and has since been modified by various studies including Lehmann et al. (1999), Foster (2003), and Altobi et al. (2004). Attempts on mapping the paleographic trend of the Cupido margin were carried out by Wilson (1999), Lehmann et al. (2000), and Foster (2003). Most of the studies combined detailed lithologic logs and petrographic analysis. Recent work Lehmann et al. (1998, 1999, and 2000) and Foster (2003) focused on the upper part of the Cupido Formation for better understanding of the platform geometry, and stratigraphic framework.

This paper combines thorough sedimentology with high-resolution sequence stratigraphic concepts to interpret platform evolution and to build a comprehensive high-resolution sequence stratigraphic framework for the entire

Cupido Formation. The paper also presents (1) evidence for the existence of a high-energy shoal margin on the eastern side of the Cupido platform, (2) evidence for back-stepping geometries caused by rising sea level, at the top of the Cupido Formation before the eventual drowning of the platform, (3) a model for breccia development and timing within the Cupido Formation, and (4) sequence stratigraphic evidence for the existence of syndepositional faulting within the Cupido Formation. A comprehensive sequence stratigraphic analysis of facies partitioning and development of models using 2D correlation, fence diagrams, and subsurface analogues allow interpretation of a refined sequence stratigraphic framework. This high-resolution framework, in turns, reveals subtle complexities of facies models and their controls not evident from previous studies. Results can be applied to similar reservoirs for better understanding of facies distribution, and their lateral variations.

Geologic setting

Tectonic and paleogeographic setting

The Cupido Formation was deposited in a passive margin setting following the opening of the Gulf of Mexico (GoM) (Wilson, 1990; Goldhammer et al., 1991a). The break up of Pangea resulted in the development of basement highs (e.g., Coahuila block and Tamaulipas arch) and lows (e.g., Sabinas basin and Monterrey trough) in NE Mexico (Anderson and Schmidt, 1983; Ross and Scotese, 1988; Pindell, 1993; Goldhammer, 1999). The Coahuila block is

composed of a Permo-Triassic basement underlain by granite and granodiorite intrusions from an island arc system that developed south of the Ouachita-Marathon orogenic belt. The Coahuila block acted as a local basement high, clastic sediment source to surrounding basins and subsequently played a major role in the distribution of carbonate deposits within northeastern Mexico throughout the late Mesozoic and early Cenozoic (Wilson, 1981; Wilson and Selvius, 1984). The Sabinas basin and Monterrey trough, which bound the Coahuila block to the north and east respectively, were developed as a result of subsidence associated with the formation of half-grabens during Triassic rifting and crustal attenuation. These basins subsequently acted as sites for evaporite precipitation followed by normal-marine carbonate sedimentation throughout the Cretaceous.

The Sierra Madre Oriental fold and thrust belt developed during the Laramide Orogeny (Late Cretaceous to Eocene), and represents the southern continuation of the Rocky Mountains in the U.S. (Marrett and Aranda-Garcia, 1999). The Sierra Madre Oriental is characterized by east-west-trending, doubly plunging, arcuate, and tight to isoclinal folds (Figure 2-1). The age of contractional deformation in the Sierra Madre Oriental has not been accurately determined. However, Eocene strata are the youngest affected suggesting that

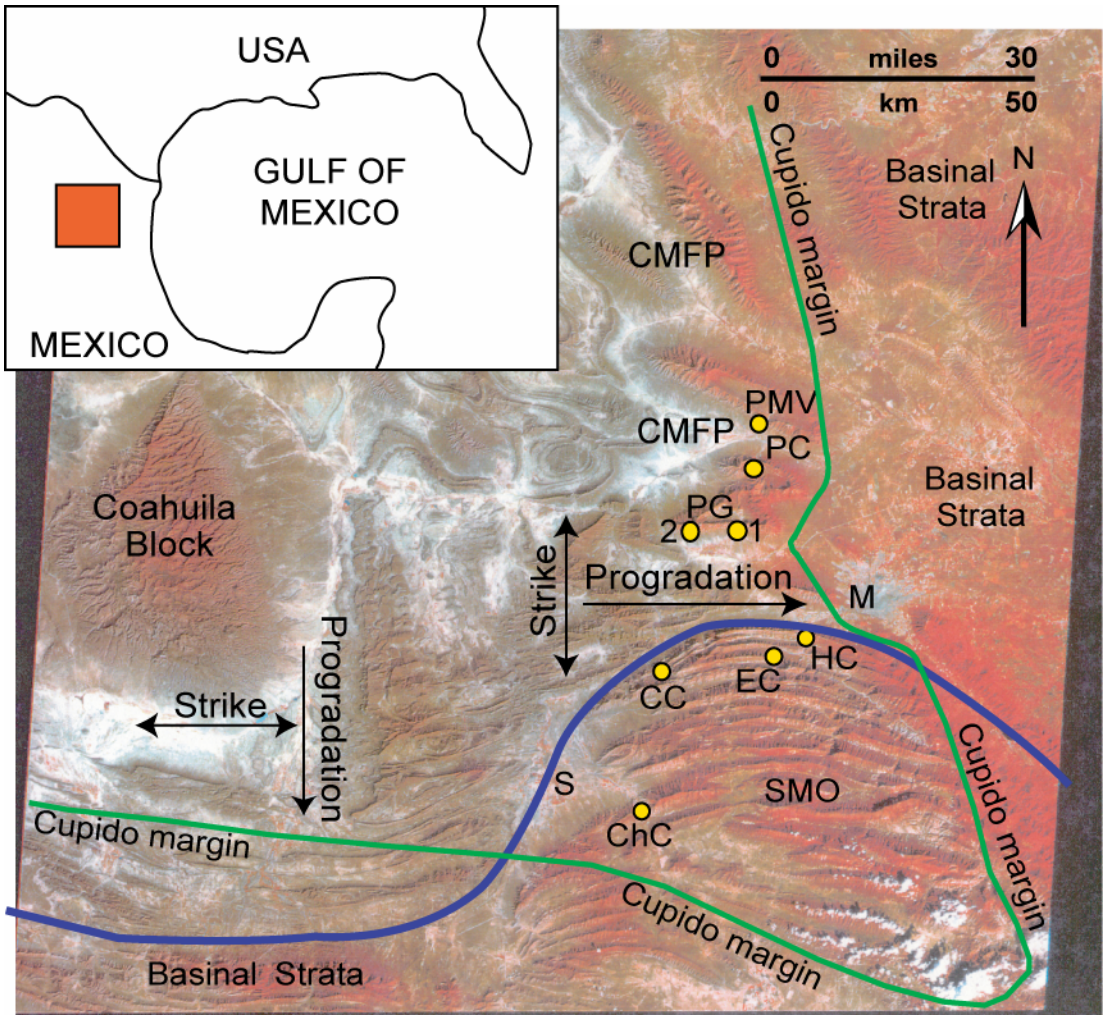

Figure 2-1. Geographic map and Landsat image.

Image illustrating the position of measured sections (yellow circles) relative to the Sierra Madre Oriental (SMO) and the Coahuila block. Monterrey (M) and Saltillo (S) Mexico are shown for orientation. The Coahuila Marginal Fold Province (CMFP) lies northward of the curvilinear thrust front (purple line) of the Sierra Madre Oriental. Anticlines and section names from north to south are Potrero Minas Viejas (PMV), Potrero Chico (PC), Potrero Garcia (PG1 and 2), Huasteca Canyon (HC), Escalera Canyon (EC), Cortinas Canyon (CC), and Chorros Canyon (ChC). The progradation of the Mesozoic passive margin is toward the east, southeast and south away from the Coahuila block. The platform margin trend (green line) is modified from Wilson (1999) and Foster (2003).

deformation ceased sometime during the Eocene (Gray et al., 2001).

Stratigraphic setting

By the Early Cretaceous rifting had ceased within the Gulf of Mexico and was replaced by 0.06 m/kyr regional subsidence rates due to lithospheric cooling (Goldhammer et al., 1991a). The Cupido Formation of northeastern Mexico was a part of a 2000 m thick carbonate platform that rimmed the ancestral Gulf of Mexico during the Early Cretaceous (Wilson, 1990; Goldhammer et al., 1991a; Lehmann et al., 1998; Goldhammer, 1999) (Figure 2-2). The platform spans Barremian through Aptian time and is contemporaneous with the Sligo shelf margin in Texas (Wilson 1975; Goldhammer, 1999; Figure 2-2). The shallow-marine Cupido shelf developed around the emergent Coahuila block. Peritidal sediments accumulated in a shallow shelf lagoon in the leeward side of the Cupido platform margin, while hemipelagic lime mudstones (Lower Tamaulipas Formation) were deposited on the surrounding deeper water off the shelf. The Cupido carbonates conformably overlie clastic deposits of the La Casita and the La Caja Formations and form a progradational highstand of a 2nd-order sequence that spans the Valanginian to Mid Aptian (Goldhammer, 1999; Figure 2-2). Subsequent deepening during the early to mid Aptian led to the retrogradation, and drowning of the Cupido platform as represented by the Cupidito member. Added to this, carbonate deposition shifted landward and a shallow-marine carbonate platform (Coahuila platform) grew over the formerly exposed Coahuila

Figure 2-2. Paleogeography and chronostratigraphic chart.

(A) Paleogeography of the Barremian to Lower Aptian in the western Gulf of Mexico, modified from Goldhammer (1999). The Cupido and Sligo platforms are shown in blue. Outline of Mexico and U.S. border is shown in black. The red line represents the approximate position and trend of the seismic lines.

(B) Chronostratigraphic chart for northeast Mexico and Texas Gulf Coast (modified from Goldhammer, 1999). The composite eustatic curve is from Haq et al. 1987. Time scale from Hardenbol et. al. (1998) and Gradstein et. al. (1995). Second-order sequence boundary ages are approximations in Ma. Abbreviations are: LST-lowstand system tracts, TST-transgressive system tracts, HST-highstand system tracts, LSW-lowstand wedge, SMW-shelf margin wedge, MFS-maximum flooding surface. Lithologies are discussed in text, border highlights interval of interest. Pinnacle reefs and buildups are shown as small domes. FW1 and FW2 refer to parts of the La Casita Formation defined by Fortunato and Ward (1982). Modified from Goldhammer (1999).

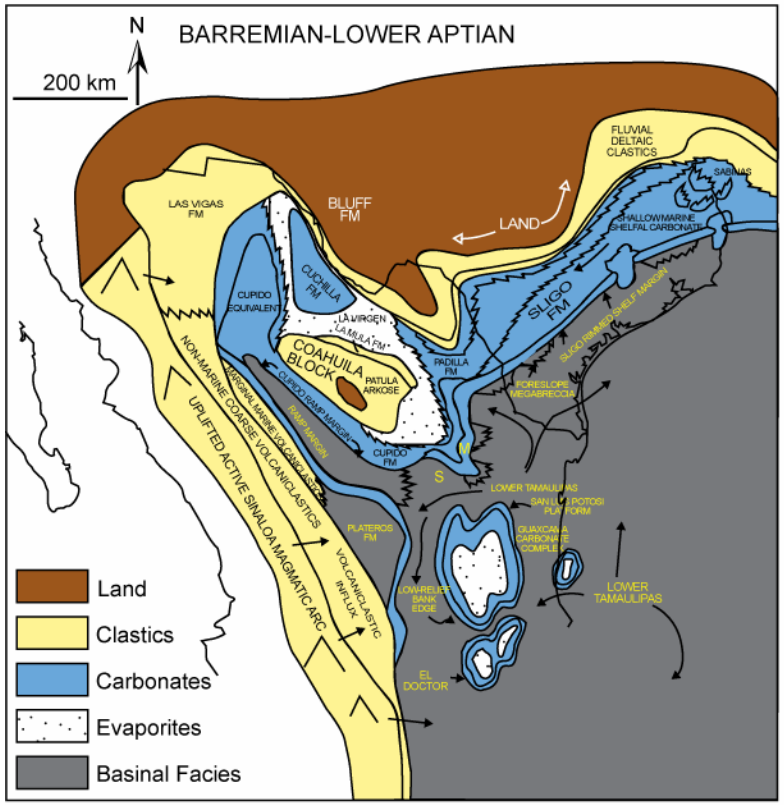
N
BARREMIAN-LOWER APTIAN
200 km
LAS VIGAS FM
BLUFF FM
LAND
FLUVIAL DELTAIC CLASTICS
SABINAS
SHALLOW MARINE SHELFAL CARBONATE
CUPIDO EQUIVALENT
CUPIDO FM
LA VIRGEN
LA MULA FM
COAHUILA BLOCK
PATULA ARKOSE
PADILLA FM
SUGO FM
SUGO RAMP-SHELF MARGIN
FORESLOPE MEGABRECCIA
RAMP MARGIN
LOWER TAMAULIPAS
SAN LUIS POTOSI PLATFORM
PLATEROS FM
GUAYCAMA CARBONATE COMPLEX
LOW-RELIEF BANK EDGE
EL DOCTOR
LOWER TAMAULIPAS
NON-MARINE COARSE VOLCANICLASTICS
UPLIFTED ACTIVE SINALOA MAGMATIC ARC
VOLCANICLASTIC INFLUX
Land
Clastics
Carbonates
Evaporites
Basinal Facies

A

B

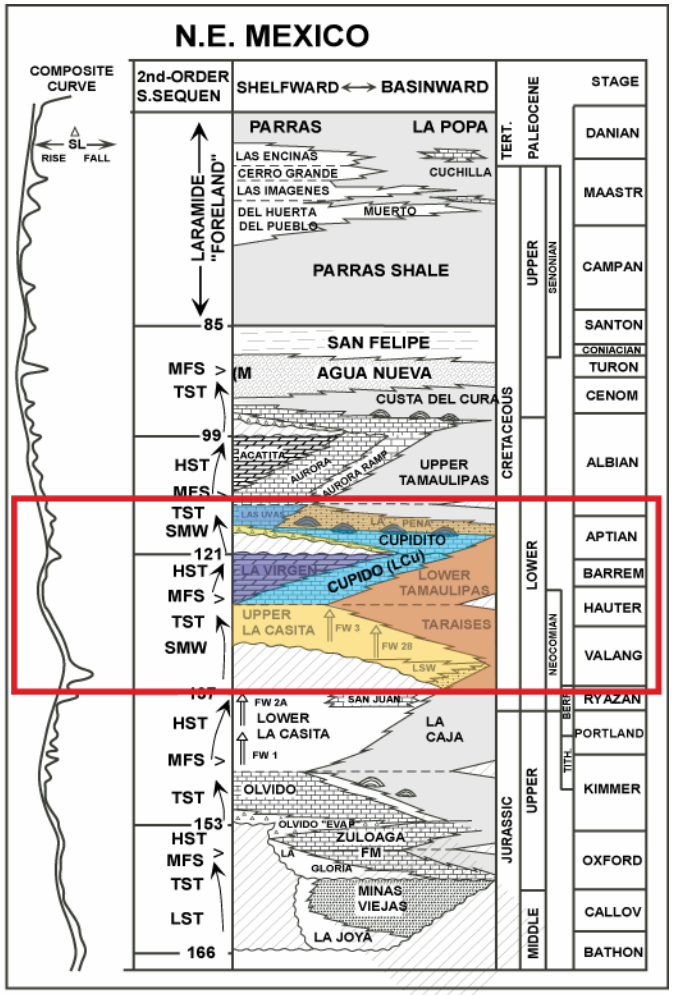
N.E. MEXICO
COMPOSITE CURVE
2nd-ORDER S.SEQUEN
SHELFWARD ⟷ BASINWARD
STAGE
SL
RISE
FALL
LARAMIDE "FORELAND"
PARRAS
LA POPA
LAS ENCINAS
CERRO GRANDE
LAS IMAGENES
DEL HUERTA
DEL PUEBLO
CUCHILLA
MUERTO
PARRAS SHALE
SAN FELIPE
AGUA NUEVA
CUSTA DEL CURA
PACATITA
AURORA
AURORA RAMP
UPPER TAMAULIPAS
LAS UVAS
LA PENA
CUPIDITO
LA VIRGEN
CUPIDO (LCu)
LOWER TAMAULIPAS
UPPER LA CASITA
FW 3
TARAISES
FW 2B
LSW
FW 2A
SAN JUAN
LOWER LA CASITA
FW 1
LA CAJA
OLVIDO
OLVIDO "EVAP"
ZULOAGA FM
LA GLORIA
MINAS VIEJAS
LA JOYA
85
99
121
137
153
166
MFS
TST
HST
SMW
LST
TERT.
PALEOCENE
CRETACEOUS
UPPER
LOWER
JURASSIC
MIDDLE
SENONIAN
NEOCOMIAN
BERR.
TITH.
DANIAN
MAASTR.
CAMPAN
SANTON
CONIACIAN
TURON
CENOM.
ALBIAN
APTIAN
BARREM.
HAUTER.
VALANG.
RYAZAN
PORTLAND
KIMMER.
OXFORD
CALLOV.
BATHON

block. The deposition of argillaceous carbonates and shales of the La Peña Formation marked the subsequent peak flooding and eventual drowning of the Cupido platform during the mid to late Aptian (Figure 2-2; Tinker, 1985). The Cupido carbonate platform developed during peak Cretaceous greenhouse climatic conditions (Read, 1995). Regionally, evaporites and sabkha carbonates of the Cupido platform indicates arid to semiarid conditions in northeastern Mexico from Barremian to Aptian time (Lehmann et al., 1998; 1999).

Methodology

The Cupido Formation is spectacularly exposed within the folds of the Sierra Madre Oriental and breached anticlines (potreros) north of it (Figure 2-3). Fifteen stratigraphic sections totaling 6000 m were measured from eight localities across the platform (Figure 2-1). The Cupido Formation is exposed and accessible in most localities. Each section was logged on a centimeter-scale documenting thickness, color, grain size, lithofacies, depositional texture, biota, sedimentary structures and any evidence for subaerial exposure. Where possible, beds were traced to determine lateral continuity and facies variability. Samples were collected at each measured section and were slabbed and polished to document depositional and diagenetic features. Thin sections were prepared and stained with Alizarin Red (Dickson, 1965) for petrographic description and to aid in grain identification. A total of 482 rock samples were

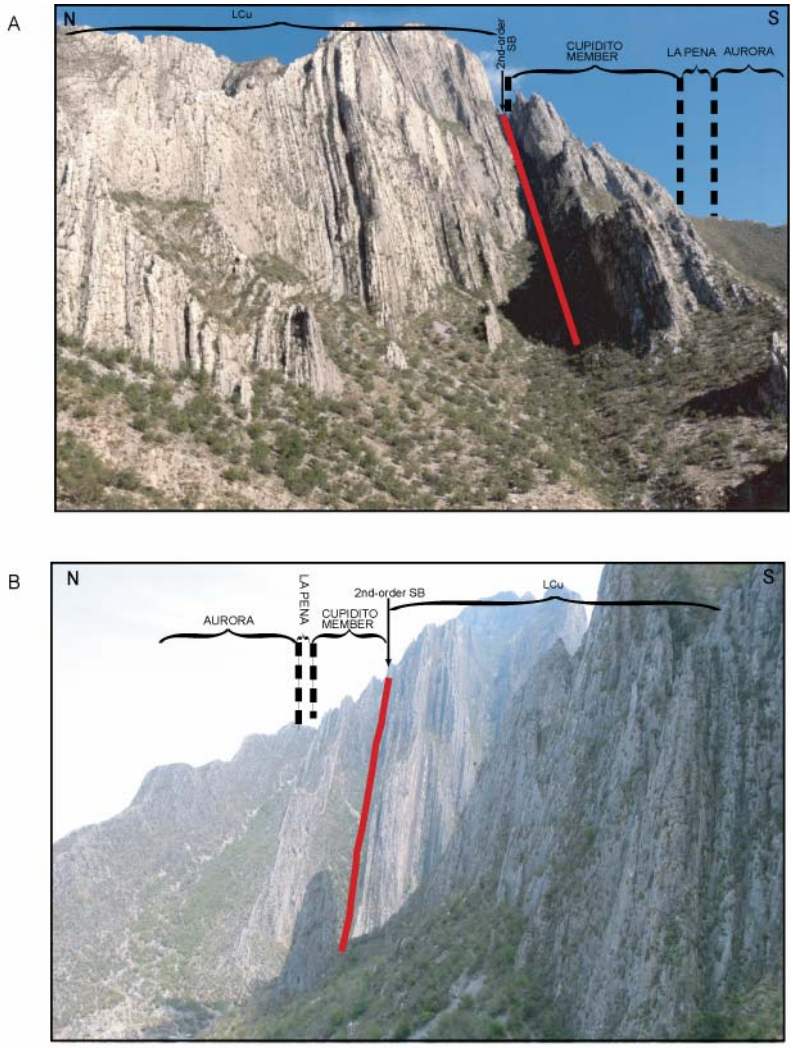

Figure 2-3. Cupido outcrop photos.

Photo panoramas of the measured stratigraphic sections in A) Potrero Garcia, and B) Potrero Chico. The Cupido Formation is a combination of the lower 2nd-order late highstand regressive part (LCu), and the upper 2nd-order early transgressive Cupidito member. The La Peña shale and Aurora Formation are not present in the measured sections. Bedding planes are near vertical. The solid red line represents the location of the 2nd-order sequence boundary (SB).

collected from the Cupido Formation, 257 slabbed samples, and 314 thin sections (250 large) were prepared for petrographic analysis. Facies were defined on the basis of depositional textures, sedimentary structures and fossil content following Dunham's (1962) classification scheme. The relative abundance of facies at each location was used to determine facies distribution, depositional processes and depositional environments.

Ginsburg's (1974) comparative sedimentology technique which utilizes the connection between recent sediments and ancient sedimentary rocks to understand and diagnose depositional environments is the focal approach taken in this study. Additionally, the building block approach of Demicco and Hardie (1994) was used to build a depositional model for the Cupido Formation. This model links identified facies and their interpreted depositional environment through by matching sedimentary and diagenetic features to certain processes that occur within specific environments. Environments matching facies descriptions can be picked out of the various modern carbonate environments through the comparison of common features and then combined to create a unique model for each ancient platform (Demicco and Hardie, 1994).

A depositional model for the Cupido platform is interpreted using overall facies transitions and distribution, and dominant depositional processes (Appendix C). The relative position of each section was interpreted along the platform profile using overall facies proportions and their dominant depositional environments. Seismic lines of the Sligo Platform of south Texas are used to

infer Cupido platform profile and stratal geometry due to lack of continuous outcrops as a result Laramide deformation.

A complete idealized shallowing-upward vertical succession of facies, grouped into 5 major facies-belts (Table 2-1), was identified from field and laboratory observations. This succession was used to identify high-frequency cycles or shoaling-upward cycles within individual measured sections. Facies and facies-belt proportions within vertically stacked high-frequency cycles vary depending on their position within lower-order depositional, composite and possibly 2nd-order sequences (Kerans, 1995; Kerans and Tinker, 1997). These high-frequency cycles are the building blocks for the stratigraphic hierarchy developed for the Cupido Formation. Recognizable patterns of deepening and shallowing facies proportions, thickening and thinning of cycles, cycle bundling, and cycle type distribution defined vertical and stacking of high-frequency cycles within the measured sections. This stacking pattern aided in interpreting changes in accommodation as recorded in the development of depositional and composite sequences. Stacking patterns of depositional and composite sequences and their system tracts components, in turn defined lower-frequency 2nd-order sequences. Correlation between each measured section was completed using the highest frequency cyclicity possible.

Cross-sections through the study area were constructed based on 1D and 2D correlation of measured stratigraphic sections. The cross-sections and fence

diagrams are hung on the 2nd-order sequence boundary that coincides with the top of the lower progradational LCu of the Cupido Formation.

LITHOFACIES AND DEPOSITIONAL ENVIRONMENTS

The characteristics of the major rock types are summarized in Table 2-1 and figures 2-4 to 2-9 and 2-10A. Using subsurface data of the equivalent Sligo, the morphology of the Cupido platform is interpreted as an aggradational-progradational rimmed shelf with a highly aggradational interior and a 15-30 degrees slope (Figure 2-10B; Goldhammer et al., 1991a; Goldhammer, 1999). Progradation has previously been interpreted to have occurred as thick turbidites are overlain by margin and slope deposits, which are in turn overlain by platform interior deposits (Wilson and Pialli, 1977; Goldhammer et al., 1991a) . Within the study area, 10 facies are observed and are grouped into five main facies-belts. Measured sections composed of deep subtidal, low-energy off-platform facies, high-energy shoal margin to rudist-reef margin facies, shallow subtidal restricted platform facies, peritidal to shallow subtidal restricted shelf-lagoon facies, and restricted evaporite interior facies. The proportions of facies and facies-belts vary within the measured sections depending on their location across the platform.

Table 2-1 Summary of facies.

Facies, types, textures, depositional processes and environment and facies-belts of the Cupido Formation. Field photo and photomicrographs of the facies are shown in Figures 2-4 to 2-9. The location of each facies within the idealized shallowing-upward vertical succession is shown in Figure 2-10A.

Facies	Subfacies	Occurrence	Color	Rock type & Depositional Texture	Grain Type	Bedding & Sedimentary Structures	Early Diagenetic Features	Depositional Environment
Evaporitic Interior facies	Polymict Solution Collapse Breccia	Common across most parts of the platform	Gray	Polymict breccia with a carbonate mud matrix	Angular clasts, <30 cm, consisting of mudstones, micritized mixed packstones and grainstones	Medium to think bedded, Brecciated	Dissolution by through flowing phreatic water, collapse and rotation of lithified rock fragments	Burial beneath supratidal environment
	Nodular - Mosaic Calcite Replaced Evaporite	Common in the shallow landward parts of the platfrom	White to light gray	Anhedral calcite replaced anhydrite nodules separated by dolomitized micrite	Peloids	Non-bedded, displacive growth distrupts surrounding sediments	Hydration of anhydrite to gypsum, sparry mosaic calcite replacement	Supratidal sabkha
Peritidal to shallow subtidal restricted shelf-lagoon facies	Planar and Stromatolitic Laminated Mudstone	Common across most parts of the platform	Light gray to tan	Dolomitic mudstones to interbedded peloidal wackstones and mudstones	Peloids and pellets	Planar to domal laminations, occasional mudcracks, wispy lenses, and contorted bedding	Fenestral fabric, early lithification dolomitization,and anhydrite precipitation	Quiet, shallow intertidal to subtidal, tidal-flat
	Heterolithic Thin Beds	Common across most parts of the platform	Tan	Alternating peloidal-skeletal grainstones, which are slightly dolomitized mudstones	Peloids (some compacted), fecal pellets, and a variety of skeletal debris	Thin bedded,10 mm, planar to flattened lenticular, no internal cross stratification	Early compaction and occacional amplitude stylolites between layers	low energy, subaqueous, shallow shelf lagoon saltern
	Intercalated Calcite Replaced Evaporite Beds	Common across most parts of the platform	White to light gray	Euhedral calcite and precipitated peloids and micrite	Peloids between crystals	Medium to thinly bedded	Sparry mosaic calcite replacement, stylolitization	Subtidal, shallow marine tidal-flat zone
Shallow subtidal restricted platform facies	Thalassanoides Burrowed Peloidal - Skeletal Packstone	Common across most central parts of the platform	Gray	Euhedral dolomitized micrite with micritized skeletal-nonskeletal W-P matrix with euhedral dolomitized skeletal-non skeletal W-P burrow fill	Peloids, Miliolidae and Vercorsella Foraminifera, mollusk and ostracod debris, and dasycladaceans	Thick to medium bedded, preserved trace fossil networks as irregular boxworks, no preservation of mechanical structures	Early lithification of mictritic matrix to support burrow networks and early dolomitization	Quiet, tide-dominated shallow lagoon/tidal-flat, dominantly open-marine conditions
	Burrowed Peloidal-Skeletal Mudstone - Grainstone	Common across most central parts of the platform	Gray	Dolomitized micritic peloidal carbonate mudstone matrix with dolomitized micrite or mixed skeletal and nonskeletal grainstone fill	Peloids, pellets, composite grains, Miliolidae and Vercorsella Foraminifera, gastrpods, bivalves and dasycladaceans	Thick to medium bedded, some trace fossil are preserved as networks, irregular boxworks, and mottling are common, no preservation of mechanical structures	Early lithification of mictritic matrix to support burrow networks under compaction	Quiet, middle shelf lagoon, to slightly open marine conditions
High energy shoal to rudist-reef margin facies	Skeletal - Nonskeletal Grainstone	Common throughout the platfrom especially across most eastern and southern parts of the platform	White to light gray	Micritized skeletal and nonskeletal grainstones and packstones with sparry mosaic clacite cement and some dolomite	Oncoids, ooids, peloids, composite grains, lumps, intraclasts, Miliolidae and Vercorsella Foraminifera, gastrpods, bivalves, dasycladaceans,echinoderms, bryozoans and ostracods	Thick to medium bedded, cross stratification to massive due to high rates of biogenic reworking	Early calcite cementation in intra and interpartical porosity within the grainstones, compaction within packstones	Active high-energy shelf crest, middle to outer shelf, subject to wave and storm influence
	Rudistid Bioherms and Beds	Common throughout the platform especially across most eastwards parts	Medium to dark gray	Micritized skeletal and nonskeletal packstones	Caprotinide, coral, Caprinidae, bryozoans, Chondrodonta ooids, Requiniidae, ostracods, bivalve shell debris,foraminifera, few peloids dasycladaceans algae, and intraclasts	Massive to thick bedded, no internalcross bedding, rudists are commonly not in growth position	Binding by encrusting algae and early cementation	Below fair weather wave base,dominated shelf edge
Deep subtidal, low-energy off platform facies	Foraminiferal wackestone/ mudstone	Common across most eastern and southern parts off the platform	Dark gray	Bioturbated mudstone and wackstone some dolomitic firmgrounds, hardgrounds and chert nodules	Planktonic Foraminifera, peloids	Thin bedded with some lamination	Early lithification of matrix and early compaction	Below storm wave base in a low-energy oxygenated setting

Deep subtidal, low-energy off-platform facies

The deep subtidal facies consists of dark-gray, homogeneous, planktonic foraminiferal mudstone and laminated micropeloidal lime wackestone. This facies is thin to thick bedded (0.2-1.0 m; Figure 2-4) and is mainly present at Iturbide section (IC; Figure 2-1). The mudstone and lime wackestone are bioturbated in some parts with occasional dolomitic firmgrounds, hardgrounds and chert nodules. Other components present in this facies are nannoconids and ostracods. Hardgrounds are synsedimentary, which indicate slow sedimentation rates or prolonged periods of non deposition (Purser, 1969; Bathurst, 1971). Due to the lack of storm beds, this facies is interpreted to have been deposited below storm wave base (Aigner, 1985) in a low-energy off-platform (basinal) setting.

High-energy shoal to rudist-reef margin facies

The high-energy platform-margin facies consist of skeletal and non-skeletal lime grainstones, bioclastic beds and rudist bioherms. These facies include a diverse assemblage of skeletal and no-skeletal gains (Figure 2-5A, B, and C; Table 2-1). The grainstones are interpreted to have been deposited under dominantly wave, but also tidal, and storm influenced processes with depths above wave base (0.1-2.5 m; Demicco and Hardie, 1994) resulting in

Figure 2-4. Deep subtidal, low-energy, off-platform facies

Field photograph of thin-thick bedded laminated micropeloidal wackestone-mudstone.

Figure 2-5. High-energy shoal to rudist-reef margin facies

Hand samples and photomicrographs of Cupido facies. (A) field photograph of unoriented *caprinid* rudists in mud rich matrix (B) field photograph of *chondrodont* bivalves in mud rich matrix (C) photomicrograph of a *requienid* bivalve-mixed packstones.


A


B

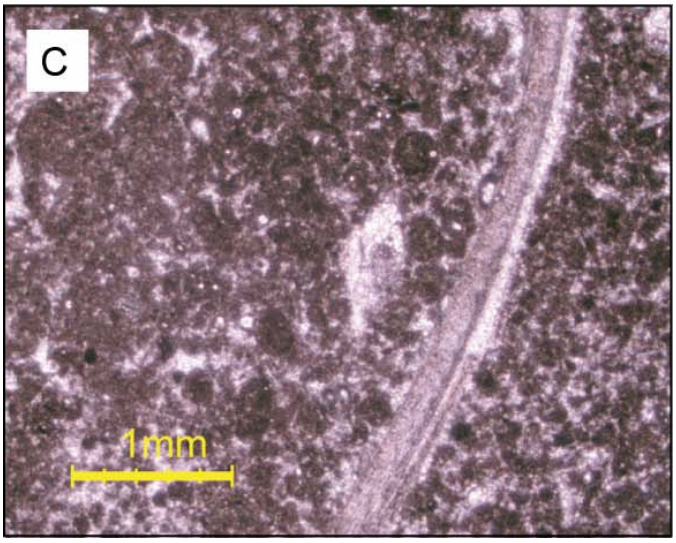
C
1mm

cross stratified, well sorted, non-skeletal grainstones on the seaward side of the shoal. Perhaps the best modern analogue of mixed grainstones is the Joulters Cay oolite shoal, a high energy, shelf edge carbonate accumulation on the Bahamian platform (Ball and Harrison, 1969; Bubb, 1970; Harris et al., 1993). The interpreted reef environment (Wilson and Pialli, 1977) was commonly developed above fair weather wave base but most of the preserved bedding described consisted of broken disoriented debris created by storm wave energy (Bebout, 1977).

Bioturbated, poorly sorted, skeletal packstones are interpreted to have been deposited below wave base and on the landward side of the shoal (1.0-4.0 m water depth). The rudist bioherms are interpreted as being deposited on the shelf edge and form isolated beds of small *requienids* and *chondrodonts* framestones (Cestari and Sartorio, 1995).

Shallow subtidal restricted platform facies

The shallow subtidal facies consists of burrowed peloidal-skeletal dolomudstones and grainstones facies and *Thalassanoides* burrowed peloidal-skeletal lime packstones and wackestones facies. The major skeletal components include Miliolids and Vercorsella foraminifera, gastropods, bivalves, dasycladaceans, and composite grains (Table 2-1; Figures 2-6A, B, C, and D). The intensity of burrowing ranges from sparsely and evenly distributed to moderately bioturbated (e.g. Figures 2-6A and C). Vertical, horizontal, and


A
2
1
0
in

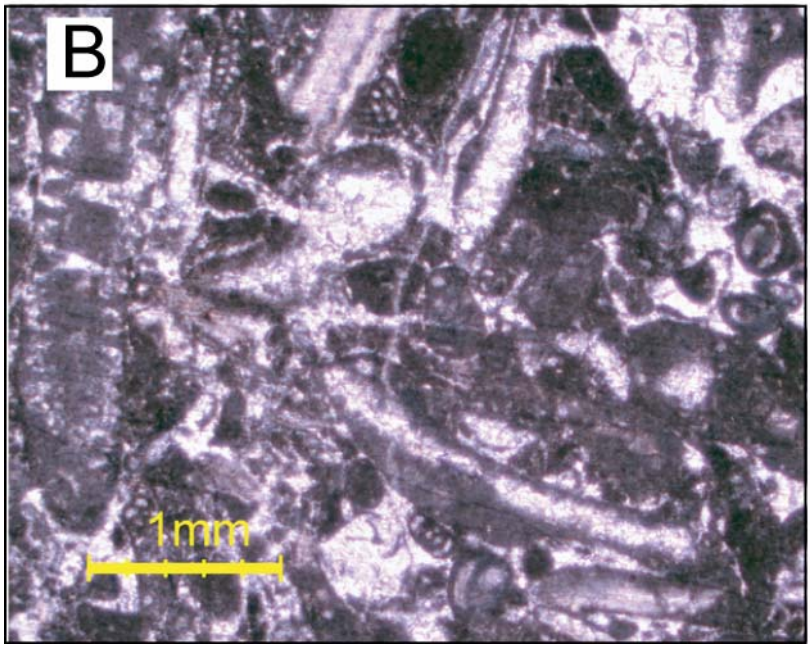
B
1mm

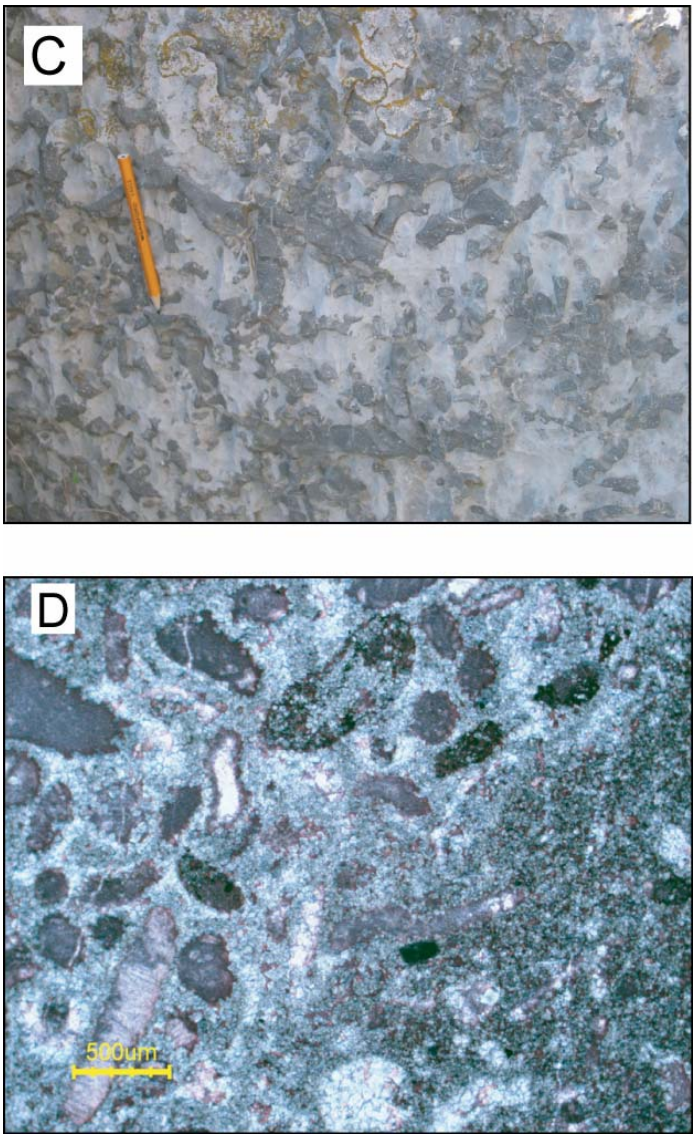

Figure 2-6. Shallow subtidal restricted platform facies

Field photos, hand samples and photomicrographs of Cupido facies. (A) hand sample of dark matrix with light colored burrow fill and the burrow network. (B) photomicrograph of poorly sorted packstone, skeletal debris with micritic or mud rich matrix. (C) field photograph of *Thalassanoides* burrow networks from a view of the bedding plane. (D) photomicrograph of dolomitized fine-grained matrix, and coarse-grained burrow fill.

diagonal burrowing patterns are commonly associated with of annelid worms, *Thalassanoides* burrows, plus potentially a variety of other organisms such as mollusks (Demicco and Hardie, 1994; Rhoads, 1967; Shinn, 1968). Bioturbation is the most dominant process in modern subtidal subenvironments, best illustrated by the lack of internal stratification. This is common in all modern carbonate platforms but has been well studied at Andros Island, Bahamas (Hardie, 1977). The presence of *Thalassanoides* burrow networks and tidally influenced sediments imply that this facies was deposited in a shallow lagoon just below or within the intertidal zone (Rhoads, 1967; Shinn, 1968). This facies is interpreted to have been deposited in a shallow lagoon (0.2-4.0 m water depth) with dominant restricted conditions with minor open-marine incursions (Demicco and Hardie, 1994; Shinn, 1968).

The peritidal to subtidal restricted facies form the bulk of the Cupido Formation. It is composed of heterolithic thin beds facies, intercalated, calcite replaced bedded evaporite facies, and laminated dolomudstone facies (Table 2-1). Heterolithic thin beds are on a lamination-scale thickness, 3-10 mm on average, and may have minor microbial influence. They are dominantly a mud rich texture of alternating light and dark bands, tan to black (Figure 2-7). Heterolithic thin beds lack mud cracks and contain abundant burrows which support a intertidal setting (Demicco and Hardie, 1994). This facies is interpreted to have been deposited on land or shoal attached tidal-flats (up to 0.5 m water depth).

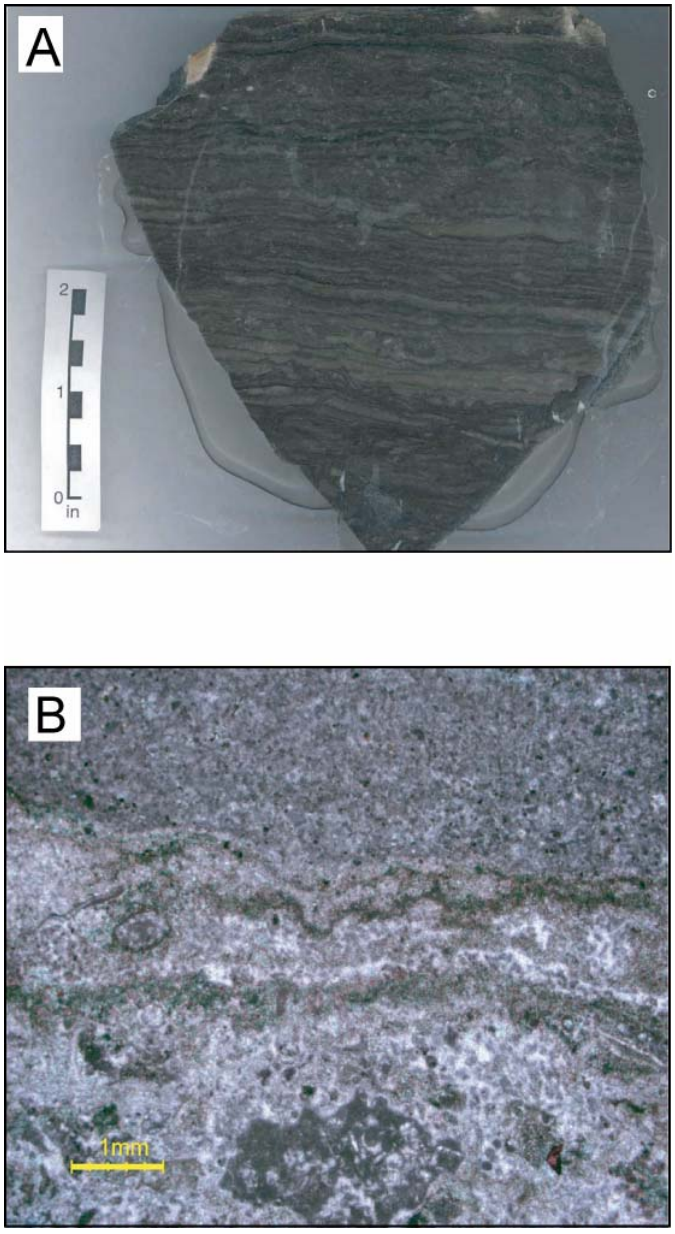

Figure 2-7. Shallow subtidal restricted platform facies

Hand sample and photomicrographs of Cupido facies. (A) hand sample illustrating the thin laminations on a mm scale, the tan layers are mudstones and the black layers are wackestones. (B) photomicrograph of alternating micrite dominated layers and wackestone layers containing fossil debris and peloids.

Bedded evaporite consists of thin to medium thick beds, 2 cm to 2 m, of calcite (Figure 2-8A). Some modern bedded evaporites occur in subaqueous settings called salinas as tens of meters thick, shoaling upward, aggradational, evaporite dominated, subtidal sequences in coastal lakes (Warren and Kendall, 1985).

Domal laminations (Stromatalites: Figure 2-8B) are micritic laminae often alternating with upward fining peloidal wackestone laminae. These laminae generally contain coarser-grained sediments than the planar-laminated mudstones (Figure 2-8D) because of the higher percentage of peloid ghosts. Laminites can be formed through several mechanisms known from modern sedimentology: 1) mechanical sedimentation unrelated to microbes, 2) microbial influenced sedimentation, 3) episodic growth f a microbial mat, and 4) chemical precipitation of carbonates (Demicco and Hardie, 1994).

Evaporitic platform interior facies

The evaporitic platform interior facies is composed of calcite-replaced bedded evaporite facies and the polymict solution collapse breccias (Table 2-1). Calcite-replaced bedded evaporite facies consists of irregular, anhydrite popcorn-like nodules generally less than 10cm in diameter (Figure 2-9A) found within a micritic dolomite dominated matrix to bedded gypsum crystals. Collapse breccias are thick to medium bedded, <2 m, with sharp bottoms and uneven tops. The upper contact of the breccias is typically irregular with areas of evaporite-infilling between clasts and the irregular topography (Figure 2-9B and

Figure 2-8. Shallow subtidal restricted platform facies

Field photographs and photomicrographs of Cupido facies. (A) photomicrograph of bed planar view of gypsum crystals with various diameters also outlined by carbonate impurities. (B) field photo of planar and domal laminations. (C) photomicrograph of dolomitized, laminated mudstone.

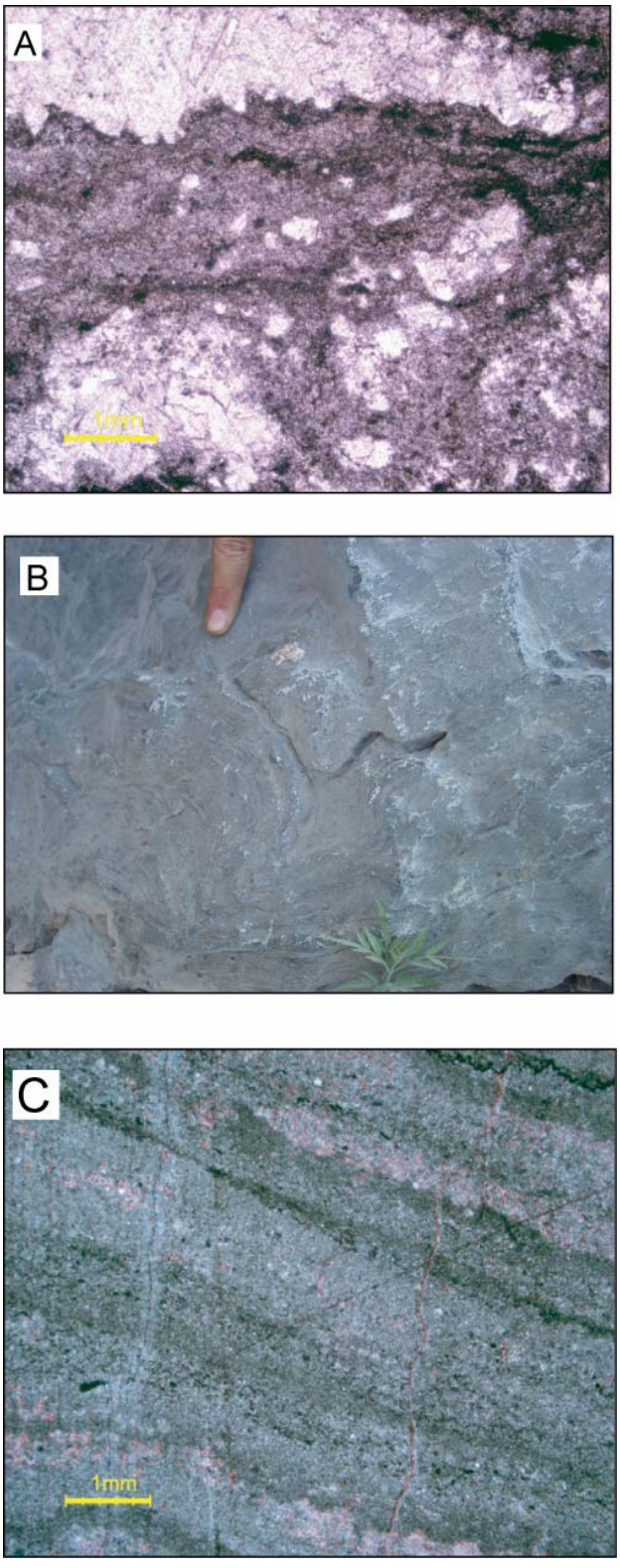
A
1mm
B
C
1mm

Figure 2-9. Evaporitic platform interior facies

Field photographs and hand samples of Cupido facies. (A) initial carbonate dominated matrix with isolated evaporite nodules causing disruption (B and C) field photographs of breccias highlighting observations that support a gradual development due to phreatic dissolution below the surfaces.


A

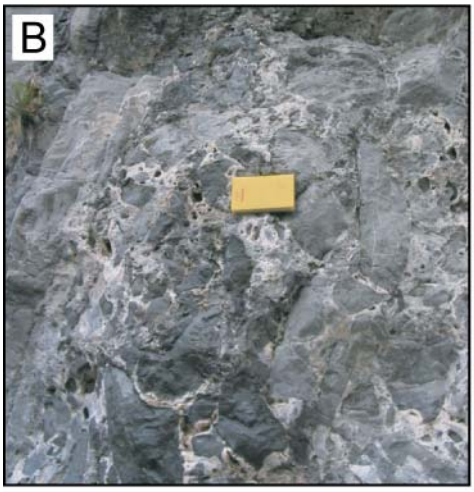
B


C

subsurface removal of bedded evaporites allows the overlying rock to settle and fragment (Warren, 1999). This facies is interpreted to have been deposited in a supratidal sabkha setting with brecciation taking place through diagenetic dissolution of underlying evaporates at a later stage (Warren, 1999).

DEPOSITIONAL MODEL

The Cupido platform has been previously interpreted to be a highly prograding/aggrading platform with a reefal rudist-coralline margin on the eastern-facing side (Wilson, 1975; Conklin and Moore, 1977; Wilson and Pialli, 1977; Wilson et al., 1984; Goldhammer et al., 1991a) and a high-energy shoal dominated margin on the south-facing side (Lehmann et al., 1999). Based on detailed analysis of facies, depositional environment and facies-belts proportions with my measured stratigraphic sections, I have reinterpreted this platform to also contain a large grainstone shoal complex rimming the east-facing side of the Cupido platform (Foster, 2003; Altobi et al., 2004: Figure 2-10). The shoal complex acted as a barrier to wave energy and open marine circulation from the platform interior and developed updip of a slightly deeper, relatively continuous reefal rudist-coralline bank. The presence of a similar shoal complex in the coeval Sligo shelf is supported by mounded reflectors developed landward of the margin seen in seismic lines from south Texas (Goldhammer, 1999; Figure 2-11). The seismic lines also suggest that the shoal developed above antecedent topography created by local movement of the Middle Jurassic

Figure 2-10. Depositional model.

(A) Idealized shallowing-upward succession of the Cupido lithofacies.

(B) Generalized schematic depositional model of the Cupido platform illustrating the depositional paleo-environments of the measured sections as they would appear projected along a dip oriented profile. The shelf crest is represented by a shoal complex, not a barrier reef. The shoal complex provided a barrier to open marine influx creating a restricted saltern environment. See text for detailed descriptions of major facies belts.

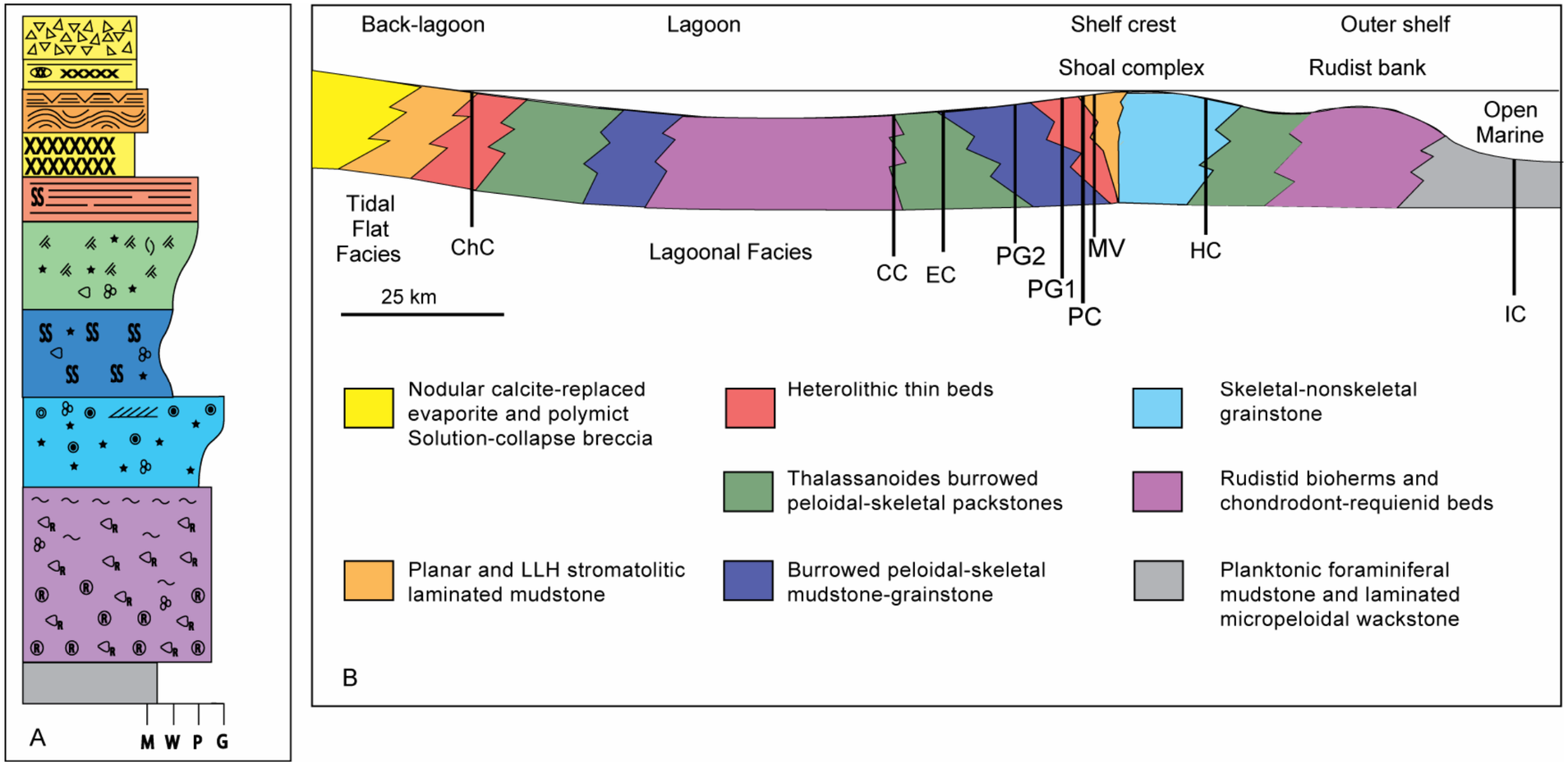
A
M W P G
Back-lagoon
Lagoon
Shelf crest
Outer shelf
Shoal complex
Rudist bank
Open Marine
Tidal Flat Facies
ChC
Lagoonal Facies
CC
EC
PG2
PG1
PC
MV
HC
IC
25 km
Nodular calcite-replaced evaporite and polymict Solution-collapse breccia
Heterolithic thin beds
Skeletal-nonskeletal grainstone
Thalassanoides burrowed peloidal-skeletal packstones
Rudistid bioherms and chondrodont-requienid beds
Planar and LLH stromatolitic laminated mudstone
Burrowed peloidal-skeletal mudstone-grainstone
Planktonic foraminiferal mudstone and laminated micropeloidal wackstone
B

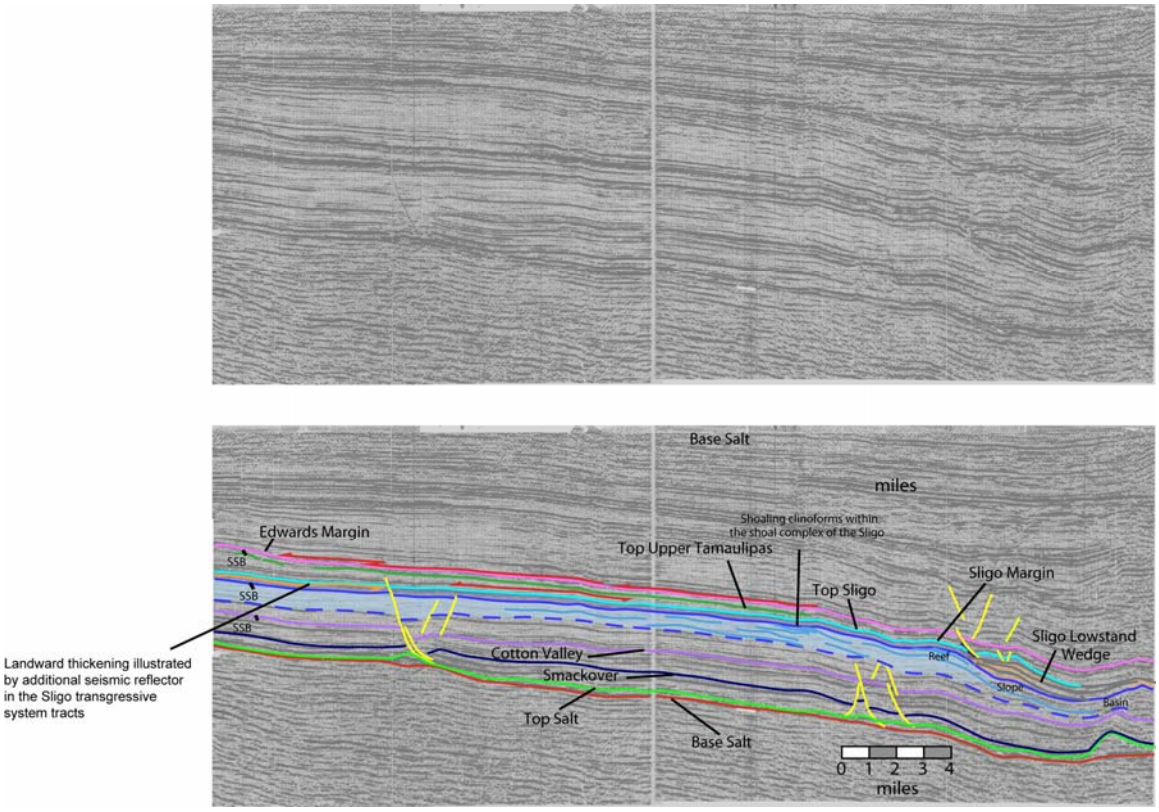

Figure 2-11. Sligo margin.

Seismic line of the Sligo margin showing platform morphology and high-energy grainstone shoal behind a rudist bank. Figure is interpreted and modified from Goldhammer (1999).

Minas Viejas Evaporite (Robert K. Goldhammer, personal communications). The stratigraphic section measured at Huasteca Canyon is dominated by thick grainstone beds, and is composed of high-energy shoal to rudist-reef margin facies which is interpreted to represent part of a narrow fringe of this high-energy grainstone shoal complex (Figure 2-10B).

In the Cupido Formation, the shoal complex provided protection from wave energy on the landward side, thus bioturbated carbonate mud-rich textures dominated lagoonal sediments (Shinn, 1968). This lagoon extended about 100 km toward to the Coahuila block (Lehmann et al., 1999). Sections measured at Escalera and Cortinas Canyons are composed dominantly of lagoonal shallow subtidal restricted platform facies (Figure 2-10B). During falling sea level, two belts of tidal-flats constitute the Cupido platform interior, tidal-flats attached to the shoal margin and land attached tidal-flats (Figure 2-10B). Within these belts, protected from most burrowing organisms and intense wave energy, laminites and heterolithic thin beds of alternating dolomudstones and packstones were deposited in minimal water depths. Facies dominating the landward portion of the lagoon were recognized at Chorros Canyon. This section is dominantly composed of heterolithic thin beds, laminites, or sabkha dominated succession. Similar facies are recognized at Potrero Garcia, Potrero Chico, and Potrero Minas Viejas (Figure 2-10B).

The presence of evaporites implies that an arid climate would produce significant sabkha and laminite facies-belts landward of Chorros Canyon,

comprising the La Virgen Formation, age equivalent to the Cupido platform (Goldhammer, 1999). A fall in sea level caused the progradation of tidal-flat environments in two different directions: seaward for the land attached tidal-flats and dominantly landward for the shoal complex tidal-flats (Figure 2-12). Occasional restriction and exposure of the shoal is also recorded by the presence of sabkha like anhydrite and rare mudcracks preserved in the laminites as well as the presence of bedded evaporites on the lagoonal side of the shoal.

DEPOSITIONAL ARCHITECTURE OF THE CUPIDO PLATFORM

Antecedent topography and carbonate production within different parts of the platform produced variable depositional architecture across the Cupido shelf (Figure 2-10B). The Cupido Formation is divided into two parts, a lower thin-bedded progradational LCu and an overlying thick-bedded retrogradational Cupidito member, separated by a 2nd-order sequence boundary (Wilson and Pialli, 1977, Goldhammer et al., 1991a; Goldhammer, 1999; Figure 2-2). The progradational LCu represents 2nd-order late highstand deposits whereas the Cupidito member was deposited during the early part of a 2nd-order Aptian transgression that caused the retrogradation of all carbonate platforms in the Gulf of Mexico and the growth of subsequent reef build-ups prior to flooding (Bebout and Loucks, 1977; McFarlan and Menes, 1991).

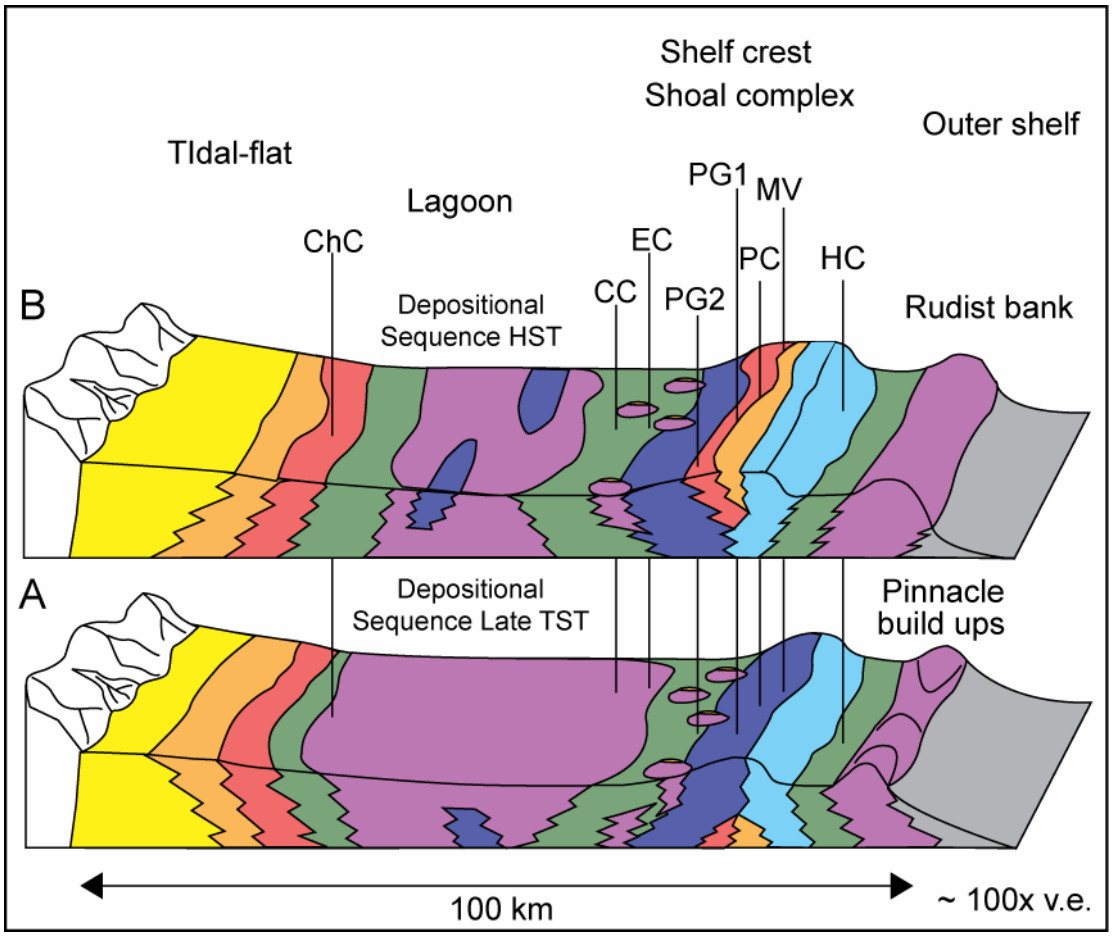

Figure 2-12. Depositional model for platform wide depositional sequences.

Schematic block diagrams showing components of a generalized depositional model for platform wide depositional sequences and tidal-flat belts prograding in two directions: A) the unrestricted late portion of the transgressive system tract (TST) of a depositional sequence, and B) depositional sequence highstand system tract (HST) capped by a sequence boundary. Facies key is found in Figure 2-5A. Vertical exaggeration is approximately 100X.

High-frequency Cycles

High-frequency cycles are equivalent to the building blocks of shallow marine carbonates which are defined as “relatively conformable successions of genetically related subtidal facies bounded by peritidal surfaces, subaerial exposure surfaces, and/or marine flooding surfaces represented by slow rates of deposition” (Wilson, 1975; James, 1984; Hardie and Shinn, 1986; Goldhammer et al., 1991b; Goldhammer et al., 1993; Kerans, 1995). Cycles are considered the thinnest succession of repetitive facies and usually contain transgressive and regressive components. The proportion of these components is a function of the cycle’s position in a lower frequency sequence as well as its position laterally across a platform. Within the Cupido Formation, meter-scale high-frequency cycles are identified using the shallowing-upward vertical succession of Cupido lithofacies (Figure 2-10A).

Variability in high-frequency cycle development

Within the Cupido platform, meter-scale deep subtidal to peritidal high-frequency cycles vary in their component facies and the percentage of those facies across the shelf (Figure 2-13). High-frequency cycles vary in thickness, facies components and type depending on their relative position laterally along the platform profile and vertically within individual depositional sequences and

Figure 2-13. High-frequency cycles.

Summary of different types of high-frequency cycles across the Cupido platform depending on their depositional setting: A) Peritidal cycle, B) Shallow subtidal cycle, C) shoal peritidal cycle, D) Deep subtidal cycle. HTB is a heterolithic thin bed. Facies key is found in Figure 2-5A.

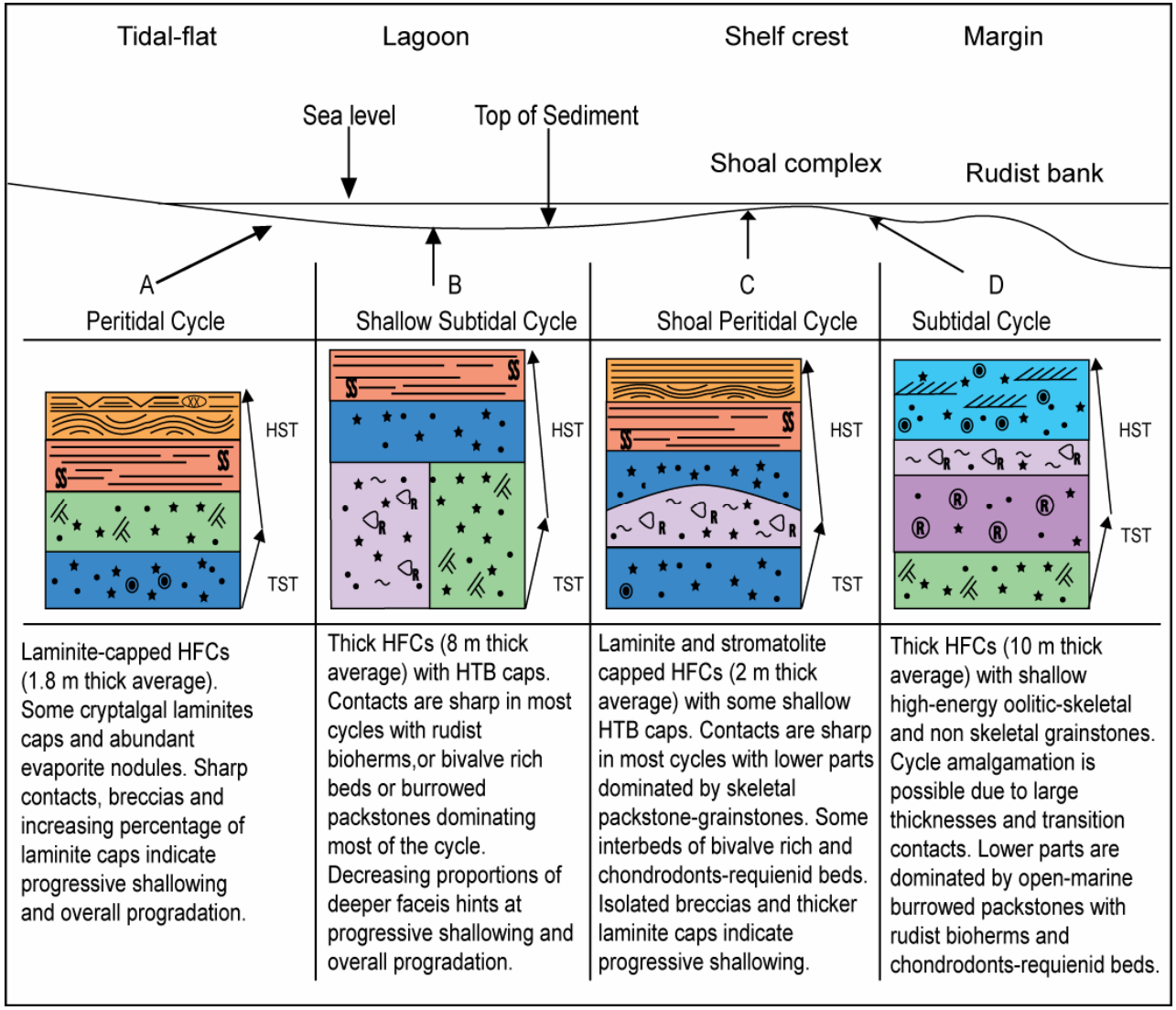
Tidal-flat
Lagoon
Shelf crest
Margin
Sea level
Top of Sediment
Shoal complex
Rudist bank
A
B
C
D
Peritidal Cycle
Shallow Subtidal Cycle
Shoal Peritidal Cycle
Subtidal Cycle
HST
TST
HST
TST
HST
TST
HST
TST
Laminite-capped HFCs (1.8 m thick average). Some cryptalgal laminites caps and abundant evaporite nodules. Sharp contacts, breccias and increasing percentage of laminite caps indicate progressive shallowing and overall progradation.
Thick HFCs (8 m thick average) with HTB caps. Contacts are sharp in most cycles with rudist bioherms,or bivalve rich beds or burrowed packstones dominating most of the cycle. Decreasing proportions of deeper faceis hints at progressive shallowing and overall progradation.
Laminite and stromatolite capped HFCs (2 m thick average) with some shallow HTB caps. Contacts are sharp in most cycles with lower parts dominated by skeletal packstone-grainstones. Some interbeds of bivalve rich and chondrodonts-requienid beds. Isolated breccias and thicker laminite caps indicate progressive shallowing.
Thick HFCs (10 m thick average) with shallow high-energy oolitic-skeletal and non skeletal grainstones. Cycle amalgamation is possible due to large thicknesses and transition contacts. Lower parts are dominated by open-marine burrowed packstones with rudist bioherms and chondrodonts-requienid beds.

the overall sequence stratigraphic framework. The proportion of peritidal to subtidal cycles and the different components of facies within individual high-frequency cycles were used to interpret dominant depositional environment, position within depositional sequences and larger system tract components. In this part, I will discuss the different high-frequency cycles (Figure 2-13) and their depositional settings; 1) outer shelf, 2) shelf crest, 3) lagoon and 4) Tidal-flat (Figure 2-10B).

1) Outer shelf

Huasteca Canyon is interpreted to have been located on the seaward side of the grainstone shoal margin and contains the greatest percentage of skeletal and non-skeletal grainstones (Figure 2-10B). Within the 2nd –order late highstand LCu deposits, shallow subtidal and peritidal cycles are dominant (Figures 2-13A, B, and C). These cycles have a base composed of skeletal packstones and rarely non-skeletal grainstones. Mounded or isolated patches of *requienids* and *Caprinids* rudists overlay and interfinger with skeletal packstones followed by heterolithic thin beds and laminite caps (Figures 2-13B and D). There are no indications of prolonged subaerial exposure or beach rock development. Also notable is the lack of any evaporites, bedded gypsum or nodular anhydrite.

Deeper subtidal high-frequency cycles dominate the Cupidito member sediments. These cycles initiate with intraclast or rip-up clast dominated

packstones, *Thalassanoides* burrowed packstones, mixed skeletal packstones and terminate in dominantly oolitic grainstone caps. The bedded deposits of *requienid*, *chondrodont*, and *caprinid* rudist packstones sometimes overlie the burrowed sediments and can also be capped by slightly burrowed to cross-stratified oolitic grainstones.

2) Shelf Crest

Sections located in the shelf crest, for example Potrero Garcia (PG), are dominated by shallow subtidal and peritidal high-frequency cycles in the lower LCu deposits (Figure 2-10B). Dominant facies include skeletal and non skeletal packstone-grainstones capped by laminites or followed by heterolithic thin beds and capped by laminites (Figure 2-13C). Microbial laminites with anhydrite nodules are interpreted as supratidal indicators (Hardie and Shinn, 1986; Demicco and Hardie, 1994). Solution collapse breccias seen within the section have been interpreted as minimum accommodation indicators by the nature of subaqueous gypsum, and therefore represent the base of the next high-frequency cycle (early transgressive).

The Cupidito member is dominated by deep subtidal high-frequency cycles with cross-stratified oolitic grainstones caps. Dominant facies include thick beds of requienid, chondrodont, and caprinid rudists dominated packstones and *Thalassanoides*-burrowed wackestone-packstone.

3) Lagoon

Escalera Canyon (EC) and Cortinas Canyon (CC) are interpreted to be in the lagoon center (Figures 2-10 and 2-12). Restricted shallow subtidal and peritidal high-frequency cycles dominate the LCu deposits. Bioturbated skeletal-peloidal packstones, *Thalassanoides*-burrowed packstones, and calcite-replaced bedded evaporites are abundant within the lagoon sections (Table 2-1). Increasing percentage of tidal-flat facies, mainly laminites and heterolithic thin beds, dominate the top part of lower LCu deposits.

Shallow and deep subtidal high-frequency cycles dominate the Cupidito member sediments. *Thalassanoides*-burrowed packstones, and bioturbated skeletal-peloidal packstones, bedded *requienids* and *chondrodonts*, and rudist bioherms dominate the thick cycles. The thick high-frequency cycles are the result of increasing accommodation space due to rising sea level and facies amalgamation caused by missed beats in sea-level fluctuations (Goldhammer et al., 1991a).

4) Tidal-flat

Chorros Canyon (ChC) is interpreted to represent the most landward portion of the lagoon (Figures 2-10 and 2-12). The LCu deposits are dominated by restricted-shallow subtidal high-frequency cycles at the base and restricted peritidal cycles toward the top (Table 2-1). *Thalassanoides*-burrowed packstones, and bioturbated skeletal-peloidal packstone facies change upward

into heterolithic thin beds and laminite, with nodular evaporites with occasional thin grainstone. Frequent exposures are indicated by the presence of nodular evaporites and microbial laminites supporting a tidal-flat and sabkha depositional environment (Hardie and Shinn, 1986; Demicco and Hardie, 1994).

The Cupidito member starts with abundant restricted-shallow subtidal and peritidal high-frequency cycles. Dominant facies include laminites, heterolithic thin beds, and bioturbated skeletal-peloidal packstones. As sea level continued to rise, deeper subtidal high-frequency cycles developed and tidal-flats facies were pushed further landward. Some bedded *requienids* and *chondrodonts*, and rudist bioherms were also deposited.

SEQUENCE STRATIGRAPHY

A variety of terminology exists for the identification and classification of cycles, sequences and for building a platform interior to basin stratigraphic framework. The terminology used herein, independent of the forcing mechanisms, was chosen to create a hierarchy that will enable the evaluation of facies arrangements in an organized manner according to a cycle's position in the next larger scale cycle, sequence or supersequence (Figure 2-14). Supersequences are composed of stacked composite sequences, which are in turn composed of depositional sequences. Depositional sequences are internally composed of stacked meter-scale high-frequency cycles (e.g. building blocks).

Depositional sequences are equivalent to high-frequency sequences of Kerans (1995) and Kerans and Tinker (1997) which are also considered equivalent to fourth-order (Vail et al., 1984; Van Wagoner et al., 1987), and are defined by surfaces or intervals representing a turn around from base sea-level fall to base sea-level rise. Composite sequences (Mitchum and Van Wagoner, 1991), composed of depositional sequences or high-frequency sequences, are equivalent to third-order (Vail et al., 1984; Van Wagoner et al., 1987), and indicate prograding and retrograding patterns within intervals (Mitchum and Van Wagoner, 1991). Supersequences are recognized as 2nd-order sequences that are bounded by either a surface or an interval of rock recording turnaround from decreasing to increasing accommodation/sediment supply ratios (Sonnenfeld, 1996).

Second-order sequence

The Barremian to Middle Aptian Cupido Formation is composed of 2nd-order late highstand LCu deposits and 2nd-order early transgressive Cupidito member (Goldhammer et al., 1991a; Goldhammer, 1999). Within the interpreted measured sections, a 2nd-order supersequence, encompassing the depositional and composite sequences, is observed. Vertical variations consist of not only different high-frequency cycle types and facies proportions, but of depositional and composite sequences overall cycle type proportions, system

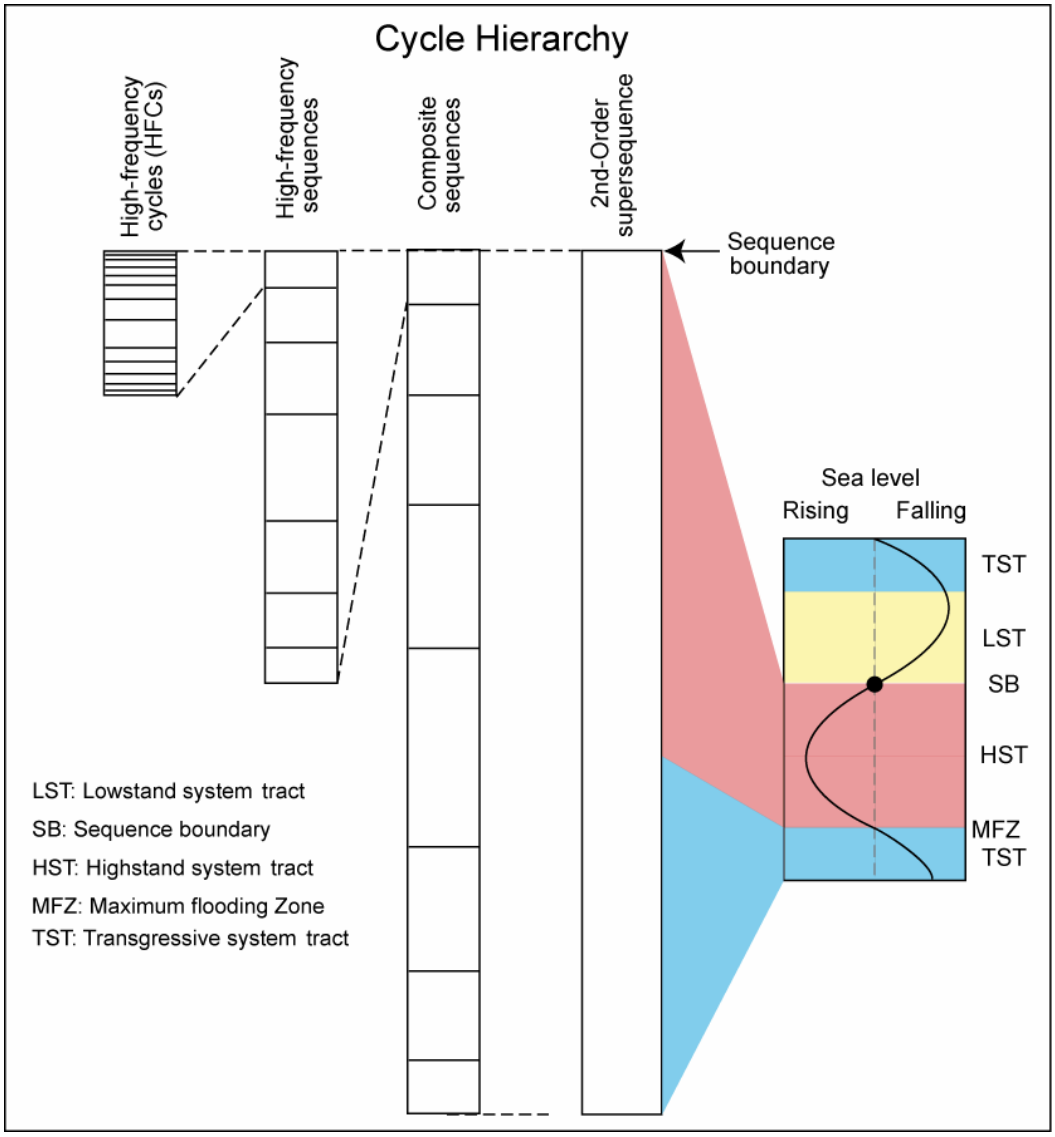

Figure 2-14. Cycle hierarchy.

The hierarchy is composed of multiple orders of cyclicity initiating with the highest frequency building block, high-frequency cycles (HFCs). HFCs stack into depositional sequences, which stack into composite sequences, then into supersequences. The cycles represent patterns in sea level rise and fall, which coordinate with system tracts (HST, LST, TST) and are bound by surfaces: sequence boundary (SB), or maximum flooding zone (MFZ).

tracts and overall thicknesses (Figures 2-15 and 2-16).

The lower parts of the measured stratigraphic sections are dominated by thinner depositional sequences with dominant peritidal and shallow subtidal high-frequency cycles and increasing abundance of tidal-flats and evaporitic facies (Table 2-2). These parts of the sections represent the LCu (Figure 2-15). The top parts of the sections are dominated by thicker depositional sequences dominated by shallow to deep subtidal high-frequency cycles with decreasing peritidal high-frequency cycles and restricted facies proportions (Table 2-2). These parts of the sections represent the upper Cupidito member (Figure 2-15). The change from progradational Cupido to retrogradational Cupidito is marked by a 2^{nd}-order sequence boundary which represents a change from decreasing accommodation space to increasing accommodation space (Figures 2-2, 2-16 and 2-17).

Composite sequences

The interpreted depositional sequences (within the Cupido stack into even larger composite sequences (Mitchum and Van Wagoner, 1991). The shallowing/deepening, peritidal/subtidal, highstand/transgressive system tract components and thinning/thickening trends of depositional sequences were used to define the composite sequences within the Cupido Formation (Figure 2-16).

Table 2-2. Sequence stratigraphic framework summary.

Sequence stratigraphic framework for the Cupido Formation showing the major characteristics of interpreted composite sequences (I-IV) and internal depositional sequences (A-L), system tract components (highstand, HST; Transgressive, TST), dominant facies, type of high-frequency cycles (HFCs) and bounding surfaces: sequence boundaries, (SB); and maximum flooding zone (MFZ).

2nd-order sequence	Composite Sequecne	Average Thickness (m)				System Tract	Comments
		Interior		Margin			
Cupidito member (TST)	IV (TST part)	L K J	125	J	49	TST	MFZ is inferred to be within the La Pena shales Composed of thick open-marine subtidal HFCs with abundant grainstones (some oolitic), beds rich in bivalves, requienids and chondront and rudist bioherms
	III	I	158	I	145	HST	SB is picked at the top thinly-stacked peritidal HFCs below thicker subtidal HFCs A thin interval of dominantly thin peritidal, laminite capped HFCs composed of relatively shallow facies
		H		H			
		G		G		TST	MFZ is interpreted within the thickest shallow subtidal HFCs Composed of thick subtidal, probably amalgamated HFCs with foraminiferal mud-packstone, a few beds rich in bivalves, requienids and chondront and some rudist bioherms/packstone
LCu (HST)	II	F	167	F	169	HST	SB is interpreted as the base of laterally correlative, thick solution collapse breccia atop thin peritidal HFCs Composed mainly of upward thining peritidal HFCs dominated by shallow tidal falt facies
		E		E			
		D		D		TST	MFZ is interpreted within 2 thick shallow subtidal HFCs Composed of thick shallow-subtidal HFCs that are mainly burrowed peloidal-skeletal packstones, thickness of subtidal HFCs decreases upwards
		C		C			
	I (HST part)	B	116	B	117	HST	SB is picked at the top stacked thin bedded peritidal HFCs Composed of massive peloidal-skeletal-oolitic packstones-grainstones and some interbeds of rudist bioherms and packstones. Some subtidal HFCs, but dominantly thin peritdal HFCs
		A		A			

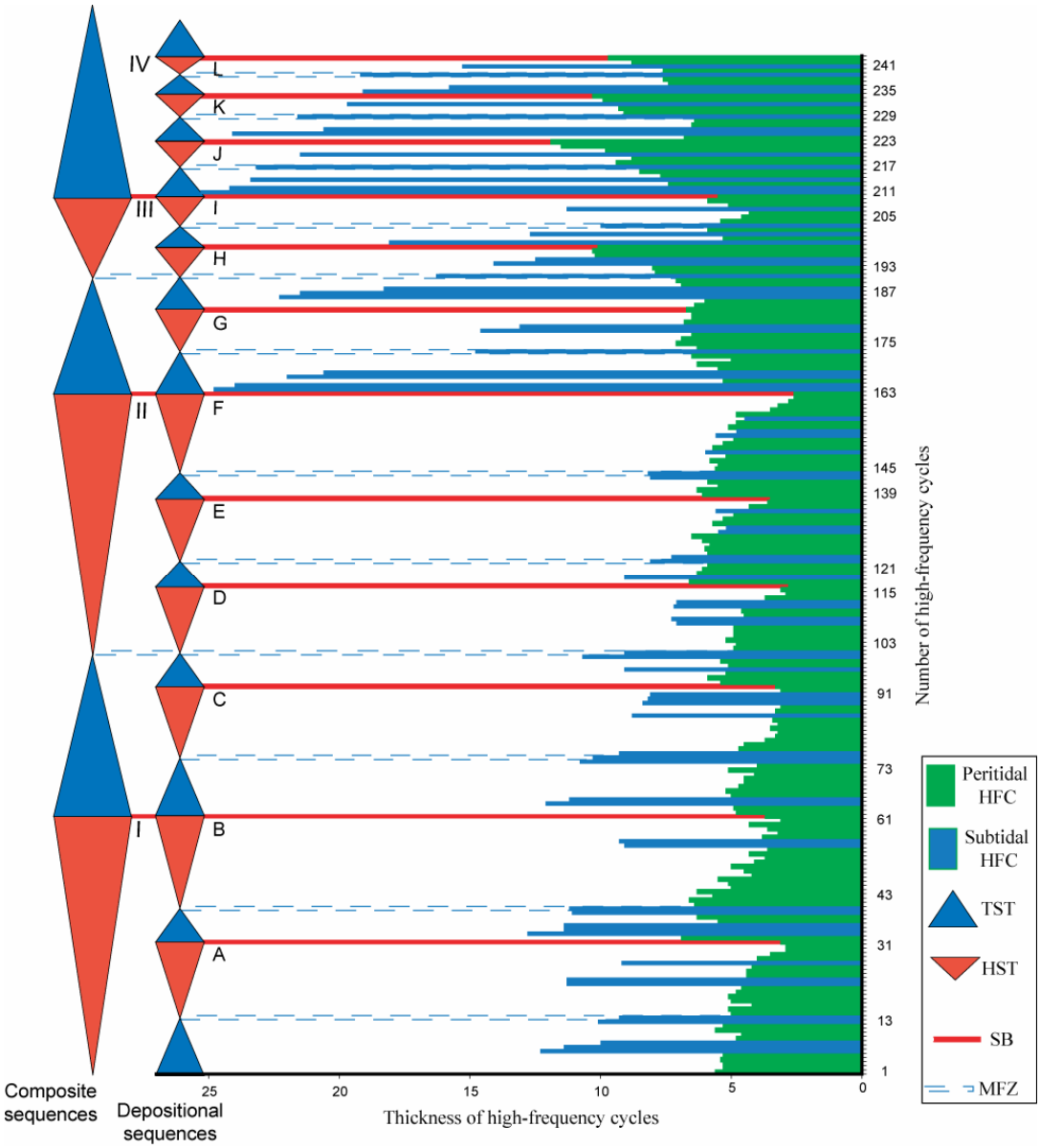

Figure 2-15. Stacking patterns of individual high-frequency cycles (HFCs).

Stacking patterns of individual peritidal and subtidal high-frequency cycles (HFCs) from Chorros Canyon into lower-order depositional and composite sequences and their component system tracts (highstand, HST; transgressive, TST). The number, type and thicknesses of HFCs determine the turnaround in accommodation and identifying sequence boundaries (SB) and maximum flooding zones (MFZ). Figure 2-16 shows stacking pattern and thicknesses of depositional sequences and their system tract components.

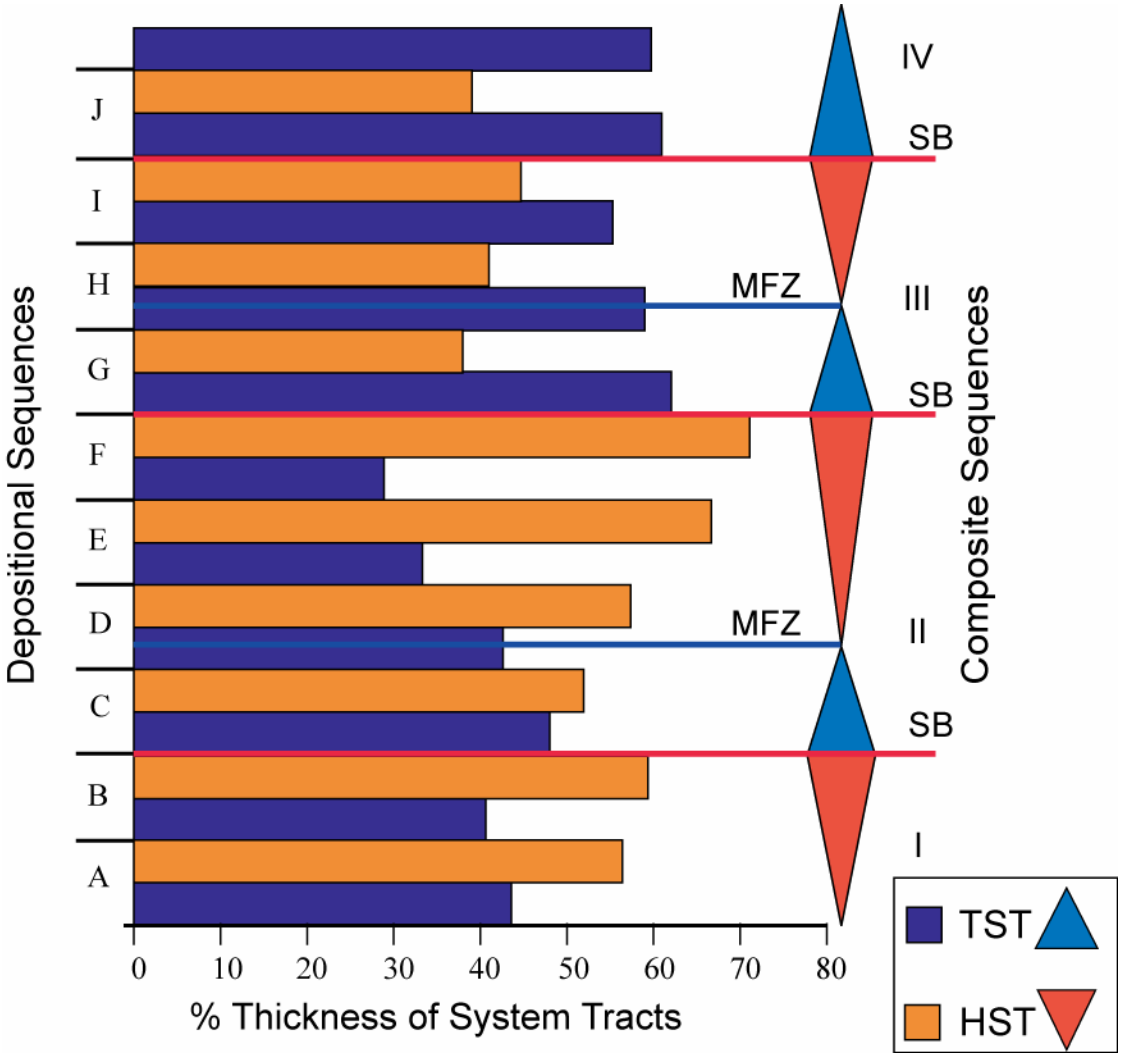

Figure 2-16. Low-order cyclicity.

Stacking pattern of system tracts components of depositional sequences interpreted from Huasteca Canyon highlights lower-order cyclicity (composite sequences). The percentage of highstand system tracts (HST) increases towards sequence boundaries (SB), whereas the percentage of transgressive system tracts (TST) decreases away from maximum flooding zones (MFZ).

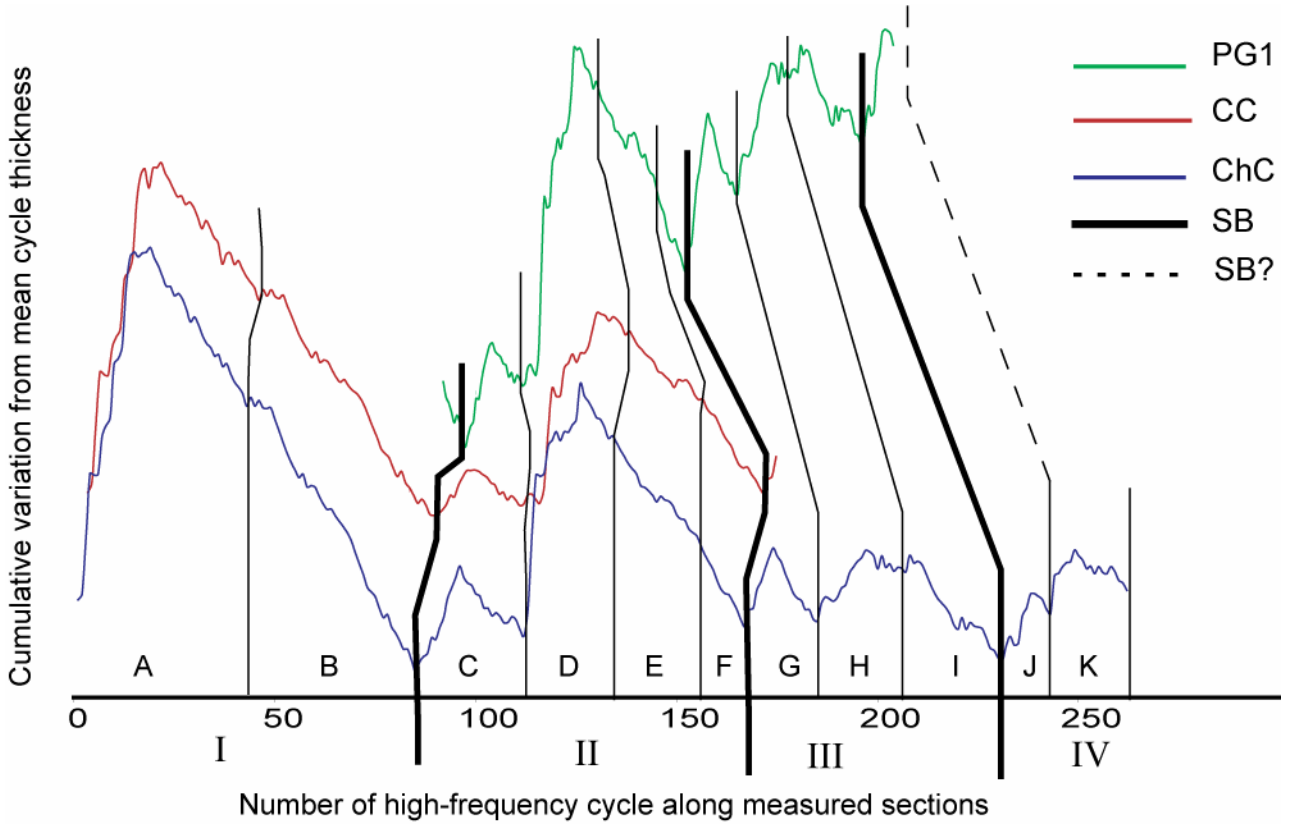

Figure 2-17. Fischer plots

Fischer plots of the Cupido Formation combining 3 sections, Chorros Canyon (ChC), Escalera Canyon (EC), and Potrero Garcia (PG1) highlighting overall change in accommodation space and lateral correlation of depositional sequences (A-K) and composite sequences (I-IV) and their bounding sequence boundaries (SB).

Two full composite sequences and 2 partial composite sequences are interpreted within the Cupido Formation (Table 2-2; Figures 2-15 and 2-16). Starting from the base of the Cupido Formation, the LCu is composed of the highstand part of composite sequence I and overlain by composite sequence II. The upper Cupidito member is composed of composite sequence III and the transgressive part of composite sequence IV (Table 2-2; Figure 2-16). These composite sequences are marked by turnaround from decreasing accommodation to increasing accommodation and changes in depositional sequences characteristics such as thickness, facies and facies-belt propportions. For example, transition from thin shallow water (peritidal-dominated) depositional sequences to thick deeper water (subtidal-dominated) depositional sequences marks an increase in overall accommodation space available for sedimentation. Sequence boundaries are marked by pronounced surfaces or zones, such as collapse breccia or stacked thinn peritidal-dominated high-frequency cycles overlain by thicker subtidal-dominated high-frequency cycles (Figure 2-16).

Depositional sequences

Within the Cupido Formation, depositional sequences are composed internally of stacked high-frequency cycles. Stacked high-frequency cycles record general deepening and shallowing trends and variations in available accommodation space across the entire platform. A total of twelve depositional sequences (A-L) are interpreted within the Cupido Formation (Figures 2-15 and

2-16). Depositional sequences A-F compose the LCu whereas depositional sequences G-L constitute the upper Cupidito member (Figures 2-15 and 2-16). Depositional sequences are separated by sequence boundaries described as unconformities and their correlative conformities (Vail et al., 1977; Vail et al., 1984; Vail, 1987; Van Wagoner et al., 1987; Vail et al., 1991; Posamentier and Allen, 1999). However, discrete surfaces are not observed in all depositional environments across the Cupido platform and stacking patterns of high-frequency cycles and major shifts in cycle type and facies components are used to interpret these turnaround surfaces. For example, maximum flooding surfaces (MFS) are difficult to recognize with certainty, and are better represented by a zone of maximum flooding (MFZ). This is normally represented by stacked thicker high-frequency cycles and greater proportion of subtidal cycles. Sequence boundaries (SB) are picked on major exposure below evaporites and breccias which are very obvious surfaces or within stacked thinner high-frequency cycles with greater proportions of peritidal cycles. Therefore, the proportion of system tracts will vary depending on the chosen maximum flooding zone and is susceptible to other interpretations due to the mosaic pattern of subtidal facies. However, it is clear that there is an overall shallowing toward the sequence boundaries followed by deepening toward the maximum flooding surfaces (Figure 2-15 and 2-16).

STRATIGRAPHIC ARCHITECTURE AND MORPHOLOGY OF THE CUPIDO PLATFORM

Two dimensional stratigraphic correlation

High-frequency cycle stacking patterns and facies-proportion analyses of 1-D measured sections (Kerans, 1995) allowed the interpretation of depositional and composite sequences for each individual section. Fischer plot analysis of deviation from mean cycle thickness was carried out to evaluate changes in accommodation space through time (Fischer, 1986; Read and Goldhammer, 1988; Osleger and Read, 1991; Lehrmann and Goldhammer, 1999; Figure 2-17). These plots were also used to display the great lateral extent of interpreted composite sequences, and therefore potential eustatic origin across the different sections. Using the 2nd-order sequence boundary as a datum, 2-D correlations of depositional sequences was accomplished across the Cupido platform (Figure 2-17). This 2nd-order sequence boundary at the top of sequence F is interpreted as an erosional unconformity below evaporite solution-collapse breccias (Figure 2-18) in all sections except Huasteca Canyon section due to the lack of evaporites. The depositional and composite sequence correlation enabled several observations and conclusions about the architecture and evolution of the Cupido platform.

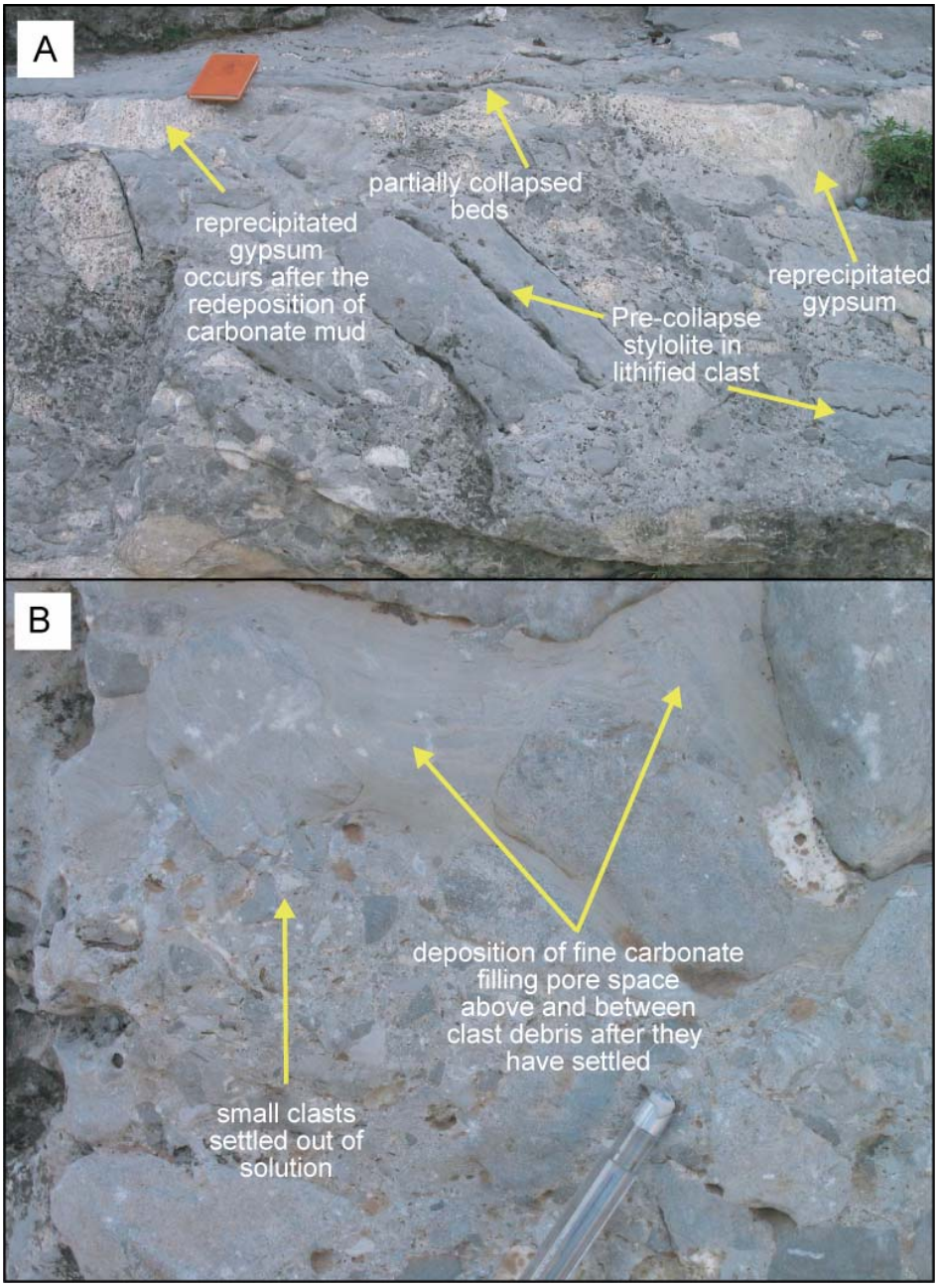

Figure 2-18. Solution-collapse breccia.

Outcrop photographs of breccias highlighting observations that support a gradual development due to phreatic dissolution below the surface.

The LCu is composed of a partial composite sequence (HST part) and a full composite sequence (Table 2-2). A total of six depositional sequences (A-F) are interpreted within the HST part of the Cupido Formation. These depositional sequences are interpreted and correlated in all measured sections (Figure 2-17 and 2-19). The overall thicknesses of these depositional sequences decrease toward the 2nd-order sequence boundary (Figure 2-16). This is attributed to overall decrease in accommodation space.

The Cupidito member is composed of a full composite sequence and a partial composite sequence (TST part) that encompass a total of six (G-L) depositional sequences (Table 2-2; Figures 2-15, 2-16, 2-17 and 2-19). Depositional sequences G-J are interpreted and correlated across the entire upper part of the platform (Figure 2-19). However, sequences K and L are not present at the margin sections (Huasteca Canyon, Potrero Garcia, Potrero Chio and Potrero Minas Viejas; Figures 2-10 and 2-19). These two extra sequences are interpreted to be a result of landward shift in sediment production as a reaction to the increasing rate of relative sea-level rise and retrogradation of the shelf. The Cupidito depositional sequences also exhibit back-stepping geometry as Sequence K is present across parts of the lagoon (sections at Escalera Canyon, Cortinas Canyon, and Chorros Canyon) and extending landwards (Figures 2-10 and 2-19). However, sequence L is only interpreted in the most landward part of the platform (Chorros Canyon section; Figures 2-10 and 2-19).

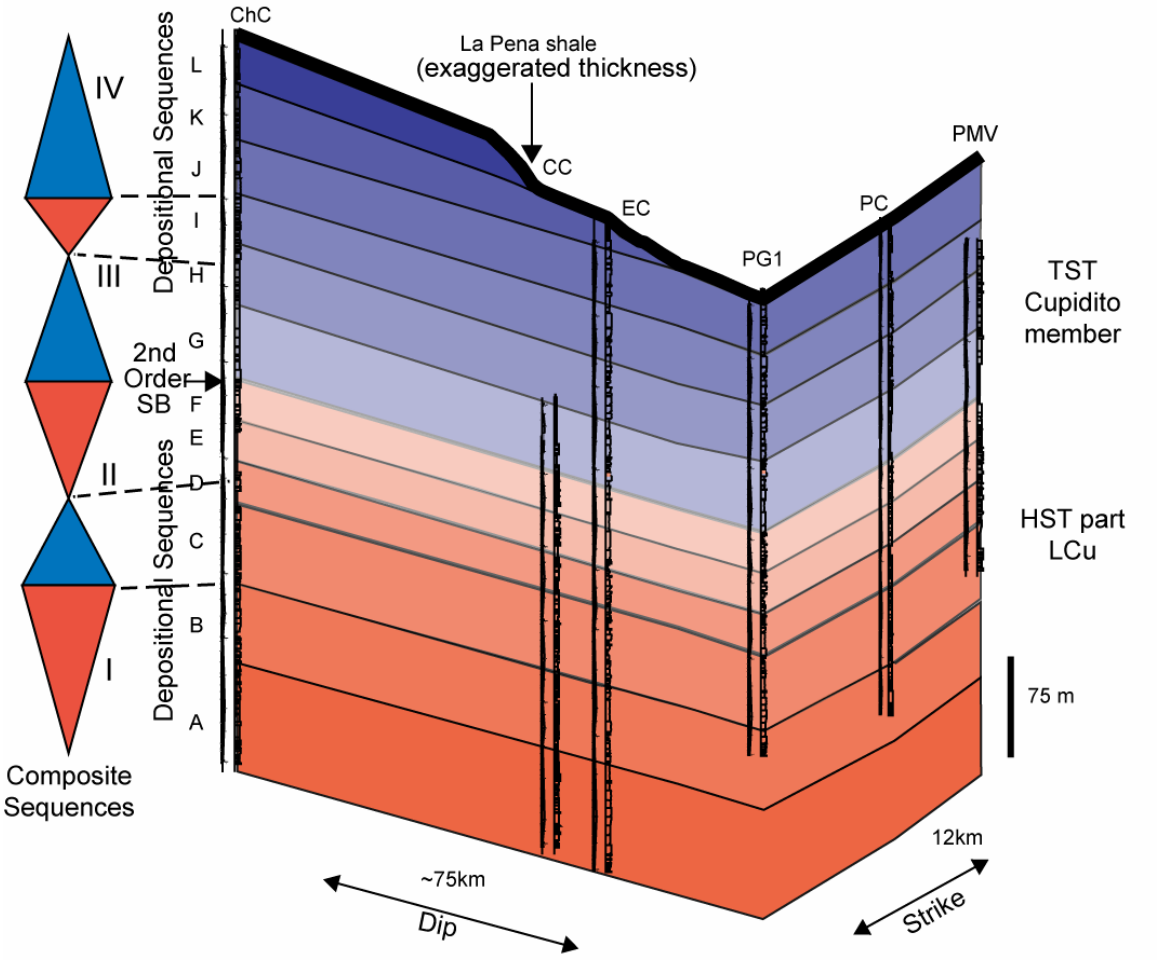

Figure 2-19. Fence diagram illustrating sequence stratigraphic framework.

Fence diagram combining six measured sections in their relative positions (Chorros Canyon, ChC; CC, Cortinas Canyon, CC; Escalera Canyon, EC; Potrero Garcia, PG1; Potrero Chico, PC; Potrero Minas Viejas, PMV). Lateral correlation of sequences and retrogradational geometry of the platform are evident. Depositional sequences (A-L) and composite sequences (I-IV) and the 2nd-order sequence boundary (SB) are outlined. Red part represents the lower highstand (HST) LCu and the blue part represents the transgressive (TST) Cupidito member. The 2nd-order sequence boundary is used as a datum. La Peña thickness is estimated. Distances in km. Modified from Foster (2003) and Altobi et al. (2004).

Stratigraphic framework for the Cupido Formation

The comprehensive high-resolution sequence stratigraphic framework developed here for the Cupido Formation matches to previous stratigraphic frameworks developed by Goldhammer et al. (1991a) and Lehmann et al. (2000) (Figure 2-19). Goldhammer et al. (1991a) interpretation is based on the analysis of one stratigraphic section measured at Potrero Garcia through the upper most LCu and Cupidito member sediments and correlates with developed framework for a section close to the Cupido margin (Figures 2-1, 2-5, 2-19 and 2-20). Lehmann et al. (2000) correlated seven widely-spaced stratigraphic measured sections exposed in a large area of northeastern Mexico that includes study area, as well as northwest and west of study area. They correlated four high-frequency sequences in the LCu and three high-frequency sequences in the Cupidito member composing a partial composite sequence (Figure 2-20). Their interpretation differs with my conclusions both in the number of depositional sequences (their high-frequency cycles) and the stacking patterns of the composite sequences (Figure 2-20). The framework developed here combines more stratigraphic sections which exhibit different depositional paleoenvironments and show a large overview of the whole platform. All sections were measured on the cm scale (Appendix A) and encompass most if not the entire Cupido Formation.

Figure 2-20. New high-resolution framework

Summary diagram comparing this study's results with previous frameworks (Goldhammer et. al., 1991a; Lehmann et. al., 2000) and highlighting the details of the study across the platform. See text for more details.

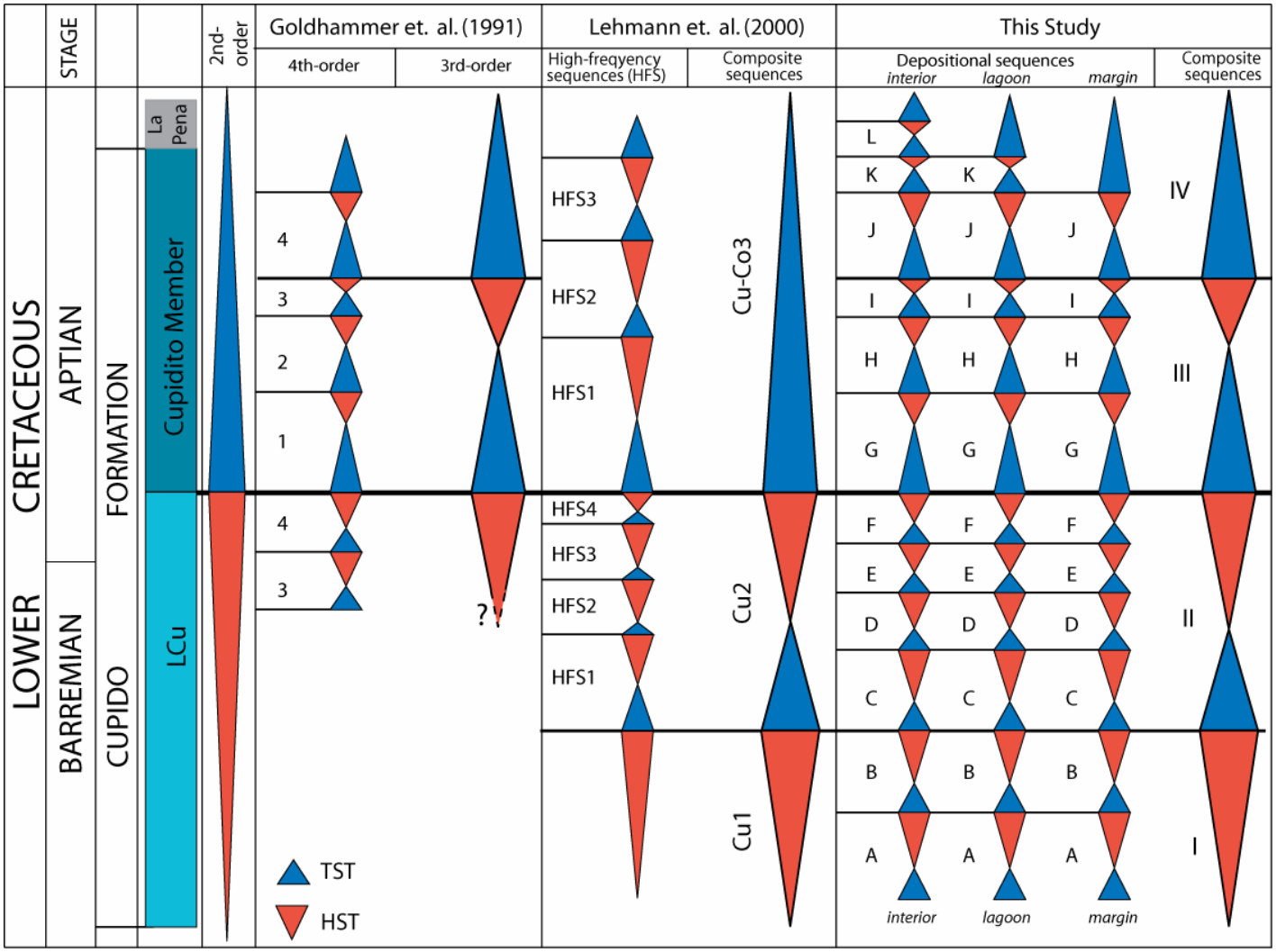
LOWER CRETACEOUS
STAGE
APTIAN
BARREMIAN
FORMATION
CUPIDO
La Pena
Cupidito Member
LCu
2nd-order
Goldhammer et. al. (1991)
4th-order
3rd-order
4
3
2
1
4
3
?
TST
HST
Lehmann et. al. (2000)
High-freqyency sequences (HFS)
Composite sequences
HFS3
HFS2
HFS1
HFS4
HFS3
HFS2
HFS1
Cu-Co3
Cu2
Cu1
This Study
Depositional sequences
interior
lagoon
margin
Composite sequences
L
K
J
I
H
G
F
E
D
C
B
A
IV
III
II
I

Stacking patterns and syndepositional faulting

In general, little variation was observed in the thickness of individual depositional sequences and their total number of high-frequency cycles in closely spaced sections. However, depositional sequences E and F are significantly thicker in Huasteca Canyon than nearby measured sections (Table 2-3; Figures 2-1 and 2-10). These sequences contain additional high-frequency cycles which could be the result of differential accommodation space created by processes beyond carbonate production and deposition. Ortega and Marrett (2001) interpreted fractures and normal faults in the Cupido Formation as early syndepositional features that are not related to the Laramide deformation. Movement along growth faults will provide differential accommodation space for carbonate sedimentation in different parts of the platform (Hardie et al., 1986). This can lead to varying number of high-frequency cycles within different parts of the platform including closely spaced sections. Subsurface data from the Sligo margin of South Texas shows intense extensional faults that die out vertically within the Sligo outer shelf and shelf margin which are believed to have originated from syndepositional salt movement (Figure 2-11).

The thicknesses of depositional sequences in Huasteca Canyon are often double those in the other sections over a short lateral distance, which is powerful evidence for intense growth faulting near the outer shelf (Table 2-3). This dramatic

Table 2-3. Thicknesses of depositional sequences.

Summary of measured thicknesses in meters, total at each section and per depositional sequence. Huasteca Canyon section has three thick sequences (red). Blank sequence thicknesses are present where the section did not extend far enough. Those sequences believed to be thicker than the current measurement are also given. Abbreviations for measured sections are similar to those given in Figure 2-1.

Section		ChC	CC	EC	PG2	PG1	PC	MV	HC
		Thickness	Thickness	Thickness	Thickness	Thickness	Thickness	Thickness	Thickness
Depositional Sequences	L	43	La Pena Shale		La Pena Shale				
	K	55		58					
	J	63		67	58	56	54	>13	**86**
	I	39		39	35	32	35	36	44
	H	75		71	71	66	67	69	73
	G	97	88	86	85	79	81	83	84
	F	49	51	52	47	45	46	45	**68**
	E	49	53	50	46	45	47	43	**56**
	D	57	61	60	52	49	47	50	53
	C	72	63	74	71	70	67	69	77
	B	71	76	77	>21	48	70	>40	75
	A	75	78	>52			>32		>68
Total (m)		747	469	687	486	488	548	440	686

variation in thickness between Huasteca Canyon and the other sections suggests that the most intense faulting occurs between the shoal and the true shelf edge. The extensional faults provide the best mechanism for increased subsidence relative to the rest of the platform, but slow enough for carbonate production rates to fill the newly created space.

Timing, formation, and significance of solution-collapse breccias

Polymict solution-collapse breccia within the Cupido carbonates can be found between any facies but is most commonly found above lagoonal sediments or above the laminated mudstone facies due to the restricted environment associated with bedded evaporites. The process of collapse is tied to the dissolution of buried bedded evaporites by continental ground waters which result in the breakage and mixture of the overlying facies (Stanton, 1966; Swennen et al., 1990; Warren, 1999). The clasts in these breccias are lithified, often stylolitized, and even fractured before breaking apart and are infilled with carbonate mud grading upward into reprecipitated gypsum (e.g. the 2nd-order sequence boundary shown in Figure 2-18).

The stratigraphic significance of bedded evaporites is their position between depositional sequences. These evaporites are formed during early rises in sea level when restricted and evaporitic conditions dominate the platform after subaerial exposure (Goldhammer, 1999; Warren, 1999; Figure 2-21). The

Figure 2-21. Schematic development of solution-collapse breccias.

(A) shallow subsurface (B) deep subsurface (~30 m). Similar observations were reported by Warren (1999).

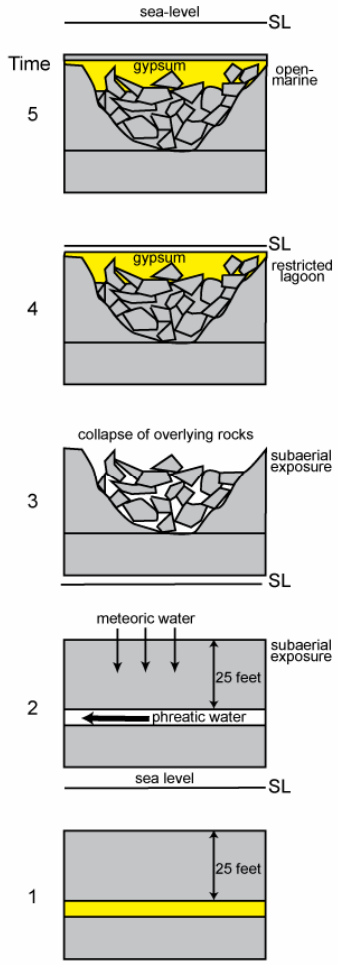

A) Solution-collapse breccia formation in the shallow subsurface

Step 5: Once sea-level has returned to normal marine salinities microbial laminites grow over the previously deposited gypsum, completing the cycle of breccia development.

Step 4: As sea-level begins to rise a restricted lagoon developes and the deposition of gypsum occurs and fills in the irregular topography above the breccia.

Step 3: The overlying strata then collapse into the dissolved bed due to over burden pressures, clasts may be poorly mixed.

Step 2: When sea-level falls, percolating meteoric water cause the dissolution of the gypsum bed.

Step 1: Subaqueous gypsum is buried to a shallow depth but deep enough for some lithification to occur in the sediments above it.

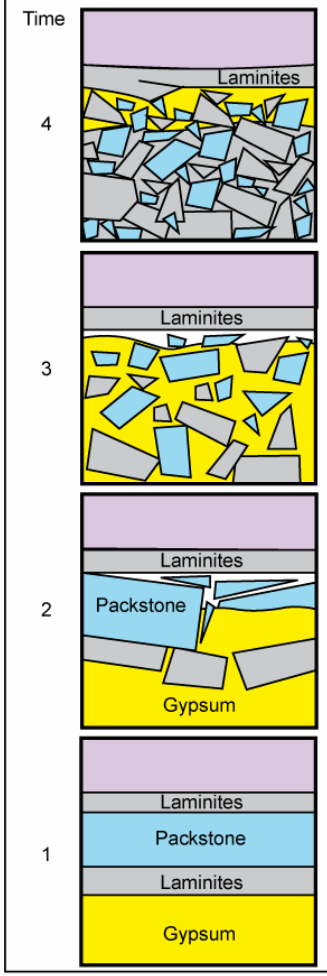

B) Development of solution-collapse breccias according to the gradational model

Step 4: Carbonate mud settles out of suspension and drapes above the clasts-supported framework. Lastly gypsum reprecipitates out of the remaining solution and the overlying beds sag into the evaporite.

Step 3: The beds break apart and the clasts rotate and mix within the gypsum. Larger clasts sink to the bottom and smaller clasts fill the space between the larger clasts as the evaporite is removed by increasingly fresh influx.

Step 2: The evaporite begins to dissolve due to the introduction of meteoric water forming a gypsum mush. The beds directly overlying the evaporite begin to break apart.

Step 1: The evaporite is deposited and buried by thick overlying sediment which becomes lithified.

correlation of depositional sequences based on evaporites further enhances the significance of breccia development. The 2nd-order sequence boundary within the Cupido Formation has been chosen by preserved extensive solution collapse breccia that formed due to the dissolution of underlying bedded evaporites. The thickest, well developed breccia is a product of a thick evaporite which was deposited, buried by successive carbonate cycles, lithified, and undisturbed until sea level dropped to a new low for an extensive period of time marking the 2nd-order sequence boundary (Figure 2-21).

The restriction of the lagoon before and during the next evaporite deposition resulted in a hydrostatically driven influx of continental water. The percolating waters would then cause the dissolution of the evaporite in the underlying sequence resulting in the development of a large solution-collapse breccia (Warren, 1999; Figure 2-21). This process could be repeated for each additional depositional sequence until the deposition of evaporites came to an end. Each succeeding breccia development would be minor to a lesser degree due to the decreasing amounts of time for exposure to continental waters (Figure 2-22). This stratigraphic stacking of breccias supports the concept that breccia formation occurs at depth due to the fall in sea level associated with the following sequence and does not occur at the surface (Warren, 1999). The inclusion of lithified clasts with stylolites and early fractures within the breccias also supports a collapse mechanism forming at depth (Figure 2-18).

Figure 2-22. Potrero Garcia section.

Stratigraphic measured section from Potrero Garcia showing the relationship between solution-collapse breccia thickness and its correlative sequence boundary (SB). The 2nd-order sequence boundary (SB F) is interpreted by thick breccia (2 m) and is interpreted to represent the longest time of minimal accommodation space (exposure) as indicated by thick breccia (3 m) below at sequence boundary E (SBE) and very thin breccia (<1 m) above at sequence boundary G (SBG). Modified from R. K. Goldhammer.

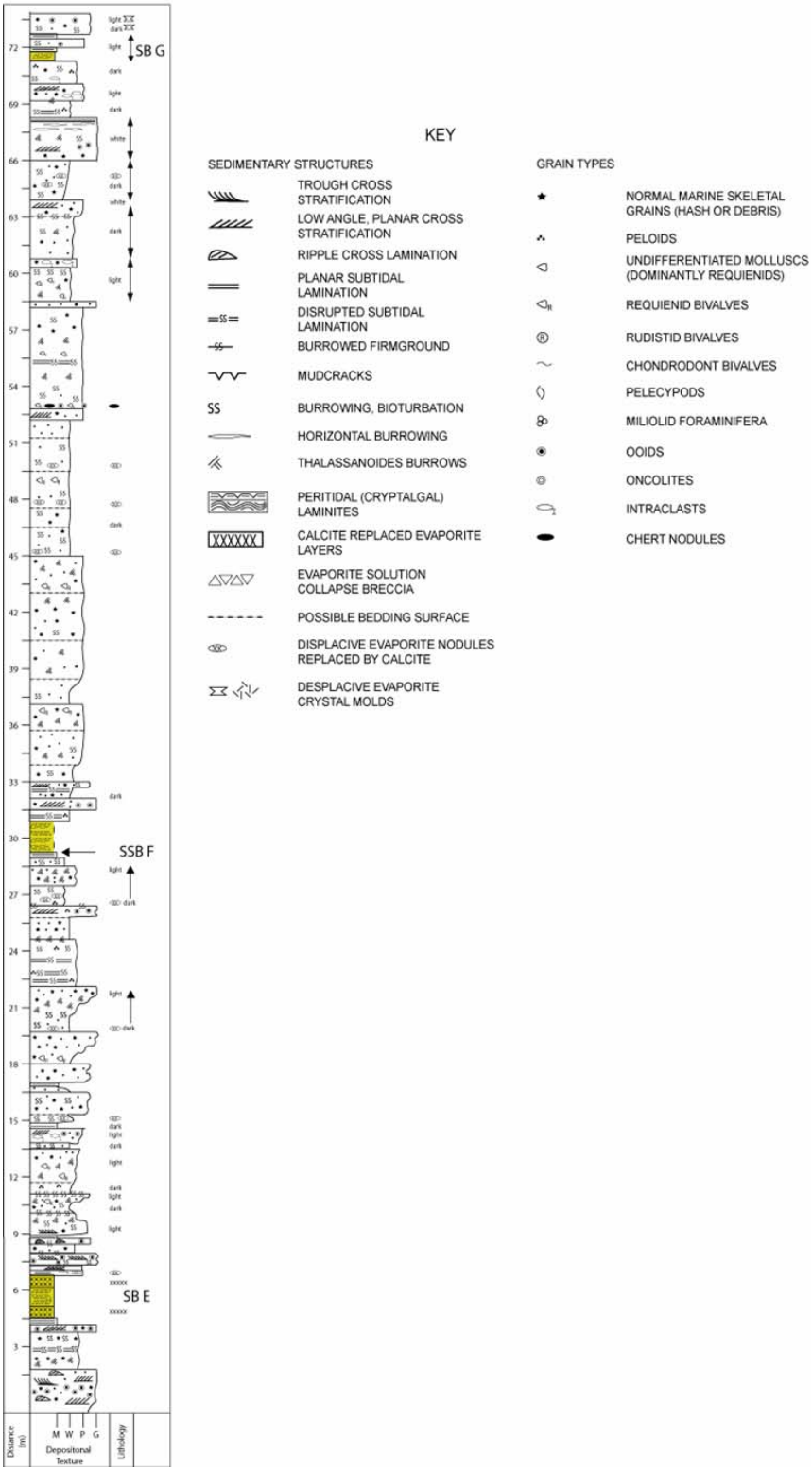
SB G
SSB F
SB E
Distance (m)
M W P G
Depositonal Texture
Lithology
KEY
SEDIMENTARY STRUCTURES
TROUGH CROSS STRATIFICATION
LOW ANGLE, PLANAR CROSS STRATIFICATION
RIPPLE CROSS LAMINATION
PLANAR SUBTIDAL LAMINATION
DISRUPTED SUBTIDAL LAMINATION
BURROWED FIRMGROUND
MUDCRACKS
BURROWING, BIOTURBATION
HORIZONTAL BURROWING
THALASSANOIDES BURROWS
PERITIDAL (CRYPTALGAL) LAMINITES
CALCITE REPLACED EVAPORITE LAYERS
EVAPORITE SOLUTION COLLAPSE BRECCIA
POSSIBLE BEDDING SURFACE
DISPLACIVE EVAPORITE NODULES REPLACED BY CALCITE
DESPLACIVE EVAPORITE CRYSTAL MOLDS
GRAIN TYPES
NORMAL MARINE SKELETAL GRAINS (HASH OR DEBRIS)
PELOIDS
UNDIFFERENTIATED MOLLUSCS (DOMINANTLY REQUIENIDS)
REQUIENID BIVALVES
RUDISTID BIVALVES
CHONDRODONT BIVALVES
PELECYPODS
MILIOLID FORAMINIFERA
OOIDS
ONCOLITES
INTRACLASTS
CHERT NODULES

Platform evolution

Thick shallow-water Cupido carbonates accumulated for more than 250 km from the shelf margin to the Coahuila block. Limited outcrops combined with the large distances between the measured sections across the platform led to interpolation of facies transitions. Cycle boundaries and interpreted depositional system tracts were used as correlation limits for dip profile continuity. Available accommodation space and subsequent system tracts were used as constraints for facies-belt distribution within the Cupido platform. The LCu of the Cupido platform has a progradational/aggradational morphology, whereas the upper Cupidito member exhibits mainly retrogradational depositional patterns leading to eventual drowning (Figure 2-23).

During the 2nd-order late highstand, the two tidal-flat belts migrated from opposite sides into the lagoon. These tidal belts were broad and parallel to the shore line (Figures 2-10, 2-12 and 2-23). The high energy shoal margin prograded and widened basinward as accommodation space decreased. The rudist-bank facies belt prograded basinward as accommodation space decreased. Subtidal lagoonal facies belt dominated the center of the platform, but decreasing accommodation space resulted in tidal-flat progradation narrowing its depositional extent.

As sea level rose during the 2nd-order transgression, the tidal-flat belt attached to land back-stepped due to rising sea level and landward shift in

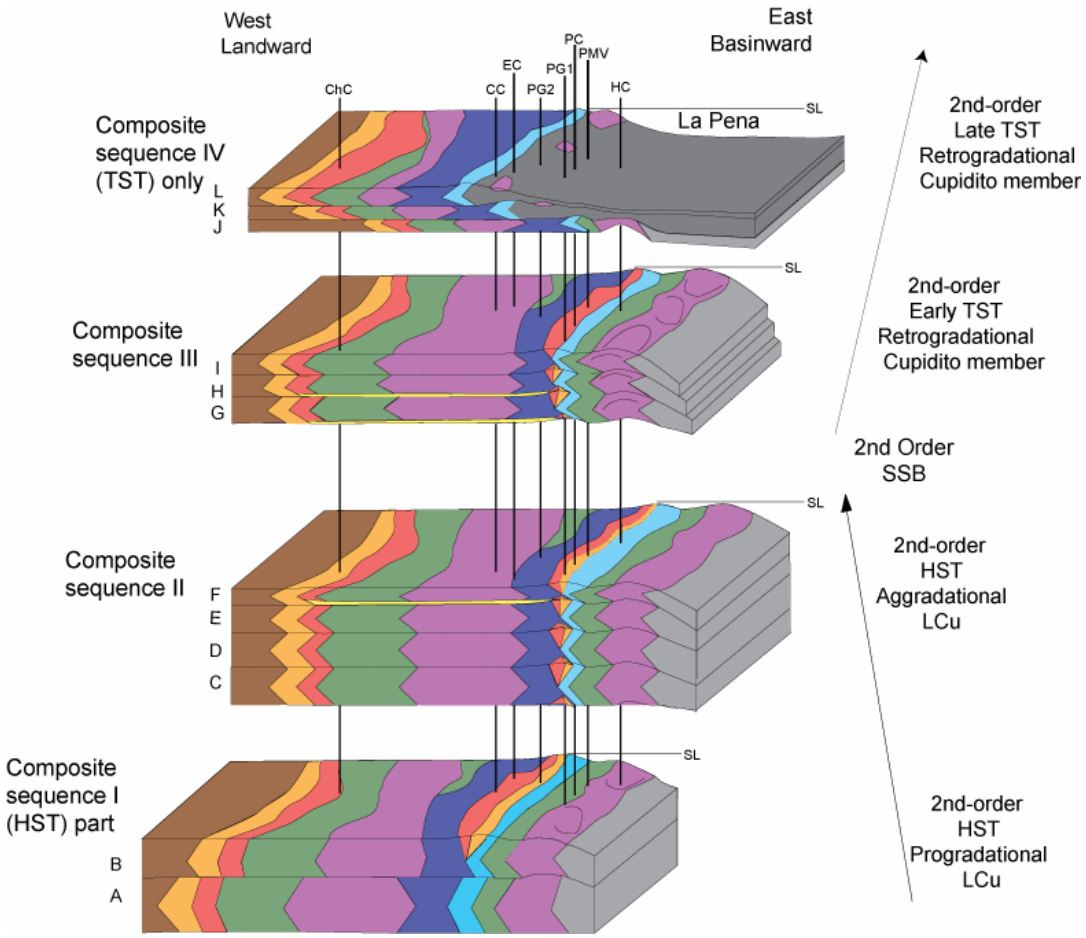

Figure 2-23. Cupido platform interior.

Block diagrams of the Cupido platform interior with eight localities of measured sections. Section names from north to south are Potrero Minas Viejas (PMV), Potrero Chico (PC), Potrero Garcia (PG), Huasteca Canyon (HC), Escalera Canyon (EC), Cortinas Canyon (CC), and Chorros Canyon (ChC). The facies color key can be found in Figure 5. The depositional sequences (A-L) are grouped according to their positions composite sequences (I-IV) and the 2nd-order supersequence. They illustrate the progradational, aggradational and retrogradational back-stepping nature of the drowning platform as sea level (SL) rises. The 2nd-order sequence boundary, (SB) divides the highstand (HST) from the transgressive (TST) and is located at the top of depositional sequence F. Modified from Foster (2003).

carbonate production (Figure 2-23). The subtidal lagoonal facies belt widened at the early stages of sea level rise but the inability of sedimentation to keep pace with rising sea level led to deepening of the lagoon and eventual drowning. The increase in accommodation space also caused the shoal-facies belt to narrow as it attempted to keep pace with optimal production window (Figure 2-23). The tidal-flat belt attached to the shoal narrowed rapidly, and eventually drowned. The rudist-bank facies belt retrograded and drowned due to rapid rise in sea level (Figure 2-23).

The platform drowned slowly during the 2nd-order transgression allowing time for the platform interior sequences to aggrade slightly while adjusting their thickness to the increasing accommodation (Figure 2-23). As sea level continued to rise, the sequence development became a function of diminishing sediment production resulting in a landward shift with a back stepping geometry (Figures 2-19 and 2-23). The sediment production on the Cupido platform kept up with sea level between depositional sequences G-I but as the rate of sea-level rise increased the focus of sediment production was forced to shift landward, removing all peritidal facies from the shoaling cycles within depositional sequence J . While depositional sequences K and L were being deposited in Chorros Canyon section, the La Peña Shale formed a condensed zone above the other sections, covering the shoal complex (Figures 2-19 and 2-23). This condensed zone could easily represent 1-2 m.y., the approximate duration required to deposit the up dip depositional sequences, K and L. The shale would

ideally be thickest in the portion of the shelf that was drowned the longest such as the outer shelf (Tinker, 1985; Figures 2-19 and 2-23).

CONCLUSIONS AND IMPLICATIONS

1) The Cupido carbonate platform of the Lower Cretaceous is a rudist reef-rimmed shelf with a shoal complex shelf crest. The reef was probably not a prominent barrier for the Cupido platform though it may be represented as such in other positions along the western Gulf of Mexico shelf-margin trend. A shallow lagoon, dominated by bioturbated carbonate mud-rich textured sediments, developed behind the shoal, which provided protection from wave energy.

2) Meter-scale deep subtidal to peritidal high-frequency cycles vary in thickness, facies components and type depending on their relative position laterally along the shelf profile, vertically within individual depositional sequences and the overall sequence stratigraphic framework. They are laterally continuous and easily correlated between closely spaced measured sections. These high-frequency cycles stack into lower-order depositional sequences that then correlate across the entire platform. These depositional sequences, in turn, stack into composite sequences that correlate regionally.

3) Six depositional sequences (A-F) are interpreted and correlated across the platform within the LCu. These sequences comprise partial

composite sequence I, and complete composite sequence (II). A total of six depositional sequences (G-L) are interpreted within the Cupidito member. These sequences comprise one complete composite sequence (III) and a partial composite sequence (IV). Depositional sequences (K-L) are part of composite sequence (IV) and are only interpreted updip and were deposited as the carbonate factory shifted landwards due to rising sea level.

4) The number, type, facies components and stacking pattern of high-frequency cycles are used to interpret lower-order cyclicity within the Cupido Formation. High-frequency cycles within the LCu are dominantly peritidal and capped by heterolithic thin beds or laminite. The proportion of subtidal to peritidal high-frequency cycles decreases in depositional sequences A-F. The total thickness of individual depositional sequences decreases toward the 2^{nd}-order sequence boundary. However, within the upper Cupidito member, the proportion of subtidal to peritidal high-frequency cycles increases as well as the thickness of high-frequency cycles due to cycle amalgamation. The top part of sequence H and sequence I include laminite capped high-frequency cycles and abundant peritidal high-frequency cycles along with some thick subtidal high-frequency cycles. Sequences J-L show mainly thick shallow and deep subtidal high-frequency cycles dominated by open marine facies.

5) The sequence stratigraphic framework developed here was compared with the frameworks developed by Goldhammer et al. (1991a) and Lehmann et al. (1999) on the basis of 1 and 6 sections, respectively. My study integrated several stratigraphic sections and thus enabled a more robust correlation and resulted in the recognition of 4 additional depositional sequences, 1 composite sequence and retrogradational geometry of the Cupidito member.

6) The Sligo Formation of south Texas contains many stratal geometries and structural features that are thought to extend into the Cupido Formation. The two formations shared the same reef trend along the western Gulf of Mexico in the Early Cretaceous. Significant variations in number of high-frequency cycles and thicknesses of depositional sequences between margin depositional sections (e.g. Potrero Garcia and Huasteca Canyon) are interpreted as the result of syndepositional faulting on the outer shelf of the Cupido Formation.

7) Solution-collapse breccias formed because of the dissolution of buried bedded evaporites by percolating continental waters which resulted in the breakage and mixing of the overlying facies. This dissolution process could be repeated for each additional depositional sequence succeeding deposition of evaporates. Each succeeding breccia development would be minor to a lesser degree due to the decreasing amounts of time for exposure to continental waters.

8) Slow drowning of the platform during the 2nd-order transgression, allowed aggradation of platform interior sequences, followed by back-stepping geometries and landward shift in facies as sequence development became a function of diminishing sediment production.

9) A high-resolution sequence stratigraphic analysis of facies partitioning and development of models using 2D correlation, fence diagrams, and subsurface analogues allow development of a refined sequence stratigraphic framework. This high-resolution framework, in turns, reveals subtle complexities of facies models and their controls which is not evident from previous studies. Results can be applied to similar reservoirs for better understanding of facies distribution, models, and their lateral continuity. Results will also add useful insights to future studies of Lower Cretaceous carbonate sequence stratigraphy and the nature of drowning carbonate platforms.

Chapter 3. The origin of meter-scale high-frequency cycles in the Lower Cretaceous Cupido Formation

ABSTRACT

The Lower Cretaceous Cupido Formation (Barremian-Aptian) of northeastern Mexico exhibits thick successions of meter-scale high-frequency shallow carbonate cycles. Facies analysis indicates deposition on a broad shallow-marine shelf lagoon behind a grainstone shoal barrier. High-frequency peritidal to subtidal cycles vary in their thickness, symmetry, facies components and stacking patterns across the shelf. The number of high-frequency cycles is laterally continuous and stack systematically into depositional sequences and large-scale composite sequences that can be correlated across the Cupido platform. Platform-wide high-frequency cyclicity supports a possible allocyclic driving mechanism.

Between Monterrey and Saltillo, six stratigraphic sections encompassing Cupido Formation were studied using Blackman-Tukey spectral analysis. A strong Milankovitch signal appeared when the time series was 'tuned' to precession and a constant sedimentation rate was assumed within each cycle. All of the principal periodicities related to eccentricity (E), both long and short, calculated for Cretaceous times are present: E1 (264-392 kyr), E2 (89-98 kyr), and E3 (107-126 kyr), along with an obliquity component with peaks at periods (38-59 kyr) near double that of the precession, which is a predicted feature of

orbitally-forced insolation at the equator. Strong correlations of Milankovitch signal vertically throughout the entire Cupido Formation and laterally across the platform supports lateral continuity of high-frequency cycles and an external driving mechanism.

External Milankovitch-driven global climatic changes produced low-amplitude, high-frequency sea-level fluctuations, resulting in meter-scale high-frequency carbonate cycles across the shallow Cupido shelf. These results support a global Milankovitch signal during Mesozoic development of cyclic shallow-marine carbonate platforms and possibly greenhouse platforms.

INTRODUCTION

Many carbonate platform depositional environments, such as tidal-flats and shallow-water lagoons, are extremely sensitive to small sea-level changes because of their location close to the shoreline and their generally flat topography (Hardie and Shinn, 1986). Furthermore, because the production of tropical carbonate sediment is related to the type and health of biological communities, carbonate platforms may also respond directly to climatic change as their short-term sedimentation rates are very high relative to rates of subsidence and eustatic change (Schlager, 1981; Enos, 1991). Therefore, sea-level fluctuations and climatic changes of very short duration can potentially be recorded if sufficient accommodation space is created. For these reasons, thick successions of cyclic carbonate platforms would seem to be favorable sites to

look for paleoenvironmental changes over periodicities encompassing the Milankovitch range (10^4–10^6 years).

Nonetheless, the ability of carbonate platforms to register environmental changes, and particularly sea-level and climatic changes produced by Milankovitch orbital periods, is still a matter of debate. The main concerns are related to the possibility that internal sedimentary processes, i.e., autocyclic processes (Ginsburg, 1971; Pratt and James, 1986; Satterley, 1996), as well as tectonic activity (Hardie et al., 1986; Hardie et al., 1991) and stochastic processes (Drummond and Wilkinson, 1993a, b; Demicco, 1998; Wilkinson et al., 1998) might overwhelm, and possibly mimic, Milankovitch-driven sea-level changes through climatic processes (Lehrmann and Goldhammer, 1999; Goldhammer, 2003). The Ginsburg autocyclic mechanism especially is often regarded as fundamental to the production of thick sequences of carbonate high-frequency cycles, although its occurrence and effectiveness still need to be more thoroughly evaluated (Schwarzacher, 1993, 2000).

Extensive and thick successions of cyclic, dominantly peritidal carbonate platforms were deposited at the margins of Tethys during the Mesozoic, with relatively few short interruptions (Bosellini, 1984; Hardie et al., 1986; Goldhammer et al., 1991a; Alsharhan and Nairn, 1993; Wilson and Ward, 1993; Gianolla et al., 1998; Strasser et al., 1999; Lehmann et al., 1998). Recognition of Milankovitch forcing in these successions would furnish crucial information about the nature of Mesozoic climate systems, sedimentary processes and

sedimentation rates, and would provide a precise time scale over intervals where biostratigraphic control remains poor. Moreover, high-precision long-distance correlation among successions may be useful in restoration of ancient sedimentary systems for hydrocarbon exploration purposes.

The Lower Cretaceous Cupido Formation (Barremian to Aptian) exposed within the Sierra Madre Oriental (SMO) exhibits well-developed meter-scale cyclicity and reveals information about platform morphology, facies composition and depositional processes and paleoenvironments (Goldhammer et al., 1991a; Lehmann et al., 1998, 1999 and 2000; Wilson, 1999; Foster, 2003; and Altobi et al., 2004; Altobi et al., *in prep.*). This study of inner platform cyclicity was conducted to evaluate various types of meter-scale high-frequency cycles, and potential mechanisms that explain their origin. Six stratigraphic sections were measured and studied in detail at three localities representing different depositional settings across the platform (Figure 3-1). The objectives of this chapter are to: 1) describe peritidal, shallow and deep subtidal high-frequency cycles across the Cupido platform; 2) evaluate, using spectral analysis, the controlling mechanisms of meter-scale high-frequency cycles (allocyclic vs. autocyclic, periodic vs. random and in particular, the role Milankovitch orbital variations); and finally, 3) illustrate the lateral continuity of stratigraphic cyclicity.

Although focusing on a limited area of the vast deposits of Mesozoic carbonate platforms developed worldwide, these results have important implications about the debate on the origin and characteristics of carbonate

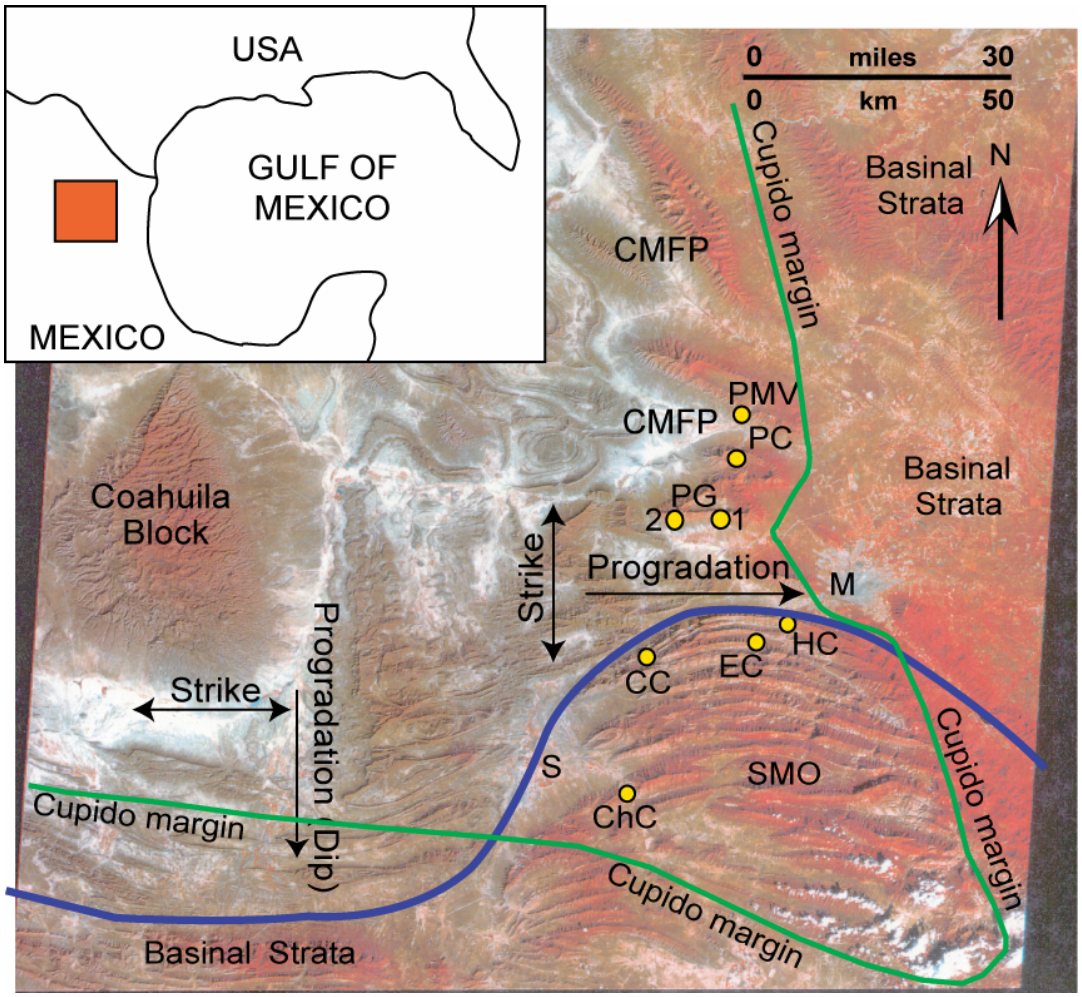

Figure 3-1. Map and Landsat image.

Geographic map and Landsat image illustrating the position of measured sections (yellow circles) relative to the Sierra Madre Oriental (SMO) and the Coahuila block. Monterrey (M) and Saltillo (S) Mexico are shown for orientation. The Coahuila Marginal Fold Province (CMFP) lies northward of the curvilinear thrust front (purple line) of the Sierra Madre Oriental. Anticlines and section names from north to south are Potrero Minas Viejas (PMV), Potrero Chico (PC), Potrero Garcia (PG1 and 2), Huasteca Canyon (HC), Escalera Canyon (EC), Cortinas Canyon (CC), and Chorros Canyon (ChC). Sections used for spectral analysis are Huasteca Canyon (HC), Escalera Canyon (EC), Cortinas Canyon (CC), and Chorros Canyon (ChC). The progradation of the Mesozoic passive margin is toward the east, southeast and south away from the Coahuila block. The platform margin trend (green line) is modified from Wilson (1999) and Foster (2003).

platform cycles, and particularly on their stochastic vs. deterministic (periodic) nature.

Geological Setting

Passive margin development along the Gulf Coast began in the Late Triassic following the continental rifting associated with the opening of the Gulf of Mexico (GoM) (Pindell, 1993; Dickinson and Lawton, 2001). Uplifted blocks of Paleozoic basement and intervening grabens, played an important role in controlling Mesozoic depositional patterns along the Mexican Gulf Coast (Wilson, 1990; Goldhammer, 1999; Dickinson and Lawton, 2001). In northeastern Mexico, the Coahuila block, presently bounded by the Sabinas and Parras basins, served as a persistent basement high and a local source of clastic sediments, which influenced evaporite and subsequent carbonate deposition throughout northern and east-central Mexico (Wilson, 1990).

By the earliest Cretaceous, extensive carbonate platforms developed around the Gulf of Mexico (Goldhammer et al., 1991a; Goldhammer, 1999; Wilson, 1999; Figure 3-2). The Cupido platform was a highly prograding/aggrading platform with a large high-energy shoal complex barrier behind a reefal rudist-coralline bank on the N-S trending margin (Altobi et al., *in prep.*; Figure 3-3) and a high-energy shoal dominated shelf on the E-W trending margin (Lehmann et al., 1999). Protection from wave energy provided by the shoal complex allowed

Figure 3-2. Stratigraphy of northeastern Mexico.

(A) Paleogeography of the Barremian to Lower Aptian in the western Gulf of Mexico, modified from Goldhammer (1999). The Cupido and Sligo platforms are shown in blue. Outline of Mexico and U.S. border is shown in black. The red box outlines the location of the study area.

(B) Chronostratigraphic chart for northeast Mexico and Texas Gulf Coast (modified from Goldhammer, 1999). The composite eustatic curve is from Haq et al. (1987). Time scale is from Hardenbol et al. (1998) and Gradstein et al. (1995). Second-order sequence boundary ages are approximations in Ma. Abbreviations are: LST-lowstand system tracts, TST-transgressive system tracts, HST-highstand system tracts, LSW-lowstand wedge, SMW-shelf margin wedge, MFS-maximum flooding surface. Lithologies are discussed in text, border highlights interval of interest. Pinnacle reefs and buildups are shown as small domes. FW1 and FW2 refer to parts of the La Casita Formation defined by Fortunato and Ward (1982).

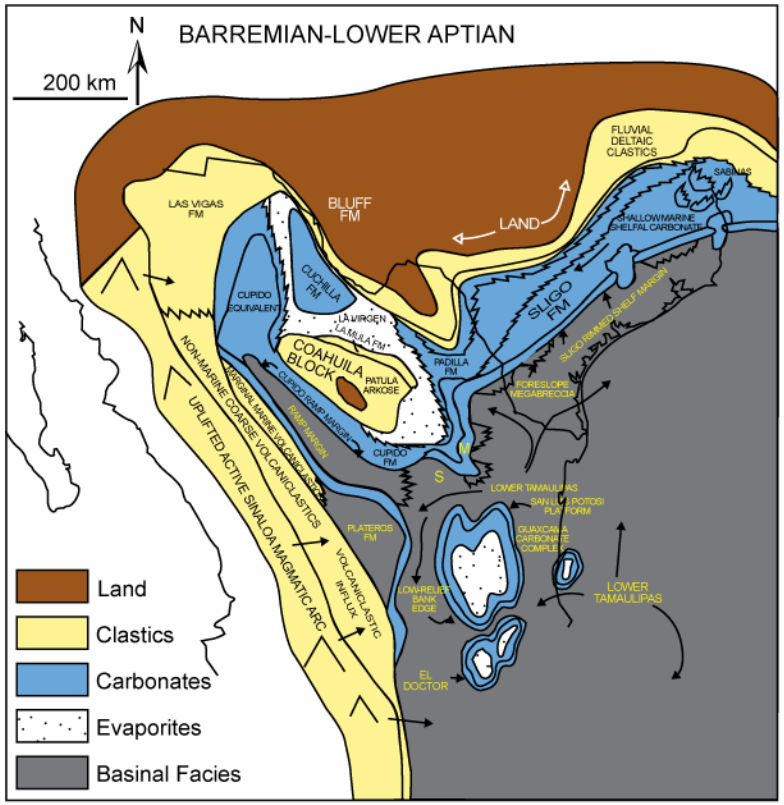
N
BARREMIAN-LOWER APTIAN
200 km
LAND
FLUVIAL DELTAIC CLASTICS
SHALLOW MARINE SHELFAL CARBONATE
LAS VIGAS FM
BLUFF FM
CUPIDO EQUIVALENT
CUPIDO FM
LA VIRGEN
LA MULA FM
SUGO FM
COAHUILA BLOCK
PATULA ARKOSE
PADILLA FM
FORESLOPE MEGABRECCIA
SUGO RAMP-SHELF MARGIN
NON-MARINE COARSE VOLCANICLASTICS
UPLIFTED ACTIVE SINALOA MAGMATIC ARC
VOLCANICLASTIC INFLUX
LOWER TAMAULIPAS
SAN LUIS POTOSI PLATFORM
PLATEROS FM
LOW-RELIEF BANK EDGE
EL DOCTOR
Land
Clastics
Carbonates
Evaporites
Basinal Facies

A

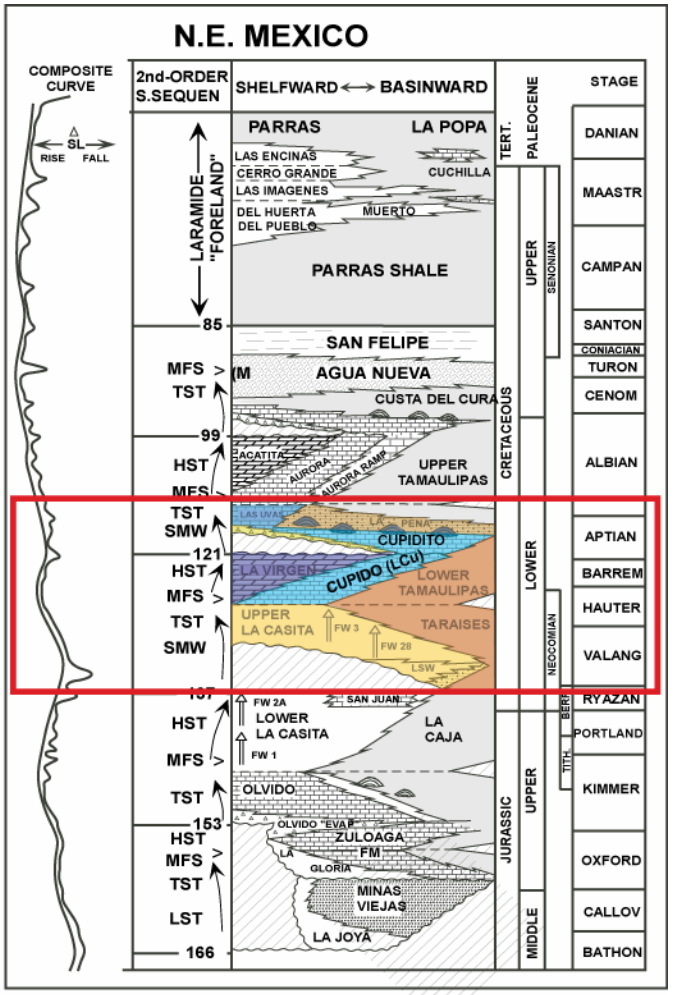
N.E. MEXICO
COMPOSITE CURVE
2nd-ORDER S.SEQUEN
SHELFWARD ⟷ BASINWARD
STAGE
SL
RISE
FALL
LARAMIDE "FORELAND"
PARRAS
LA POPA
LAS ENCINAS
CERRO GRANDE
LAS IMAGENES
DEL HUERTA
DEL PUEBLO
CUCHILLA
MUERTO
PARRAS SHALE
SAN FELIPE
AGUA NUEVA
CUSTA DEL CURA
PACATITA
AURORA
AURORA RAMP
UPPER TAMAULIPAS
LAS UVAS
LA PENA
CUPIDITO
LA VIRGEN
CUPIDO (LCu)
LOWER TAMAULIPAS
UPPER LA CASITA
FW 3
FW 28
TARAISES
LSW
SAN JUAN
FW 2A
LOWER LA CASITA
FW 1
LA CAJA
OLVIDO
OLVIDO "EVAP"
ZULOAGA FM
LA GLORIA
MINAS VIEJAS
LA JOYA
85
99
121
137
153
166
MFS
TST
HST
SMW
LST
TERT.
PALEOCENE
CRETACEOUS
UPPER
LOWER
JURASSIC
MIDDLE
SENONIAN
NEOCOMIAN
BERR.
TITH.
DANIAN
MAASTR.
CAMPAN.
SANTON
CONIACIAN
TURON
CENOM.
ALBIAN
APTIAN
BARREM.
HAUTER.
VALANG.
RYAZAN
PORTLAND
KIMMER.
OXFORD
CALLOV.
BATHON

B

the development of mud-dominated lagoonal facies on the landward side (Figure 3-3). The Cupido Formation (about 800 m thick) consists of a platform interior succession composed of hundreds of meter-scale upward-shallowing carbonate cycles (Wilson and Pialli, 1977; Wilson and Selvius, 1984; Wilson, 1981; Goldhammer et al., 1991a; Wilson and Ward, 1993; Lehmann et al., 2000; Foster, 2003; Altobi et al., 2004; Altobi et al., *in prep.*). Two thirds of the Cupido Formation is regressive, progradational LCu (lower Cupido part) and the upper third is transgressive, aggradational-retrogradational Cupidito member (Wilson and Pialli, 1977). During the Upper Aptian, the Cupido platform was drowned by the deposition of La Peña Shale, which is composed of alternating pelagic carbonates and shale (Tinker, 1985).

PROPOSED MECHANISMS CONTROLLING METER-SCALE HIGH-FREQUENCY CYCLES

Causal mechanisms for meter-scale cyclicity observed in greenhouse Cretaceous carbonates are poorly understood. During greenhouse periods little or no polar ice existed on the continents due to high amounts of carbon dioxide in the atmosphere and the luminosity of the sun (Read, 1995). Climate-controlled sea-level variations (up to 8 m in amplitude) during greenhouse periods have been proposed as a result of thermal expansion and contraction of ocean volumes, and waxing and waning of alpine glaciers and lakes (Jacobs and Sahagian, 1995). Greenhouse conditions have noticeable effects on sea level

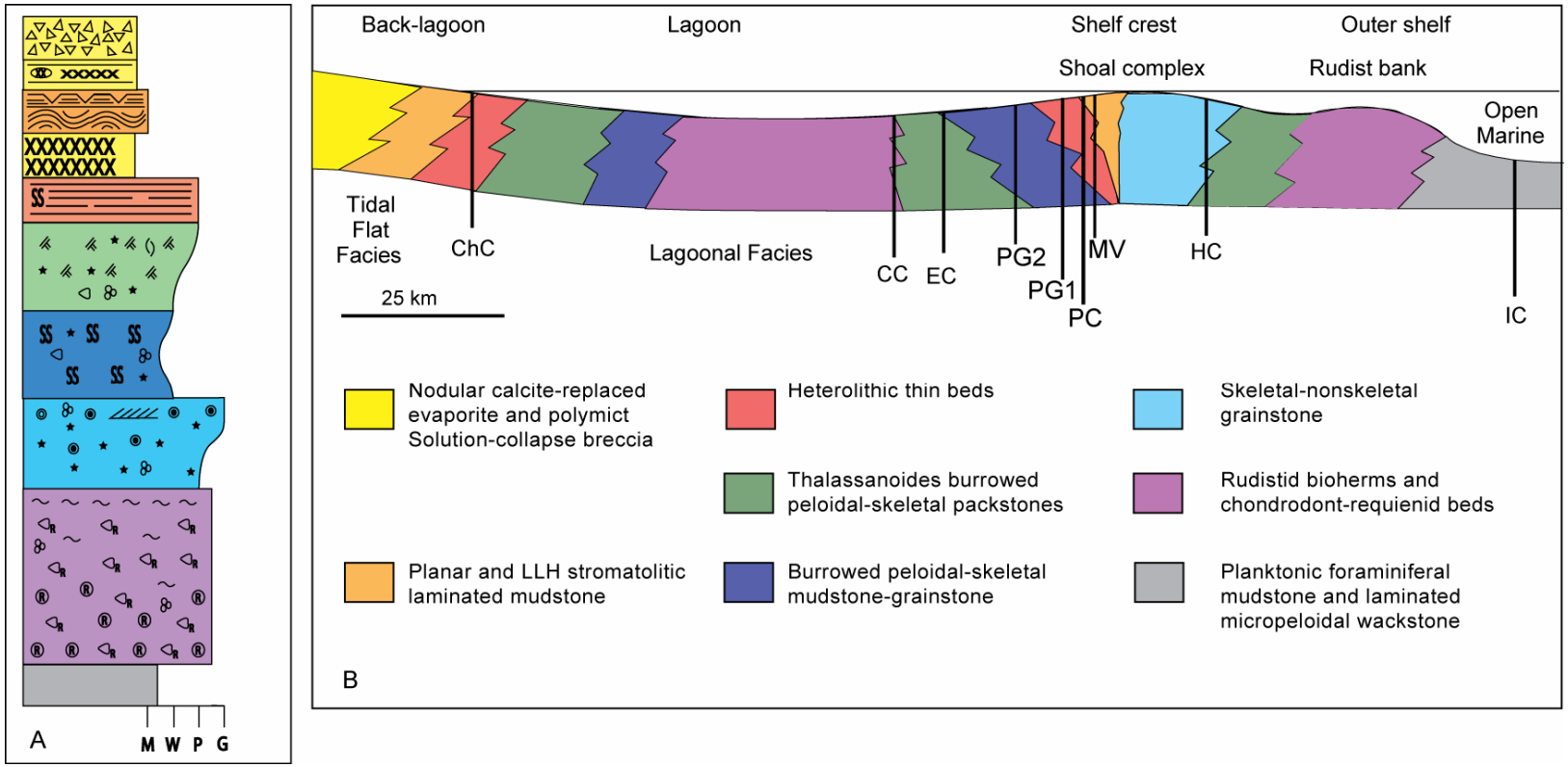

Figure 3-3. Depositional environments across the Cupido platform.

(A) Idealized shallowing-upward succession of the Cupido lithofacies. Key for structures is in Appendix A.
(B) Generalized schematic depositional model of the Cupido platform illustrating the depositional paleo-environments of the measured sections as they would appear projected along a dip oriented profile. The shelf crest is represented by a shoal complex, not a barrier reef. The shoal complex provided a barrier to open marine influx creating a restricted saltern environment. See text for detailed descriptions of major facies belts.

resulting in low amplitude and short-time periods for fluctuations of less than 10-20 m (Koerschner and Read, 1989; Osleger and Read, 1991; Read, 1995; Kerans, 1995; Kerans and Tinker, 1997: Figure 3-4). Sloan and Huber (2001) demonstrated, using general circulation models, that precessional-driven changes in insolation could result in significant variability in net ocean surface moisture balance and the amount of continental runoff at low latitudes during greenhouse conditions similar to northeastern Mexico during the Cretaceous. Because of this, several models, both allocyclic and autocyclic, have been proposed to explain the repetitive nature of upward-shallowing cycles deposited on large shallow-water Cretaceous platforms (Loucks and Longman 1982; Strasser, 1988; Bosellini, 1989; Goldhammer et al., 1991a; Hunt and Tucker, 1993; Röhl and Ogg 1996; Lehmann et al., 1998). Allocyclic models require that processes external to the depositional system are responsible for cyclic deposition. Proposed allocyclic mechanisms include: 1) episodic subsidence (Hardie and Shinn, 1986; Hardie et al., 1991), 2) stochastically induced aperiodic sea-level oscillations (Drummond and Wilkinson, 1993a, b; Demicco 1998; Wilkinson et al., 1998), and 3) Milankovitch-forced glacio-eustatic oscillations (Goldhammer et al., 1987; Berger, 1988; Hinnov, 2000). On the other hand, autocyclic models call upon processes internal to the depositional system, totally independent of external influences, to generate stacked, meter-scale cycles (Ginsburg, 1971; Pratt and James, 1986; Wilkinson et al., 1998).

Along with the rhythmic cyclicity, each mechanism must explain the

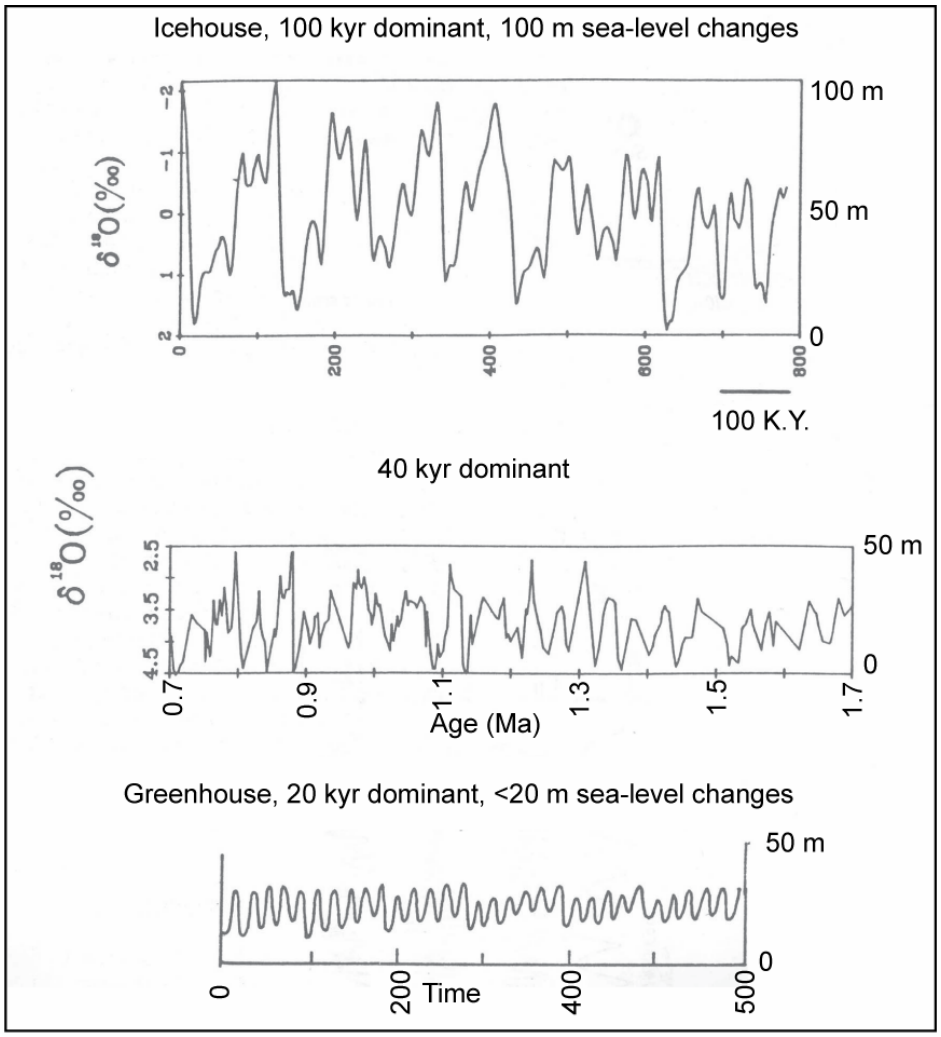

Figure 3-4. Milankovitch driven climate changes.

Amplitude signals from Milankovitch driven climate changes. Amplitudes are in meters on the right with time on the horizontal axis decreasing to the left. The top curve is from ice house oxygen isotopes which are believed to reflect 100 kyr sea-level cycles over the last 700 kyr of the Late Pleistocene (modified from Ruddiman and Wright, 1987). The middle curve is oxygen isotopes of the earlier Pleistocene with lower amplitude and 40 kyr cycles (modified from Ruddiman and Wright, 1987). The bottom curve is inferred greenhouse sea-level amplitudes of around 20 meters for ~20 kyr cycles. Figure modified from Read (1995).

upward shoaling of individual high-frequency cycles, the vertical stacking pattern into sequences, concurrent development of subtidal and peritidal cycles across the platform, and, importantly, model long-term third and 2nd-order temporal variations.

Autocyclicity

Ginsburg (1971) proposed progradation-driven autocyclicity as a possible cause of repetitive stacks of meter-scale high-frequency carbonate cycles. Under constant subsidence and static sea-level conditions, tidal-flat belts prograde over subtidal deposits producing a shallowing upward cycle (Figure 3-5A). In the tidal-flat island model, meter-scale high-frequency cycles represent tidal-flat islands that accreted vertically and migrated laterally as local sediment supply from neighboring subtidal areas waxed and waned during relatively constant subsidence (Pratt and James, 1986). However, Osleger (1991) concluded that eustasy coupled with storm and wave reworking is the dominant control on stacked subtidal cycles' formation. Variability in shifting the focus of carbonate sedimentation and deposition only, cannot explain the persistent lateral and vertical repetition of stacked subtidal cycles (Osleger and Read, 1991; Osleger, 1991)

Stochastic cyclicity

Drummond and Wilkinson (1993a, b) applied statistical analyses to cyclic

Figure 3-5. Autocyclic and allocyclic mechanisms.

Two possible driving mechanisms for cyclic record in carbonates.
(A) Repetition of shallowing-upward cycles by tidal flat progradation (Ginsburg, 1971). Modified from James (1984).
(B) Diagram of Milankovitch orbital forcing of climate, discussed in text. These are considered to be the causes of oscillations in solar radiation which produce high-frequency cycles in the rock record. Modified from House (1995).

A

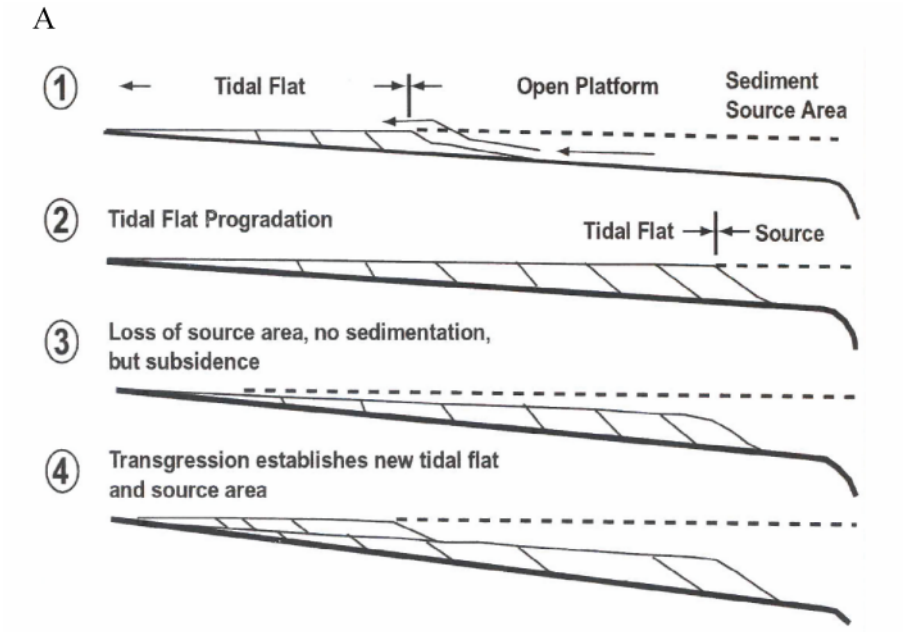

B

OBLIQUITY: the tilt of Earth's axis changes in a 41 ka cycle

PRECESSION: wobble of Earth's axis has a 18 to 23 ka cycle

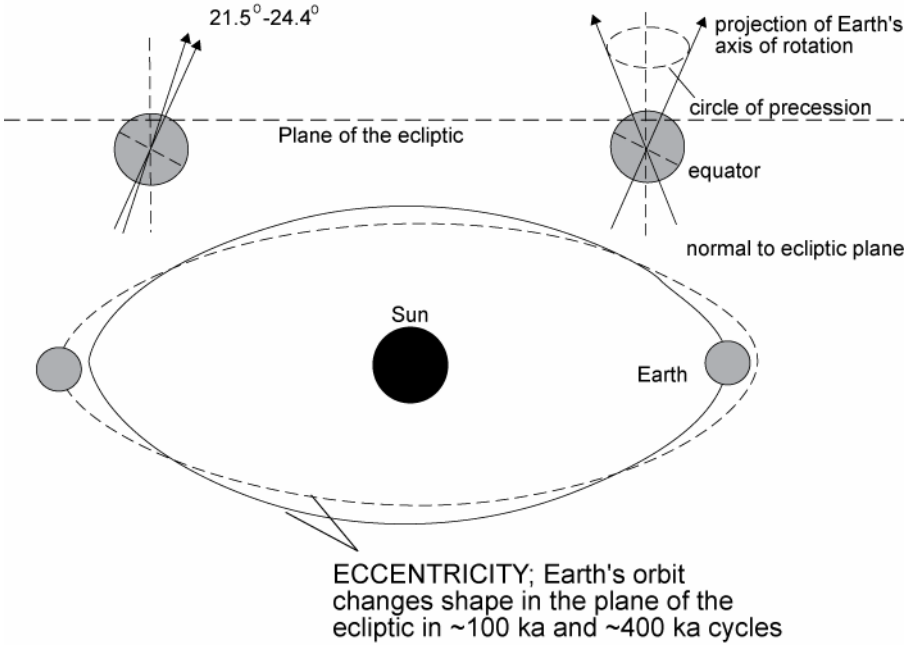

ECCENTRICITY; Earth's orbit changes shape in the plane of the ecliptic in ~100 ka and ~400 ka cycles

carbonate successions and concluded that the vertical arrangement of meter-scale high-frequency cycles and facies is random. Either the periodicity of high-frequency oscillations, the amplitudes, or both may be governed by stochastic forces or autocyclicity, and therefore, are unpredictable. In contrast, Sadler (1993) and Lehrmann and Goldhammer (1999) concluded that there is some element of order to high-frequency cycles which could be age and scale dependant.

Episodic subsidence

Meter-scale high-frequency cycles might be formed by repeated tectonic pulses of uplift (subaerial exposure) and downdropping (submergence) of a shallow shelf area (Hardie and Shinn, 1986). Repeated tectonic pulses of uplift and downdropping would provide accommodation space required for individual high-frequency cycles (Hardie and Shinn, 1986; Hardie et al., 1991). Tectonic pulses can also be random and are expected to produce subtidal and peritidal cycles with limited lateral extent.

Milankovitch-forced oscillations

The simplest explanation for meter-scale high-frequency cyclicity is that it results from high-frequency oscillations in sea level caused by fluctuations in glacial ice volume (Fischer, 1964; Goldhammer et al., 1987; Berger, 1988; Koerschner and Read, 1989). Milankovitch orbital forcing has been proposed as

a potential control of global ice volume and local sea-level changes which produce shallowing upward cycles. Waxing and waning of ice sheets accumulating on land would yield patterns of emergence and submergence across shallow-marine shelves (Hardie and Shinn, 1986). Milankovitch orbital forcing could also affect 1) ocean temperature, ocean water volume, lake storage of water, and 2) climate and carbonate production. The periodicities of meter-scale high-frequency cycles are often compared to Milankovitch orbital periods for eccentricity, obliquity and precession (Figure 3-5B).

CYCLE HIERARCHY OF THE CUPIDO FORMATION

Previous sequence stratigraphic studies of the Cupido Formation are relatively few and have been somewhat general. Goldhammer et al. (1991a) established a regional sequence stratigraphic framework for Middle-Upper Jurassic to Lower Cretaceous strata in northeastern Mexico. This regional sequence stratigraphic framework has since been modified to focus on the Cupido Formation by various studies including Lehmann et al. (1998), Lehmann et al. (2000), Foster (2003) and Altobi et al. (2004). Altobi et al. (*in prep.*) focused on the Cupido outcrops in the SMO near Saltillo and Monterrey to build a comprehensive high-resolution sequence stratigraphic framework. Basin-wide sea-level and climate changes have been proposed as causes of meter-scale high-frequency cycles within the Cupido Formation (Goldhammer et al., 1991a; Lehmann et al., 2000; Foster, 2003; Altobi et al., 2004).

The Cupido Formation is divided into two parts, a thin-bedded progradational LCu and a thicker bedded retrogradational Cupidito member, separated by a 2nd-order sequence boundary (Wilson and Pialli, 1977, Goldhammer et al., 1991a; Goldhammer, 1999; Figures 3-2B and 3-6). The stratigraphically lower part of the platform (Cupido) is composed of a partial composite sequence (HST part) and a full composite sequence (Figure 3-7). A total of six depositional sequences (A-F) are interpreted within the HST part of the Cupido Formation (Figure 3-7). The overlying Cupidito member is composed of a full composite sequence and a partial composite sequence (TST part) that encompass a total of six depositional sequences (G-L; Figure 3-7). These sequences are interpreted and correlated in all measured sections (Figure 3-7; Appendix D). The thickness of individual depositional sequences decreases toward the 2nd-order sequence boundary. This is attributed to a progressive decrease in accommodation space available for sediment accumulation. The Cupidito depositional sequences also exhibit a back-stepping geometry as Sequence K is present across parts of the lagoon and extends landward. However, Sequence L is only interpreted in the most landward part of the platform.

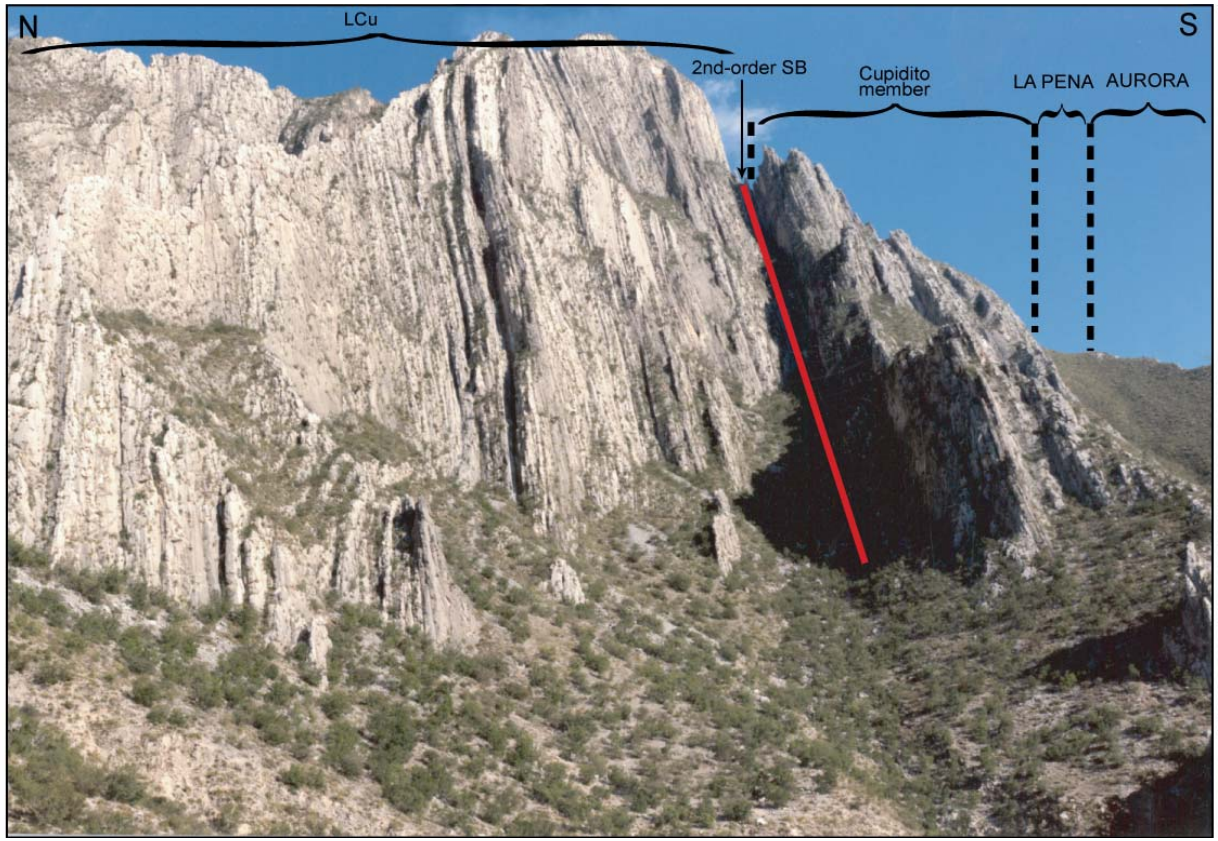

Figure 3-6. Potrero Garcia anticline.

Photo panorama of the measured stratigraphic section in Potrero Garcia, bedding plane is near vertical. The Cupido Formation is a combination of the Cupido, regressive, and the Cupidito, transgressive. The Aurora Formation is not present in the measured section. The 2nd-order sequence boundary (SB) is drawn in red.

Figure 3-7. Sequence stratigraphic framework

Fence diagram combining six measured sections in their relative positions (Chorros Canyon, ChC; CC, Cortinas Canyon, CC; Escalera Canyon, EC; Potrero Garcia, PG1; Potrero Chico, PC; Potrero Minas Viejas, PMV). Lateral correlation of sequences and retrogradational geometry of the platform are evident. Depositional sequences (A-L) and composite sequences (I-IV) and the 2nd-order sequence boundary (SB) are outlined. Red part represents the lower highstand (HST) LCu and the blue part represents the transgressive (TST) Cupidito member. The 2nd-order sequence boundary is used as a datum. La Peña thickness is estimated. Distances in km. Modified from Foster (2003) and Altobi et al. (2004).

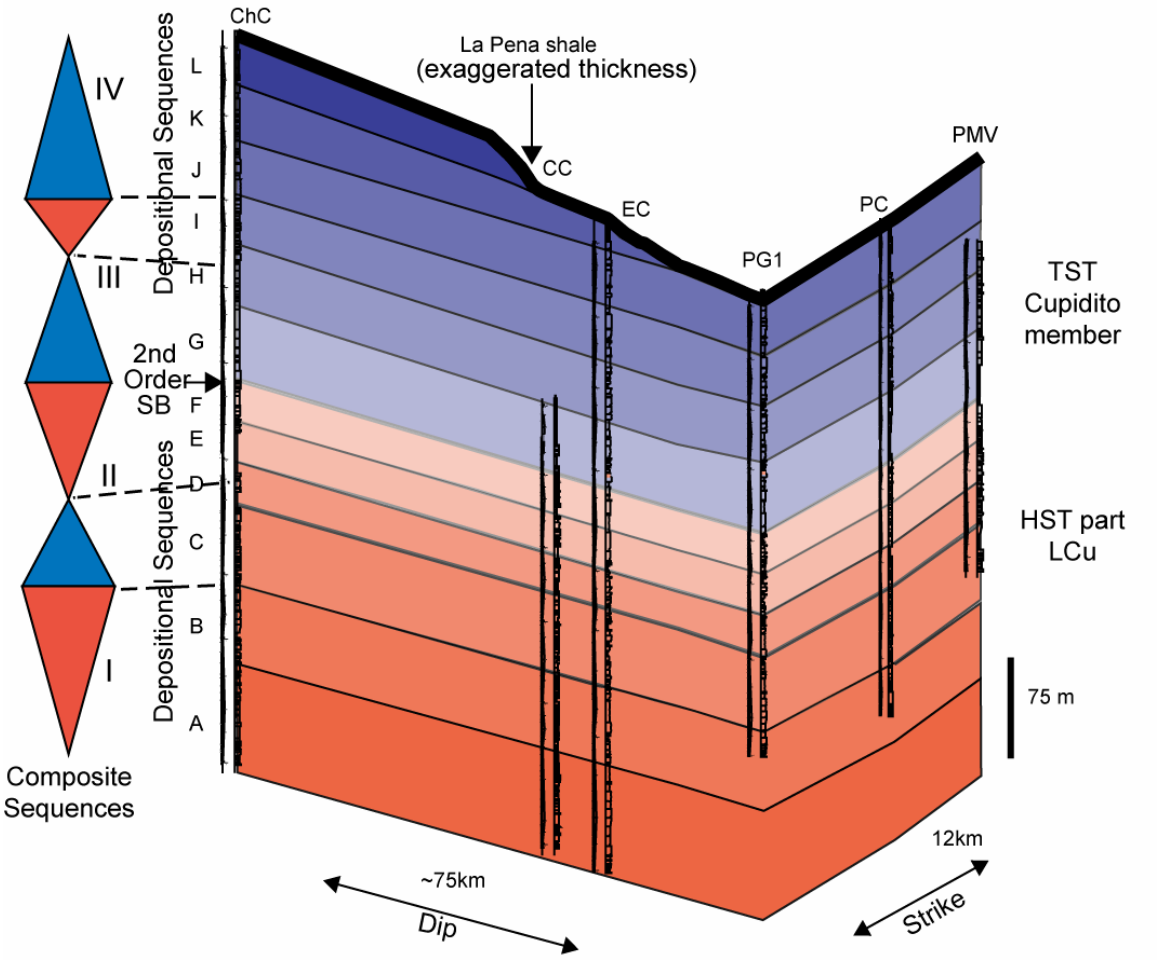

Figure 3-7. Sequence stratigraphic framework

Fence diagram combining six measured sections in their relative positions (Chorros Canyon, ChC; CC, Cortinas Canyon, CC; Escalera Canyon, EC; Potrero Garcia, PG1; Potrero Chico, PC; Potrero Minas Viejas, PMV). Lateral correlation of sequences and retrogradational geometry of the platform are evident. Depositional sequences (A-L) and composite sequences (I-IV) and the 2nd-order sequence boundary (SB) are outlined. Red part represents the lower highstand (HST) LCu and the blue part represents the transgressive (TST) Cupidito member. The 2nd-order sequence boundary is used as a datum. La Peña thickness is estimated. Distances in km. Modified from Foster (2003) and Altobi et al. (2004).

Table 3-1. Summary of facies.

Facies, types, textures, depositional processes and environment and facies-belts of the Cupido Formation. The location of each facies within the idealized shallowing-upward vertical succession is shown in Figure 2-3.

Facies	Subfacies	Occurrence	Color	Rock type & Depositional Texture	Grain Type	Bedding & Sedimentary Structures	Early Diagenetic Features	Depositional Environment
Evaporitic Interior facies	Polymict Solution Collapse Breccia	Common across most parts of the platform	Gray	Polymict breccia with a carbonate mud matrix	Angular clasts, <30 cm, consisting of mudstones, micritized mixed packstones and grainstones	Medium to think bedded, Brecciated	Dissolution by through flowing phreatic water, collapse and rotation of lithified rock fragments	Burial beneath supratidal environment
	Nodular - Mosaic Calcite Replaced Evaporite	Common in the shallow landward parts of the platfrom	White to light gray	Anhedral calcite replaced anhydrite nodules separated by dolomitized micrite	Peloids	Non-bedded, displacive growth distrupts surrounding sediments	Hydration of anhydrite to gypsum, sparry mosaic calcite replacement	Supratidal sabkha
Peritidal to shallow subtidal restricted shelf-lagoon facies	Planar and Stromatolitic Laminated Mudstone	Common across most parts of the platform	Light gray to tan	Dolomitic mudstones to interbedded peloidal wackstones and mudstones	Peloids and pellets	Planar to domal laminations, occasional mudcracks, wispy lenses, and contorted bedding	Fenestral fabric, early lithification dolomitization,and anhydrite precipitation	Quiet, shallow intertidal to subtidal, tidal-flat
	Heterolithic Thin Beds	Common across most parts of the platform	Tan	Alternating peloidal-skeletal grainstones, which are slightly dolomitized mudstones	Peloids (some compacted), fecal pellets, and a variety of skeletal debris	Thin bedded,10 mm, planar to flattened lenticular, no internal cross stratification	Early compaction and occacional amplitude stylolites between layers	low energy, subaqueous, shallow shelf lagoon saltern
	Intercalated Calcite Replaced Evaporite Beds	Common across most parts of the platform	White to light gray	Euhedral calcite and precipitated peloids and micrite	Peloids between crystals	Medium to thinly bedded	Sparry mosaic calcite replacement, stylolitization	Subtidal, shallow marine tidal-flat zone
Shallow subtidal restricted platform facies	Thalassanoides Burrowed Peloidal - Skeletal Packstone	Common across most central parts of the platform	Gray	Euhedral dolomitized micrite with micritized skeletal-nonskeletal W-P matrix with euhedral dolomitized skeletal-non skeletal W-P burrow fill	Peloids, Miliolidae and Vercorsella Foraminifera, mollusk and ostracod debris, and dasycladaceans	Thick to medium bedded, preserved trace fossil networks as irregular boxworks, no preservation of mechanical structures	Early lithification of mictritic matrix to support burrow networks and early dolomitization	Quiet, tide-dominated shallow lagoon/tidal-flat, dominantly open-marine conditions
	Burrowed Peloidal-Skeletal Mudstone - Grainstone	Common across most central parts of the platform	Gray	Dolomitized micritic peloidal carbonate mudstone matrix with dolomitized micrite or mixed skeletal and nonskeletal grainstone fill	Peloids, pellets, composite grains, Miliolidae and Vercorsella Foraminifera, gastrpods, bivalves and dasycladaceans	Thick to medium bedded, some trace fossil are preserved as networks, irregular boxworks, and mottling are common, no preservation of mechanical structures	Early lithification of mictritic matrix to support burrow networks under compaction	Quiet, middle shelf lagoon, to slightly open marine conditions
High energy shoal to rudist-reef margin facies	Skeletal - Nonskeletal Grainstone	Common throughout the platfrom especially across most eastern and southern parts of the platform	White to light gray	Micritized skeletal and nonskeletal grainstones and packstones with sparry mosaic clacite cement and some dolomite	Oncoids, ooids, peloids, composite grains, lumps, intraclasts, Miliolidae and Vercorsella Foraminifera, gastrpods, bivalves, dasycladaceans,echinoderms, bryozoans and ostracods	Thick to medium bedded, cross stratification to massive due to high rates of biogenic reworking	Early calcite cementation in intra and interpartical porosity within the grainstones, compaction within packstones	Active high-energy shelf crest, middle to outer shelf, subject to wave and storm influence
	Rudistid Bioherms and Beds	Common throughout the platform especially across most eastwards parts	Medium to dark gray	Micritized skeletal and nonskeletal packstones	Caprotinide, coral, Caprinidae, bryozoans, Chondrodonta ooids, Requiniidae, ostracods, bivalve shell debris,foraminifera, few peloids dasycladaceans algae, and intraclasts	Massive to thick bedded, no internalcross bedding, rudists are commonly not in growth position	Binding by encrusting algae and early cementation	Below fair weather wave base,dominated shelf edge
Deep subtidal, low-energy off platform facies	Foraminiferal wackestone/ mudstone	Common across most eastern and southern parts off the platform	Dark gray	Bioturbated mudstone and wackstone some dolomitic firmgrounds, hardgrounds and chert nodules	Planktonic Foraminifera, peloids	Thin bedded with some lamination	Early lithification of matrix and early compaction	Below storm wave base in a low-energy oxygenated setting

Variations of high-frequency cycles across the platform

Within the Cupido platform, meter-scale deep subtidal to peritidal high-frequency cycles vary in their component facies and the percentage of those facies across the shelf (Table 3-1; Figure 3-8). High-frequency cycles vary in thickness, facies components and type depending on their relative position laterally across the Cupido shelf, vertically within individual depositional sequences, and the overall sequence stratigraphic framework. The proportion of peritidal to subtidal cycles and the different components of facies within individual high-frequency cycles were used to interpret dominant depositional environment, position within depositional sequences and larger system tract components (Table 3-2). A spectrum of meter-scale high-frequency cycles (1-10 m) from peritidal to deep subtidal cycles are recognized within the Cupido Formation (Figure 3-8). The peritidal cycles are commonly asymmetric with thick subtidal components and a thinner shallow facies or peritidal component. Subtidal cycles are relatively symmetric or contain equal percentages of deep-water and shallow-water facies components and commonly occur in the deep-water portions of the shelf. Subtidal cycles do not contain intertidal caps or exhibit exposure features.

Peritidal cycles related to the land-attached tidal-flats (1.8 m thick average; Figure 3-3) are composed of mixed skeletal packstones followed by *Thalassanoides*-burrowed peloidal wackestones/packstones in turn overlain by

Figure 3-8. High-frequency cycles across the Cupido platform.

Summary of different types of high-frequency cycles (HFCs) across the Cupido platform depending on their depositional setting: A) Peritidal cycle, B) Shallow subtidal cycle, C) shoal peritidal cycle, D) Deep subtidal cycle. Facies key is found in Figure 3. HTB is a heterolithic thin bed.

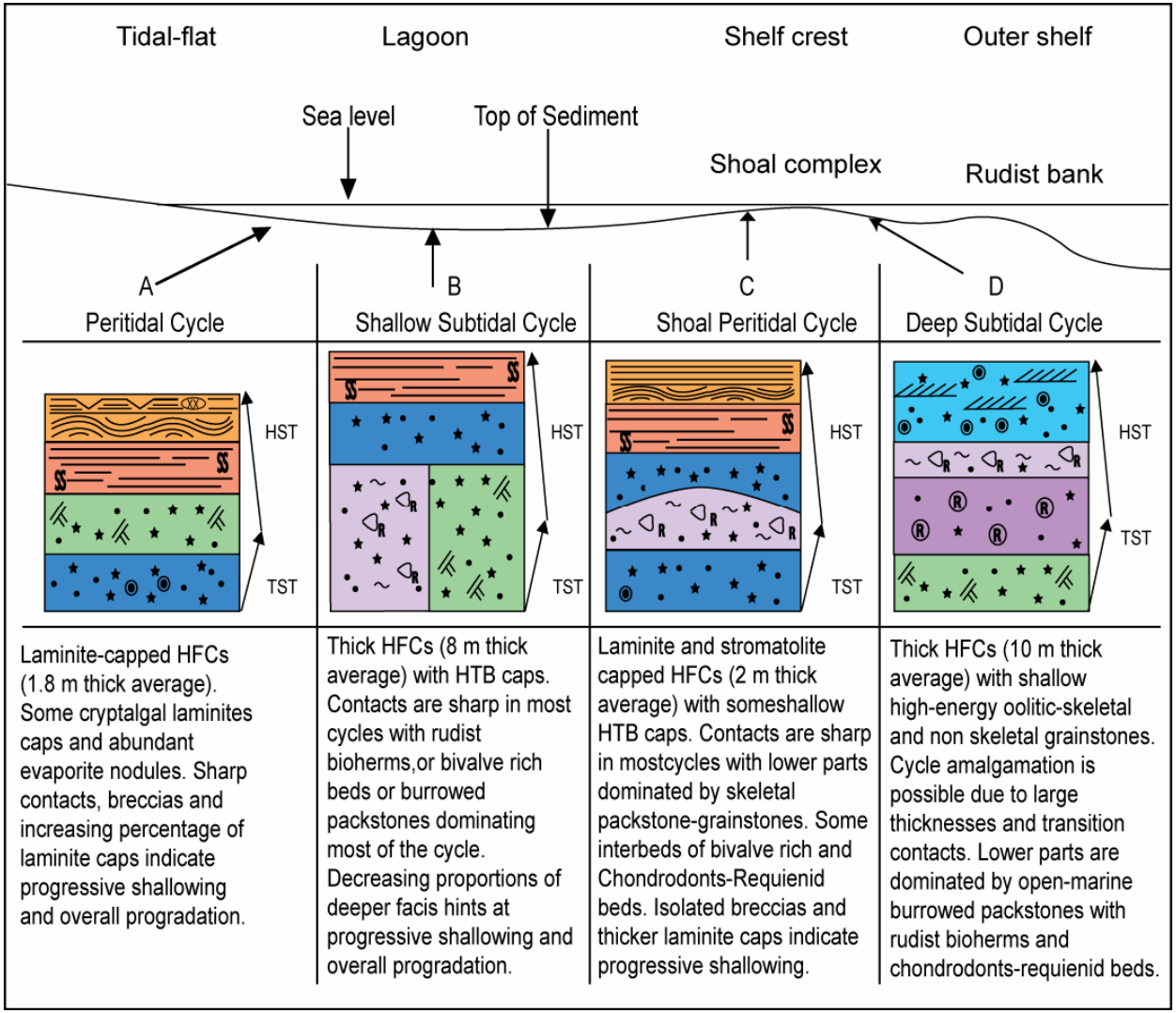
Tidal-flat
Lagoon
Shelf crest
Outer shelf
Sea level
Top of Sediment
Shoal complex
Rudist bank
A
B
C
D
Peritidal Cycle
Shallow Subtidal Cycle
Shoal Peritidal Cycle
Deep Subtidal Cycle
HST
TST
HST
TST
HST
TST
HST
TST
Laminite-capped HFCs (1.8 m thick average). Some cryptalgal laminites caps and abundant evaporite nodules. Sharp contacts, breccias and increasing percentage of laminite caps indicate progressive shallowing and overall progradation.
Thick HFCs (8 m thick average) with HTB caps. Contacts are sharp in most cycles with rudist bioherms,or bivalve rich beds or burrowed packstones dominating most of the cycle. Decreasing proportions of deeper facis hints at progressive shallowing and overall progradation.
Laminite and stromatolite capped HFCs (2 m thick average) with someshallow HTB caps. Contacts are sharp in mostcycles with lower parts dominated by skeletal packstone-grainstones. Some interbeds of bivalve rich and Chondrodonts-Requienid beds. Isolated breccias and thicker laminite caps indicate progressive shallowing.
Thick HFCs (10 m thick average) with shallow high-energy oolitic-skeletal and non skeletal grainstones. Cycle amalgamation is possible due to large thicknesses and transition contacts. Lower parts are dominated by open-marine burrowed packstones with rudist bioherms and chondrodonts-requienid beds.

Table 3-2. Sequence stratigraphic framework summary.

Sequence stratigraphic framework for the Cupido Formation showing the major characteristics of interpreted composite sequences (I-IV) and internal depositional sequences (A-L), system tract components (highstand, HST; Transgressive, TST), dominant facies, type of high-frequency cycles (HFCs) and bounding surfaces: sequence boundaries, (SB); and maximum flooding zone (MFZ).

2nd-order sequence	Composite Sequecne	Average Thickness (m)				System Tract	Comments
		Interior		Margin			
Cupidito member (TST)	IV (TST part)	L K J	125	J	49	TST	MFZ is inferred to be within the La Pena shales Composed of thick open-marine subtidal HFCs with abundant grainstones (some oolitic), beds rich in bivalves, requienids and chondront and rudist bioherms
	III	I	158	I	145	HST	SB is picked at the top thinly-stacked peritidal HFCs below thicker subtidal HFCs A thin interval of dominantly thin peritidal, laminite capped HFCs composed of relatively shallow facies
		H		H			
		G		G		TST	MFZ is interpreted within the thickest shallow subtidal HFCs Composed of thick subtidal, probably amalgamated HFCs with foraminiferal mud-packstone, a few beds rich in bivalves, requienids and chondront and some rudist bioherms/packstone
LCu (HST)	II	F	167	F	169	HST	SB is interpreted as the base of laterally correlative, thick solution collapse breccia atop thin peritidal HFCs Composed mainly of upward thining peritidal HFCs dominated by shallow tidal falt facies
		E		E			
		D		D		TST	MFZ is interpreted within 2 thick shallow subtidal HFCs Composed of thick shallow-subtidal HFCs that are mainly burrowed peloidal-skeletal packstones, thickness of subtidal HFCs decreases upwards
		C		C			
	I (HST part)	B	116	B	117	HST	SB is picked at the top stacked thin bedded peritidal HFCs Composed of massive peloidal-skeletal-oolitic packstones-grainstones and some interbeds of rudist bioherms and packstones. Some subtidal HFCs, but dominantly thin peritdal HFCs
		A		A			

heterolithic thin beds of alternating mudstones and skeletal packstones (Figure 3-8A). The cycles are capped by cryptalgal laminites with some mudcracks and calcitized nodules (originally anhydrite; Table 3-1; Figure 3-9A). The basal skeletal packstones were deposited as skeletal debris that was brought landward and reworked during the initial transgression (TST). As the rate of sea-level rise decreased, bioturbation became more effective at reworking sediments and ultimately produced a cap of peloidal sediment (Figure 3-8A). *Thalassanoides* burrows are commonly filled with the mixed skeletal debris (Figure 3-9B). Heterolithic thin beds were deposited during relative sea-level fall (HST). Thin laminite caps suggest continued shallowing and progradation during highstand. The presence of evaporite nodules on top of cycles implies sabkha-like conditions landward of the laminites (Hardie and Shinn, 1986; Demicco and Hardie, 1994).

Shallow subtidal high-frequency cycles of the lagoon interior (8 m thick average; Figure 3-3) are dominated by *thalassanoides* burrows and bedded *requienids* and *chondrodonts* packstones. They are sometimes overlain by mixed skeletal packstones and capped by burrowed heterolithic thin beds. Other common lagoonal subtidal cycles are capped by *Thalassanoides* burrows or skeletal packstones (Figure 3-8B). The presence of *thalassanoides*-burrow networks (Figure 3-10A) and tidally influenced sediments imply that this facies was deposited in a shallow lagoon just below or within the intertidal zone (Rhoads, 1967; Shinn, 1968). The requienid and chondrodont packstones

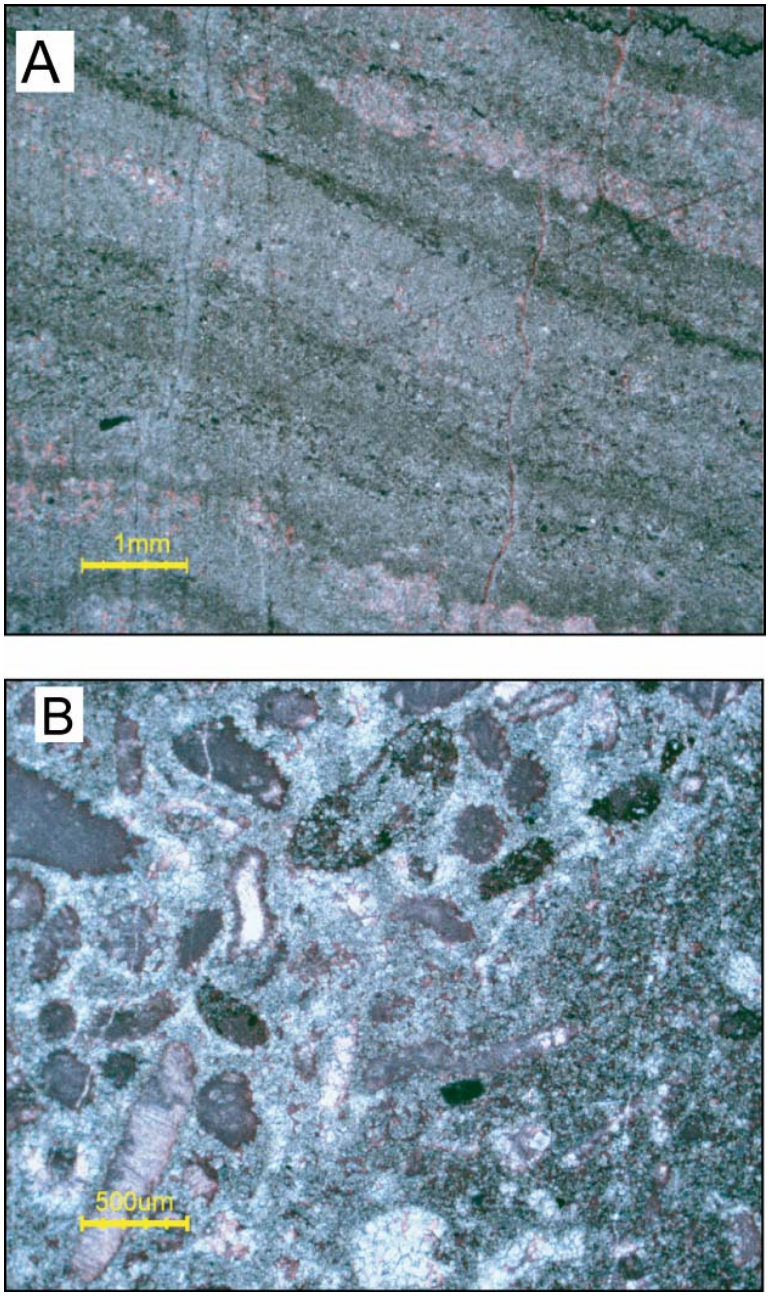

Figure 3-9. Peritidal facies.

Photomicrographs of selected Cupido carbonates. (A) photomicrograph of dolomitized laminated mudstone. (B) photomicrograph of dolomitized matrix, fine grained, and burrow fill, coarse grained.

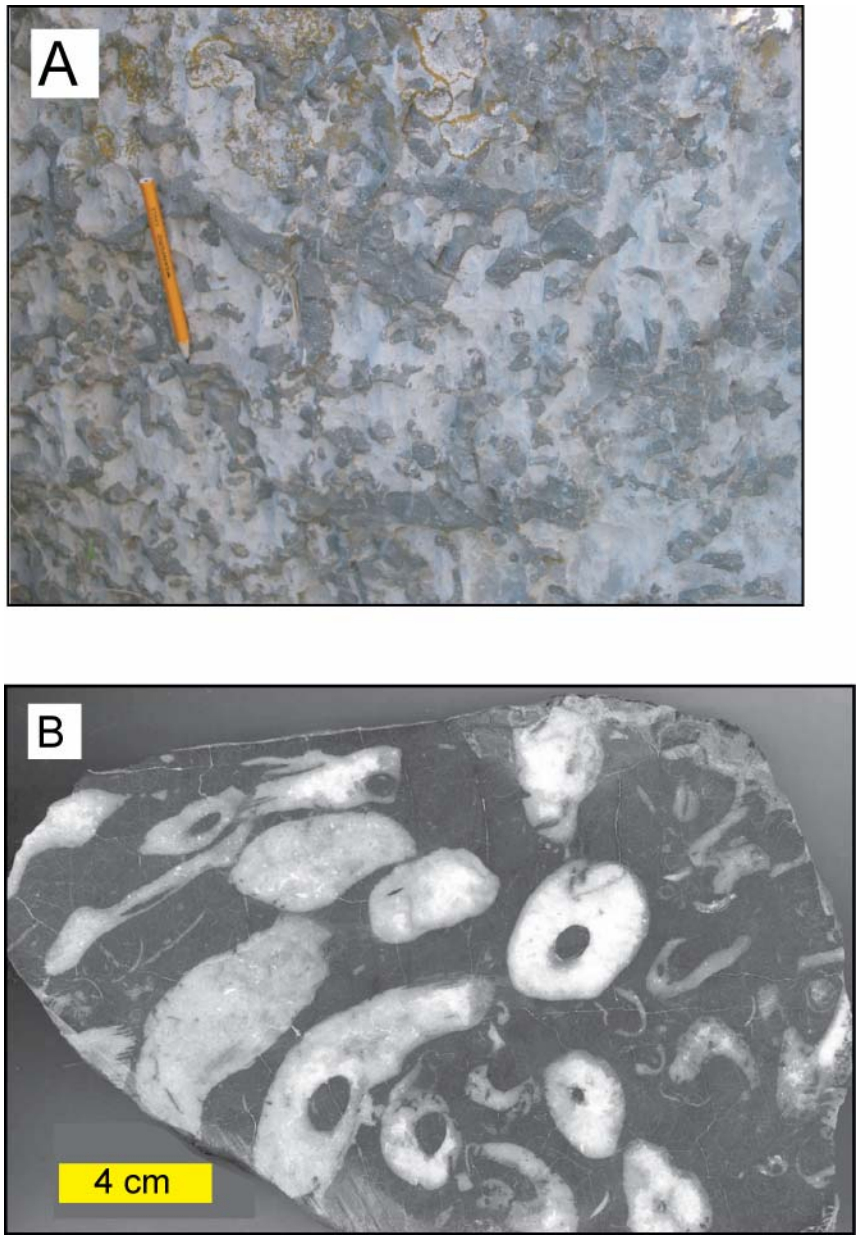

Figure 3-10. Subtidal facies.

(A) Field photograph of *thalassanoides* burrow networks from a bedding plane view. Pencil for scale is 12 cm long.

(B) Hand sample of unoriented *caprinid* rudists in mud rich matrix.

(Figure 3-10 B) develop during transgression (TST) and opening of the marine circulation. The highstand that follows is represented by shallow-water deposition of thin heterolithic beds which lack mudcracks, calcitized nodules or any evidence for exposure (Demicco and Hardie, 1994). Deeper lagoonal pure subtidal cycles without tidal-flat caps are also present (Osleger, 1991).

Peritidal high-frequency cycles, related to the shoal complex (Figure 3-3) on the outer shelf (2 m thick average), and are composed of skeletal and non-skeletal packstones-grainstones capped by laminites or followed by heterolithic thin beds and capped by laminites (Figures 3-8C and 3-11A). Microbial laminites with anhydrite nodules are interpreted as supratidal conditions indicators (HST: Hardie and Shinn, 1986; Demicco and Hardie, 1994). Solution collapse breccias (Figure 3-11B) seen within the section have been interpreted as minimum accommodation indicators and therefore represent high-frequency cycle tops (Warren, 1999).

Deeper subtidal high-frequency cycles (10 m thick average) are found in sections between the shoal complex or shelf crest and shelf margin (Figure 3-3). These cycles have a base composed of skeletal packstones and rarely non-skeletal grainstones. Mounded or isolated patches of *requienids* and *chondrodonts* rudists (TST; Figures 3-8D and 3-12A) overlay and interfinger with skeletal packstones and terminate in dominantly oolitic grainstone caps (HST; Figure 3-8D). The bedded deposits of *requienid*, *chondrodonts*, and *caprinid* rudist packstones sometimes overlie the burrowed sediments and can also be

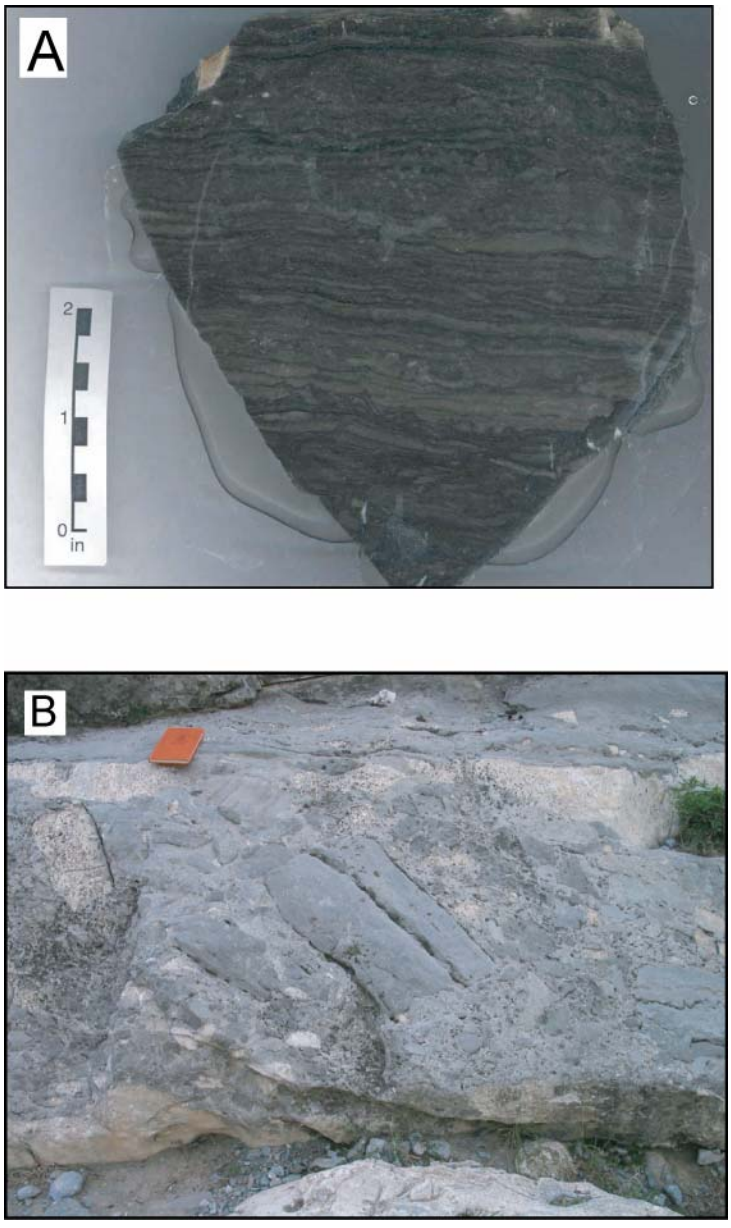

Figure 3-11. Platform interior facies.

(A) Hand sample illustrating the thin laminations on a mm scale, the tan layers are mudstones and the black layers are packstones.

(B) Outcrop photograph of solution-collapse breccias.

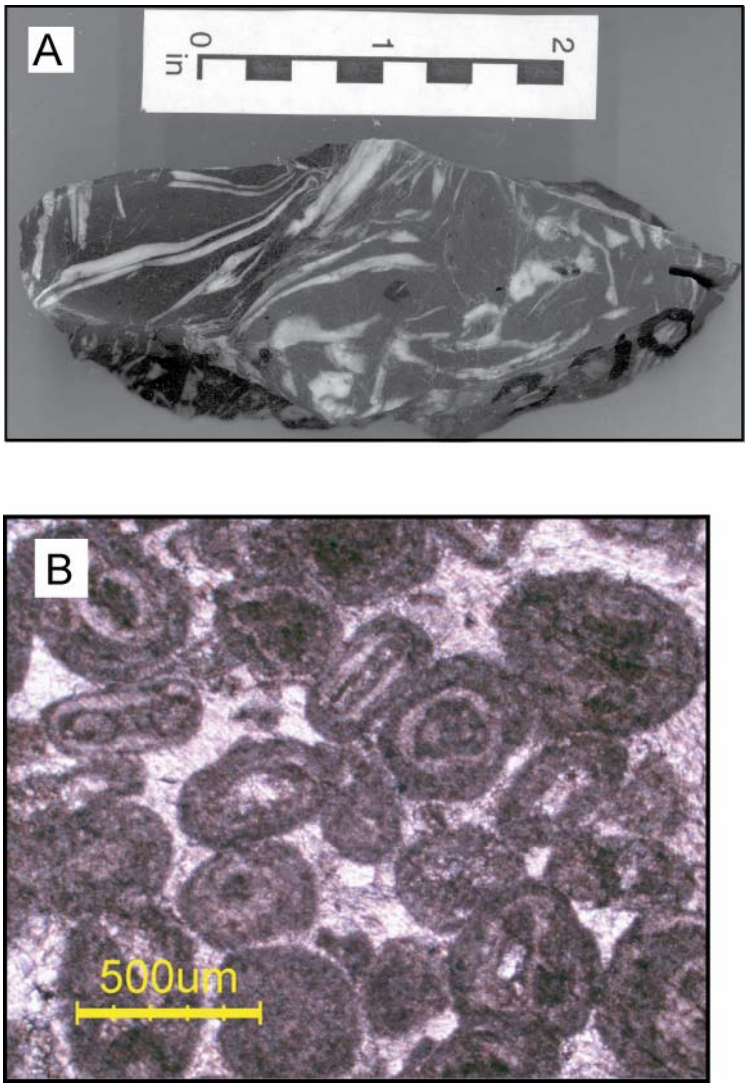

Figure 3-12. Platform margin facies.

(A) Hand sample of *chondrodont* bivalves in mud rich matrix.

(B) Photomicrograph of well sorted grainstone, ooids and lumps with skeletal nuclei.

capped by slightly burrowed to cross-stratified oolitic grainstones (Figure 3-12B). Pure subtidal cycles (Osleger, 1991) are abundant in outer shelf sections.

Peritidal high-frequency cycles attached to land and those attached to the shoal and subtidal cycles in the lagoon are time-correlative according to their positions within larger sequences. Notably while all cycles shallow upward, the peritidal cycles shoal up to sea level but the subtidal cycles of the lagoon did not always fill the available accommodation space. Most of the high-frequency cycles recognized in the Cupido are asymmetric with thin transgressive basal facies and thick regressive upper facies indicating steady shallowing (Goldhammer et al., 1991a; Altobi et al., *in prep.*). Vertical variations in thickness (stacking pattern) and facies components of high-frequency cycles stack vertically reveal a lower order cyclicity pattern (Table 3-2; Figure 3-13).

ORIGIN OF HIGH-FREQUENCY CYCLES IN THE CUPIDO FORMATION

Distinguishing between autocyclic and allocyclic processes is a key step in interpreting of the origin of meter-scale high-frequency cycles of the Cupido Formation. Autocyclic processes are internally caused by changes within a sedimentary system, whereas, allocyclic processes are system changes caused by external forces.

One potential external forcing mechanism is tectonic subsidence/uplift. Growth faulting (Hooker et al., 2002) provided accommodation space for extra high-frequency cycles near the Cupido margin (Altobi et al., *in prep.*). However,

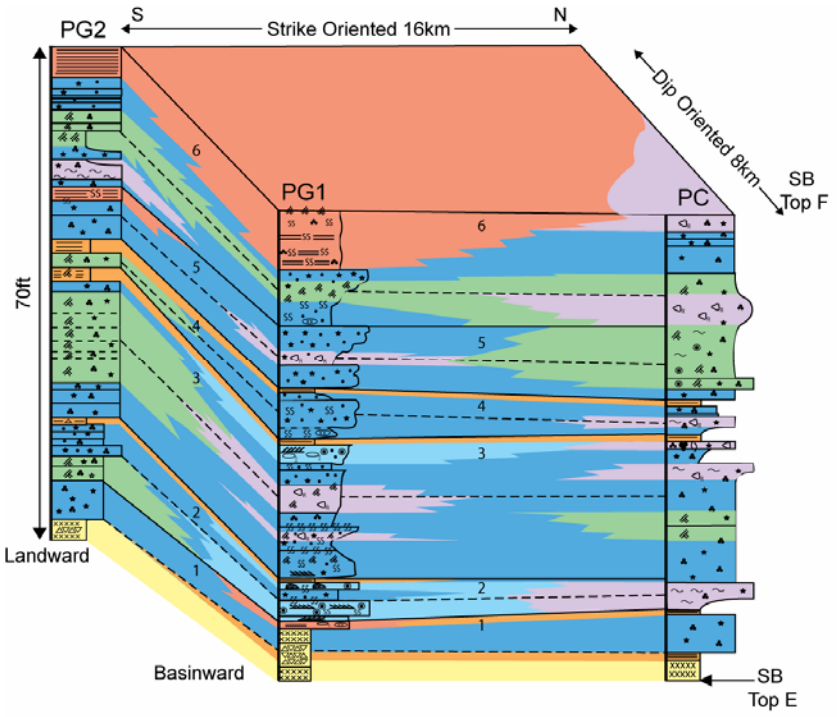

Figure 3-13. Cycle stacking and lateral continuity.

Block diagram of Sequence F (above sequence boundary (SB) E, high-frequency cycles 1-6, composed of correlated sections PG2, PG1, and PC (left to right: Figure 1). High-frequency cycles stack vertically and correlate laterally with closely-spaced measured sections cutting across cycle boundaries. A facies key can be found in Figure 3-3. Solid correlation lines represent cycle boundaries and dashed correlation lines represent the approximate position of flooding surfaces. Cycles are numbered according to their position in the stratigraphic section.

these faults have a limited spatial distribution and small displacement, so they fail to explain the widespread cyclicity seen within the Cupido carbonates. Added to this, an active tectonic setting would be required to produce such shallowing-upward high-frequency cycles.

A potential internal forcing mechanism is autocyclicity. In Ginsburg's (1971) model, cycles should be laterally continuous, asymmetric, tidal-flat capped, of constant thickness and display no significant progradational or retrogradational facies shifts in the two-dimensional stacking patterns. For the Pratt and James (1986) island autocyclic model, cycles should be laterally discontinuous, asymmetric, tidal-flat capped, and of varying thickness. Within the Cupido Formation, characteristics of high-frequency cycles support an allocyclic origin as indicated by the following observations:

1) Both peritidal and subtidal cycles are interpreted across the margin with peritidal cycles being the dominant type in certain parts (Figure 3-8).

2) High-frequency cycles are laterally continuous and correlate across facies tracts (Figure 3-13).

3) Both symmetric and asymmetric high-frequency cycles are seen in different parts of the platform (Figure 3-8).

4) Most cycles are capped by tidal-flat facies, however, incomplete subtidal cycles (pure subtidal cycles that lack tidal-flat caps) were also interpreted within the Cupido Formation.

5) High-frequency cycle thickness is highly variable and ranges from 1 m to 10 m (Figure 3-8) indicating highly variable sedimentation rates.

These observations and interpretations support an allocyclic origin for the high-frequency cycles of the Cupido Formation, but they provide very little information about the allocyclic process that determined their origin. Clues can be obtained through time-series analysis, which require a reasonably long and continuous cyclic series to be analyzed. For example, spectral analysis is a widely used statistical tool in cyclostratigraphy to detect hidden periodicities in noisy temporal (or spatial) series derived from stratigraphic sequences at outcrops or boreholes (Hinnov, 2000).

Time series analysis

Time series analysis provides tools for recognizing Milankovitch frequencies within cyclic platform carbonates (Einsele et al., 1991; Hinnov and Goldhammer, 1991; Hinnov, 2000). Spectral analyses of sedimentation rate-cumulative time series (constant sedimentation rate within individual high-frequency cycle assumed to represent equal time duration) from measured stratigraphic sections were performed to detect the presence of cycle periodicity and quantify their frequency and amplitude (Bloomfield, 1976). The frequencies of periodic components can then be compared to known Milankovitch frequency ratios to determine compatibility. Six stratigraphic sections were measured and studied in detail at four localities representing different depositional settings

across the platform (Figures 3-1 and 3-3). Three are located at Chorros Canyon (ChC: tidal flat; Figure 3-14), one at Cortinas canyon (CC: lagoon), one at Escalera Canyon (EC: lagoon), and another section at Huasteca Canyon (HC: platform margin). In most localities, most of the Cupido Formation, if not all, is exposed and accessible. For high-resolution statistical analysis, each section was measured at the centimeter scale documenting thickness, color, grain size, lithofacies, depositional texture, biota, sedimentary structures and any evidence for subaerial exposure for each bed. The total length of the sections ranged from 177 m to 679 m (ChC M: 274 m; ChC S: 347 m; ChC N: 270 m; CC: 177 m; EC: 679 m; HC: 251 m; Appendix A). The sections expose a continuous cyclic succession of the Cupido Formation, and were chosen to compare and contrast dominant meter-scale cycles and their driving mechanisms across the platform.

The interior deposits of the Cupido platform outcrops offer a great opportunity to test cycle periodicity, as they are characterized by the repetition of a discrete number of facies, as opposed to the extremely complicated facies (Altobi et al., *in prep.*). In addition to providing valuable statistical information, sedimentation rate-cumulative time series analysis of the Cupido Formation is useful for the following purposes. 1) Detecting superimposed frequencies and hierarchy of stratigraphic cycles from stratigraphic data. 2). Offering information about the lateral extent and variations of Milankovitch forcing because high-frequency cycles are present at all five stratigraphic measured sections and

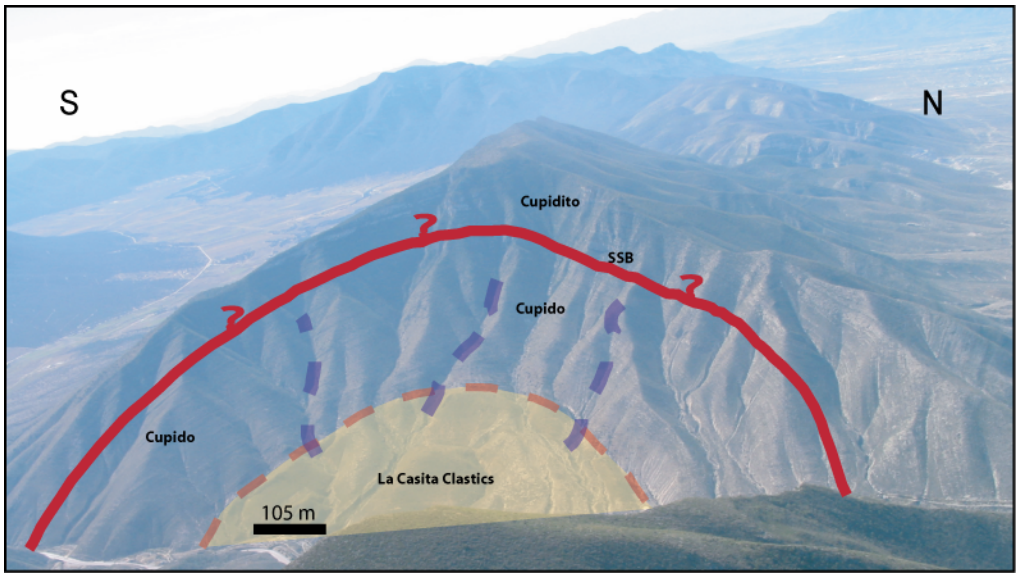

Figure 3-14. Chorros Canyon.

Aerial photograph of Chorros Canyon (ChC), SMO near Saltillo, with locations of measured stratigraphic sections (dashed purple lines). The Cupido Formation is a combination of the Cupido, regressive part, and the Cupidito, transgressive part. The Cupidito transgressive portion is difficult to measure within the anticline and it therefore was measured along the road cut. The solid red line represents the approximate location of the 2nd-order sequence boundary (SB). Photo taken by Goldhammer (2002).

correlate across the platform. 3) Providing a wavelength signal for a specific (e.g., precession or obliquity) or a mixed (e.g., allocyclic and autocyclic) orbital forcing mechanism for high-frequency cycles in the Cupido Formation (Hinnov, 2000).

Herein, numerical representation of the rock record is created using sedimentation rate-cumulative time series (similar in principle to cycle-thickness series of Goldhammer et al. 1987; Hinnov and Goldhammer 1991). The rock record is converted into a time series by assuming an equal duration for each high-frequency cycle (18.4 kyr, Milankovitch precession period during the Cretaceous: Berger et al., 1992). Precession was chosen as the dominant cycle period because of field observations (low average high-frequency cycle thickness) and previous conclusions from Cretaceous sections (Goldhammer et al., 1991a; D'Aregenio et al., 1997; Lehmann et al., 1998) and Triassic carbonate platforms (Goldhammer et al., 1987; Preto and Hinnov, 2003; Zühlke, 2004). Within each cycle, a second assumption is that the sedimentation rate is constant during each cycle, regardless of lithofacies. Additionally, I assume that no significant hiatuses occurred during deposition. Sedimentation rates of individual high-frequency cycles give the variable used in time-series analysis and register time variations in accommodation space (Goldhammer et al., 1990). Cycles are defined by vertical facies shifts and subaerial exposure surfaces and are recognized mainly during field work.

Using POWGRAF2 program (see Pardo-Igúzquiza and Rodriguez-Tovar, 2004, for details), Fourier transform converts the sedimentation rate-cumulative time series into a frequency spectrum based on cyclic sinusoids, thereby quantifying the relative amplitudes of individual frequencies representing groups of cycles in the form of their power spectrum using a variety of methodologies. In this study, smoothed periodogram (Papoulis, 1984; Pardo-Igúzquiza and Rodriguez-Tovar, 2004) and Blackman-Tukey approaches (Blackman and Tukey, 1958; Pardo-Igúzquiza and Rodriguez-Tovar, 2004) were used. To show dominant cyclicity, frequency is converted into period (kyr) and the spectra are compared to red noise and its 90%, 95%, 99% statistical confidence limits (Figure 3-15).

Limitations

Sedimentation rate-cumulative time series analysis assumes a complete cyclic record in which each cycle equates directly to a sea-level pulse. This assumption limits this analysis as the corresponding stratigraphic record may not preserve every pulse, regardless of their driving force, due to complexity of sedimentation.

Sedimentation rate-cumulative time series cannot be used to investigate directly the generating process of the high-frequency cycles, because the frequency of such a process falls beyond the highest frequency represented in

Figure 3-15. Spectrum of sedimentation rate-cumulative time series.

Chorros Canyon South (ChC S) stacked cycle series and precession tuned spectrum.
(A) Stacked high-frequency cycles interpreted from Chorros Canyon South section. Horizontal axis is position within the section and vertical axis is relative thickness of individual cycles.
(B) Tuned spectra of Chorros Canyon South section obtained by Blackman-Tukey spectral analysis. Highly-significant peaks (above 90% confidence limit) are labeled.

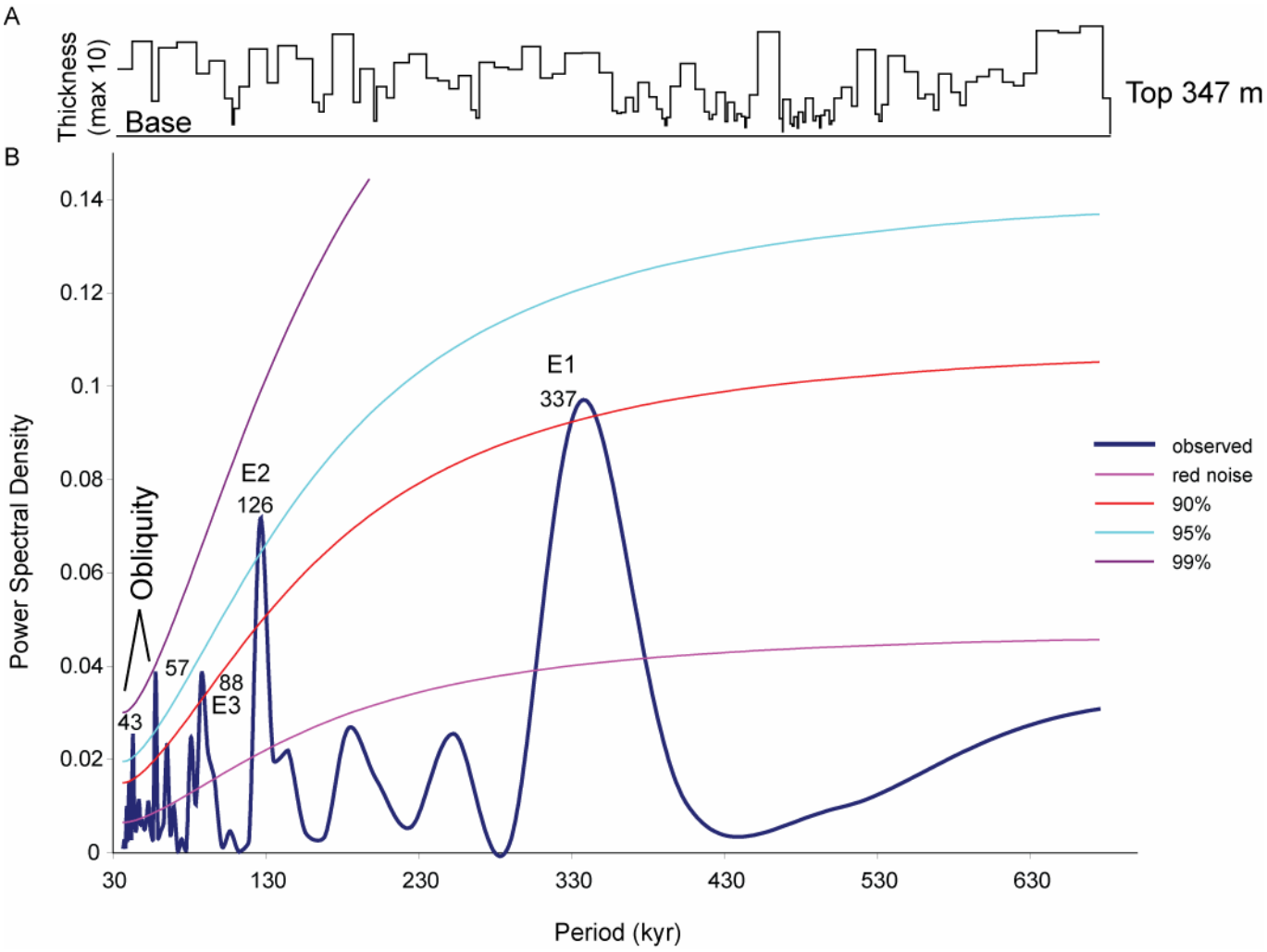
A
Thickness (max 10)
Base
Top 347 m
B
Power Spectral Density
0.14
0.12
0.1
0.08
0.06
0.04
0.02
0
Obliquity
43
57
88
E3
E2
126
E1
337
30
130
230
330
430
530
630
Period (kyr)
observed
red noise
90%
95%
99%

the series. This holds true for all processes that may have operated at wavelengths shorter than that of two successive high-frequency cycles. As a result, careful interpretations of results are needed for the following reasons.

1) The assumption of equal cycle duration should not generally be held (Hinnov, 2000; Preto and Hinnov, 2003). Metronomic analysis (Hinnov, 2000) contemplates a hypothesis that considers the natural duration variability of orbital cycles, but requires that all high-frequency cycles represent orbital cycles. This approach, however, does not fully exploit the thorough information provided in the facies of shallow-marine carbonate platforms, such as those in the Cupido Formation, in reconstructing continuous, fine-scale paleoenvironmental signals.

2) A cycle is typically constructed by the stacking of different lithofacies, which have variable sedimentation rates (Kominz and Bond, 1990). A lithofacies-rank series (Olson, 1986; D'Argenio et al., 1997; Preto and Hinnov, 2004) contains more information than the sedimentation rate-cumulative time series.

3) Subtidal cycle amalgamation and 'missed beats' are common in shallow platform carbonates (Hardie and Shinn, 1986; Koerschner and Read, 1989; Goldhammer et al., 1990). Here, sediments do not aggrade to sea level within each sea-level pulse and therefore, the cycle does not register subtidal deposition to exposure or tidal-flat deposition (Koerschner and Read, 1989; Goldhammer et al., 1990).

4) If a specific orbital forcing mechanism (e.g., precession) is suspected as a dominant driver for sea-level oscillations, which in turn provide

accommodation space and a constant sedimentation rate for individual cycles, then its indirect assessment is possible through the analysis of frequency and/or time modulations expressed in the sedimentation rate-cumulative time series (Hinnov, 2000). But if a mixed orbital signal was the source of the forcing with or without variable sedimentation rates, then an individual cycle would be expected to contain a mix of frequency and time modulations that cannot be evaluated by a sedimentation rate-cumulative time series alone.

Despite the limitations above, time-series analysis, such as spectral analysis, offers the best techniques to determine the possible allocyclic process behind cyclic shallow-marine carbonate platforms.

RESULTS

I hypothesize that high-frequency cycles have a constant duration equal to precession periodicity and that sedimentation rate is constant within individual cycles. Under this hypothesis, the spectrum is tuned to a frequency of 1 cycle/kyr (i.e., the short precession frequency calculated for Lower Cretaceous by Berger et al., 1992). Therefore other frequencies related to the Milankovitch forcing (eccentricity and obliquity) should appear as sharp peaks in the spectrum. If the hypothesis does not hold, then tuning of the time series according to precession should not result in any sharp peaks at non-Milankovitch frequencies, or any other systematic frequency. Herein, the frequency is converted into time and all the plots are shown in period (kyr).

The ‘tuned’ sedimentation rate-cumulative time series and its power spectrum are shown for Chorros Canyon South section in Figure 3-15B. High spectral density peaks are observed at 337, 126, 88, 53 and 43 kyr, the predicted periods of long eccentricity (E1: labeled as in Hinnov, 2000), short eccentricity (E2 and E3: labeled as in Hinnov, 2000) and obliquity times, respectively. The peaks at 53 and 43 kyr can be interpreted as a double beat of obliquity, as expected from insolation at the equator (Berger and Loutre, 1997) with most of the power concentrated in the higher period (53 kyr). The spectral density peak values are well above the 90% confidence limit for red noise, indicating statistically significant deviation from random (Figure 3-15).

In summary, the observed distribution of spectral peaks in the sedimentation rate- cumulative time series strongly supports the hypothesis that Milankovitch cycles forced the deposition of the Cupido Formation. The presence of Milankovitch signal can be further tested by tuning and filtering techniques beyond the scope of this chapter. However, I carried out the same analysis to check for signal continuity in three other different depositional settings and paleoenvironments.

1) Testing for vertical continuity of Milankovitch signal for the entire Cupido Formation section at Escalera Canyon using sliding window approach (After Stage, 1999)

The entire Cupido section at Escalera Canyon (Figure 3-1; Appendix A) was analyzed using the Blackman-Tukey (Blackman and Tukey, 1958) spectral

analysis. The section was divided into six overlapping windows and data in each window were analyzed independently using the technique described above (Figure 3-16). The sliding window approach helps in minimizing variations in sedimentation rates by focusing on specific parts of the section at discrete times. Sedimentation rates vary depending on position within the larger sequence and system tract (Schlager, 1989). Moderate random variations from mean sedimentation rate can alter the spectrum slightly, but original signal peaks are still highly significant (Schwarzacher, 1989; Stage, 1999).

The analysis reveals a persistent Milankovitch signal throughout the entire section (Figure 3-16). High spectral density peaks are observed at long (E1) eccentricity (336-392 kyr), short (E2 and E3) eccentricity (89-123 kyr) and obliquity (39-57) periods (Figure 3-16). Variations occur in period and power of the spectral peaks, however, most of the variation in period is limited to known Milankovitch bandwidths (Figure 3-16). Again, the labeled spectral density peak values are well above the 90% confidence limit for red noise (Figure 3-16).

The same peaks are present in the power spectra for all windows, which is interpreted as an indication that the high-frequency cycles are robust and not limited to the special intervals of the stratigraphic column (Stage, 1999; Zühlke, 2004).

Figure 3-16. Sliding window spectral analysis.

Blackman-Tukey spectral analysis of entire Cupido Formation section exposed at Escalera Canyon (Figure 3-1) using the sliding window approach (see text for details). Color bars indicate vertically correlated spectral peaks at known Milankovitch periods. Labeled peaks are highly-significant (above the 90% statistical confidence limit). Horizontal axis is stretched to better show condensed peaks at lower periods.

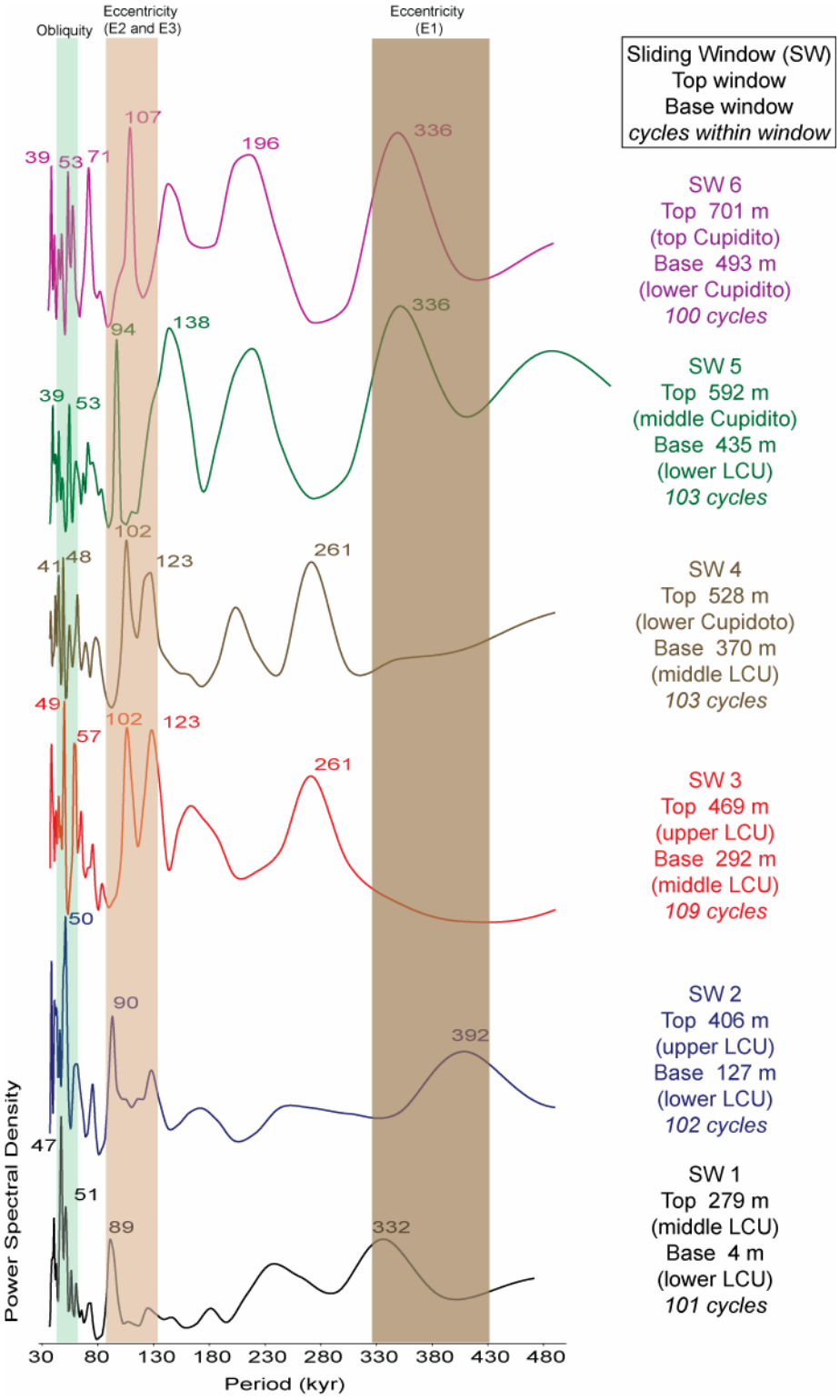
Obliquity
Eccentricity (E2 and E3)
Eccentricity (E1)
Sliding Window (SW)
Top window
Base window
cycles within window
39
53
71
107
196
336
SW 6
Top 701 m
(top Cupidito)
Base 493 m
(lower Cupidito)
100 cycles
39
53
94
138
336
SW 5
Top 592 m
(middle Cupidito)
Base 435 m
(lower LCU)
103 cycles
41
48
102
123
261
SW 4
Top 528 m
(lower Cupidoto)
Base 370 m
(middle LCU)
103 cycles
49
57
102
123
261
SW 3
Top 469 m
(upper LCU)
Base 292 m
(middle LCU)
109 cycles
47
50
90
392
SW 2
Top 406 m
(upper LCU)
Base 127 m
(lower LCU)
102 cycles
51
89
332
SW 1
Top 279 m
(middle LCU)
Base 4 m
(lower LCU)
101 cycles
Power Spectral Density
30
80
130
180
230
280
330
380
430
480
Period (kyr)

Period variability is probably caused by subtle variations in sedimentation rates or orbital forcing periods (Yang et al., 1995; Hinnov, 2000). Autocyclic processes can not be rules out completely and they alone or maybe coupled with tectonics might be responsible for peak variations. The variations in peak periods for E1 in windows 3 and 4 (SW3 and SW4) might also be because of missing cycles (e.g. missed beats) below and above the 2nd-order sequence boundary.

2) Testing for lateral continuity of Milankovitch signal between closely spaced section in a tidal-flat depositional environment (Chorros Canyon)

Three stratigraphic sections were measured at shortspacing (less than 150 m apart) at Chorros Canyon (Figures 3-1 and 3-14). Blackman-Tukey spectral analysis of sedimentation rate-cumulative time was applied to the sections. Signal correlation between the sections supports the hypothesis of an external control on high-frequency cyclicity.

High spectral density peaks are observed at 334-392, 107-126, 88-98, and 38-57 kyr, the predicted periods of long eccentricity (E1), short eccentricity (E2 and E3) and obliquity bandwidths, respectively (Figure 3-17). Little variations occur in period and power of the spectral peaks, however, most of the variation is limited to known Milankovitch bandwidths (Figure 3-17).

The same peaks are present in the power spectra and correlate between the three measured sections (Figure 3-17) indicating lateral continuity of

Figure 3-17. Spectral analysis of Chorros Canyon.

Blackman-Tukey spectral analysis of measured sections through the Cupido Formation exposed at Chorros Canyon (Figures 3-1 and 3-14). Color bars indicate laterally correlated spectral peaks at known Milankovitch periods. Labeled peaks are highly-significant (above the 90% statistical confidence limit).

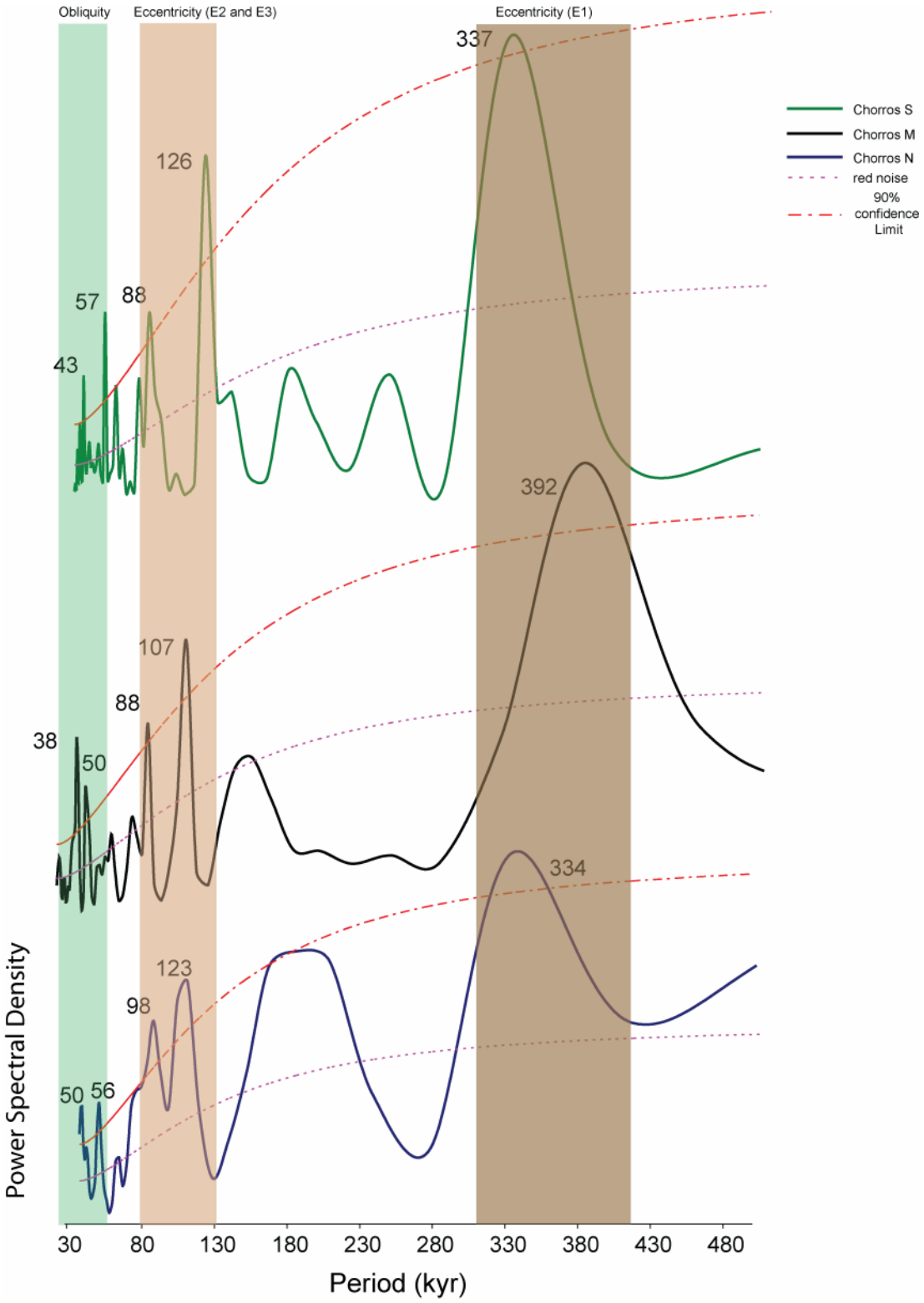
Obliquity
Eccentricity (E2 and E3)
Eccentricity (E1)
337
126
57
88
43
392
107
88
38
50
334
123
98
50
56
Chorros S
Chorros M
Chorros N
red noise
90% confidence Limit
Power Spectral Density
30
80
130
180
230
280
330
380
430
480
Period (kyr)

Milankovitch forcing at Chorros Canyon (Figure 3-14). Period variability is probably caused by subtle variations in sedimentation rates or orbital forcing periods (Yang et al., 1995; Hinnov, 2000). Autocyclic processes can not be rules out completely and they alone or maybe coupled with tectonics might be responsible for peak variations.

3) Testing for lateral continuity of Milankovitch signal across the Cupido platform from widely-spaced sections

Four stratigraphic sections from four different depositional paleoenvironments (Figures 3-1 and 3-3) were examined for cyclic periodicity using Blackman-Tukey (Blackman and Tukey, 1958) spectral analysis. If high-frequency cycles are driven by an external force such as Milankovitch orbital forces, then their periodicities should correlate across the platform.

High spectral densities peaks are observed at periods of 264-337, 122-143, 88-92, and 39-59 kyr, the predicted periods of long eccentricity (E1), short eccentricity (E2 and E3) and obliquity bandwidths, respectively (Figure 3-18). The same high-spectral density peaks are present in all four power spectra with little variation of period and power of the spectral peaks from locality to locality (Figure 3-18) and correlate with limited variation of peak periods to known Milankovitch bandwidths (Figure 3-18).

Peak variation is probably caused by subtle variations in subsidence and sedimentation rates across the platform, completeness of stratigraphic sections,

Figure 3-18. Spectral analysis across the Cupido shelf.

Blackman-Tukey spectral analysis of measured sections through the Cupido Formation exposed at Chorros Canyon, Cortinas Canyon, Escalera Canyon and Huasteca Canyon (Figures 3-1). Color bars indicate platform-wide laterally correlated spectral peaks at known Milankovitch periods. Labeled peaks are highly-significant (above the 90% statistical confidence limit).

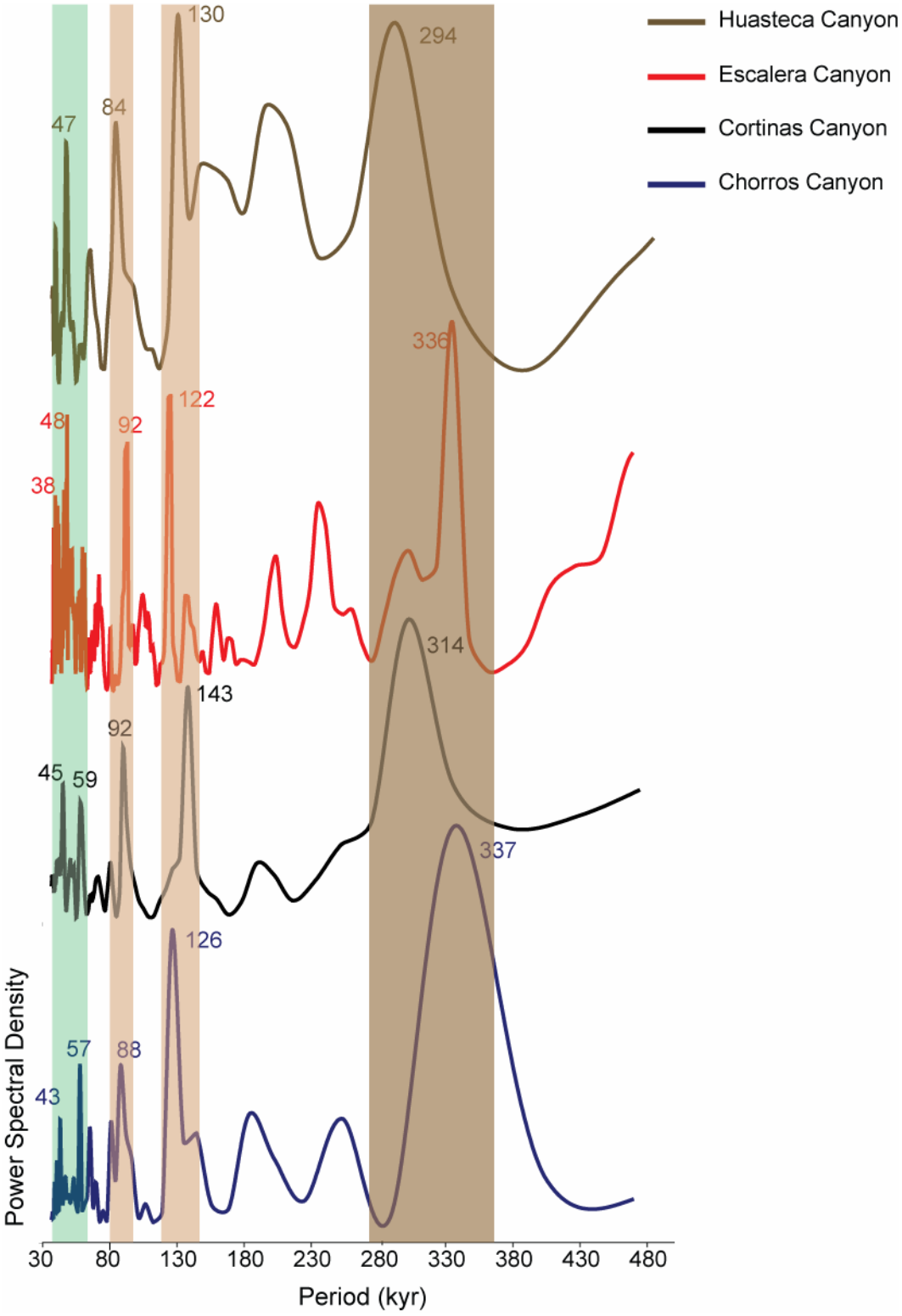
Huasteca Canyon
Escalera Canyon
Cortinas Canyon
Chorros Canyon
130
294
84
47
336
122
92
48
38
143
314
92
45
59
337
126
57
88
43
Power Spectral Density
30
80
130
180
230
280
330
380
430
480
Period (kyr)

or orbital forcing periods (Yang et al., 1995; Hinnov, 2000). Autocyclic processes can not be rules out completely and they alone or maybe coupled with tectonics might be responsible for peak variations. This strong correlation supports previous interpretations of lateral continuity of high-frequency cycles across the platform (Goldhammer et al., 1991a; Lehmann et al., 2000; Foster, 2003; Altobi et al., *in prep.*). More importantly, it supports the hypothesis of an external driver (e.g., Milankovitch orbital forcing) for high-frequency cyclicity across the Cupido platform.

DISCUSSION

Autocyclicity and allocyclicity

Through sedimentological and stratigraphic criteria, I have been able to infer that at least some high-frequency cycles of the Cupido Formation are best interpreted as allocyclic, but this does not exclude the possibility that autocyclic processes were at play as well. Autocyclic models assume local changes in carbonate accumulation rates as the driving force of high-frequency cycles in carbonate platforms. Autocyclic processes (Ginsburg, 1971; Pratt and James, 1986) can generate cyclic successions similar to those produced by orbitally-driven sea-level oscillations. However, the recognition of autocyclic processes in cyclic carbonate successions is difficult because of their stochastic nature. Therefore, proposed models of autocyclic generation of cycles (Ginsburg, 1971; Pratt and James, 1986) can be used to explain individual cycles occurring on

some parts of the platform. However, they are unlikely to be the only driver for cyclicity (Schwarzacher, 1993, 2000). Periodic autocycles have been generated in simple carbonate platform models (Drummond and Wilkinson, 1993a, b; Demicco, 1998) but have not been widely interpreted in actual stratigraphic successions.

The internal architecture of the Cupido platform is characterized by laterally continuous shallowing-upward meter-scale high-frequency cycles which stack into larger depositional and composite sequences (Goldhammer et al., 1991a; Lehmann et al., 2000; Foster, 2003; Altobi et al., *in prep.*). Assuming that the sedimentological criteria for allocyclicity discussed above are valid, I interpret a common allocyclic origin for shallow-marine carbonate high-frequency cycles (Goodwin and Anderson 1985; Hardie et al., 1986; Goldhammer et al., 1987; Osleger, 1991; D'Argenio et al., 1997; Strasser et al., 1999; Preto et al., 2001; Hinnov, 2000). However, autocyclic processes can still be functioning at different scales within individual cycles as they display differences in symmetry, type, and thickness. In the present study, almost all of the Cupido cycles are defined by exposure surfaces and lithofacies shifts indicating transgressions and regressions (Table 3-2; Figure 3-13).

Spectral analysis of the six measured sections, tuned to precession (18.4 kyr), allowed the identification of obliquity and eccentricity (E1, E2 and E3; labeled as in Hinnov, 2000). Tuning the spectrum to precession (18.4 kyr) period in each section focused spectral peaks into narrow frequency bands consistent

with other Milankovitch components. Periodicities are persistent within the measured sections as revealed by vertical and lateral correlation of closely and widely spaced sections (Figures 3-15, 3-16, 3-17 and 3-18). Therefore, I suggest that the Cupido cycles were produced by basin-wide sea-level variations under Milankovitch control. The peaks variations could also be the result of different autocyclic processes acting on top of allocyclic drivers and causing a slight shift in the location of the peak, hence slightly different period. These allocyclic overprints make it hard to interpret of maybe observe a periodicity range for autocyclic processes.

Milankovitch cyclicity

Because of the absence of polar ice sheets during the Cretaceous greenhouse climate, a significant problem exists in generating climatic modulators for sea-level oscillations, the proposed primary control on high-frequency cycle development on shallow-marine carbonate platforms. Combinations of climate-driven processes that affect sea level may be necessary to generate the minimum sea-level changes required to form shallow-marine high-frequency cycles.

(1) Even though major continental glaciations were absent during the Cretaceous (Barron 1983), small ice caps or alpine glaciers might have existed. Cretaceous dropstone deposits found in Australia, Arctic Canada, Siberia, and Alaska indicate that seasonal ice rafting occurred (Frakes and Francis, 1988).

Global falls in sea level seem to coincide with cooler temperatures recorded in oxygen isotopes of Cretaceous sedimentary rocks, which suggests that minor glaciations in the 10^5 year range existed during Cretaceous greenhouse time (Weissert and Lini, 1991). Melting of alpine glaciers and small ice caps has produced minor sea-level rises within the last century (Meier, 1984; Wigley and Raper, 1987).

(2) Thermal expansion and contraction of ocean water responding to global changes in sea-surface temperatures might cause geologically significant sea-level changes. An increase of 18ºC throughout the water column would increase sea level by about 1 m (Donovan and Jones 1979; Revelle, 1990; Elder et al., 1994).

(3) Climate-driven changes in water volume stored in lakes and groundwater reservoirs (e.g., monsoonal rainfall) have been calculated to potentially produce 2–8 m changes in sea level (Hay and Leslie, 1990; Jacobs and Sahagian, 1993; 1995). The Tethyan distribution of continents around the Cretaceous equator should have generated a monsoonal climate (Barron et al., 1995).

These processes, driven by Milankovitch orbital forces, individually or collectively generated the low-amplitude sea-level fluctuations responsible for the cyclic Cupido succession in northeastern Mexico (Lehmann et al., 1998).

Implications for the geologic time scale

If the periodicity displayed by the spectral plots indicates a support for Milankovitch orbital forcing, then the total amount of time represented by the Cupido Formation in the study area can be constrained. Each high frequency cycle has duration of 18.4 kyr. This tuning produced excellent matches to known Milankovitch periodicities. The amount of time represented by the Cupido Formation can be estimated from the spectral results assuming that each high-frequency cycle represents 18.4 kyr. Since the entire Cupido Formation in the study area is interpreted to consist of 337 high-frequency cycles, the amount of time represented by this cyclic interval is 6.2 Myr.

The total amount of time (6.2 Myr) represented by the Cupido Formation calculated using tuned cycle periods (18.4 kyr) is less than that indicated by different geologic time scales (Gradstein et al., 1995; Lehmann et al., 1999; Gradstein and Ogg, 2004). These three scales assigned 7 ±2 Myr, 9 ±2 Myr, and 10 ±2 Myr, respectively (for the Cupido Formation, these are assigned ranges derived from biostratigraphy and not exact dated-surfaces) to this stratigraphic interval. Using the Gradstein et al. (1995) time scale, the duration of each high-frequency cycles is roughly 20.8 kyr (14.8-26.7 kyr). Using ages provided by Lehmann et al. (1999), the duration of each high-frequency cycle is about 26.7 kyr (20.8-32.6 kyr). Lastly, using Gradstein and Ogg (2004) time-scale, the duration of each high-frequency cycle is about 29.7 kyr (23.7-35.6 kyr).

The discrepancies between the total amount of time estimated from tuned spectra and that estimated from different geologic time scales may be explained

in several ways. First, it is possible that there are a number of high-frequency cycles missing from the Cupido sections. Missing high-frequency cycles range from 43, 152, and 206 cycles according to the time scales of Gradstein et al. (1995), Lehmann et al. (1999); Gradstein and Ogg (2004), respectively. It is also possible that the major 2nd-order unconformity at the top of the LCu interval (e.g. heterolithic breccia at Potrero Garcia) may represent a significantly larger period of time than assumed.

CONCLUSIONS

(1) High-frequency cycles of the Cupido formation were deposited in a shallow-marine carbonate shelf environment as the result of high-frequency sea-level variations.

(2) The number of high-frequency cycles correlate laterally and they vary in thickness, facies components, type (subtidal vs. peritidal) and correlate across facies tracts. Symmetric and asymmetric high-frequency cycles are mostly capped by tidal-flat facies, however, incomplete subtidal cycles (pure subtidal cycles that lack tidal-flat caps) were also interpreted in some parts of the Cupido shelf. These observations and interpretations strongly support an allocyclic origin for high-frequency cycles of the Cupido platform.

(3) Sedimentation rate-cumulative time series analysis of precession-tuned spectra revealed three persistent eccentricity (E1, E2, and E3) and two obliquity peaks throughout the sections. The peaks occur at the principal orbital

eccentricity periodicities E1 (264-392 kyr), E2 (89-98 kyr), and E3 (107-126 kyr) and components related to the obliquity with peaks at period (38-59 kyr) near double that of precession, which is a predicted feature of orbitally-forced insolation at the equator. Variable subsidence and sedimentation rates across the platform, completeness of the sections, missed beats, and subtle variations in orbital forces may have caused the little period variation in peak periods and power spectral density. Autocyclic processes can not be rules out completely and they alone or maybe coupled with tectonics might be responsible for peak variations. However, peak variation was limited to known Milankovitch periods.

(4) Sliding window analysis of one section, combined with lateral analysis of closely to widely spaced sections show strong correlation of all high spectral density peaks. This supports the lateral continuity of high-frequency cycles and an external forcing mechanism.

(5) External Milankovitch-driven global climatic changes produced low-amplitude, high-frequency sea-level fluctuations through a combination of climatic processes to produce meter-scale cycles across the Cupido platform. These results support a global Milankovitch signal embedded in the development of Mesozoic cyclic shallow-marine carbonate platforms and possibly other greenhouse platforms.

Chapter 4. Evidence for Milankovitch control on early dolomite distribution in the Lower Cretaceous Cupido Formation, NE Mexico

ABSTRACT

The Lower Cretaceous Cupido Formation is characterized by stacked meter-scale high-frequency cycles bundled into depositional sequences which recur at scales similar to those of Milankovitch eccentricity periods. Variations in facies components and stacking patterns of high-frequency cycles define a total of twelve depositional sequences that stack into two complete and 2 partial composite sequences. Depositional and composite sequences correlate suggesting a global eustatic control on sedimentation.

The lower 2nd-order highstand of the Cupido Formation (LCu) is extensively dolomitized. Most of the dolomite is stratiform synsedimentary 'early' dolomite with little evidence for pervasive modification by burial diagenetic fluids. Early dolomitization formed within individual high-frequency cycles during both early sea-level rises and during late sea-level falls in the basal subtidal sediments and in tidal-flat caps, respectively. Evidence for syndepositional dolomitization in subtidal sediments includes the extensive dolomitization of basal subtidal parts of individual cycles underlying partially dolomitized or limestone middle part. Evidences for syndepositional dolomitization in cycle caps include the common occurrence of dolomitized clasts, eroded from the underlying cycle cap, in the transgressive base of cycles, and systematic decrease in

dolomite abundance below dolomitized caps of peritidal cycles and association of dolomite with laminites. The distribution of early fractures within the LCu is dominantly controlled by the degree of predating or contemporaneous dolomitization. Synsedimentary dolomitization of the cyclic LCu carbonates occurred in modified seawater within subtidal and supratidal zones, both at high-frequency cycle-scale and depositional sequence-scale. Hypersaline conditions during early dolomitization are indicated by the presence of local bedded evaporite.

Cyclic sedimentation and synsedimentary dolomitization within Cupido carbonates are strongly controlled by sea-level changes. Meter-scale high-frequency cycles formed in response to Milankovitch-induced high-frequency sea-level fluctuation superimposed on larger sea-level events. Distribution of early dolomite shows a strong relationship to 4^{th}-order sea-level events as the transgressive portions of 4^{th}-order depositional sequences are dolomitized compared to the regressive portions. The proposed dolomitization model, influenced largely by evaporitic setting and gradual rises and falls in sea level, can generate vertically and laterally extensive dolomite given enough time and a broad area (up to 61 m thick and 10s of kilometers wide across the shallow shelf) of active dolomitization than modern Holocene dolomitizing environments.

Thickness (Escalera Canyon) and periodicity (Chorros Canyon) clusters of completely dolomitized cycles within the LCu sediments are equivalent to 4^{th}-order depositional sequences in thickness (58 m thick on average) and in

duration (294-338 kyr). Therefore, Milankovitch-induced 4th-order sea-level events may exert a significant influence on early dolomite distribution within the LCu interval. These 4th-order sea-level fluctuations can provide the necessary fluids and Magnesium/calcium ratio partly required for platform-wide dolomitization.

Even though thickness and periodicity clusters of dolomitized cycles were quantified, they are not uniform across the Cupido platform. I also speculate that Milankovitch forcing may have influenced dolomite distribution in other geologic periods and settings. It is unlikely, however, that the Cupido model is valid for all shallow-marine carbonate platforms. This is because the operating dolomitization mechanisms vary with location and time across a single platform, depending on sea-level fluctuations.

INTRODUCTION

The relationship between dolomite distribution, stratigraphic age of dolomitized strata and global eustasy have been studied to link dolomite and sea-level history (Given and Wilkinson, 1987; Lumsden, 1989; Sibley, 1991; Montañez and Read, 1992; Table 4-1). The studies suggested that most ancient dolomite formed during periods of prolonged sea-level highstands associated with long-term rising sea level. Other studies, however, linked dolomite to regressive depositional facies and associated limestone with transgressive facies (Harris, 1973; Gorody, 1980; Kerans and Lucia, 1989; Montañez and Read,

1992; Table 4-1). Various authors (Mackenzie and Pigott, 1981; Wilkinson et al, 1985; Wilkinson and Given, 1986; Mackenzie and Agegian, 1989; Wilkinson and Algeo, 1989) suggested that periods of significant dolomite occurrence may be related to variation in atmosphere-hydrosphere environmental conditions. For example, Mackenzie and Morse (1992) postulated that times of high sea level, coupled with high atmospheric CO_2 levels and low saturation state of seawater with respect to carbonate minerals, are favorable dolomitization times. Balog et al. (1999) suggested that vertical distribution of early dolomite might not reflect eustasy, but instead, it indicates control by long-term climatic changes. More recently, dolomite distribution has been linked to transgressive depositional lithofacies of cycles and sequences (Smith et al., 2004; Altobi, 2006; Table 4-1).

Dolomitized meter-scale high-frequency cycles often characterize thick carbonate successions (Wilson, 1975; Grotzinger, 1986; Koerschner and Read, 1989; Gao and Land, 1991; Montañez and Read, 1992; Altobi et al., 2004; Altobi, 2006). These cycles range between extensively dolomitized to partly dolomitized high-frequency cycles, which stack into lower-order depositional, composite and larger-scale partially to completely dolomitized sequences. However, the origin of dolomite in these cyclic carbonate successions remains a mystery. The discovery of Holocene dolomicrite and protodolomite in supratidal, coastal lagoon, and saline lake settings confined dolomite development to saline and/or evaporitic conditions (Shinn et al., 1965; Folk and Land, 1975). Actually, many dolostones display evidence of just such a depositional setting (for example, the

Table 4-1. Previous studies.

Summary of previous conclusions linking dolomite distribution and sea level.

Author	Age	Formation	Conclusions
Harris (1973)	Upper Cambrian and Lower Ordovician	Knox Group	Dolomite is concentrated in shallow water, prograding tidal flats
Gorody (1980)	Lower Ordovician	Mascot Formation	Dolomite is linked to salinity gradient and transition from normal marine to highly saline dolomite facies
Given and Wilkinson (1987)	Phanerozoic Dolostones	A study of dolomitized Phanerozoic Formations	Dolomitization may be enhanced during times of global transgression
Kerans and Lucia (1989)	Lower Ordovician	El Paso Group	Dolomitized tidal flat caps form during third order sea-level fall
Montañez and Read (1992)	Lower Ordovician	Upper Knox Group	Dolomite distribution is linked to third-order eustatic events
Balog (1999)	Late Triassic	Hungarian Carbonates	Cyclic dolomite might be controlled by high frequency by high frequency eustatic changes; Overall vertical distribution is controlled by climate
Smith et al. (2004)	Late Mississippian	Madison Formation	Porous dolomite is common in the trangressive portions of composite sequences, high frequency sequences and cycles

presence of algal laminae, mudcracks, and associated evaporite minerals), and some authors concluded that all dolomite is a type of evaporite deposit (Friedman, 1980). Vasconceloes et al. (1995) suggested direct involvement of bacteria (possibly including sulphate-reducing bacteria) in dolomite precipitation. However, these models alone, cannot adequately explain many massive dolostones of the geologic record (Land, 1985).

To date, the 'dolomite problem' is still unresolved. This stems from our inability to synthesize dolomite inorganically in the laboratory under standard temperature and pressure (STP, 25 ºC and 1 atm) despite its widespread occurrence in carbonate rocks of different ages and different depositional environments (Warren, 2000). Because of this, dolomitization models derived from modern analogs are used to interpret ancient massive dolomite with different textural and geochemical compositions. The initial texture and geochemical compositions of ancient dolomite, especially syndepositional dolomite, are highly likely to have been extensively altered by a variety of diagenetic fluids and processes (Land, 1980; 1985; Banner et al., 1988; Smith and Dorobeck, 1989; Shelton et al., 1990; Gao and Land, 1991; Montañez and Read, 1992; Allan and Wiggins 1993; Warren, 2000). Therefore, our current understanding of dolomite genesis is inhibited by complex diagenetic overprinting on initial early dolomite characteristics. Added to this, knowledge of the timing and mechanism of dolomite formation is important if we are to understand the

emplacement and distribution of hydrocarbons and base metal ores into a dolostone.

To evaluate the origin of synsedimentary dolomite, this chapter quantifies the relationship between early dolomite distribution, stratigraphic surfaces, lithofacies and high-frequency cycles recording sea-level changes. Extensive early dolomite within the Lower Cretaceous Cupido carbonates is coupled with 2nd-order regressive sediments and is controlled by sea-level oscillations. The chapter demonstrates a primary relationship between dolomite distribution, lateral continuity, stratigraphic surfaces and sea-level changes. The chapter also presents a model for synsedimentary dolomitization processes within cyclic carbonates.

Methods

Fifteen stratigraphic sections through the Cupido Formation were logged and described in detail on a decimeter-scale. The locations of the measured sections were chosen for best accessibility to the outcrop and exposure of large section of the Cupido Formation. Six sections measured at Chorros Canyon (Figure 4-1) were used for an extensive study of lateral and vertical early dolomite distribution (Figure 4-2). Samples were collected at 15 m intervals or less depending on facies variability.

A total of 482 rock samples were collected from the Cupido Formation, 257 slabbed samples, and 314 thin sections (250 large) were prepared for

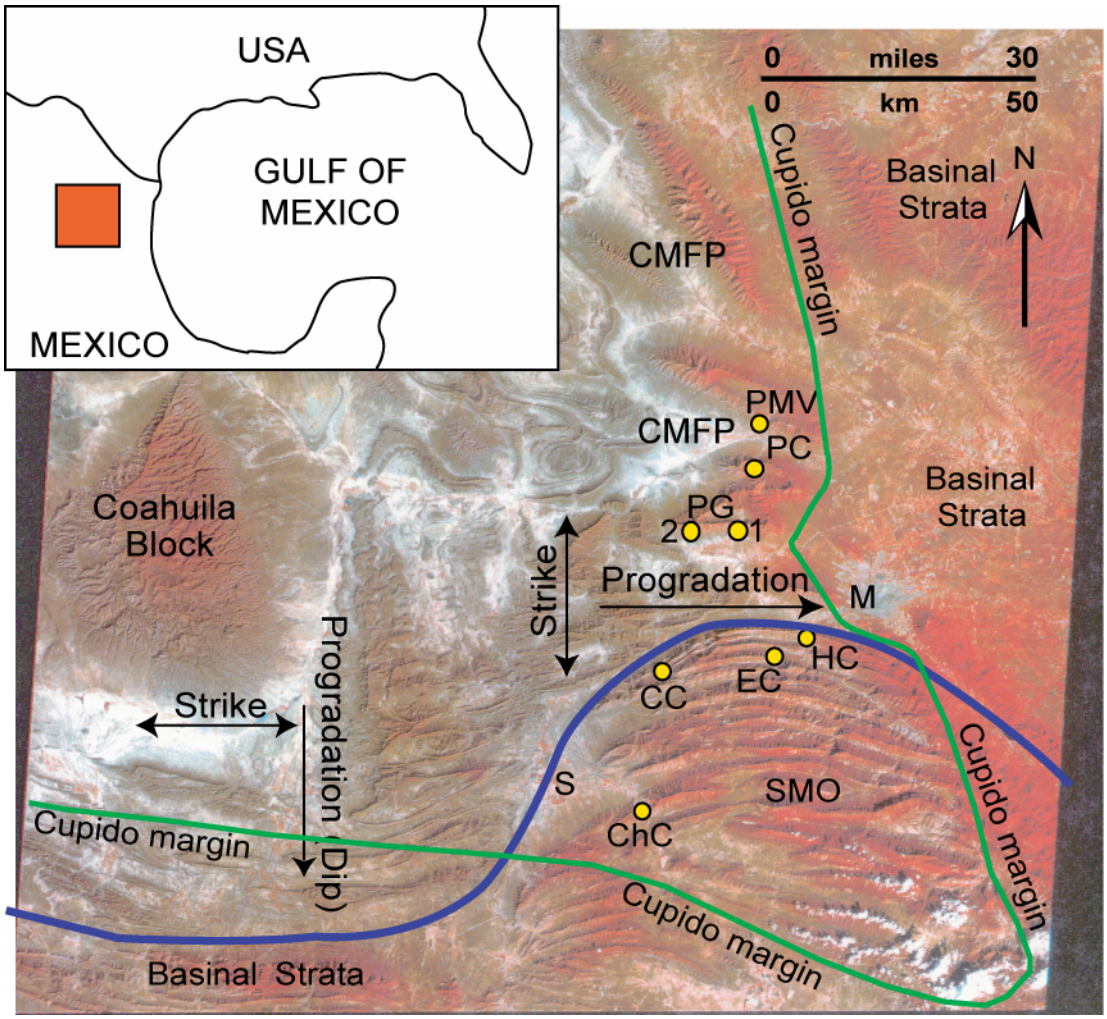

Figure 4-1. Location of study area.

Geographic map and Landsat image illustrating the position of measured sections (yellow circles) relative to the Sierra Madre Oriental (SMO) and the Coahuila block. Monterrey (M) and Saltillo (S) Mexico are shown for orientation. The Coahuila Marginal Fold Province (CMFP) lies northward of the curvilinear thrust front (purple line) of the Sierra Madre Oriental. Anticlines and section names from north to south are Potrero Minas Viejas (PMV), Potrero Chico (PC), Potrero Garcia (PG1 and 2), Huasteca Canyon (HC), Escalera Canyon (EC), Cortinas Canyon (CC), and Chorros Canyon (ChC). Sections used for spectral analysis are Huasteca Canyon (HC), Escalera Canyon (EC), Cortinas Canyon (CC), and Chorros Canyon (ChC). The progradation of the Mesozoic passive margin is toward the east, southeast and south away from the Coahuila block. The platform margin trend is modified from Wilson (1999) and Foster (2003).

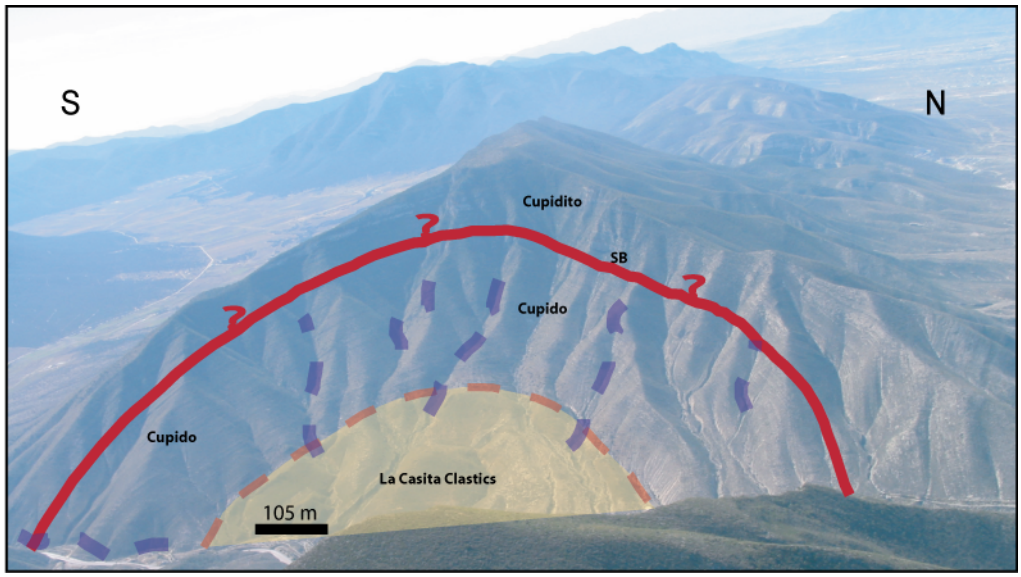

Figure 4-2. Chorros Canyon.

Aerial photograph of Chorros Canyon (ChC), SMO near Saltillo, with locations of measured stratigraphic sections (dashed purple lines). The Cupido Formation is a combination of the Cupido, regressive, and the Cupidito, transgressive. The Cupidito transgressive portion is difficult to measure within the anticline and it therefore was measured along the road cut. The solid red line represents the approximate location of the 2nd-order sequence boundary (SB). Photo taken by Goldhammer (2002).

petrographic analysis. Thin sections were stained with Alizarin Red (Dickson, 1965) for petrographic description and to identify calcite and aid in grain identification. Thin sections were examined using both conventional transmitted light and cathodoluminescent petrography with a Technosyn Cold Cathodoluminescence Model 8200 Mk-II (16–20 kV gun potential, 400-600 μA beam current, 1 cm diameter focused beam current, and 0.3 torr vacuum). Facies were defined on the basis of depositional textures, sedimentary structures and fossil content following Dunham's (1962) classification scheme. Dolomite textures were described following Sibley and Greg's (1987) classification scheme. Estimating the degree of dolomitization of lithofacies in outcrops was carried out by calibrating point-count data of dolomite crystals from 37 thin sections, and detailed descriptions of hand samples, with field observations and descriptions of lithofacies from outcrops.

Through detailed petrographic analysis using standard transmitted light and cathodoluminescence techniques, fabric-preserving syndepositional dolomites with minimal petrographic evidence for recrystallization and allochems with least visible evidence for alteration were identified. Samples for isotope analysis were ultrasonically cleaned. Dolomite and calcite types were microsamples (3–15 mg) were collected from ultrasonically cleaned, thick sections (500 mm thick) using a bench-mounted milling machine equipped with dental drills (250–500 mm Tungsten carbide tips) and a binocular microscope.

Oxygen and carbon isotope analyses were conducted at the University of Texas, Austin, on a Prism II, dual-inlet, isotope ratio spectrometer. Samples were dissolved in anhydrous H_3PO_4 at 25ºC for limestone and both 25ºC and 50ºC for dolomite following procedures outlined in McCrea (1950) and Gao et al. (1995). Precisions for $\delta^{18}O$ and $\delta^{13}C$ were better than ±0.15‰ and ±0.11‰, respectively.

Stratigraphic setting

The Barremian to Middle Aptian Cupido Formation is exposed in the Sierra Madre Oriental (SMO) and the Coahuila Marginal Fold Province (CMFP; Figure 4-1). It forms part of an extensive carbonate system that developed around the ancestral Gulf of Mexico (Wilson, 1990; Goldhammer et al., 1991a; Lehmann et al., 1998; Goldhammer, 1999: Figure 4-3). The study area is located within the uplifted Sierra Madre Oriental fold belt between Monterrey and Saltillo in northeastern Mexico as well as north of the fold belt in the form of isolated doubly plunging potreros (Figure 4-1).

Figure 4-3. Stratigraphy of northeastern Mexico.

(A) Paleogeography of the Barremian to Lower Aptian in the western Gulf of Mexico, modified from Goldhammer (1999). The Cupido and Sligo platforms are shown in blue. Outline of Mexico and U.S. border is shown in black. The red box outlines the location of the study area.

(B) Chronostratigraphic chart for northeast Mexico and Texas Gulf Coast (modified from Goldhammer, 1999). The composite eustatic curve from Haq et al. (1987). Time scale from Hardenbol et al. (1998) and Gradstein et al. (1995). Second-order sequence boundary ages are approximations in Ma. Abbreviations are: LST-lowstand system tracts, TST-transgressive system tracts, HST-highstand system tracts, LSW-lowstand wedge, SMW-shelf margin wedge, MFS-maximum flooding surface. Lithologies are discussed in text, border highlights interval of interest. Pinnacle reefs and buildups are shown as small domes. FW1 and FW2 refer to parts of the La Casita Formation defined by Fortunato and Ward (1982).

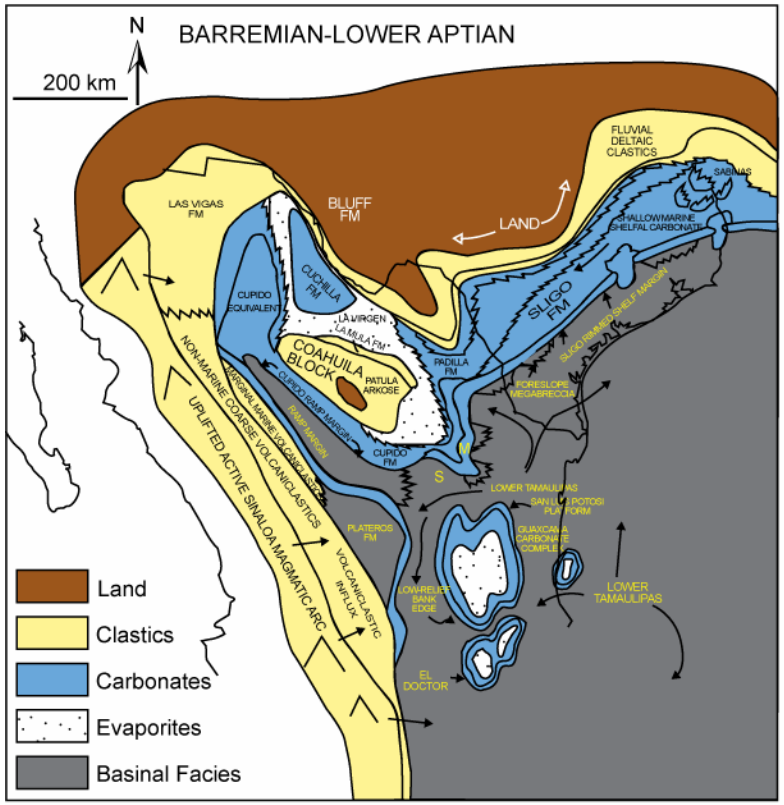
N
BARREMIAN-LOWER APTIAN
200 km
LAND
FLUVIAL DELTAIC CLASTICS
SHALLOW MARINE SHELFAL CARBONATE
LAS VIGAS FM
BLUFF FM
SABINAS
CUPIDO EQUIVALENT
CUCHILLA FM
LA VIRGEN
LA MULA FM
SUGO FM
COAHUILA BLOCK
PATULA ARKOSE
PADILLA FM
FORESLOPE MEGABRECCIA
SUGO RAMP-SHELF MARGIN
NON-MARINE COARSE VOLCANICLASTICS
UPLIFTED ACTIVE SINALOA MAGMATIC ARC
CUPIDO RAMP MARGIN
CUPIDO FM
LOWER TAMAULIPAS
SAN LUIS POTOSI PLATFORM
PLATEROS FM
GUAYCAMA CARBONATE COMPLEX
VOLCANICLASTIC INFLUX
LOW-RELIEF BANK EDGE
LOWER TAMAULIPAS
EL DOCTOR
Land
Clastics
Carbonates
Evaporites
Basinal Facies

A

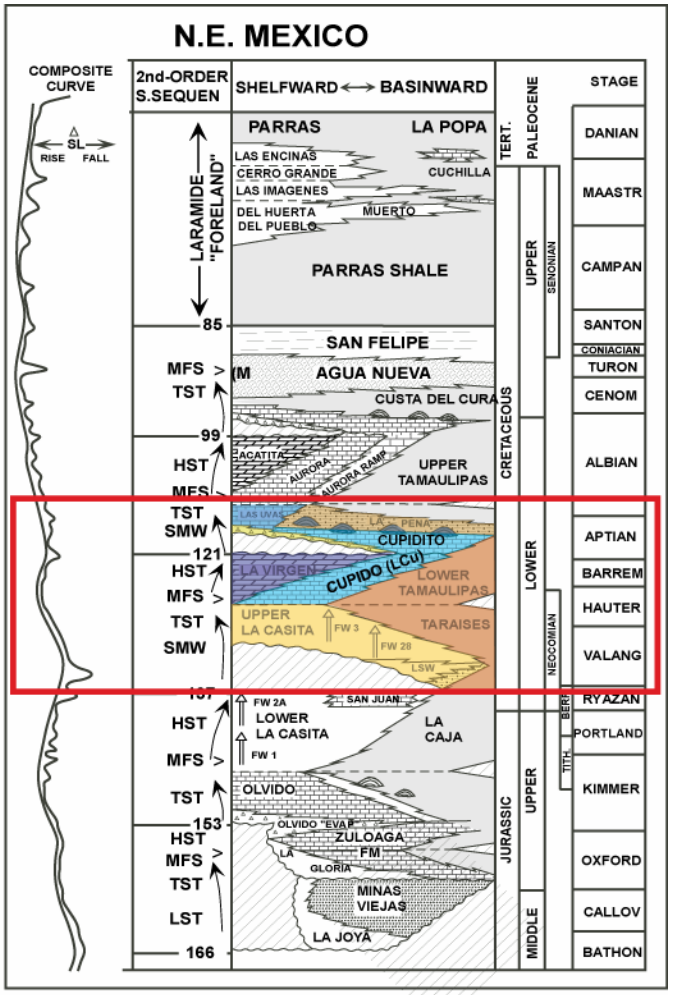
N.E. MEXICO
COMPOSITE CURVE
2nd-ORDER S.SEQUEN
SHELFWARD ⟷ BASINWARD
STAGE
SL
RISE
FALL
LARAMIDE "FORELAND"
PARRAS
LA POPA
LAS ENCINAS
CERRO GRANDE
LAS IMAGENES
DEL HUERTA
DEL PUEBLO
CUCHILLA
MUERTO
PARRAS SHALE
85
SAN FELIPE
MFS
TST
AGUA NEUVA
CUSTA DEL CURA
99
HST
MFS
TACATITA
AURORA
AURORA RAMP
UPPER TAMAULIPAS
TST
SMW
LAS UVAS
LA PENA
CUPIDITO
121
HST
MFS
LA VIRGEN
CUPIDO (LCu)
LOWER TAMAULIPAS
TST
SMW
UPPER LA CASITA
FW 3
TARAISES
FW 2B
LSW
137
FW 2A
SAN JUAN
HST
LOWER LA CASITA
LA CAJA
MFS
FW 1
TST
OLVIDO
153
OLVIDO "EVAP"
HST
ZULOAGA FM
MFS
LA GLORIA
TST
MINAS VIEJAS
LST
LA JOYA
166
TERT.
PALEOCENE
CRETACEOUS
UPPER
SENONIAN
LOWER
NEOCOMIAN
JURASSIC
UPPER
MIDDLE
BERR.
TITH.
DANIAN
MAASTR.
CAMPAN
SANTON
CONIACIAN
TURON
CENOM.
ALBIAN
APTIAN
BARREM.
HAUTER.
VALANG.
RYAZAN
PORTLAND
KIMMER.
OXFORD
CALLOV.
BATHON

B

Depositional model for the Cupido Formation

Cupido carbonates developed on a shallow grainstone-rimmed margin (Lehmann et al., 1998; Altobi et al., *in prep.*; Figure 4-4) that was several hundred kilometers wide and extended from NE Mexico to Texas and Louisiana (Wilson, 1990; Goldhammer et al., 1991a; Lehmann et al., 1998; Goldhammer, 1999: Figure 4-3). A shallow lagoon, protected from wave-energy by a grainstone shoal complex developed within the shelf and was dominated by bioturbated carbonate mud-rich sediments. In the landward direction, this lagoon was about 100 km wide adjacent to the Coahuila block (Lehmann et al., 2000; Altobi et al., *in prep.*; Figure 4-4).

The Cupido Formation is divided into two parts, a thin-bedded progradational LCu (lower Cupido interval) and an overlying thick-bedded retrogradational Cupidito member, separated by a 2^{nd}-order sequence boundary (Wilson and Pialli, 1977, Goldhammer et al., 1991a; Goldhammer, 1999; Figure 4-3). The progradational LCu represents 2^{nd}-order late highstand deposits whereas the Cupidito member was deposited during the early part of a 2^{nd}-order transgression that caused the retrogradation of all carbonate platforms in the Gulf of Mexico and the growth of subsequent reef build-ups prior to drowning (Bebout and Loucks, 1977; McFarlan and Menes, 1991; Figure 4-3).

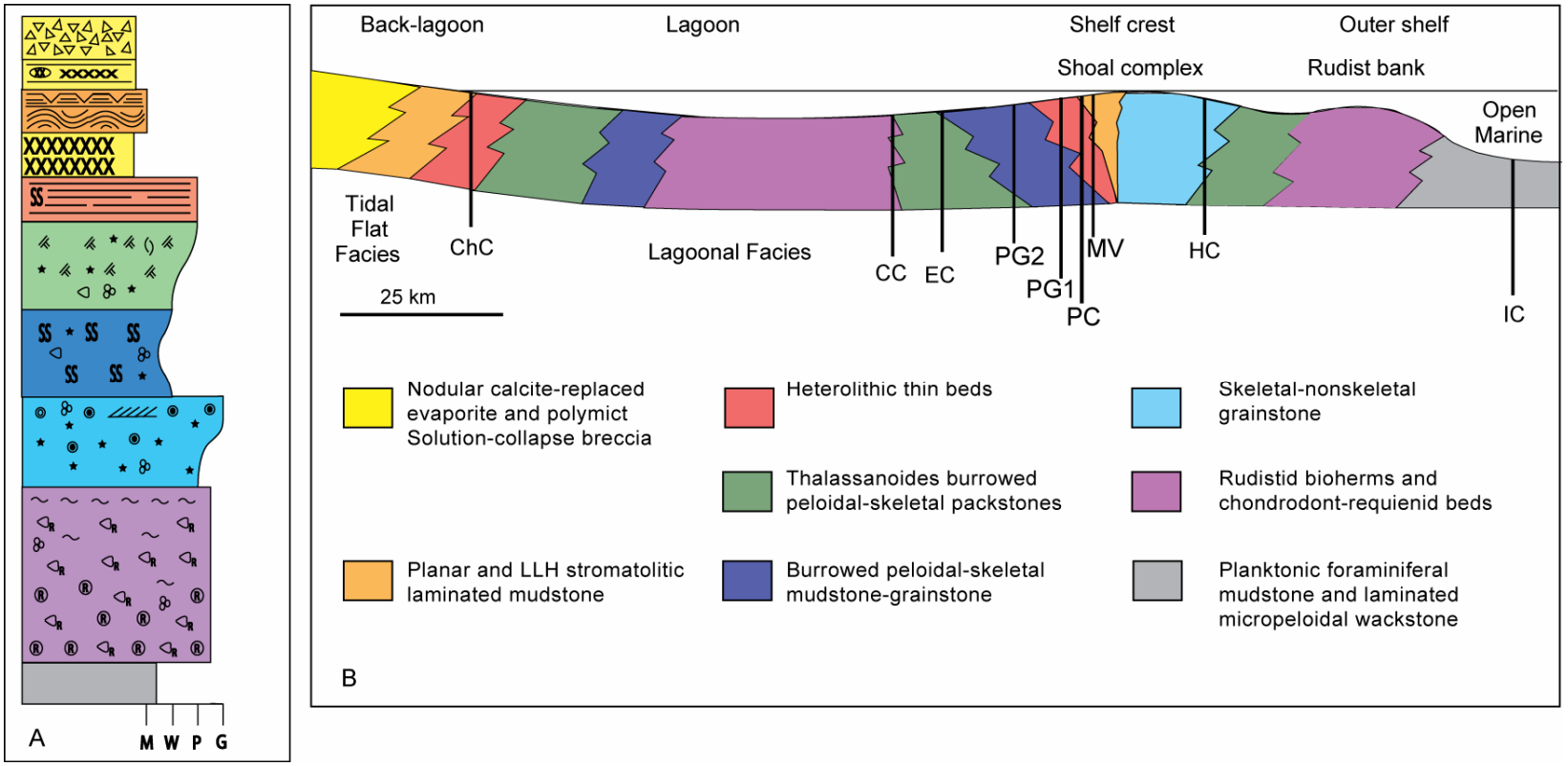

Figure 4-4. Depositional model.

Depositional environments across the Cupido platform.
(A) Idealized shallowing-upward succession of the Cupido lithofacies. See Appendix A for Key.
(B) Generalized schematic depositional model of the Cupido platform illustrating the depositional paleo-environments of the measured sections as they would appear projected along a dip oriented profile. The shelf crest is represented by a shoal complex, not a barrier reef. The shoal complex provided a barrier to open marine influx creating a restricted saltern environment. See text for detailed descriptions of major facies belts.

CUPIDO FORMATION CYCLOSTRATIGRAPHY

Meter-scale high-frequency cycles

The Cupido Formation is characterized by stacked peritidal and subtidal high-frequency cycles (Goldhammer et al., 1991a; Goldhammer, 1999; Lehmann et al., 1999; Foster, 2003 and Altobi et al., 2004; Altobi et al., *in prep.*; Figure 4-5). It consists of as many as 283 meter-scale (0.2-18 m; average 6 m) shallowing-upwards cycles, which can be classified as restricted or open-marine (Figure 4-5). Subtidal facies of restricted peritidal cycles (Table 4-2) consist of (1) moderately to intensely bioturbated, thick- to medium-bedded peloidal-skeletal dolomudstone to grainstone; (2) weakly to moderately bioturbated, thick- to medium-bedded *thalassanoides* burrowed peloidal-skeletal dolopackstone; and (3) massive to thick-bedded rudist bioherms and rudist-rich beds. Subtidal facies of open-marine cycles (Table 4-2) are dominated by deeper-water lithofacies such as (1) moderately to intensely bioturbated, thick-bedded dolomudstone to packstones, and (2) massive to thick-bedded rudist-rich beds. Subtidal facies of most peritidal cycles grade up into cycle caps (Figure 4-5) composed of cross-stratified grainstone, planar and stromatolitic laminated dolomudstone and heterolithic thin-beds.

Table 4-2 Summary of facies.

Facies, types, textures, depositional processes and environment and facies-belts of the Cupido Formation. The location of each facies within the idealized shallowing-upward vertical succession is shown in Figure 4-4.

Facies	Subfacies	Occurrence	Color	Rock type & Depositional Texture	Grain Type	Bedding & Sedimentary Structures	Early Diagenetic Features	Depositional Environment
Evaporitic Interior facies	Polymict Solution Collapse Breccia	Common across most parts of the platform	Gray	Polymict breccia with a carbonate mud matrix	Angular clasts, <30 cm, consisting of mudstones, micritized mixed packstones and grainstones	Medium to think bedded, Brecciated	Dissolution by through flowing phreatic water, collapse and rotation of lithified rock fragments	Burial beneath supratidal environment
	Nodular - Mosaic Calcite Replaced Evaporite	Common in the shallow landward parts of the platfrom	White to light gray	Anhedral calcite replaced anhydrite nodules separated by dolomitized micrite	Peloids	Non-bedded, displacive growth distrupts surrounding sediments	Hydration of anhydrite to gypsum, sparry mosaic calcite replacement	Supratidal sabkha
Peritidal to shallow subtidal restricted shelf-lagoon facies	Planar and Stromatolitic Laminated Mudstone	Common across most parts of the platform	Light gray to tan	Dolomitic mudstones to interbedded peloidal wackstones and mudstones	Peloids and pellets	Planar to domal laminations, occasional mudcracks, wispy lenses, and contorted bedding	Fenestral fabric, early lithification dolomitization,and anhydrite precipitation	Quiet, shallow intertidal to subtidal, tidal-flat
	Heterolithic Thin Beds	Common across most parts of the platform	Tan	Alternating peloidal-skeletal grainstones, which are slightly dolomitized mudstones	Peloids (some compacted), fecal pellets, and a variety of skeletal debris	Thin bedded,10 mm, planar to flattened lenticular, no internal cross stratification	Early compaction and occacional amplitude stylolites between layers	low energy, subaqueous, shallow shelf lagoon saltern
	Intercalated Calcite Replaced Evaporite Beds	Common across most parts of the platform	White to light gray	Euhedral calcite and precipitated peloids and micrite	Peloids between crystals	Medium to thinly bedded	Sparry mosaic calcite replacement, stylolitization	Subtidal, shallow marine tidal-flat zone
Shallow subtidal restricted platform facies	Thalassanoides Burrowed Peloidal - Skeletal Packstone	Common across most central parts of the platform	Gray	Euhedral dolomitized micrite with micritized skeletal-nonskeletal W-P matrix with euhedral dolomitized skeletal-non skeletal W-P burrow fill	Peloids, Miliolidae and Vercorsella Foraminifera, mollusk and ostracod debris, and dasycladaceans	Thick to medium bedded, preserved trace fossil networks as irregular boxworks, no preservation of mechanical structures	Early lithification of mictritic matrix to support burrow networks and early dolomitization	Quiet, tide-dominated shallow lagoon/tidal-flat, dominantly open-marine conditions
	Burrowed Peloidal-Skeletal Mudstone - Grainstone	Common across most central parts of the platform	Gray	Dolomitized micritic peloidal carbonate mudstone matrix with dolomitized micrite or mixed skeletal and nonskeletal grainstone fill	Peloids, pellets, composite grains, Miliolidae and Vercorsella Foraminifera, gastrpods, bivalves and dasycladaceans	Thick to medium bedded, some trace fossil are preserved as networks, irregular boxworks, and mottling are common, no preservation of mechanical structures	Early lithification of mictritic matrix to support burrow networks under compaction	Quiet, middle shelf lagoon, to slightly open marine conditions
High energy shoal to rudist-reef margin facies	Skeletal - Nonskeletal Grainstone	Common throughout the platfrom especially across most eastern and southern parts of the platform	White to light gray	Micritized skeletal and nonskeletal grainstones and packstones with sparry mosaic clacite cement and some dolomite	Oncoids, ooids, peloids, composite grains, lumps, intraclasts, Miliolidae and Vercorsella Foraminifera, gastrpods, bivalves, dasycladaceans,echinoderms, bryozoans and ostracods	Thick to medium bedded, cross stratification to massive due to high rates of biogenic reworking	Early calcite cementation in intra and interpartical porosity within the grainstones, compaction within packstones	Active high-energy shelf crest, middle to outer shelf, subject to wave and storm influence
	Rudistid Bioherms and Beds	Common throughout the platform especially across most eastwards parts	Medium to dark gray	Micritized skeletal and nonskeletal packstones	Caprotinide, coral, Caprinidae, bryozoans, Chondrodonta ooids, Requiniidae, ostracods, bivalve shell debris,foraminifera, few peloids dasycladaceans algae, and intraclasts	Massive to thick bedded, no internalcross bedding, rudists are commonly not in growth position	Binding by encrusting algae and early cementation	Below fair weather wave base,dominated shelf edge
Deep subtidal, low-energy off platform facies	Foraminiferal wackestone/ mudstone	Common across most eastern and southern parts off the platform	Dark gray	Bioturbated mudstone and wackstone some dolomitic firmgrounds, hardgrounds and chert nodules	Planktonic Foraminifera, peloids	Thin bedded with some lamination	Early lithification of matrix and early compaction	Below storm wave base in a low-energy oxygenated setting

Figure 4-5. High-frequency cycles across the Cupido platform.

Types of high-frequency cycles across the Cupido platform depending on their depositional setting: A) Peritidal cycle, B) Shallow subtidal cycle, C) shoal peritidal cycle, D) Deep subtidal cycle. Facies key is found in Figure 4-4. HTB is a heterolithic thin bed. The solid orange bar to the left of each cycle represents the degree of dolomitization.

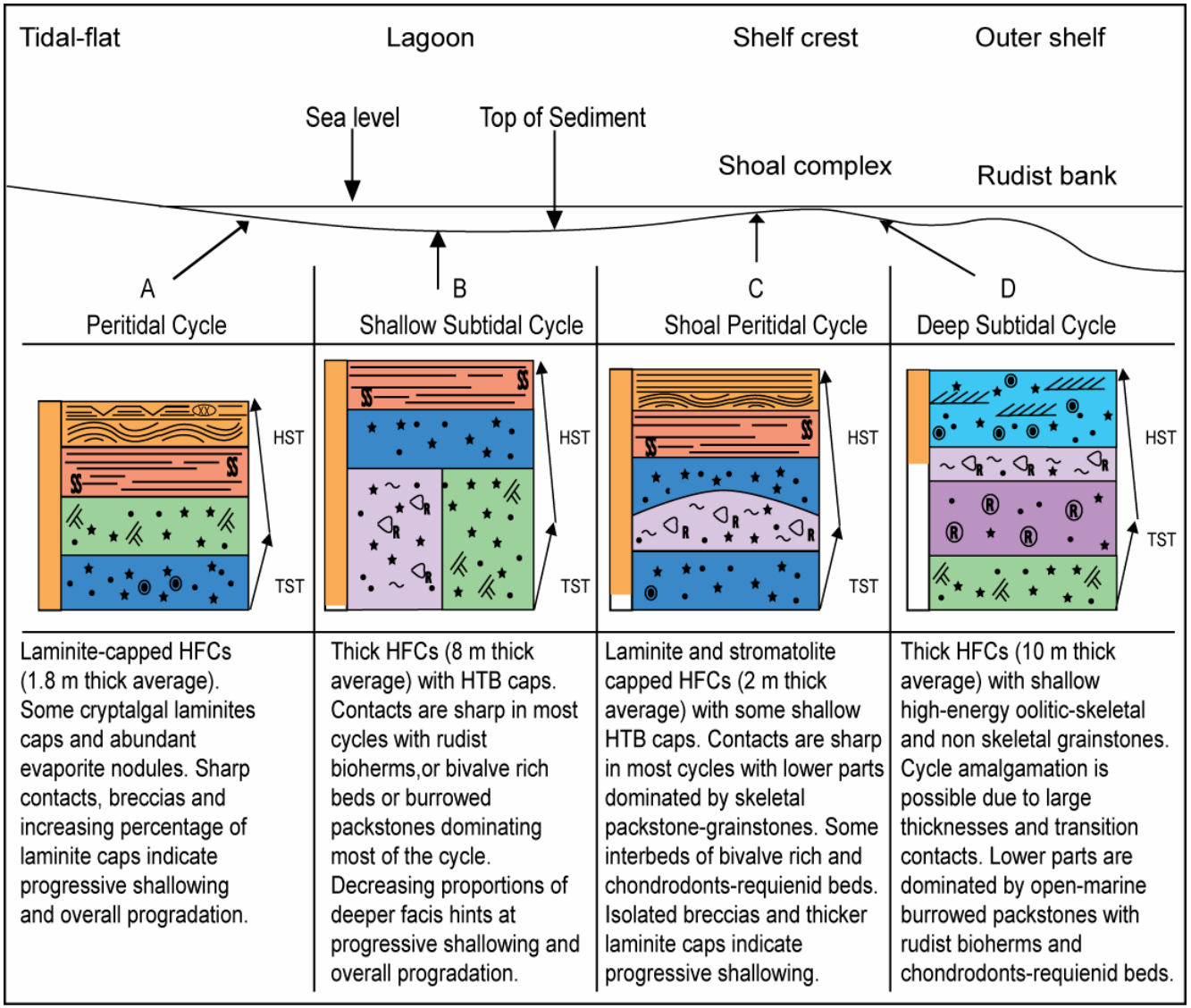
Tidal-flat
Lagoon
Shelf crest
Outer shelf
Sea level
Top of Sediment
Shoal complex
Rudist bank
A
Peritidal Cycle
B
Shallow Subtidal Cycle
C
Shoal Peritidal Cycle
D
Deep Subtidal Cycle
HST
TST
Laminite-capped HFCs (1.8 m thick average). Some cryptalgal laminites caps and abundant evaporite nodules. Sharp contacts, breccias and increasing percentage of laminite caps indicate progressive shallowing and overall progradation.
Thick HFCs (8 m thick average) with HTB caps. Contacts are sharp in most cycles with rudist bioherms,or bivalve rich beds or burrowed packstones dominating most of the cycle. Decreasing proportions of deeper facis hints at progressive shallowing and overall progradation.
Laminite and stromatolite capped HFCs (2 m thick average) with some shallow HTB caps. Contacts are sharp in most cycles with lower parts dominated by skeletal packstone-grainstones. Some interbeds of bivalve rich and chondrodonts-requienid beds. Isolated breccias and thicker laminite caps indicate progressive shallowing.
Thick HFCs (10 m thick average) with shallow high-energy oolitic-skeletal and non skeletal grainstones. Cycle amalgamation is possible due to large thicknesses and transition contacts. Lower parts are dominated by open-marine burrowed packstones with rudist bioherms and chondrodonts-requienid beds.

Most of the high-frequency peritidal cycles are asymmetric, capped by tidal-flats and vary in type, facies composition, and thickness across the platform (Figure 4-5). Thinner restricted cycles are abundant in the platform interior, whereas thicker, amalgamated open-marine cycles are abundant at the shelf margin. Evidence for emergence in cycle caps include sabkha like anhydrite and rare mudcracks preserved in cryptalgal laminites (Figure 4-6) as well as the presence of bedded evaporites on the lagoonal side of the shoal. Outer shelf cycles, which lack tidal-flat caps, are capped by cross-stratified mixed grainstones analogous to those high-energy grainstones in the Joulters Cay oolite shoal (Bubb, 1970; Harris et al., 1993).

Depositional and composite sequences

Stacked high-frequency cycles record general deepening and shallowing trends and variations in available accommodation space across the platform. Meter-scale high-frequency cycles stack into larger-scale depositional sequences (43-96 m), which in turn stack into even larger composite sequences (145-169 m; Table 4-3). Systematic changes in stacking-patterns of high-frequency cycles, outlined on the basis of long-term changes in cycle types and variations in cycle thickness, define twelve depositional sequences (A-L) and two full and two partial composite sequences (I-IV; Figure 4-7). These depositional sequences correlate across the platform. Composite sequences of the Cupido Formation regionally

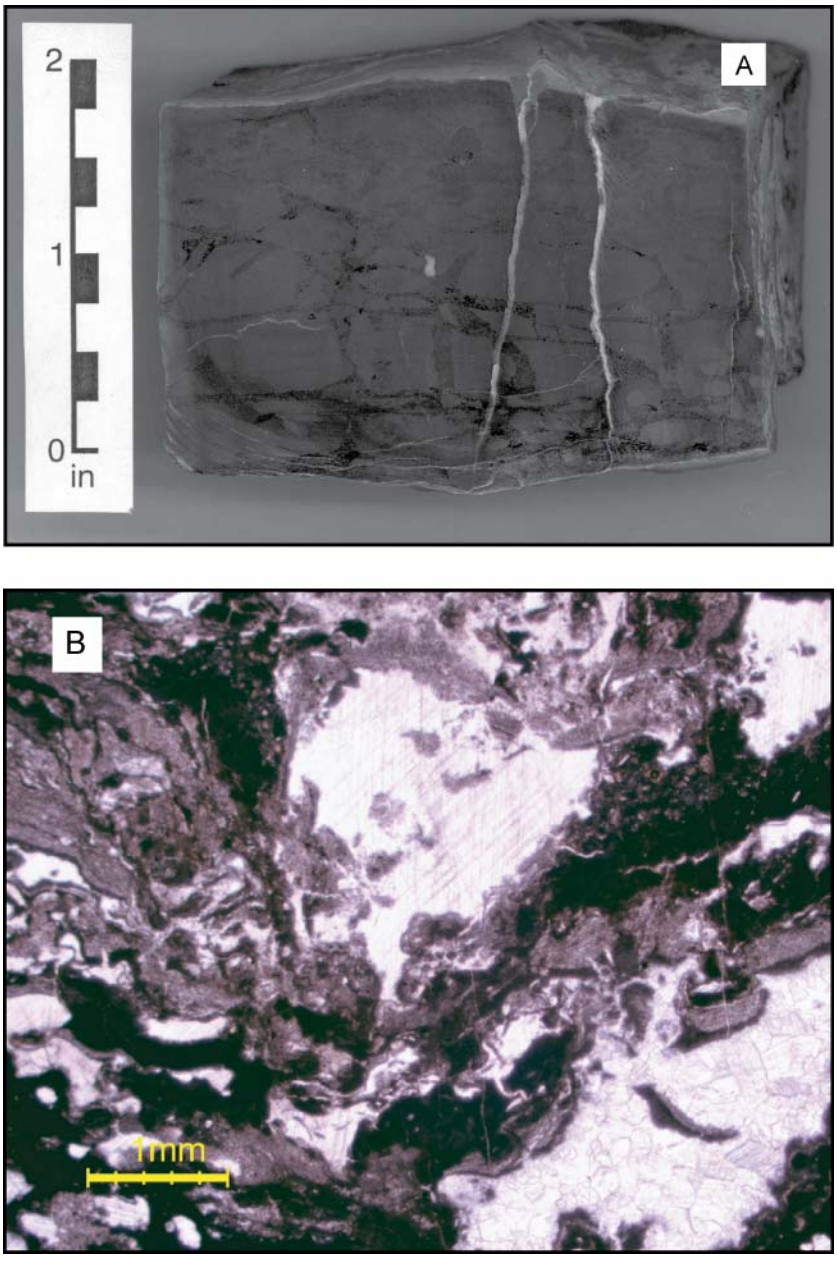

Figure 4-6. Exposure features within Cupido facies.

(A) Hand sample of a brecciated, laminated mudstone with cryptmicrobial origin. (B) Photomicrograph of evaporite disrupted laminations with inferred cryptmicrobial origin.

Table 4-3. Sequence stratigraphic framework summary.

Sequence stratigraphic framework for the Cupido Formation showing the major characteristics of interpreted composite sequences (I-IV) and internal depositional sequences (A-L), system tract components (highstand, HST; Transgressive, TST), dominant facies, type of high-frequency cycles (HFCs) and bounding surfaces: sequence boundaries, (SB); and maximum flooding zone (MFZ).

2nd-order sequence	Composite Sequecne	Average Thickness (m)				System Tract	Comments
		Interior		Margin			
Cupidito member (TST)	IV (TST part)	L K J	125	J	49	TST	MFZ is inferred to be within the La Pena shales Composed of thick open-marine subtidal HFCs with abundant grainstones (some oolitic), beds rich in bivalves, requienids and chondront and rudist bioherms
	III	I H	158	I H	145	HST	SB is picked at the top thinly-stacked peritidal HFCs below thicker subtidal HFCs A thin interval of dominantly thin peritidal, laminite capped HFCs composed of relatively shallow facies
		G		G		TST	MFZ is interpreted within the thickest shallow subtidal HFCs Composed of thick subtidal, probably amalgamated HFCs with foraminiferal mud-packstone, a few beds rich in bivalves, requienids and chondront and some rudist bioherms/packstone
LCu (HST)	II	F E	167	F E	169	HST	SB is interpreted as the base of laterally correlative, thick solution collapse breccia atop thin peritidal HFCs Composed mainly of upward thining peritidal HFCs dominated by shallow tidal falt facies
		D C		D C		TST	MFZ is interpreted within 2 thick shallow subtidal HFCs Composed of thick shallow-subtidal HFCs that are mainly burrowed peloidal-skeletal packstones, thickness of subtidal HFCs decreases upwards
	I (HST part)	B A	116	B A	117	HST	SB is picked at the top stacked thin bedded peritidal HFCs Composed of massive peloidal-skeletal-oolitic packstones-grainstones and some interbeds of rudist bioherms and packstones. Some subtidal HFCs, but dominantly thin peritdal HFCs

Figure 4-7. Sequence stratigraphic framework.

Fence diagram combining six measured sections in their relative positions (Chorros Canyon, ChC; CC, Cortinas Canyon, CC; Escalera Canyon, EC; Potrero Garcia, PG1; Potrero Chico, PC; Potrero Minas Viejas, PMV). Lateral correlation of sequences and retrogradational geometry of the platform are evident. Depositional sequences (A-L) and composite sequences (I-IV) and the 2nd-order sequence boundary (SB) are outlined. Orange part represents the dolomitized lower highstand LCu and the blue part represents the transgressive (TST) Cupidito member which is dominantly limestone. The 2nd-order sequence boundary is used as a datum. La Peña thickness is estimated. Distances in km. Modified from Foster (2003) and Altobi et al. (2004).

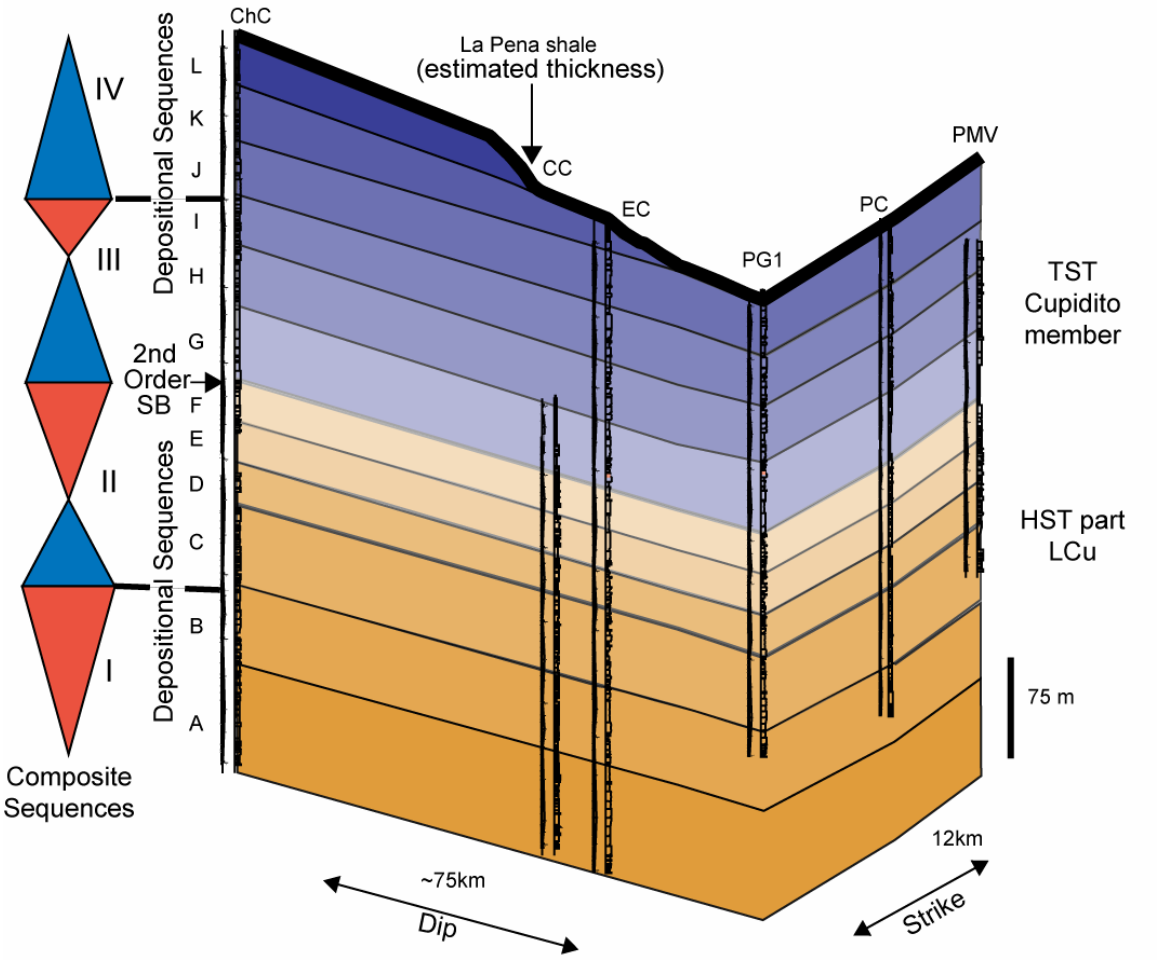

Figure 4-7. Sequence stratigraphic framework.

Fence diagram combining six measured sections in their relative positions (Chorros Canyon, ChC; CC, Cortinas Canyon, CC; Escalera Canyon, EC; Potrero Garcia, PG1; Potrero Chico, PC; Potrero Minas Viejas, PMV). Lateral correlation of sequences and retrogradational geometry of the platform are evident. Depositional sequences (A-L) and composite sequences (I-IV) and the 2nd-order sequence boundary (SB) are outlined. Orange part represents the dolomitized lower highstand LCu and the blue part represents the transgressive (TST) Cupidito member which is dominantly limestone. The 2nd-order sequence boundary is used as a datum. La Peña thickness is estimated. Distances in km. Modified from Foster (2003) and Altobi et al. (2004).

correlate with those in the coeval, nearby, Texas platform (Goldhammer, 1999; Lehmann et al., 2000; Altobi et al., 2004).

Depositional and composite sequences are bounded by sequence boundaries which exhibit changes in high-frequency cycle type and facies characteristics and record turnaround from decreasing accommodation space to increasing accommodation space (Mitchum and Van Wagoner, 1991; Kerans and Tinker, 1997; Goldhammer, 2003). The LCu interval is dominated by thinner depositional sequences with dominant peritidal and shallow subtidal high-frequency cycles and increasing abundance of tidal-flats and evaporitic facies. The Cupidito member is dominated by thicker depositional sequences composed of shallow to deep subtidal high-frequency cycles with decreasing peritidal high-frequency cycles and restricted facies proportions.

PETROGRAPHIC AND STRATIGRAPHIC DISTRIBUTION OF DOLOMITE

Petrography

Two main types of dolomite were recognized in the Cupido carbonates based on textural characteristics and cathodoluminescence (Figure 4-8). Differences in petrographic characteristics of the Cupido dolomites distinguish early from late dolomite and indicate that early dolomite is distinct in origin from late dolomite. Early dolomite occurs primarily as a replacive phase in the Cupido carbonates, whereas late dolomite occurs as possible multiple generations of dolomite cements within fractures only (Figure 4-8H and I). Early replacive

dolomite is polymodal fine to medium crystalline, has abundant planar (euhedral-subhedral) crystal boundaries, rare zoning (plane light, PL; and cathodoluminescent, CL), and nonluminescent cores (Figure 4-8). Fine crystalline dolomite is associated with mm-scale laminites occurring as cycle caps (Figure 4-8A) whereas fine to medium crystalline dolomite is associated with subtidal parts of high-frequency cycles (Figure 4-8B). Early dolomite replaced the matrix and some of the grains (partial to full replacement; Figure 4-8J and K). In contrast, late replacive dolomite is seen only in fractures within the Cupido Formation and is unimodal 50 um to 200's um in size), has a common nonplanar (anhedral) crystal boundaries, and dark luminescent cores and (Figure 4-8H and I).

Stratigraphic distribution of early dolomite

The distribution and abundance of early replacive dolomite are stratigraphically controlled and constitutes most dolomite in the Cupido carbonates. Early replacive dolomite exhibits minor to extensive replacement and overgrowth by late dolomite. Late replacive dolomite occurs as selective replacement of limestone closely associated with fractures and stylolites. Whether some late replacive dolomite has had an early dolomite precursor cannot be determined given destruction of early dolomite textures and geochemistry within those samples.

Figure 4-8. Dolomite textures from the Cupido Formation.

(A) Photomicrograph of fine-grained dolomite within the matrix and a fracture filled with different dolomite texture.

(B) Photomicrograph of coarse-grained euhedral early dolomite completely altering the original fabric.

(C) and (D) PL and CL photomicrograph showing uniform early dolomite crystals (D) and limestone (L).

(E) and (F) PL and CL photomicrograph showing fine-dolomitized matrix (D) with some limestone (L).

(H) and (I) PL and CL photomicrograph showing large and small fractures (F) filled with large dolomite (D) crystals and limestone (L).

(J) and (K) PL and CL photomicrograph showing fabric selective dolomite (D) and remaining limestone (L).

(L) and (M) Scanning electron microscope (SEM) showing planar euhedral early dolomite crystals.

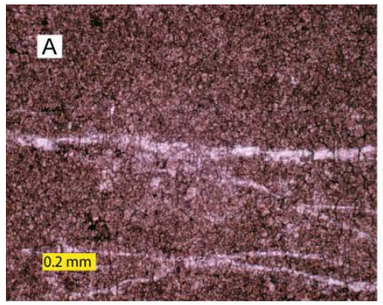
A
0.2 mm

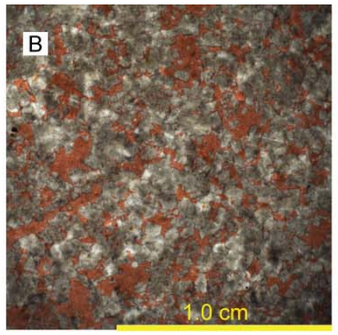
B
1.0 cm

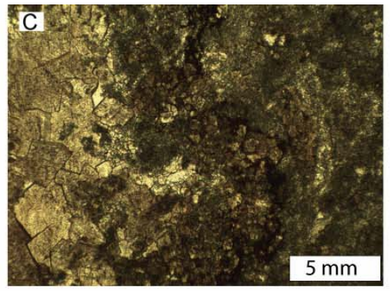
C
5 mm

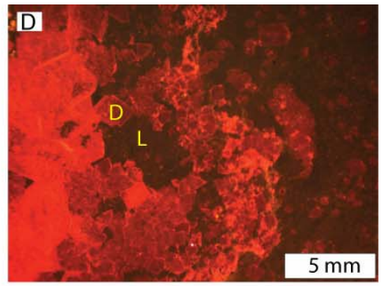
D
D
L
5 mm

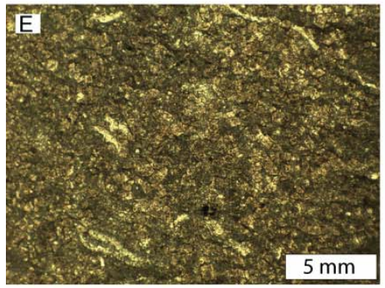
E
5 mm

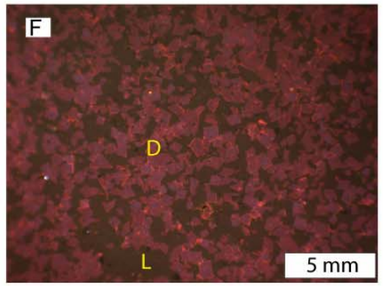
F
D
L
5 mm

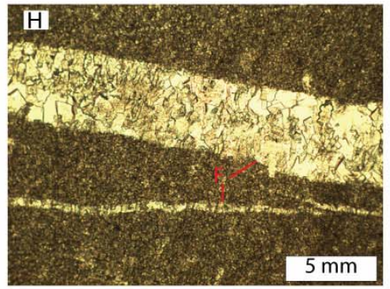
H
5 mm

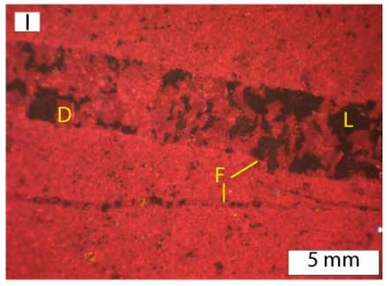
I
D
L
F
5 mm

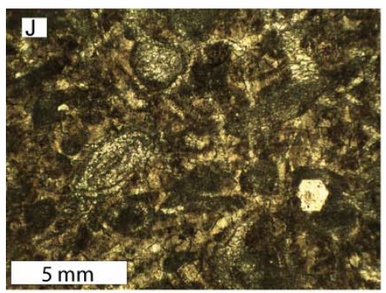
J
5 mm

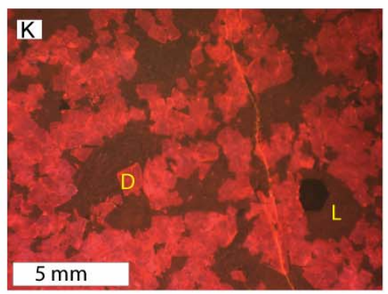
K
D
L
5 mm

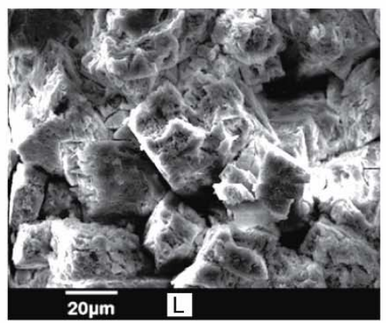
20µm
L

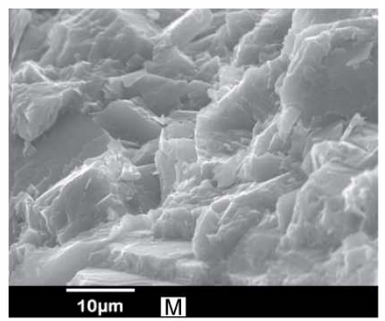
10µm
M

Early dolomite is abundant within the lower 2nd-order late highstand, thin-bedded progradational LCu deposits of the Cupido Formation compared with the upper 2nd-order early transgressive Cupidito member (Figure 4-9). Consequently, my study focuses on the early dolomite distribution within the LCu of the Cupido Formation.

Table 4-4 summarizes the cross-platform, early dolomite distribution within high-frequency cycles and depositional sequences of the Cupido Formation. The degree of dolomitization of individual high-frequency cycles is calculated from percentage thickness of dolomitized lithofacies within the cycle. Early dolomite is common in most peritidal high-frequency cycles, where less than 30% of the total cycles that have remained limestone. The remaining 70% of the cycles are partially (20% to 90% dolomite replacement) to completely dolomitized (≥ 90% dolomite replacement). The distribution of early dolomite within partially dolomitized cycles consistently exhibit a systematic decrease in early dolomite abundance downward from the cycle cap (tidal-flat facies) regardless of the precursor grain size. Within restricted subtidal cycles, early dolomite is abundant, and less than 15% of the total cycles that have remained limestone. The remaining 85% of the cycles are partially (10% to 90% dolomite replacement) to completely dolomitized (≥ 90% dolomite replacement). The intracyclic variation in abundance of early dolomite within peritidal and restricted subtidal cycles is closely related to (1) the position of the cycle within the depositional sequence and overall stratigraphic hierarchy (Figures 4-9 and 4-10),

(2) the proportion of tidal-flat to subtidal facies (Table 4-4), and (3) the location on the platform (Figure 4-11).

Stratigraphic distribution of early dolomite is also controlled by position within depositional sequences and overall stacking geometry within the lower 2nd-order late highstand LCu deposits of the Cupido Formation (Figure 4-9). Transgressive system tracts of depositional sequences (A-L) contain abundant early dolomite compared to highstand system tracts (Figure 4-10; Smith et al., 2004). Transgressive intervals of depositional sequences are composed of 65% cycles that are completely dolomitized, 20% cycles that are partially dolomitized and 15% cycles that remain limestone. Regressive intervals of depositional sequences are composed of 30% cycles that are completely dolomitized, 55% cycles that are partially dolomitized and 15% cycles that remain limestone. The large-scale distribution of early dolomite shows a close relationship to the 2nd-order sequence boundary within the Cupido Formation as most of the 2nd-order LCu is dolomitized (Figures 4-9 and 4-10).

Intracyclic early dolomite distribution varies with tidal-flat to subtidal facies ratio (Table 4-4). Thick subtidal cycles (average = 8 m) are commonly completely dolomitized, whereas thinner, tidal-flat dominated cycles (average = 3 m) are partially dolomitized. The relationship between tidal-flat to subtidal facies ratios in cycles, dolomite abundance and cycle thickness also correlate with lithologic evidence for minimal accommodation or exposure (Figure 4-12). Tidal-flat facies in subtidal-dominated completely dolomitized cycles rarely show any

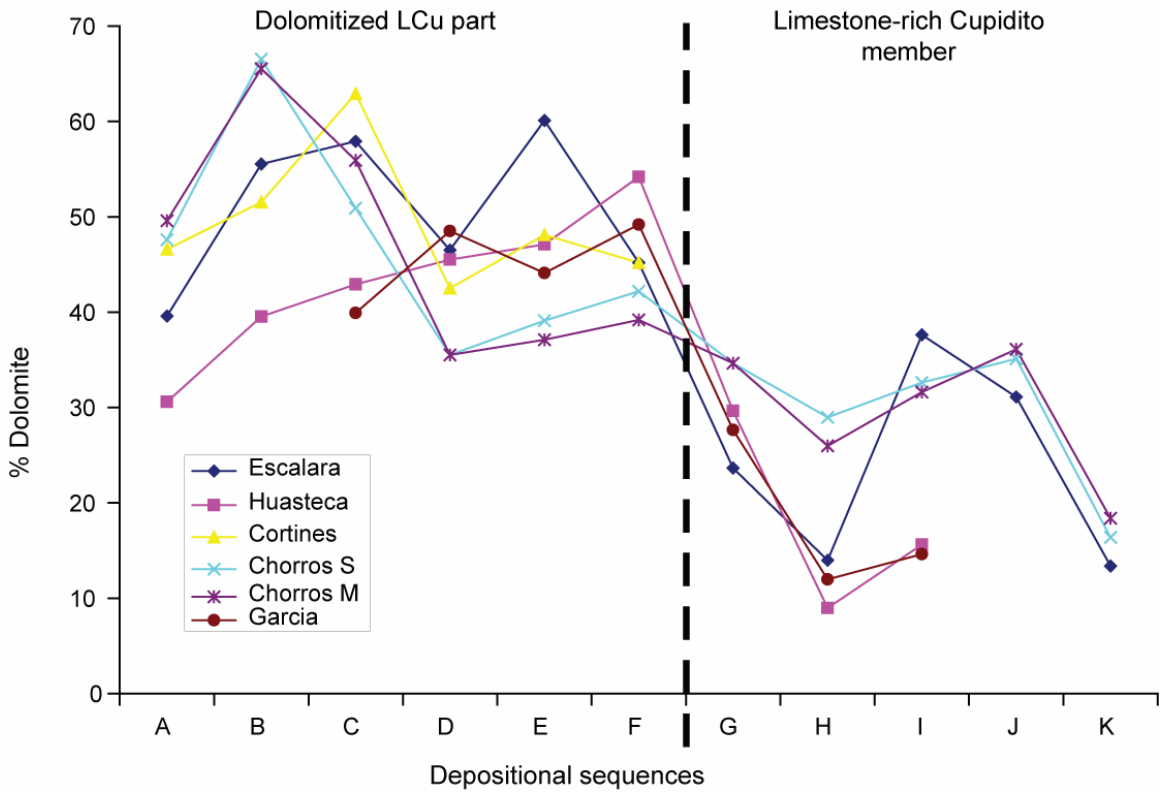

Figure 4-9. Dolomite distribution trend.

Trend showing significant decrease in dolomite distribution between the regressive dolomitized LCu and the transgressive lime-rich Cupidito member of the Cupido Formation. Data are averaged by sequence.

Table 4-4. Intracyclic dolomite distribution within system tracts..

Summary of intracyclic dolomite distribution within high-frequency cycles (HFC) from transgressive and highstand system tracts of depositional sequences interpreted from different stratigraphic sections from across the platform. Abbreviations and section names are similar to those in Figure 4-1.

System Tract	Depos. Setting Section	Cycle thickness Average (m) *(range)*	Tidal-flat to subtidal Facies ratio	Early dolomite in cycle (%)	Early dolomite in tidal-flat facies (%)	Early dolomite in subtidal facies (%)
Depositional sequences transgressive system tracts cycles	Total HFC	6.3	0.6	98	73	99
	Tidal-flat *ChC sections*	5.6 *(0.1-16.0)*	0.7	85	83	95
	Lagoon *EC and CC sections*	8.2 *(1.1-18.3)*	0.7	97	91	99
	Shoal tidal-flats *PG, PC and PMV sections*	4.9 *(0.2-15.9)*	0.6	86	80	94
	Shoal *HC section*	5.3 *(0.6-19.0)*	0.4	76	71	83
Depositional sequences highstand system tracts cycles	Total HFC	3	0.7	79	91	58
	Tidal-flat	1.3 *(0.1-6.6)*	0.9	79	95	65
	Lagoon	1.4 *(0.6-5.9)*	0.8	76	88	69
	Shoal tidal-flats	1.4 *(0.3-6.1)*	0.9	75	93	53
	Shoal	1.9 *(0.1-4.9)*	0.4	52	70	41

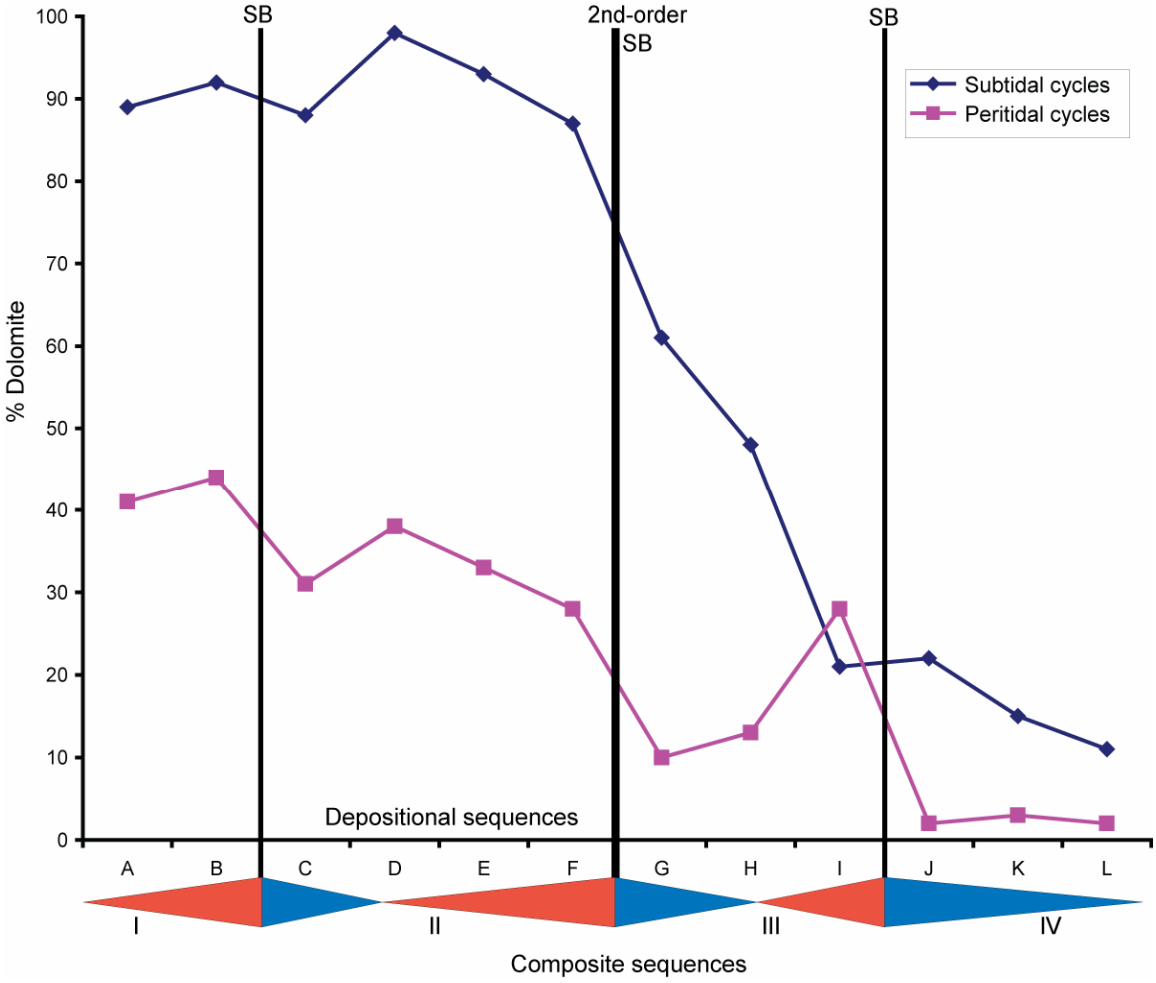

Figure 4-10. Early dolomite distribution within subtidal and peritidal cycles.

Intracyclic dolomite variations with respect to depositional sequences and overall stratigraphic framework. Data collected from all measured stratigraphic sections.

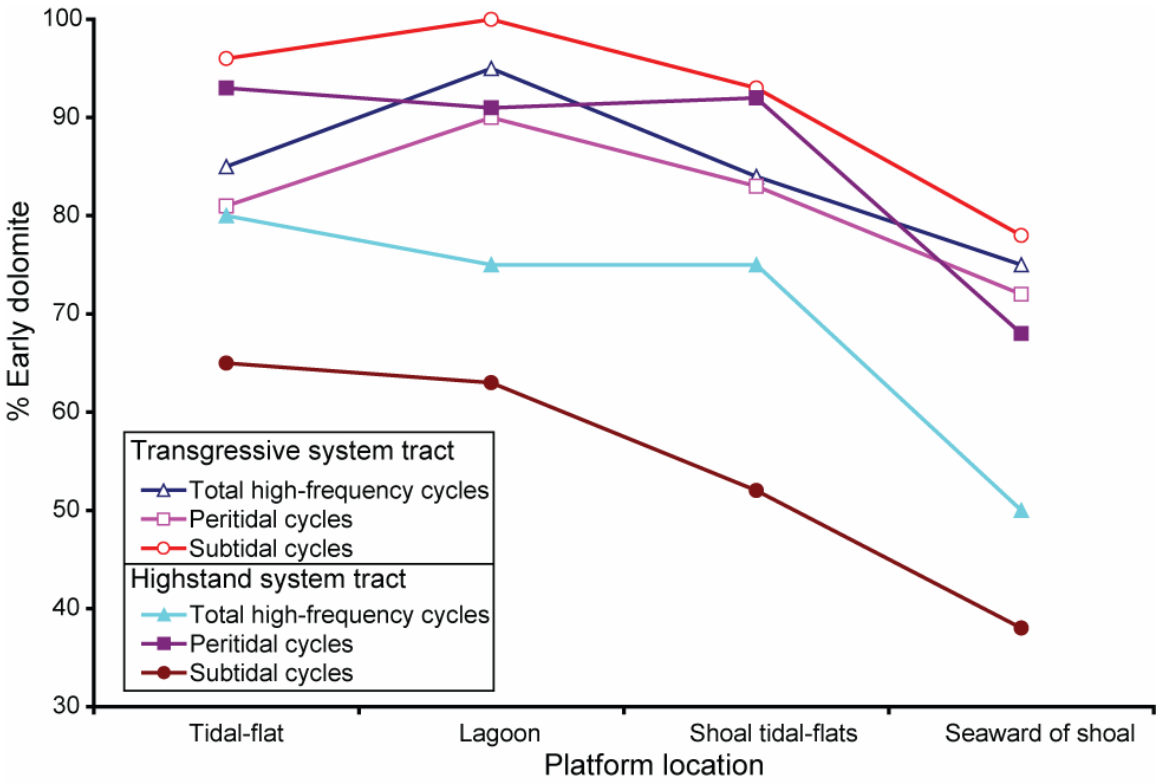

Figure 4-11. Intracyclic dolomite distribution across the platform.

Intracyclic dolomite distribution across the Cupido platform. Transgressive high-frequency cycles are more dolomitized compared to regressive cycles. Degree of dolomitization varies across the shallow platform. Tidal-flat and lagoonal facies contain more abundant dolomitized cycles relative ton shoal tidal-flats and shoal crest deposits. Transgressive subtidal cycles are commonly dolomitized, followed by regressive peritidal cycles, transgressive peritidal cycles and least dolomitized are regressive subtidal cycles.

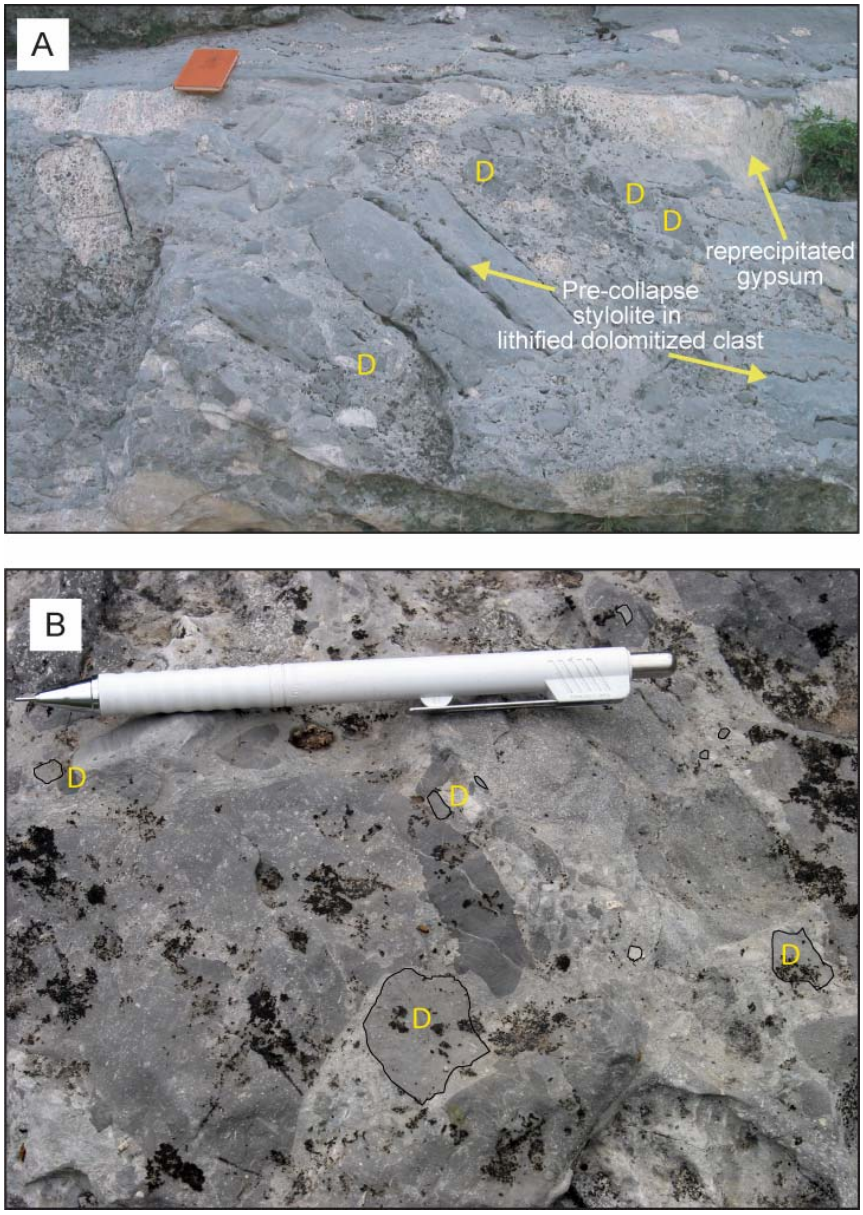

Figure 4-12. Solution-collapse breccias.

(A) thick solution-collapse breccia with clasts up to 3.0 m long, dolomitized lithified clasts (D).

(B) small-scale collapse breccia with abundant dolomitized clasts (D) and large clast sizes (<0.3 m)

evidence of exposure (e.g., sabkha like anhydrite or mudcracks). In contrast, partially dolomitized thinner, tidal-flat dominated cycles show laminites with increasing extent of anhydrite nodules and mudcracks (Figure 4-5).

Intracyclic formation of early dolomite controls the larger-scale platform-wide distribution of early dolomite. In general, the abundance of early dolomite within cycles decreases from landward to seaward systematically across the platform (Table 4-4; Figure 4-11). Intervals of stacked peritidal cycles dominated by dolomite are abundant on the inner platform, whereas, partially dolomitized to limestone-rich cyclic intervals are best developed toward the outer platform (Table 4-4; Figure 4-11). On the inner shelf, 70% of the cycles are completely dolomitized, 26% are partially dolomitized, and 4% remain limestone. On the middle shelf, 73% of the cycles are completely dolomitized, 24% are partially dolomitized, and 3% remain limestone. On the outer shelf, 41% of the cycles are completely dolomitized, 37% are partially dolomitized, and 22% remain limestone.

Lateral continuity and vertical distribution of early dolomite

The most dolomitized cycles in the Cupido Formation occur in the restricted subtidal-dominated carbonates in the transgressive portions of 4^{th}-order depositional sequences in the progradational LCu interval (Figure 4-11). Partially to completely dolomitized high-frequency cycles dominate the thin tidal-flat dominated cycles at the top of highstand system tracts of depositional

sequences. The dolomitized peritidal and restricted subtidal cycles are abundant in the middle and inner parts of the platform. Figure 4-13 shows the distribution of dolomitized cycles in a sequence stratigraphic framework from Cupido outcrop at Chorros Canyon (ChC; Figure 4-1). Dolomitization of cycles is pervasive and laterally continuous in the transgressive system tracts. The dolomite bodies cut facies tracts and decrease in thickness upward toward the top of the LCu (Figure 4-13). Downdip in the lagoon, nearly all the cycles in the transgressive system tracts of depositional sequences within the LCu are pervasively dolomitized. However, the highstand system tracts of depositional sequences are increasingly dominated by partially dolomitized to limestone cycles toward the top of the LCu interval (Figure 4-14).

Figure 4-13. Early dolomite distribution at Chorros Canyon.

Correlation of depositional sequences into larger composite sequences within the Cupido Formation in Chorros Canyon (ChC). Six detailed sections within the LCu show vertical and lateral changes in facies components, high-frequency cycles type and stacking patterns. Dolomite (Orange) is abundant and laterally extensive in the transgressive portion of depositional sequences compared to the regressive portion. The systematic change in cycle types and dolomite abundance at Chorros Canyon offers a unique opportunity to investigate any possible links between ecstatically-induced stratigraphic surfaces and dolomite distribution. Vertical scale divisions are in meters.

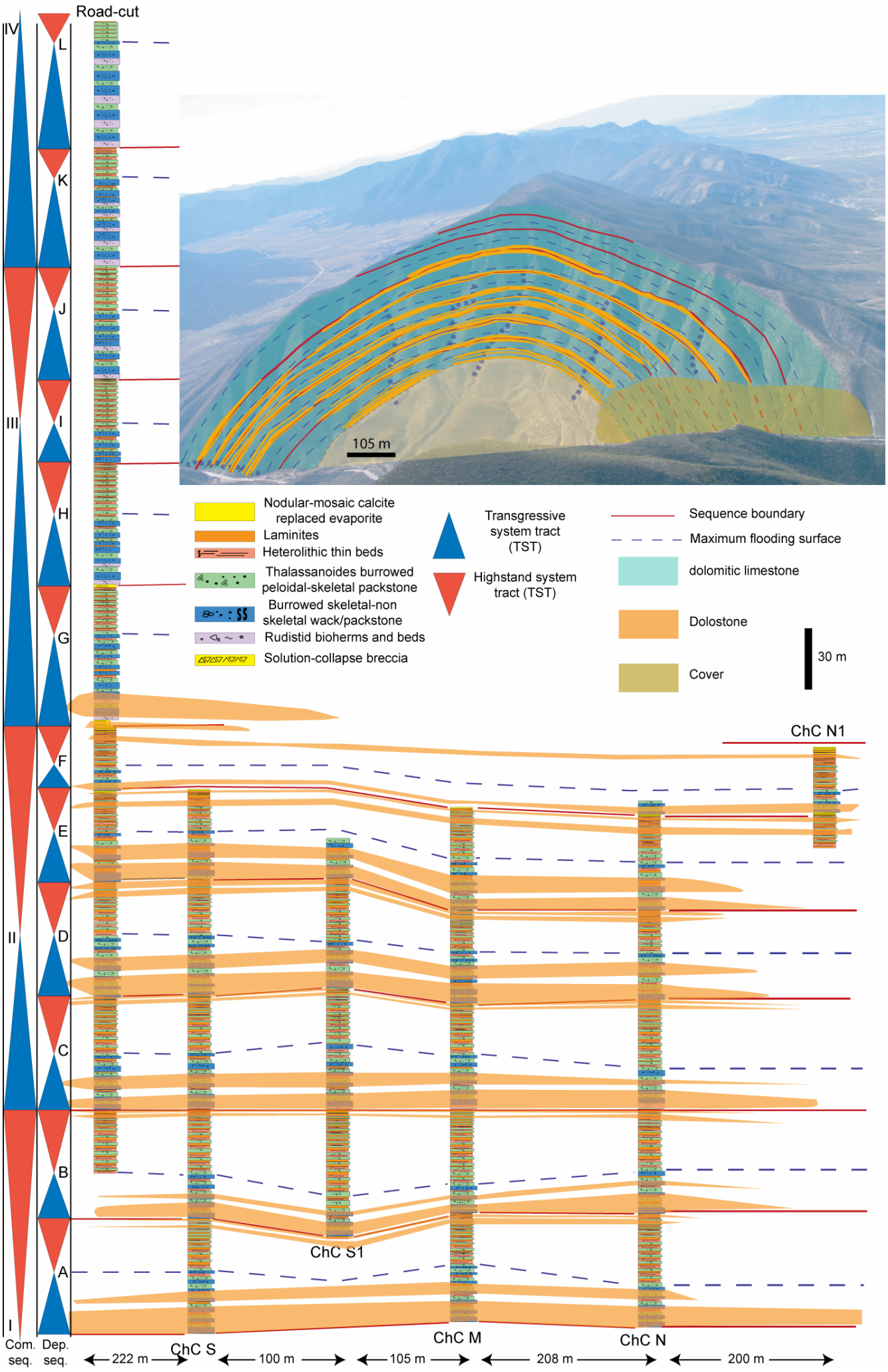
Road-cut
IV
III
II
I
L
K
J
I
H
G
F
E
D
C
B
A
105 m
Nodular-mosaic calcite replaced evaporite
Laminites
Heterolithic thin beds
Thalassanoides burrowed peloidal-skeletal packstone
Burrowed skeletal-non skeletal wack/packstone
Rudistid bioherms and beds
Solution-collapse breccia
Transgressive system tract (TST)
Highstand system tract (TST)
Sequence boundary
Maximum flooding surface
dolomitic limestone
Dolostone
Cover
30 m
ChC N1
ChC S1
ChC M
ChC N
ChC S
Com. seq.
Dep. seq.
222 m
100 m
105 m
208 m
200 m

Spatial distribution of completely dolomitized beds along a continuous measured section were analyzed using normalized correlation count technique (Marrett et al., in review) to determine length scale of clusters if any (Figure 4-15). Limestone and dolostones (>90% dolomite) beds from Escalera Canyon were to document the spacing between dolomitized beds. This was achieved by identifying the contacts between limestone and dolostone beds and measuring the distances separating dolostones (thickness of limestone beds). These distances (contacts length) were analyzed, to determine cluster widths if any, between the dolomitized beds. The contacts at Escalera Canyon (EC; Figure 4-1) have a cluster width of 60 m which is the average thickness of depositional sequences encompassed within the measured section (Figure 4-15). The spatial correlation forms a plateau profile (Marrett et al., in review; Figure 4-15) above the 95% confidence limit. This indicates that clustering of dolostone/limestone contacts is non-random, and is inherited or forced by an external process as opposed to being self organized (Marrett et al., in review).

Farther downdip, the outer shelf section is dominated by partially dolomitized and limestone cycles with no apparent relationship between dolomite distribution and sequence stratigraphic surfaces (Figures 4-11 and 4-16). The overall dolomite distribution pattern within the LCu of the Cupido Formation indicates that dolomitization is more focused across the restricted shelf interior by local alteration process or processes that are in turn controlled by an external process (e.g., sea-level fluctuations).

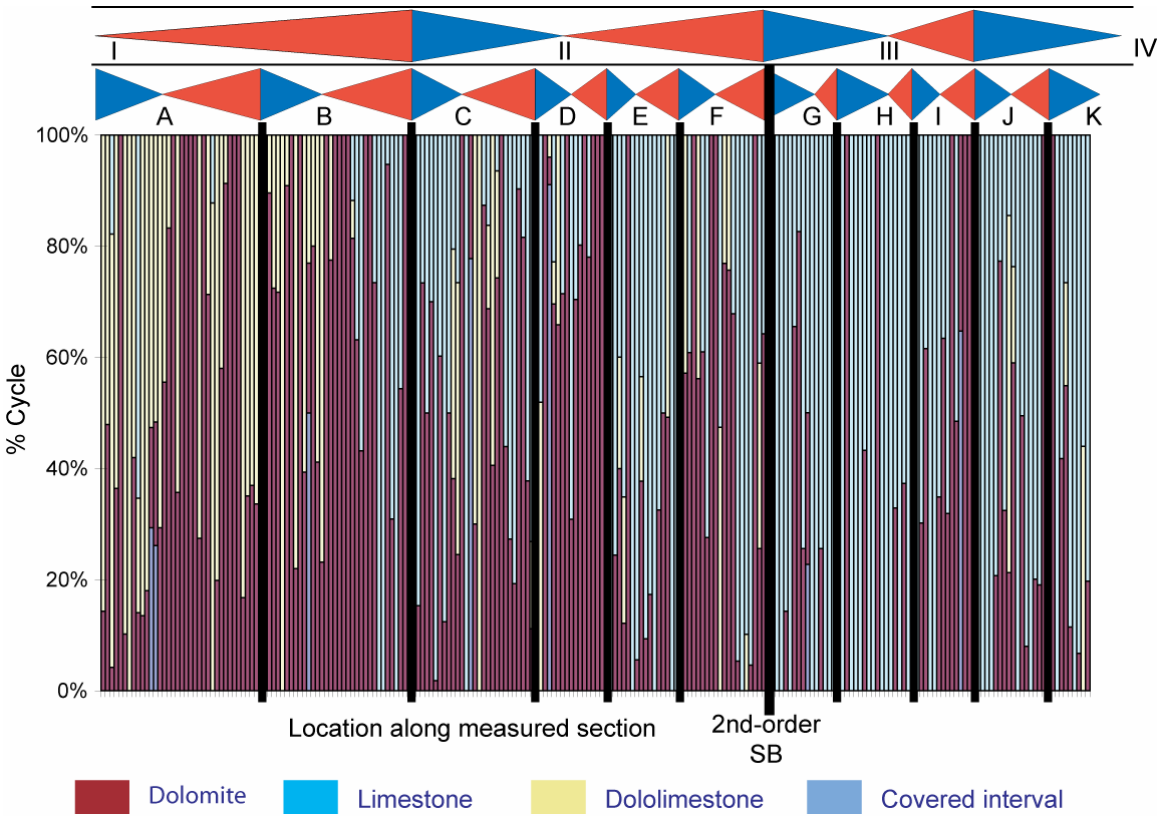

Figure 4-14. Early dolomite distribution at Escalera Canyon.

Extensive dolomitization in the transgressive portions of depositional sequences (A-K) within the LCu. Composite sequences (I-IV) show no apparent relation to early dolomite distribution. The top of depositional sequence F marks the 2nd-order sequence boundary. The degree of dolomitization decreases dramatically in the transgressive Cupidito member (see Figure 4-9). Balck lines mark depositional sequence boundaries. Blue triangle represents transgressive system tract, red triangle represents highstand system tract.

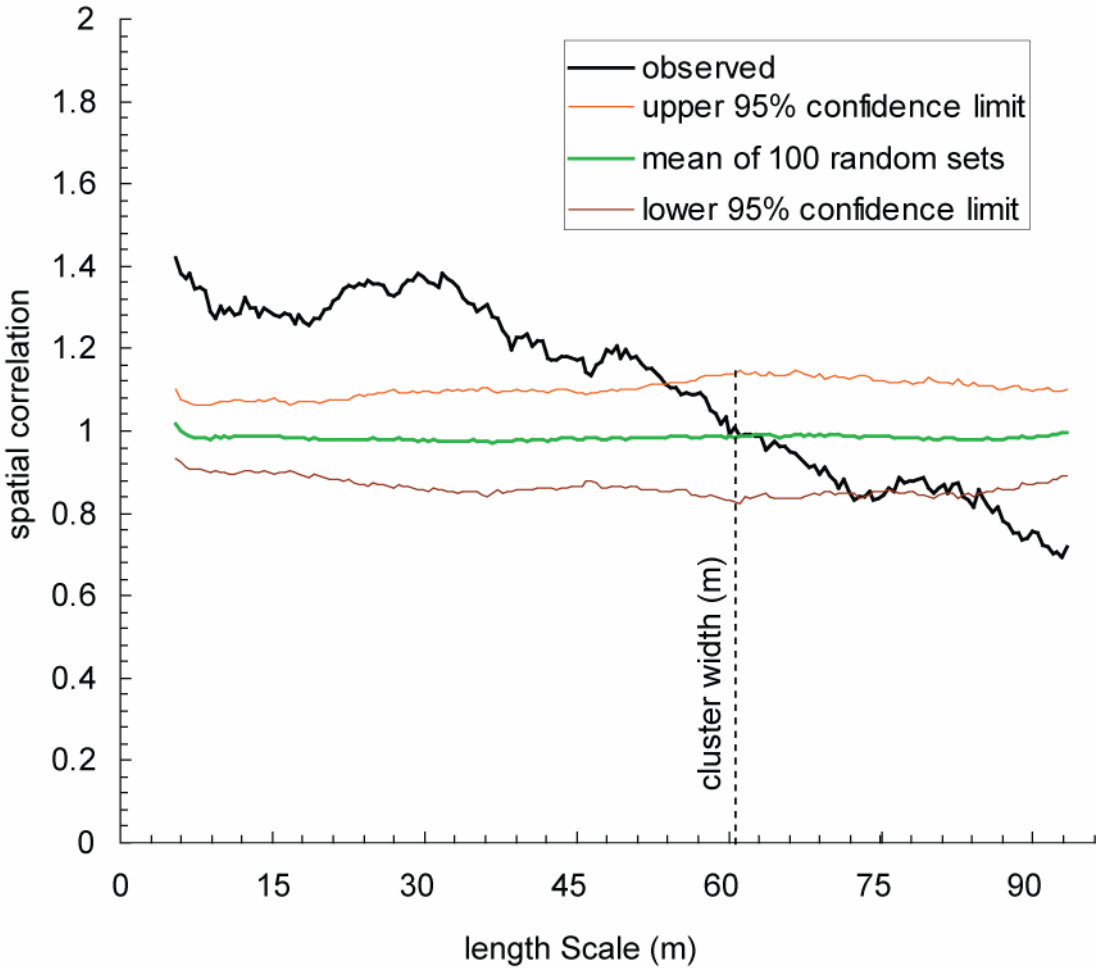

Figure 4-15. Clustering of dolomite beds.

Correlation count of dolomite/limestone contacts along a measured line from Escalera Canyon (Figure 4-1). The X-axis represents the length scale of clusters, if any, and the Y-axis represents distribution relative to random data sets. Identified cluster length (width) is 61 m.

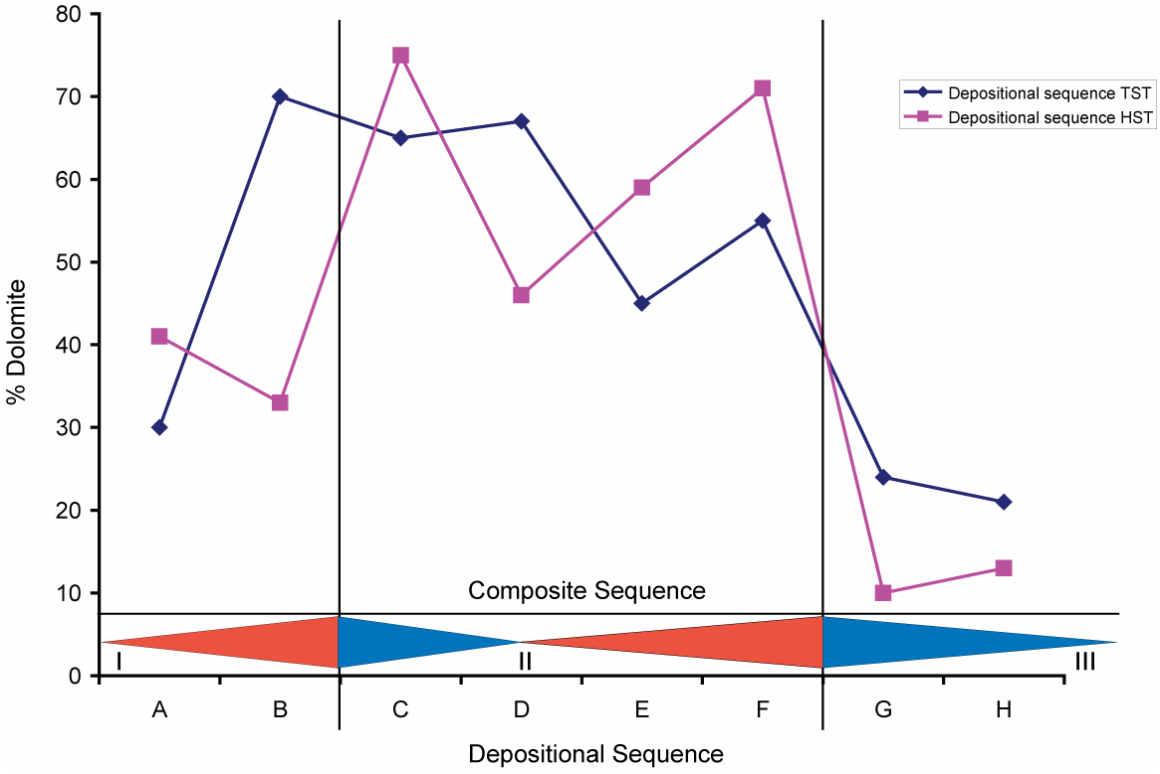

Figure 4-16. Early dolomite distribution at shelf margin.

Dolomite distribution at Huasteca Canyon showing no apparent relationship to system tract components of depositional and composite sequences.

ORIGIN OF SYNSEDIMENTARY DOLOMITIZATION AND HIGH-FREQUENCY CYCLICITY OF THE CUPIDO FORMATION

Synsedimentary dolomitization

Dolomitization of the Cupido carbonates occurred within individual cycle periods as indicated by early dolomite clasts reworked in the overlying transgressive base of the next cycle (Figure 4-17). The presence of layered early dolomite in peloidal laminites and mudstones also indicate synsedimentary dolomitization. Dolomitization 'fronts' do not cross cut cycle boundaries. Stylolites developed within dolomitized beds suggest that dolomitization occurred prior to significant burial compaction. Ortega and Marrett (2001) suggested that the degree of dolomitization had the dominant control on early burial fracture distribution within the Cupido carbonates. Hence, dolomitization predated or is concurrent with early fracture development.

Additional evidence for initial dolomitization occurring during deposition of individual cycles includes (1) a systematic decrease in dolomite abundance with distance downward beneath cycle caps in partly dolomitized cycles (James, 1984; Strasser, 1988; Figure 4-18), and (2) the restricted basal parts of subtidal cycles are dolomitized and the degree of dolomitization decreases systematically as slightly open-marine facies were deposited before partially to completely dolomitized tidal-flat cycle caps (Table 4-4). Early dolomite alteration by burial diagenetic processes is interpreted to be minimal because fractures are

Figure 4-17. Reworked early dolomite clasts.

(A) Dolomitized laminite clasts are included in the transgressive base of the overlying cycle as rip-up clasts in a dolomitized burrowed wackestone/packstone. (B) Abundant dolomitized clasts from the underlying cycle cap are mixed in with a partially dolomitized transgressive base in skeletal wackestone.
(C) Dolomitized cryptalgal laminites are broken up in a mini teepee structure and some clasts are included in the dolomitized base of the overlying cycle.

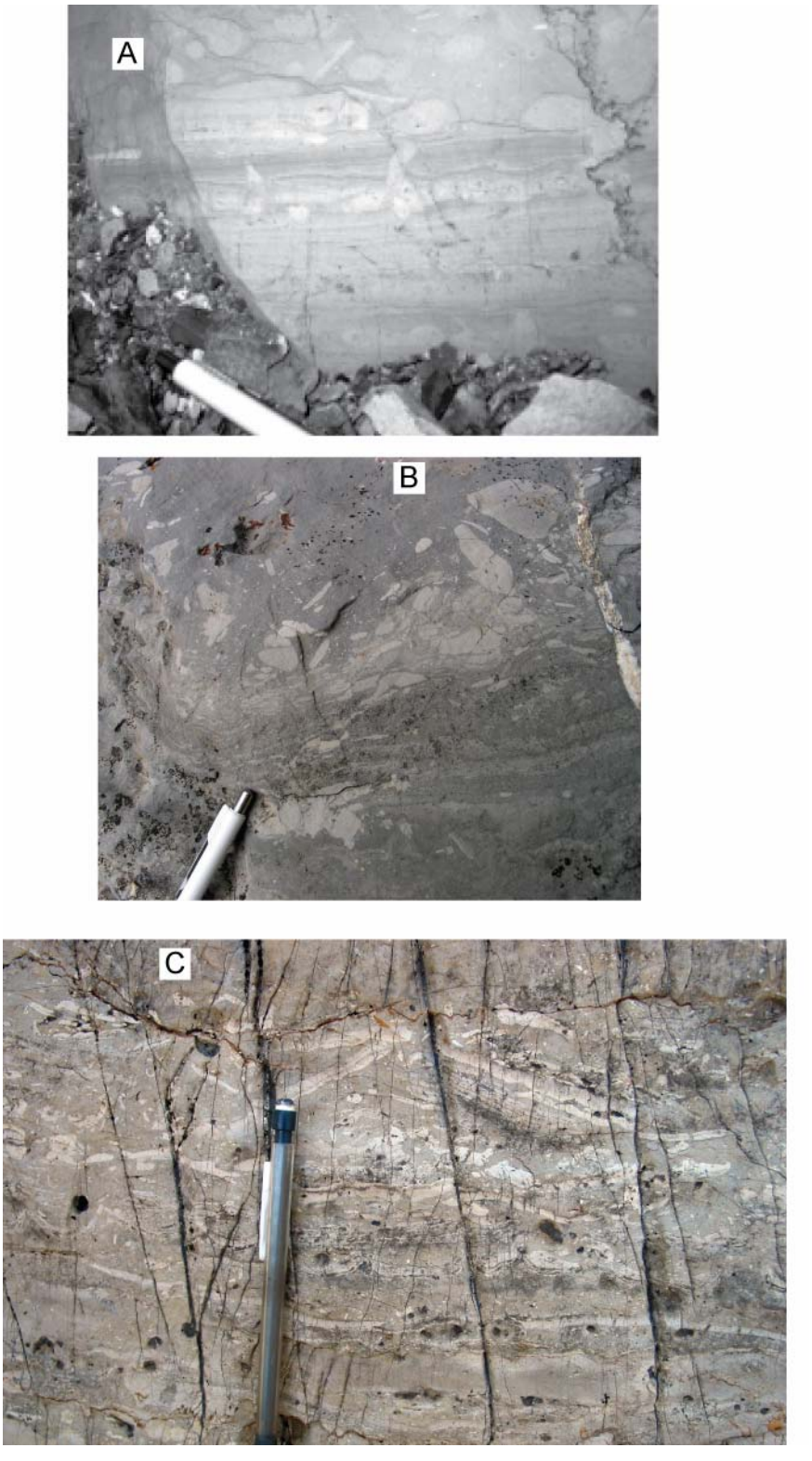
A
B
C

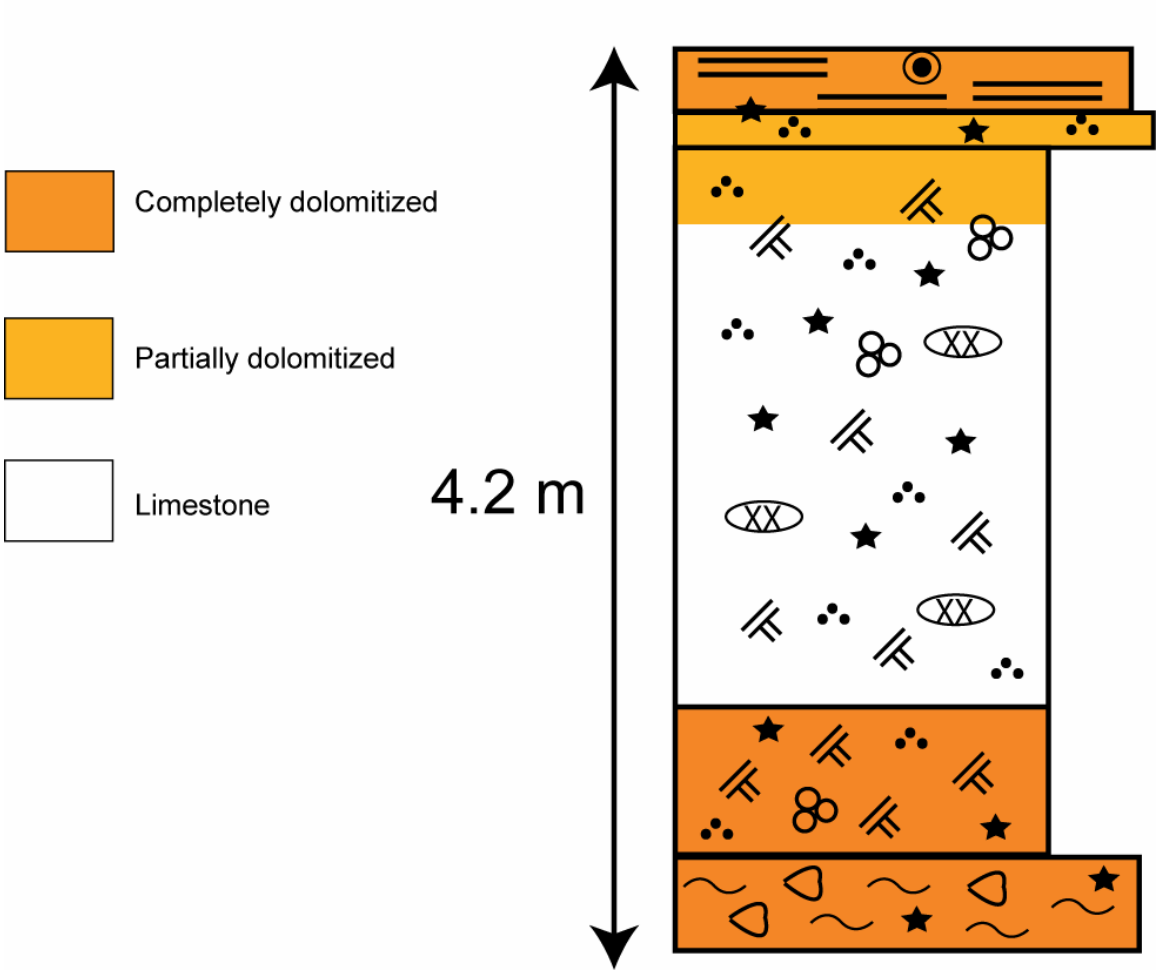

Figure 4-18. Schematic intracyclic early dolomite distribution.

Early dolomite distribution within a 4.2 meter thick high-frequency cycle from Escalera Canyon. The transgressive base and the regressive top of the cycle are dolomitized. Degree of dolomitization decreases downward from the cycle cap.

interpreted to have acted as conduits for late dolomitizing diagenetic fluids.

High-frequency cycles

Meter-scale, shallowing-upward peritidal and restricted subtidal facies in the Cupido carbonates were deposited in shallow evaporitic shallow lagoons, tidal-flat zones, and supratidal sabkhas during peak Cretaceous greenhouse climate conditions (Read, 1995). Regionally extensive evaporites, solution-collapse breccia and sabkha carbonates indicate arid to semiarid conditions in northeastern Mexico from Barremian to Aptian time similar to the modern arid Persian Gulf (Purser, 1973). Abundant anhydrite nodules in laminites and peloidal dolomudstones also suggests arid to semiarid conditions during deposition (Hardie and Shinn, 1986; Demicco and Hardie, 1994).

Meter-scale high-frequency cycles formed in response to high-frequency sea-level fluctuations caused by variations in Milankovitch orbital forces (Fischer, 1964; Berger, 1984; Grotzinger, 1986; Goldhammer et al., 1987; Hinnov, 2000). Most individual Cupido cycles are composed of a transgressive base (shallow-restricted subtidal platform facies) capped by tidal-flat (peritidal to evaporitic interior facies) and formed during pulses of short-term high-frequency sea-level rises caused by Milankovitch-induced climate changes (Figure 4-19). Lags in sedimentation may have occurred as initial sea level rise outpaced sedimentation rates with the sediment surface aggrading to sea level within 15% to 20% of each

Figure 4-19. Milankovitch-signal across the Cupido shelf.

Blackman-Tukey spectral analysis of measured sections through the Cupido Formation exposed at Chorros Canyon, Cortinas Canyon, Escalera Canyon and Huasteca Canyon (Figures 4-1). Color bars indicate platform-wide laterally correlated spectral peaks at known Milankovitch periods (Yang et al., 1995; Hinnov, 2000). Labeled peaks are highly-significant (above the 90% statistical confidence limit).

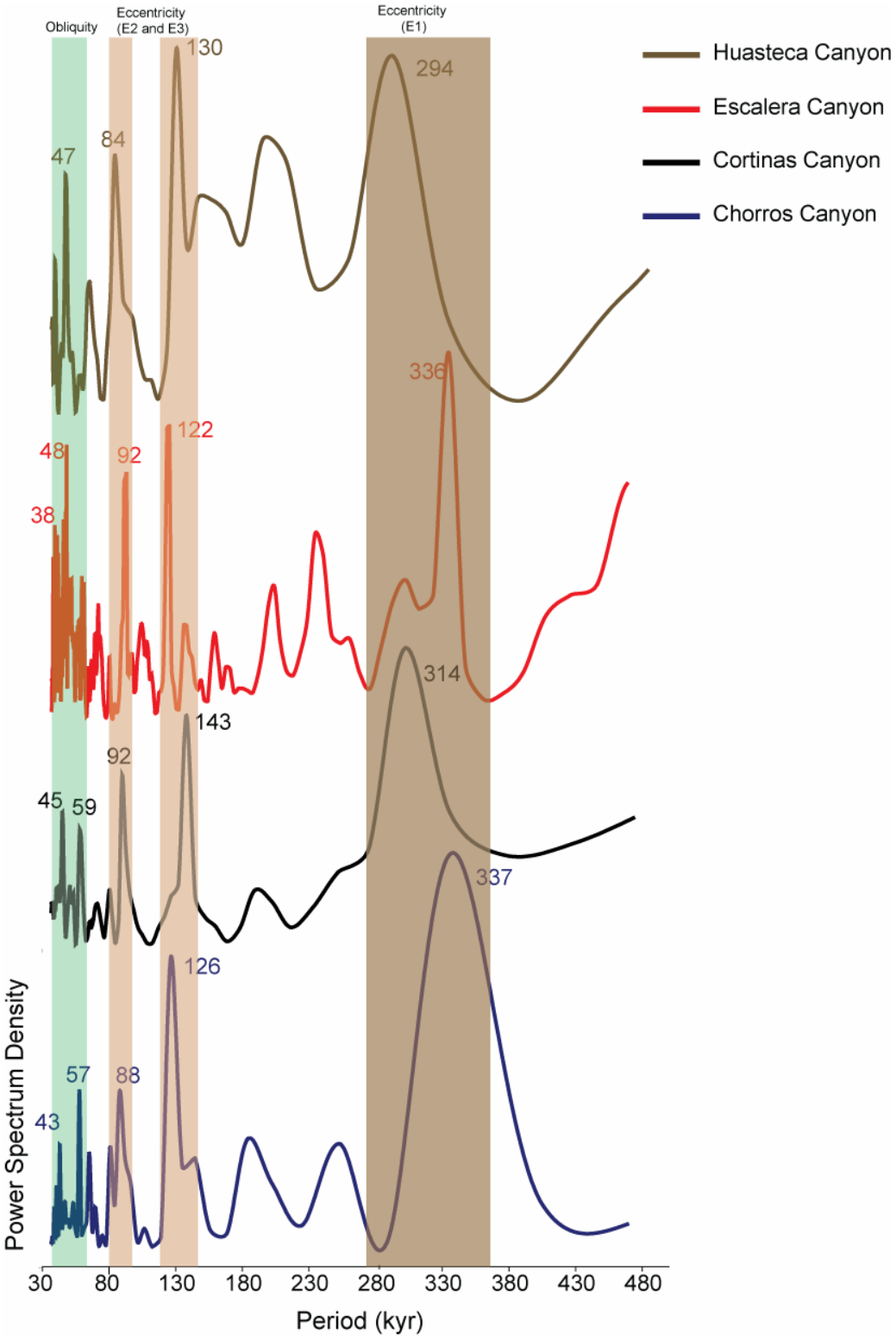
Obliquity
Eccentricity (E2 and E3)
Eccentricity (E1)
Huasteca Canyon
Escalera Canyon
Cortinas Canyon
Chorros Canyon
47
84
130
294
48
38
92
122
336
45
59
92
143
314
43
57
88
126
337
Power Spectrum Density
30
80
130
180
230
280
330
380
430
480
Period (kyr)

cycle period (Koerschner and Read, 1989). Assuming reasonable progradation rates (Holocene rates equal 0.5 to 20 km/kyr; Patterson, 1972; Hardie and Shinn, 1986), the supratidal portion of the tidal-flats would become emergent with continued progradation.

EUSTATIC CONTROL ON SEQUENCES AND DOLOMITE DISTRIBUTION

Within the study area, the lower 2nd-order late highstand progradational LCu of the Cupido Formation is more dolomitized than the upper 2nd-order order transgressive Cupidito member (Altobi, 2006; Figures 4-7 and 4-9). The 2nd-order sea-level rise caused gradual increase in accommodation space, open-marine conditions, and backstepping of shallow-carbonate sedimentation farther landward. This resulted in lesser basinward progradational extent of tidal-flats (Goldhammer, 1999, Lehmann et al., 2000) and possibly restricted early dolomite deposition updip close to the Coahuila block (Montañez and Read, 1992). The LCu is composed of partial composite sequence I and composite sequence II (Figure 4-7) with both sequences showing an overall decrease in degree of dolomitization upward toward the 2nd-order sequence boundary (top of LCu; Altobi, 2006; Figure 4-7).

Fischer plot analysis of meter-scale high-frequency cycles deviations from mean cycle thickness was carried out to evaluate changes in accommodation space through time (Fischer, 1986; Read and Goldhammer, 1988; Osleger and

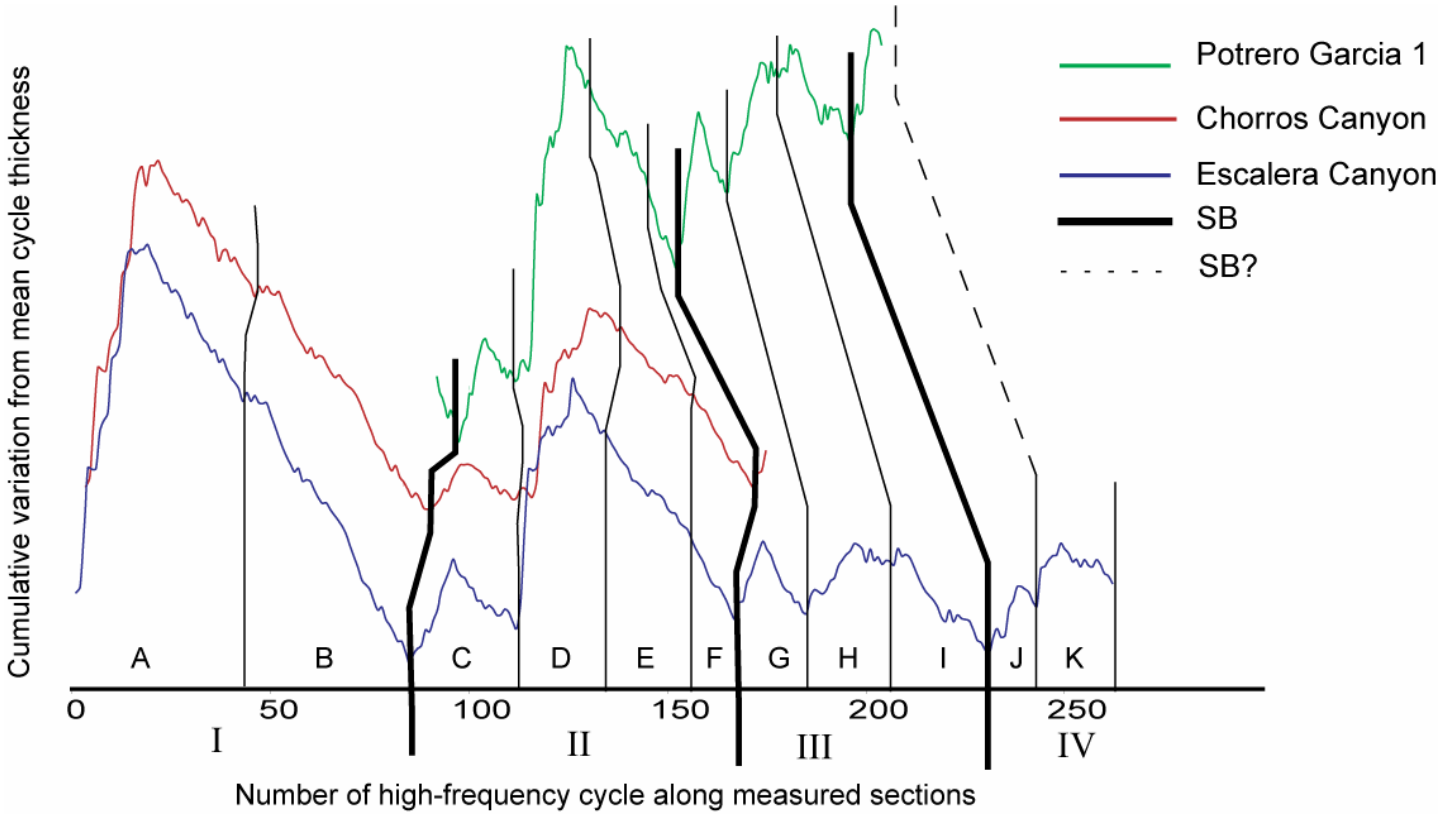

Figure 4-20. Accommodation plots.

Fischer plots of the Cupido Formation are combining 3 sections, Chorros Canyon (ChC), Escalera Canyon (EC), and Potrero Garcia (PG1) highlighting overall change in accommodation space and lateral correlation of depositional sequences (A-K) and composite sequences (I-IV) and their bounding sequence boundaries (SB).

Read, 1991; Lehrmann and Goldhammer, 1999; Figure 4-20). Systematic deviations in cycle thickness from the mean can be used to infer changes in relative sea level (Read and Goldhammer, 1988; Osleger and Read, 1991). These plots were also used to display the great lateral extent of interpreted composite and depositional sequences, therefore reveal potential eustatic origin across the different sections.

In the Cupido Formation, changes in facies components, cycle thickness, and stacking patterns of high-frequency cycles were used to define depositional sequences. Stacked thin peritidal cycles, exposure surfaces, or solution-collapse breccia are interpreted as indicators of minimum accommodation space and sequence boundaries for individual depositional sequences. Correlated Fischer plots indicate platform-wide changes in sea level generated the interpreted depositional sequences within the Cupido Formation. Sea-level variations (fourth-order scale) are probably caused by a combination of climatic processes induced by Milankovitch orbital forcing (Figure 4-19).

Six depositional sequences (A-F) are interpreted in the dolomitized LCu and the degree of dolomitization of these depositional sequences decreases systematically upward (Figures 4-7 and 4-10). Variations in abundance of early dolomite distribution within the LCu are associated with changes in cycle stacking patterns and depositional sequences, suggesting that Milankovitch-driven sea-level variations coupled with the environmental processes/model strongly controlled early dolomite distribution.

During 4th-order sea-level rises on Fischer plots, stacks of thick (average = 10 m) shallow subtidal cycles developed that are characterized on the inner shelf by restricted environment lithofacies such as *thalassanoides* burrows (Figure 4-21A); bedded *requienids* and *chondrodonts* packstones; mixed skeletal packstones; and capped by burrowed heterolithic thin beds (Figure 4-5). On the outer platform, stacks of thick deeper subtidal cycles are dominated by bedded *requienids* and *chondrodonts* packstones (Figure 4-21B), and caprinid rudists that overlie the burrowed sediments and interfinger with skeletal packstones before terminating in dominantly oolitic grainstone caps (Figures 4-5 and 4-21C). These transgressive cycles are commonly dolomitized (Table 4-4), especially their lower parts. Stacks of thick, subtidal cycles define relative increase in accommodation space during 4th-order rises in sea level. This increase in accommodation space is recorded in these transgressive cycles by their thick proportions of subtidal facies and (Table 4-4) and limited evidence of exposure in their tidal-facies caps. Gradual rises in sea level transformed the depositional condition, especially on the inner platform, from dominantly evaporitic to restricted resulting in abundant early dolomitization. These Milankovitch-induced 4th-order sea-level rises possibly supplied the required fluids onto the shallow evaporitic platform and elevated the Mg/Ca ratio resulting in efficient dolomitization of subtidal sediments. Overall, early dolomitization was abundant during 4th-order sea-level rises as indicated by 70% of all transgressive cycles being completely dolomitized.

Figure 4-21. Subtidal Cupido carbonate facies.

(A) Field photograph of *thalassanoides* burrow networks from a view of the bedding plane.

(B) Hand sample of unoriented *caprinid* rudists in mud rich matrix.

(C) Photomicrograph of well sorted grainstone, ooids and lumps with skeletal nuclei.


A

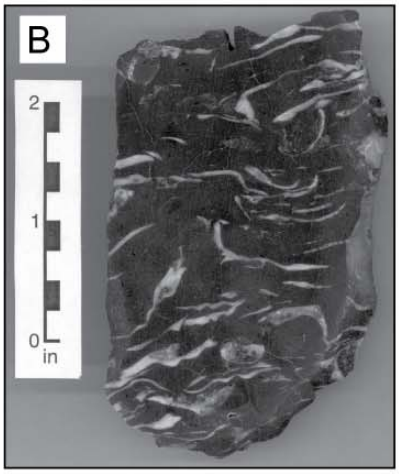
B
2
1
0
in

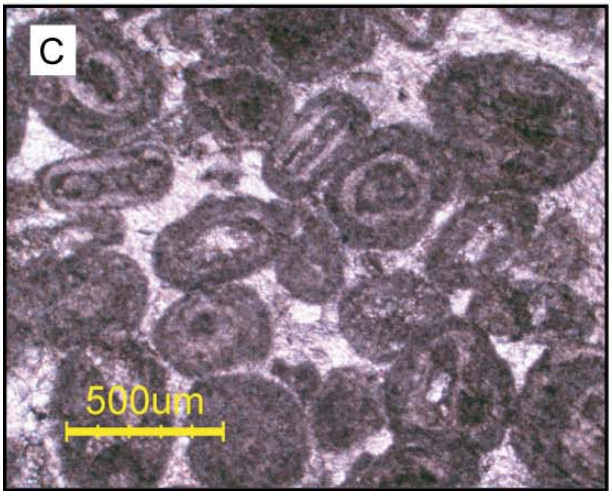
C
500um

During 4th-order relative sea-level falls on Fischer plots, stacks of thin (average = 3 m) tidal-flat dominated peritidal cycles dominate the platform. These cycles are dominantly composed of evaporitic-restricted lithofacies such as *thalassanoides*-burrowed peloidal wackestones/packstones overlain by heterolithic thin beds of alternating mudstones and skeletal packstones (Figures 4-5 and 4-22A). The cycles are capped by cryptalgal laminites with mudcracks and calcitized nodules (originally anhydrite; Figures 4-5, 4-6 and 4-22B). These restricted peritidal cycles likely record reduced accommodation space during 4th-order sea-level falls. Extended durations of tidal-flat progradation, evaporitic conditions and emergence are indicated by high proportions of tidal-flat facies, mudcracks, evaporite nodules and solution-collapse breccia (Figures 4-6 and 4-12). These regressive cycles dominantly are partially to completely dolomitized (Table 4-4). Dolomite, however, is restricted to cycle caps and decreases systematically away from the cycle cap suggesting limited synsedimentary dolomitization during highly evaporitic conditions (Folk and Land, 1975).

Other controls: (1) Rates of sea-level rise

Rates of sea-level rise may have influenced dolomite distribution in the Cupido platform. Rapid rates of some 4th-order sea-level rises could have resulted in platform-wide occurrence of limestone, partially dolomitized, and maybe some dolomitized cycles within transgressive parts of depositional sequences in open-marine conditions. However, dolomitization would have been

Figure 4-22. Peritidal Cupido carbonate facies.

(A) Hand sample illustrating the thin laminations on a mm scale, the tan layers are mudstones and the black layers are packstones.

(B) Photomicrograph of alternating micrite dominated layers and packstone layers containing fossil debris and peloids.

(C) Photomicrograph of dolomitized laminated mudstone.


A
2
1
0
in

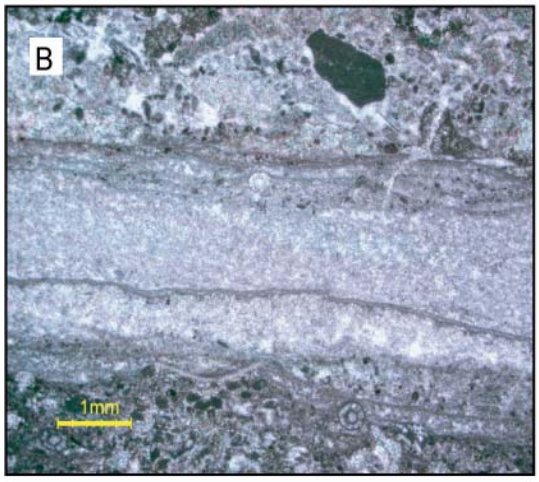
B
1mm

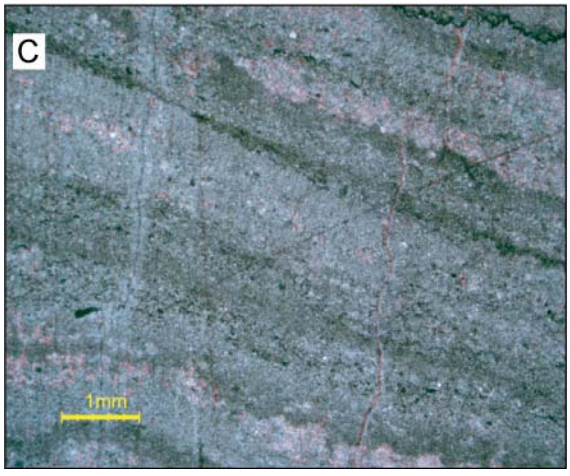
C
1mm

more abundant during slow rates of 4th-order sea-level rise. With gradual increase in accommodation space, the depositional environments slowly switched from dominantly evaporitic to restricted and maybe slightly open-marine settings for brief time periods. The resultant depositional environments would have been dominated by dense hypersaline fluids capable of dolomitizing large areas and rock volumes. Simultaneously, a landward shift in tidal-flat deposition (Altobi et al., *in prep.*) would induce synsedimentary dolomitization farther updip resulting in platform-wide early dolomite deposition.

(2) Shoal crest geometry

Tidal-flats are interpreted to have developed on the landward side of the shoal, close to the lagoon (Altobi et al., *in prep.*; Figure 4-4). These tidal-flats prograded toward the lagoon depocenter during 4th-order sea-level falls and narrowed as the shoal aggraded to keep up with increasing accommodation during 4th-order sea-level rises (Figure 4-23). Most high-frequency cycles from the outer shelf remain limestone with some being partially dolomitized (10% are completely dolomitized cycles, 52% are partially dolomitized and 38% remain limestone; Table 4-4). This dolomite distribution probably controlled by variation in accommodation space is caused by sea-level variations or sediment accumulation or both.

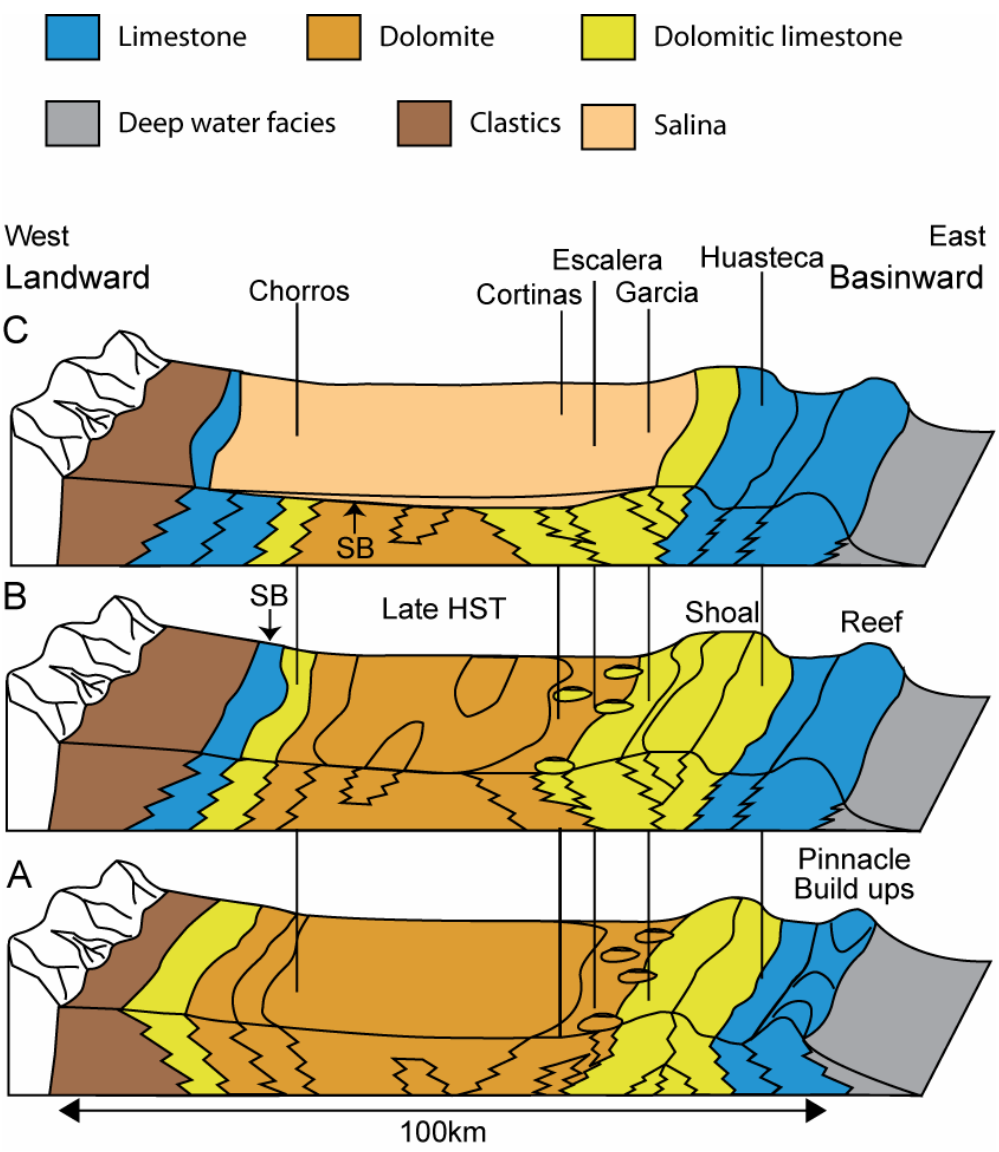

Figure 4-23. Generalized depositional and platform wide dolomitization.

(A) The restricted early portion of the transgressive system tract.

(B) The unrestricted late portion of the transgressive system tract.

C) Highstand system tract capped by a sequence boundary represented by a broad gypsum layer lying above a sequence boundary (SB) and highstand package of facies. Vertical exaggeration is approximately 100X.

(3) Platform geometry

Montañez and Read (1992) documented early dolomite distribution within the Early Ordovician Upper Knox carbonates. The Upper Knox platform developed as a gently dipping ramp which is now exposed in the fold and thrust belt of the Valley and Ridge province of the central and southern Appalachians. They investigated early dolomite distribution at both high-frequency cycle- and larger-scale 3rd-order sequences. Upper Know cyclic carbonates are extensively dolomitized; as much as 85% of all dolomite is stratiform and consists of early dolomite exhibiting minor to extensive modification by burial dolomite (Montañez and Read, 1992). They interpreted that third-order depositional sequences control the stratigraphic positions of early dolomite as regressive facies tend to be predominantly dolomitized whereas transgressive facies retain abundant limestone. Within the Upper Knox carbonates, third-order transgressive deposits, high-frequency cycles are dominantly subtidal with limestone facies and dolomitized cycle cap. However, most of the high-frequency cycles within third-order highstand deposits are partially to completely dolomitized. The large-scale, cross platform distribution of early dolomite within cycles deceases systematically across the platform. Peritidal cycles of regional highs and inner platform are dominated by dolomite, whereas limestone-rich cyclic intervals are best developed towards depocenters and on the outer platform. The large-scale

patterns are similar to Smith et al. (2004) study of dolomite distribution within the Madison carbonate ramp in central Wyoming.

On the contrary, subtidal facies are dominantly dolomitized within the Cupido carbonates with peritidal cycle caps being dominantly dolomitized in 3rd-order regressive deposits. The Cupido is a rimmed platform with well developed lagoon in the shallow shelf. This ramp to rimmed variation in platform geometry might have played a role in controlling early dolomite distribution patters between the two formations.

EVIDENCE AGAINST DOLOMITIZATION BY BURIAL PROCESSES

Cupido carbonate, tidal-flats and subtidal, facies were dolomitized syndepositionally early in their history. Preferential selective burial dolomitization has been suggested as an alteration process for fine-grained facies, similar to those of Cupido, due to their mineralogy, grain size and increased reactivity with burial temperatures (Bullen and Sibley, 1984; Sibley et al., 1987). Hardie (1989) suggested that fine-grained facies are preferentially dolomitized because of their higher permeabilities compared to coarse-grained facies. Basic conditions required for burial dolomitization include a through flow of warm to hot, magnesium-rich basinal fluids. However, more recent concepts of burial dolomitization suggest that it is part of a continuing series of dolomitization events that begin early in the depositional, diagenetic cycle and are over-printed during burial (Banner et al., 1988; Gao et al., 1995; Amthor et al., 1993; Kupecz

et al., 1993; Wojcik et al., 1994; Montañez, 1994; Kupecz and Land, 1994; Ayalon and Longstaffe, 1995; Warren, 2000).

Selective burial dolomitization is unlikely in the Cupido Formation because different fracture sets developed at different stages during burial (Oretga and Marrett, 2001; Monroy-Santiago et al., 2001; Ortega, 2002) and may have acted as flow pathways for burial fluids. Added to this, dolomitized fractures have different luminescence (dull-dark) compared to matrix dolomite (Figure 4-8). More evidence against burial dolomitization is indicated by some facies remaining limestone in some parts of the platform and completely dolomitized in other parts. This supports a sea-level control on dolomite distribution instead of selective dolomitization during burial (Montañez and Read, 1992).

DOLOMITIZATION ENVIRONMENT AND MODEL FOR THE CUPIDO FORMATION

Dolomitization environment

The close associations of evaporitic to restricted lagoonal conditions and pulses of platform-wide flooding with early dolomite distribution in the Cupido Formation suggests that early dolomitization occurred in an arid climate and was caused by dense altered sea-water brines. Applying modern models of near surface dolomitization to the origin of ancient dolomitized platforms, such as the Cupido platform, is made difficult by several factors. The fabrics and geochemistry of ancient dolomite differ significantly from modern dolomite because of complex history of stabilization and maybe several generations of

dolomitization fluids (Gao and Land, 1991; Montañez and Read, 1992; Kupecz et al., 1993; Warren, 2000). Secondly, stable-hydrologic systems sustaining continuous flow of dolomitizing fluids, which are not present in modern environments, are required for massive dolomitization. Finally, there is very little modern dolomite compared to ancient dolomite (Warren, 2000). Ortega (2002) suggested that hypersaline reflux-induced dolomitization (Lucia and Major, 1994) as a possible alteration process within the Cupido Formation.

Sabkha dolomitization (similar to Holocene Persian Gulf) has been proposed as a modern analog model for tidal-flat dolomitization (Mackenzie, 1981; Shinn, 1983; Montañez and Read, 1992; Illing and Taylor, 1993; Wenk et al., 1993; Chafetz and Rush, 1994; Warren, 2000). Given space and individual cycle time, the sabkha model can generate early dolomite with significant vertical and lateral extent (Patterson, 1972; Purser, 1973; Mackenzie, 1981; Shinn, 1983; Montañez and Read, 1992; Wenk et al., 1993). With seawater supplying magnesium, the dolomitization zone would be very broad (10s of km) during continued tidal-flat progradation within individual high-frequency cycle durations (Montañez and Read, 1992; Wenk et al., 1993).

Model for synsedimentary dolomitization

Within the Cupido Formation, early dolomite is abundant in the early transgressive deposits of depositional sequences and late regressive sediments

capping these depositional sequences. This can be the result of dolomitization process or processes operating at different scales and times.

Widespread evaporite deposition similar to the Cupido is associated with brine-reflux dolomitization (Adams and Rhodes, 1960; Hsu and Siegenthaler, 1969; Warren, 1999; 2000). This model explained the massive dolomitization of the Permian reef complex where backreef, shelf and lagoonal carbonates are intensely dolomitized, while shelf edge carbonates, such as the Capitan reef, are not. However, there are no modern counterparts to most types of ancient marine-platform and basin-wide evaporites, hence, there are no modern counterparts to brine-reflux dolomites. There are, nevertheless, other islands in the tropics where localized brine reflux, associated with hypersaline conditions, is apparently forming Holocene dolomites. Müller and Teitz (1971) documented brine-reflux dolomite replacing earlier carbonate cement in skeletal grainstones on the shoreline in Fuerteventura in the Canary Islands. Kocurko (1979) found brine-reflux dolomite a few meters above the high tide line, in the spray-zone pools of the shoreline of San Andres, Columbia. However, the hydrologies of modern brine-reflux dolomites never approach the scale of processes required to dolomitize shelf carbonates adjacent to ancient evaporites. In the Cupido, a broad shallow lagoon protected from open-marine circulation by a grainstone shoal complex (Figure 4-4) allowed evaporite deposition during falling sea level and sinking dense brines to form reflux dolomite. This reflux process is tied up to falling stages of sea level (Adams and Rhodes, 1960; Warren, 1999, 2000).

Early dolomitization forming in tidal-flat cycle caps is analogous to modern day dolomitization in coastal sabkha of the Persian Gulf (Illing et al., 1965; McKenzie, 1981; Patterson and Kinsman, 1982; Montañez and Read, 1992; Warren, 2000). In sabkhas, dolomite forms from modified (evaporitic) seawater within and below the tidal-flats surface in response to falling sea level and progradation (Illing et al., 1965; Patterson, 1972; McKenzie, 1981; Patterson and Kinsman, 1982; Warren, 2000). Dolomite abundance decreases away from sabkha surface with distance underneath (McKenzie et al., 1980; Patterson and Kinsman, 1982) which is similar to decreasing dolomite abundance away from cycle caps in peritidal cycles in the Cupido Formation (Altobi et al., 2004; Altobi, 2006) and many ancient peritidal cycles (James, 1984; Strasser, 1988; Montañez and Read, 1992; Kupecz and Land, 1994). However, distribution of modern dolomite in the Persian Gulf is limited to narrow discontinuous zones of the sabkha (Purser, 1973; Patterson and Kinsman, 1982; Warren, 2000). Furthermore, early dolomitization of tidal-flats in the Persian Gulf has been active only for less than 4000 years (Purser, 1973; Patterson and Kinsman, 1982; Montañez and Read, 1992). On the other hand, as much as 80% of the Cupido Formation has been replaced by early dolomite over large broad areas. Added to this, early dolomitization occurred during the deposition of most high-frequency cycles (~278) in the Cupido and was active for part if not the entire duration of each cycle (18.4 kyr).

Subtidal dolomitization forming due to gradual rise in sea level over broad and evaporitic areas produced thick dolomitized successions of Upper Cambrian and Lower Ordovician carbonate rocks in the Eastern U.S (Harris, 1973) with sea water being the fluid source (Land, 1985; Morrow, 1982; Machel and Mountjoy, 1986). The dilution of brines developed over the shallow shelf by seawater can move the solution into the dolomite stability field (Folk and Land, 1975). Mazzullo et al. (1997) documented occurrence of Holocene dolomite forming syndepositionally in the shallow-subtidal sediments in northern Belize. Isotopic analysis of surface water and pore fluids suggest normal-marine salinities for dolomitizing fluids (Teal et al., 1998). However, dolomitization in northern Belize is limited (Mazzullo et al., 1997) compared to the dolomitization extent of the Cupido platform.

A gradual rise in sea level flooding the evaporitic shallow Cupido shelf would result in restricted conditions and evaporite deposition within the broad restricted shallow lagoon. Deposition of evaporites may have been responsible for dolomite formation near the top underlying sediments by refluxing brines (Figure 4-24A). Continued evaporation and anhydrite deposition within the lagoon would result in hypersaline brines. As sea level continued to rise, early transgressive mud-dominated high-frequency cycles with low tidal-flat to subtidal ratio are deposited in a low energy setting. Added seawater dilutes the hypersaline brines in the lagoon, shifting the solution into the dolomite stability field (Figure 4-24B and 25; Folk and Land, 1975). Continued rise in sea level

switches the depositional setting within the lagoon from restricted to open-marine and shifts tidal-flat deposition further landwards. Grain- to mud-dominated open-marine cycles with no tidal-flat caps or low tidal-flat to subtidal ratio are deposited within the lagoon (Figure 4-24C). Early transgressive high-frequency cycles are dominantly dolomitized (70% of the cycles are partially to completely dolomitized; Table 4-4).

As sea level starts to fall, thinner progradational peritidal cycles with increasing tidal-flat to subtidal ratios are deposited on either side of the lagoon (Figure 4-24D). Most of these cycles have dolomitized caps and dolomite abundance decreases with distance below the cycle cap (Figure 4-19). This limited extent of dolomitization is similar to the Holocene sabkha of the Persian Gulf (Purser, 1973; Mackenzie, 1981; Patterson and Kinsman, 1982; Shinn, 1983; Montañez and Read, 1992; Wenk et al., 1993; Warren, 2000). Continued falling sea level and progradation will lead to platform-wide tidal-flat deposition and periods of emergence resulting in evaporitic conditions and early dolomitization (Purser, 1973; Patterson and Kinsman, 1982; Montañez and Read, 1992; Warren, 1999, 2000; Figure 4-24E). Regressive high-frequency cycles are dominantly dolomitized (85% of the cycles are partially to completely dolomitized; Table 4-4).

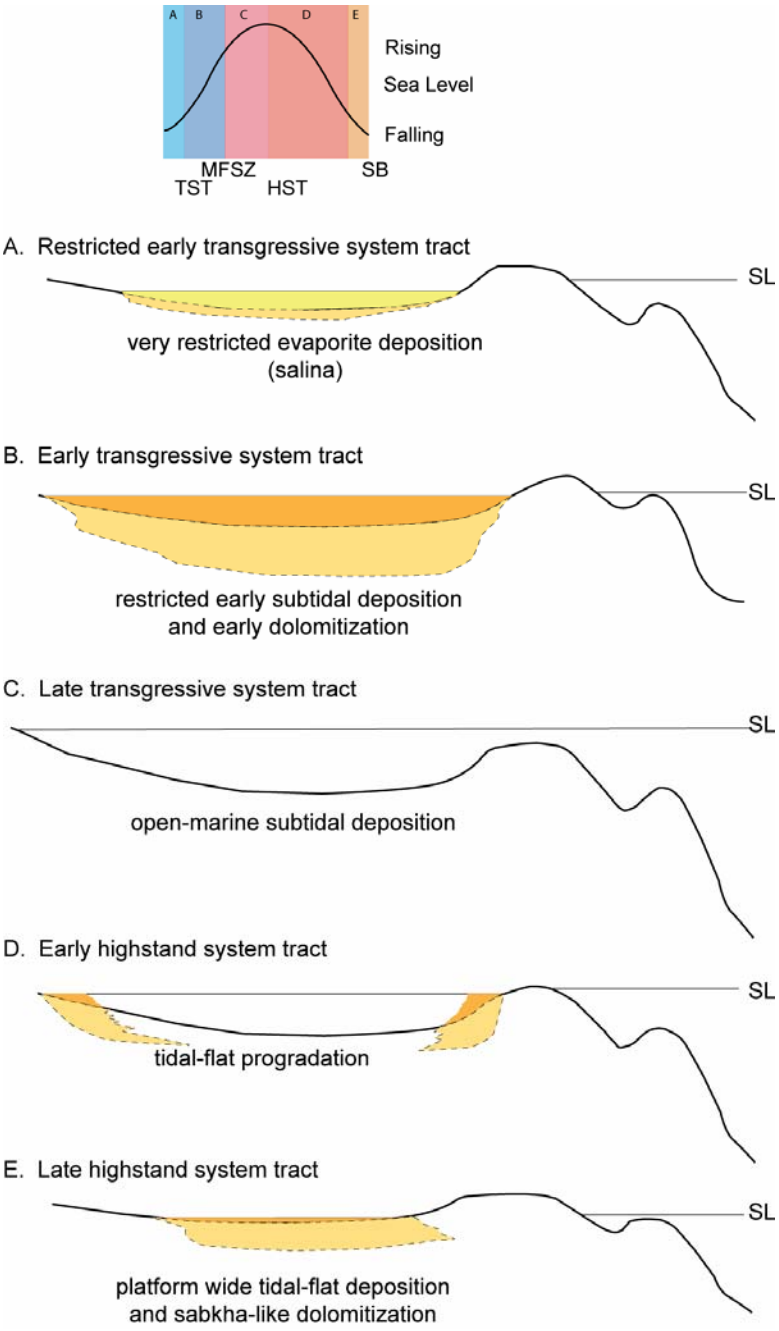

Figure 4-24. Dolomitization model.

Proposed mechanisms for dolomitization across the Cupido platform with a single pulse of sea-level fluctuation. See text for details.

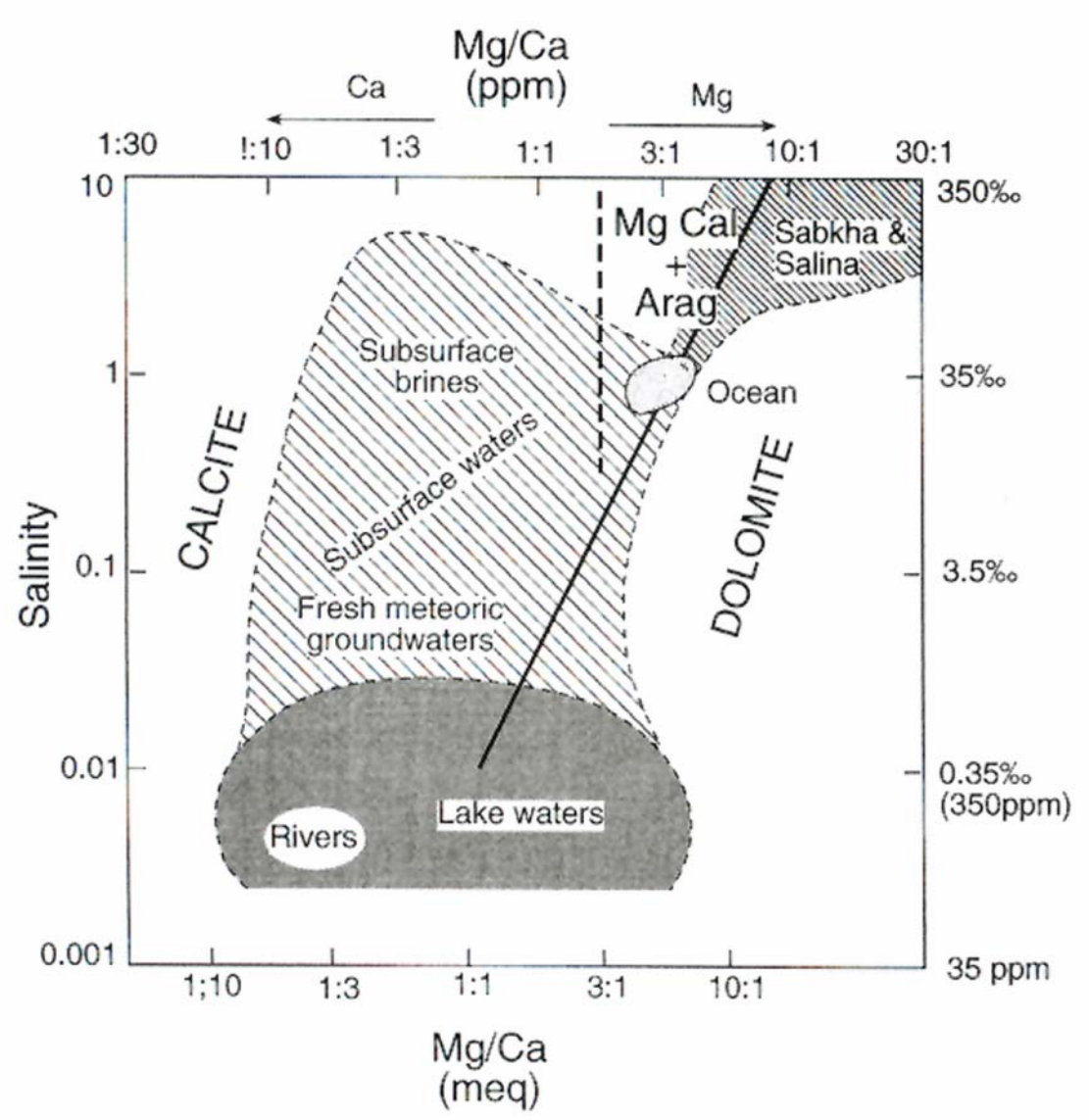

Figure 4-25. Dilution and dolomitization.

Stability of major carbonate minerals in relation to Mg/Ca ratio and salinity of Fluids. Note how dilution of brine by seawaters can move the solution into the dolomite stability field (after Folk and Land, 1975).

The variation in degree of dolomitization of transgressive and regressive system tracts of depositional sequences is probably controlled overall trend in accommodation space. Within the LCu of the Cupido Formation, the degree of dolomitization decreases toward the 2nd-order sequence boundary. It also indicates that subtidal dolomitization is dominant as overall dolomite distribution decreases with decreasing thicknesses of transgressive system tracts (Figures 4-13 and 4-14).

Stable isotopes

The present day fabrics and geochemistry of Cupido dolomites likely record multiple events of dolomitization and recrystallization (Monroy-Santiago et al., 2001). Figure 4-26 shows stable isotope values for 17 samples from the LCu of the Cupido Formation. Oxygen isotope values for the dolomites range from +4 to -10‰, with a median $\delta^{18}O$ value of -1.2‰ PDB (Figure 4-26). Carbon isotope values range from +1 to +7‰ with a median $\delta^{13}C$ value of+2.6‰ PDB (Figure 4-26; Appendix E). If the dolomite had formed solely because of seepage reflux of evaporated seawater without further modification, the $\delta^{18}O$ values would be approximately +4‰ (Warren, 2000; Moore, 2001). The median oxygen value is approximately 5‰ more negative, and the range is 2-14‰ more negative than expected of evaporated sea-water values. This supports a complex dolomitization and recrystallization history recorded by present day isotopic analyses of Cupido dolomites.

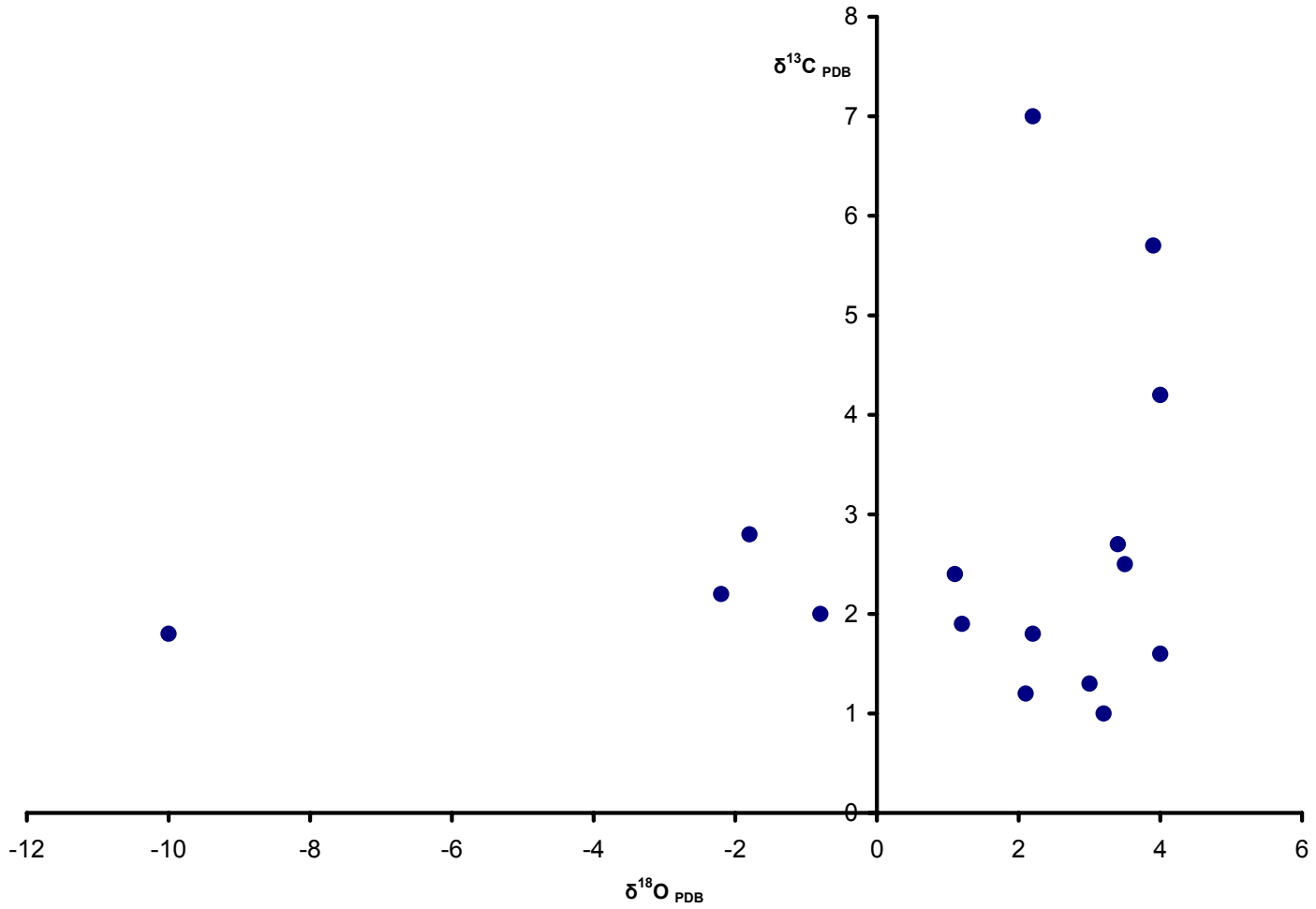

Figure 4-26. Stable isotope values for Cupido dolomites.

Dolomitization periodicity

The calculated order of magnitude of time required for dolomite replacement of a volume of sediment representative of deposition over one cycle period vary over large area of fluid recharge and volume of carbonate to be dolomitized (Montañez and Read, 1992; Fullmer, 2005). Required time ranges from 0.3-1 kyr (Fullmer, 2005) to 40-400 kyr (Montañez and Read, 1992). Temporal correlation of completely dolomitized high-frequency cycles within the LCu of the Cupido Formation at Chorros Canyon (ChC; Figure 4-1) shows periodic arrangement (Figure 4-27A) with clustering every 319 kyr (Figure 4-27B). However, the analysis does not identify the location of the clusters. This period cluster should vary in different locations as the dolomitization pattern varies across the platform. For example, thickness clustering of completely dolomitized cycles from Escalera Canyon shows a cluster with 61 m length scale (Figure 4-15). The paleogeographic position of Escalera Canyon is different from Chorros Canyon (Figure 4-4) and the pattern of dolomitization varies as facies and system tract components of each depositional sequence changes along the LCu carbonates (Figures 4-5, 4-7, 4-9, 4-10, and 4-11).

Despite the above limitations, thickness clusters of completely dolomitized cycles at Escalera Canyon (Figure 4-15) and periodicity clusters of completely dolomitized cycles within the LCu sediments at Chorros Canyon (Figure 4-27) are equivalent to depositional sequences in thickness (58 m thick average) and

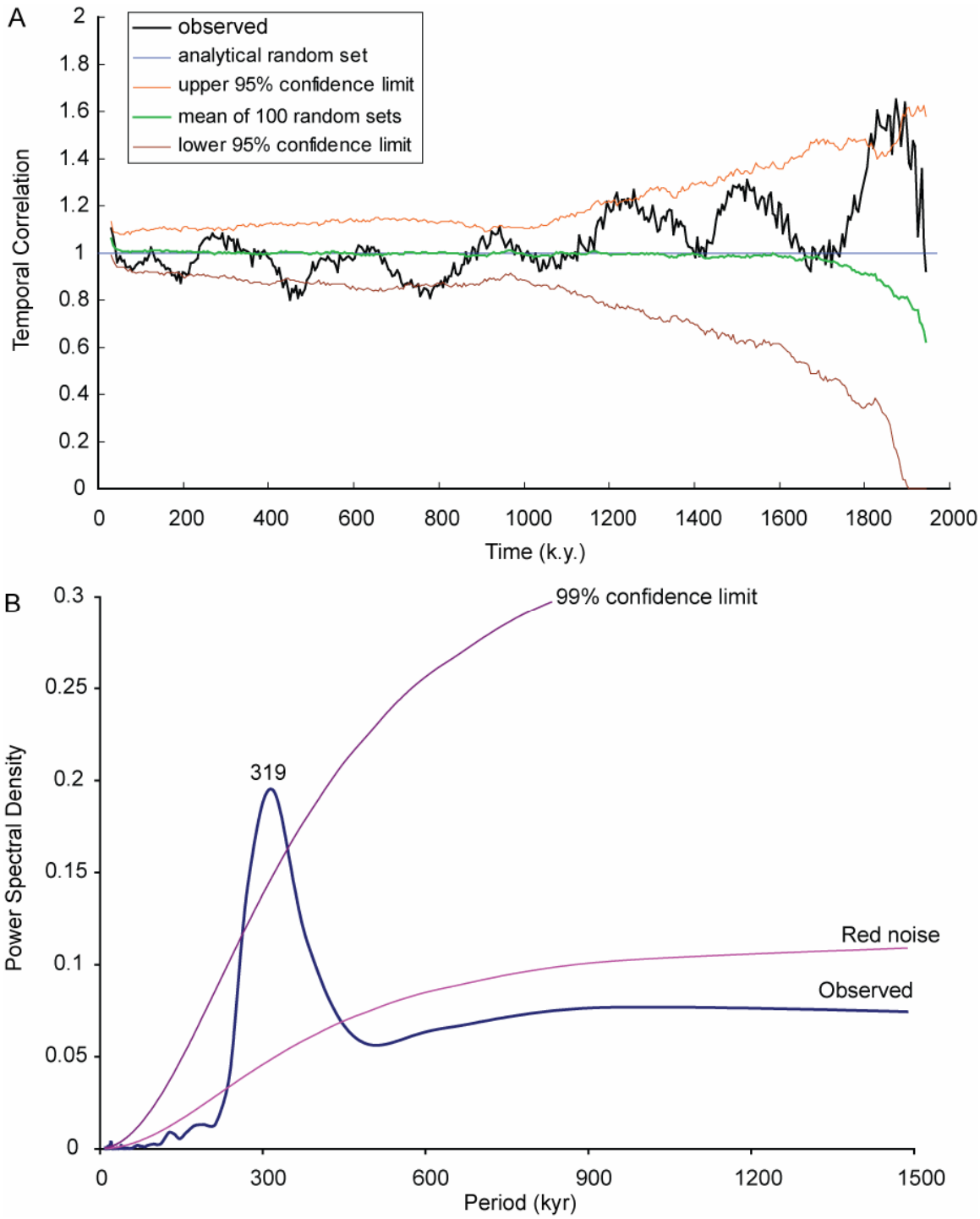

Figure 4-27. Period control on dolomitization.

Correlation and significance of dolomitized cycles distribution with time. (A) Temporal correlation of completely dolomitized high frequency cycles from Chorros South section (ChC S in Figure 13) showing periodic character. (B) Power spectrum of periodicity for dolomite distribution using Blackman-Tukey transform (Blackman and Tukey, 1958 and Pardo-Igúzquiza and Rodriguez-Tovar, 2004). Dolomitized cycles cluster in period every 319 kyr at Chorros Canyon section.

in duration (294-338 kyr; 337 kyr at Chorros South section). Milankovitch-induced 4th-order sea-level events are interpreted to be the driver behind depositional sequences in the Cupido carbonates and therefore may also control early dolomite distribution within the LCu. This eccentricity equivalent periodicity (E1; Figure 4-17; Yang et al., 1995; Hinnov, 2000) can produce required sea-level changes to form shallow-marine high-frequency cycles in carbonate platforms by different climate processes.

1. Melting of small ice caps or alpine glaciers (Frakes and Francis 1988).
2. Thermal expansion and contraction of ocean water (Donovan and Jones 1979; Revelle, 1990; Elder et al., 1994).
3. Changes in water volume stored in lakes and groundwater reservoirs (Hay and Leslie, 1990; Jacobs and Sahagian, 1995; Barron et al., 1995).

The interpreted dolomite clustering and time periodicity is not assumed to be valid for all shallow-marine carbonate platforms and expected to vary. Variation is expected within the Cupido platform itself due to different characteristics within different depositional environment and setting. Also, the operating dolomitization mechanisms vary between different location and times across the platform depending on sea-level fluctuations (Figure 4-24).

CONCLUSION

Platform-wide dolomitization of the cyclic LCu carbonates occurred in modified seawater/brine within subtidal and supratidal zones, both at high-

frequency cycle-scale and depositional sequence-scale. Synsedimentary dolomitization is suggested by the presence of dolomitized clasts, eroded from the underlying cycle caps, in the transgressive base of cycles. The degree of dolomitization of lithofacies is the dominant control on early fracture distribution within the cyclic LCu carbonates indicating that dolomitization predates or concurs early fracture development. Hypersaline conditions during early dolomitization are indicated by the presence of bedded evaporite, the common occurrence of early dolomite in laminites and restricted subtidal facies.

Cyclic sedimentation and synsedimentary dolomitization within Cupido carbonates are strongly controlled by sea-level changes. Meter-scale high-frequency cycles formed in response to Milankovitch-induced high-frequency sea-level fluctuation superimposed on larger sea-level events. Early dolomitization occurred within each high-frequency cycle during early sea-level rises in subtidal sediments and during sea-level falls and progradation in tidal-flat caps. Distribution of early dolomite shows a strong relationship to 4^{th}-order sea-level events suggesting that low-frequency (3^{rd} and 2^{nd}) sea-level changes also play a major role in overall early dolomite distribution. The transgressive portions of 4^{th}-order depositional sequences are pervasively dolomitized compared to the regressive portions. Thicknesses of dolomitized cycles clusters at Escalera Canyon are equal to the thicknesses of 4^{th}-order depositional sequences.

The proposed dolomitization processes, influenced largely by evaporitic conditions and gradual rises and falls in sea level, overcomes the restrictions of

applying modern analogs only to constrain the origin of ancient massive dolomitized successions. These processes can generate vertically and laterally extensive dolomite given enough time and a broader area (10s of kilometers of shallow shelf) of active dolomitization than modern Holocene dolomitizing environments. Stable isotopes likely recorded multiple episodes of dolomitization and recrystallization instead of a single evaporitic-induced dolomitization.

Thickness (Escalera Canyon) and periodicity (Chorros Canyon) clusters of completely dolomitized cycles within the LCu sediments are equivalent to 4^{th}-order depositional sequences in thickness (58 m thick average) and in duration (294-338 kyr). Therefore, Milankovitch-induced 4^{th}-order sea-level events may control early dolomite distribution within the LCu. Even though thickness and periodicity clusters of dolomitized cycles were quantified, they are not assumed to be uniform across the Cupido platform, and not in the least valid for all shallow-marine carbonate platforms. This is because the operating dolomitization mechanisms vary with locations and time across a single platform, depending on sea-level fluctuations.

Chapter 5. Conclusions

SUMMARY

The shallow-marine Cupido shelf exhibits well-developed cyclicity. Meter-scale deep subtidal to peritidal high-frequency cycles vary in thickness, facies components, type, and degree of early dolomitization depending on their relative lateral position along the platform profile, their vertical position within individual depositional sequences and the overall sequence stratigraphic framework. This study integrated several stratigraphic sections, enabling a more robust correlation that resulted in the recognition of 4 additional depositional sequences, one composite sequence and the retrogradational nature of the Cupidito member. This high-resolution framework, in turns, reveals subtle complexities and controls on facies models not evident from previous studies.

Two full and two partial 3rd-order composite sequences, and a total of twelve 4th-order depositional sequences were interpreted within the Cupido Formation. Six depositional sequences (A-F), comprising the highstand part of composite sequence I and composite sequence II, are interpreted and correlated across the platform within the LCu of the Cupido Formation. They are dominated by peritidal cycles capped by heterolithic thin beds or laminites. The proportion of subtidal to peritidal high-frequency cycles decreases in depositional sequences A-F, along with the thickness of these depositional sequences. A total of six depositional sequences (G-L), comprising composite sequence (III)

and a partial composite sequence (IV), are interpreted within the Cupidito member with a back-stepping geometry caused by landward shift in carbonate sedimentation due to rising sea level. This aggradational to retrogradational geometry supports a gradual rise in sea level allowing sediment production to keep pace during the early stages of transgression.

Field observations and interpretation coupled with time-series analysis of high-frequency cycle thicknesses within the shallow-marine Cupido shelf support an allocyclic driving mechanism. Symmetric and asymmetric peritidal and subtidal cycles correlate across facies tracts and are mostly capped by tidal-flat facies, however, incomplete subtidal cycles (pure subtidal cycles that lack tidal-flat caps) were also interpreted in different parts of the Cupido shelf. Cycles also vary in thickness and facies components as a result of progradation and retrogradation.

Sedimentation rate-cumulative time-series analysis of precession-tuned spectra of this cyclicity revealed the persistence of three eccentricity (E1, E2, and E3) signals and two obliquity peaks with Milankovitch periodicities throughout the sections. The peaks occur at the principal orbital eccentricity periodicities E1 (264-392 kyr), E2 (89-98 kyr), and E3 (107-126 kyr) and related obliquity component peaks at period (38-59 kyr). These peaks show strong vertical and lateral correlation across the shelf further supporting lateral continuity of high-frequency cycles and Milankovitch-induced sea-level fluctuation as driving mechanism for the cyclic hierarchy interpreted within the Cupido Formation.

These fluctuations might subsequently play a role in controlling the distribution of diagenetic processes within the Cupido carbonates.

Platform-wide dolomitization of the cyclic LCu carbonates occurred in modified seawater within subtidal and supratidal zones, both at high-frequency cycle-scale and depositional sequence-scale. Hypersaline conditions during early dolomitization are indicated by the presence of bedded evaporite, and the common occurrence of early dolomite in laminated and restricted facies. The proposed dolomitization processes, influenced largely by evaporitic conditions and gradual rises and falls in sea level, can generate vertically and laterally extensive dolomite given enough time and a broader area (10s of kilometers of shallow shelf) of active dolomitization than that observed in modern Holocene dolomitizing environments. Stable isotopes appear to record multiple episodes of dolomitization and recrystallization instead of a single evaporitic-induced dolomitization events.

Cyclic sedimentation and synsedimentary dolomitization within Cupido carbonates are strongly controlled by changes in basin-wide sea level. Synsedimentary dolomitization took place in subtidal sediments during sea-level rises and in tidal-flat caps during sea-level falls and progradation. Distribution of early dolomite shows a strong relationship to 4^{th}-order sea-level events as transgressive portions of depositional sequences are dolomitized compared to the regressive portions.

Thickness (Escalera Canyon) and periodicity (Chorros Canyon) clusters of completely dolomitized cycles within the LCu sediments are equivalent to 4th-order depositional sequences in thickness (58 m thick average) and in duration (294-338 kyr). Therefore, Milankovitch-induced 4th-order sea-level events may control early dolomite distribution within the LCu.

IMPLICATIONS

(1) External Milankovitch-driven global climatic changes produced low-amplitude, high-frequency sea-level fluctuations through a combination of climatic processes to produce meter-scale high-frequency cycles during greenhouse conditions. These results support global widespread Milankovitch signal embedded in the development of Mesozoic cyclic shallow-marine carbonate platforms and possibly other greenhouse platforms.

(2) The high-resolution sequence stratigraphic framework for the Cupido Formation, and detailed depositional and facies model can be applied to similar reservoirs for better understanding of facies distribution, high-frequency cycle development and their lateral continuity. This high-resolution framework will also add useful insights to future studies of Lower Cretaceous carbonate sequence stratigraphy and the nature of drowning carbonate platforms.

(3) Even though thickness and periodicity clusters of dolomitized cycles were quantified, they are not assumed to be uniform across the Cupido platform, and not in the least valid for all shallow-marine carbonate platforms. This is

because the operating dolomitization mechanisms vary with location and time across a single platform, depending on sea-level fluctuations. However, the Cupido outcrops offer a great opportunity to further investigate eustatic controls on dolomitization. Different outcrops across the platform offer multiple variables that possible control early dolomite distribution. For example, period, thickness, cycle type, paleogeographic location, stratigraphic position and extent of hydraulic area, can all be used to evaluate the extent of operating dolomitizing mechanisms for specific platforms at specific depositional setting, sea levels and/or climate periods.

Appendices

Paper copies of this dissertation are kept at the Perry Castañeda Library, The University of Austin, and the Geology Library, Jackson School of Geosciences, The University of Texas at Austin. These paper copies contain a CD with the appendices in digital PDF (http://adobe.com) format. Additional copies of the appendices in digital form can be provided by the author.

APPENDIX A: MEASURED STRATIGRAPHIC SECTIONS

Fifteen measured section from the Cupido Formation, are located in folder (Appendix A). The symbol key used is included as KEY.PDF.

APPENDIX B: PETROGRAPHY

A list of all the samples and thin sections with brief descriptions is located in folder (Appendix B). A subfolder (photos) contains all the images used in the dissertation and petrography.

APPENDIX C: FACIES DISTRIBUTION AT EACH STRATIGRAPHIC SECTION

Histogram plots of total facies distribution at individual stratigraphic section are found in (Appendix C).

APPENDIX D: CORRELATIONS

Fence diagrams and larger prints containing correlation of the measured sections are located in folder (Appendix D).

APPENDIX E: CORRELATIONS

Stable isotope analyses technique and collected data are found in (Appendix E).

References

Adams, J. F., Rhodes, M. L., 1960, Dolomitization by seepage refluxion: American Association of Petroleum Geologists Bulletin, v. 44, p. 1912-1920.

Allan, J. R., and Wiggins, W. D., 1993, Dolomite reservoirs; geochemical techniques for evaluating origin and distribution: American Association of petroleum Geologists Continuing Education Course Note Series, v. 36, 129p.

Alsharhan, A.S., and Nairn, A.E.M., 1993, Carbonate platform models of Arabian Cretaceous reservoirs, *in* J. A. Simo, R. W. Scott, and J. P. Masse, (eds.), Cretaceous Carbonate Platforms: American Association of Petroleum Geologists, Memoir 56, p. 176-182.

Altobi, Y. K., Goldhammer, R. K., and Lehrmann, D. J., 2004, Sequence Stratigraphic Controls on Dolomitization, Structural Deformation and Fracture Distribution in Carbonate Strata, the Cupido Formation, Sierra Madre Oriental, NE Mexico (Abstarct): American Association of Petroleum Geologists, 2004 Annual Convention, p. A5.

Altobi, Y. K., 2006, High Frequency Cycles to Supersequences: Stratigraphic Controls on Early Dolomite Distribution within Peritidal and Subtidal Carbonates, the Cupido Formation, Sierra Madre Oriental, NE Mexico (abstract): American Association of Petroleum Geologists, Annual Convention, Abstracts, p. 3.

Amthor, J. E., Mountjoy, E. W., and Machel, H.G., 1993, Subsurface dolomites in Upper Devonian Leduc Formation buildups, central part of Rimbey-Meadowbrook reef trend, Alberta, Canada: Bulletin of Canadian Petroleum Geologists, v. 41 (2), p. 164-185.

Anderson, T. H., and Schmidt, V. A., 1983, The evution of Middle America and the Gulf of Mexico-Caribbean Sea region during Mesozoic time: Geological Society of America Bulletin, v. 94, p. 941-966.

Ayalon, A., and Longstaffe, F. J., 1995, Stable isotope evidence for the origin of diagenetic carbonate minerals from the Lower Jurassic Inmar Formation, southern Israel: Sedimentology, v. 42 (1), p. 147-160.

Ball, M. M., and Harrison, C. G. A., 1969, Origin of the Gulf and Caribbean and implications regarding ocean ridge extension, migration, and shear: Gulf

Coast Association of Geological Societies: Transactions, v. 19, p. 287-294.

Balog, A., Read, J. F., and Haas, J. 1999, Climate-controlled early dolomite, Late Triassic cyclic platform carbonates, Hungary: Journal of Sedimentary Research, v. 69, No. 1, p. 267-282.

Banner, J. L., Hanson, G. N., and Meyers, W .J., 1988, Water–rock interaction history of regionally extensive dolomites of the Burlington-Keokuk FormationMississippian.; isotopic evidence, *in* V. Shukla, P. A. Baker, (eds.)., Sedimentology and Geochemistry of Dolostones, Based on a Symposium: Special Publication-Society of Economic Paleontologists and Mineralogists v. 43, p. 97-113.

Barron, E. J., 1983, A warm, equable Cretaceous: The nature of the problem: Earth-Science Reviews, v. 19, p. 305–338.

Barron, E. J., Arthur, M. A., and Kauffman, E.G., 1985, Cretaceous rhythmic bedding sequences: a plausible link between orbital variations and climate: Earth and Planetary Science Letters, v. 72, p. 327-340.

Bartok, P., 1993, Prebreakup geology of the Gulf of Mexico-Caribbean: its relation to Triassic and Jurassic rift systems of the region: Tectonics, v. 12, p. 441-459.

Bathurst, R. G. C., 1971, Carbonate sediments and their diagenesis: Development in sedimentology no. 12, Elsevier (Amsterdam), 658 p.

Bebout, D. G., 1977, Sligo and Hosston depositional patterns, subsurface of south Texas, *in* R. G. Loucks, (ed.), Cretaceous Carbonates of Texas and Mexico: Applications to Subsurface Exploration: University of Texas Bureau of Economic Geology Report of Investigations no. 89: Austin, The Bureau of Economic Geology, p. 79-96.

Bebout, D. G., and R. G. Loucks, (eds.), 1977, Cretaceous Carbonates of Texas and Mexico: Applications to Subsurface Exploration: University of Texas Bureau of Economic Geology Report of Investigations no. 89: Austin, The Bureau of Economic Geology, 332 p.

Berger, A, Loutre, M. F., and Laskar, J., 1992, Stability of the astronomical frequencies over the Earth's history for paleoclimatic studies: *Science* v. 255, p. 560-66.

Berger, A. (eds)., 1984, New perspectives in climate modeling: Elsevier Science Publishing, Amsterdam, v. 16, 403p.

Berger, A., 1988, Milankovitch theory and clime: Reviews of Geophysics, v. 26, p. 624-657.

Berger, A., and Loutre, M. F., 1997, Intertropical latitudes and precessional and half-precessional cycles: Science, v. 278, p. 1476-1478.

Blackman, R. B., and Tukey, J. W., 1958, The measurement of power spectra from the point of view of communication engineering: New York, Dover Publications, 190p.

Blauser, W. H., 1981, The stratigraphy of the Taraises Formation, Lower Cretaceous, Mexico, *in* C. I. Smith, (ed.), Lower Cretaceous Stratigraphy and Structure, Northern Mexico: West Texas Geological Society Publication 81-74, p. 37-42.

Bosellini, A., 1989, Dynamics of the Theyan carbonate platforms, *in* P. D. Crevello, (eds.), Controls on carbonate platform and basin development: Society of Economic Paleontologists and Mineralogists Special publication No. 44, p. 3-13.

Boselllini, A., 1984, Progradation geometries of carbonate platforms: examples from the Triassic of the Dolomites, Northern Italy: Sedimentology, v. 31, p. 1-24.

Bubb, J. N., 1970, Modern Shelf Carbonates, Joulters Cay Oolite Shoal, Great Bahama Bank: Esso Production Research Company Report EPR-39ER-70.

Bullen, S. B., and Sibley, D. F., 1984, Dolomite selectivity and mimic replacive: Geology, v. 12, p. 655-658.

Cestari, R., and Sartorio, D., 1995, Rudists and Facies of the Periadriatic Domain: Milan, Agip S. P. A., 207 p.

Charleston, S., 1974, Stratigraphy, Tectonics, and Hydrocarbon Potential of the Lower Cretaceous, Coahuila Series, Coahuila, Mexico: Ph. D. thesis, University of Michigan, Ann Arbor, 268 p.

Conklin, J., and Moore, C., 1977, Paleoenvironmental analysis of the lower Cretaceous Cupido Formation, northeast Mexico, *in* R. G. Loucks, (ed.), Cretaceous Carbonates of Texas and Mexico: Applications to Subsurface Exploration: University of Texas Bureau of Economic Geology Report of Investigations no. 89: Austin, Bureau of Economic Geology, p. 302-323.

D'Aregenio, B., Ferreri, V., Amodio, S., and Pelosi, N., 1997, Hierarchy of high-frequency orbital cycles in Cretaceous carbonate platform strata: Sedimentary Geology, v. 113, p. 169-193.

Demicco, R. V., and L. A. Hardie, 1994, Sedimentary Structures and Early Diagenetic Features of Shallow Marine Carbonate Deposits: Society of Economic Paleontologists and Mineralogists Atlas Series No. 1: Tulsa, Oklahoma, Society of Economic Paleontologists and Mineralogists, 265 p.

Demicco, R. V., 1998, Cycopath 2D-a two dimensional, forward-model of cyclic sedimentation on carbonate platforms: Computers & Geosciences, v. 24, p. 405-424.

Dickson, J. A. D., 1965, A Modified Staining Technique for Carbonates in Thin Section: Nature, v. 205, p. 587.

Donovan, D.T., and Jones, E.J., 1979, Causes of world-wide changes in sea level: Geological Society of London, Journal, v. 136, p. 187-192.

Drummond, C.N., and Wilkinson, B.H., 1993a, Aperiodic accumulation of cyclic peritidal carbonate: Geology, v. 21, p. 1023-1026.

Drummond, C.N., and Wilkinson, B.H., 1993b, on the use of cycle thickness diagrams as records of long-term sea-level change during accumulation of carbonate sequences, The Journal of Geology, v.101, p. 687-702.

Dunham, R. J., 1962, Classification of carbonate rocks according to depositional texture, *in* W. E. Ham, (ed.), Classification of Carbonate Rocks, American Association of Petroleum Geologists Memoir 1, p. 108-121.

Einsele, G., Ricken, W., and Seilacher, A., 1991, Cycles and evend in stratigraphy, Springer Verlag: Berlin, 955pp.

Ekdale, A. A., Ekdale, S. F., and Wilson, J. L., 1976, Numerical analysis of carbonate microfacies in the Cupido Limestone (Neocomian-Aptian), Coahuila, Mexico: Journal of Sedimentary Petrology, v. 46, p. 362-368.

Elder, W. P., Gustason, E. R., and Sageman, B. B., 1994, Correlation of basinal carbonate cycles to nearshore parasequences in the Late Cretaceous Greenhorn seaway, Western Interior U.S.A.: Geological Society of America, Bulletin, v. 106, p. 892-90.

Enos, P., 1991, Sedimentary parameters for computer modeling, *in* E. K. Franseen, W. L. Watney, and w. Ross, (ed.), Sedimentary modeling: Computer Simulations and Methods for Improved Parameter Definition: State Geological Survey of Kansas, Bulletin, v. 233, p. 63-99.

Fischer, A. G., 1964, The Lofer cyclothems of the Alpine Triassic: Geological Survey of Kansas Bulletin, v. 169, p. 107-149.

Fischer, A. G., 1986, Climatic rhythms recorded in strata: Annual Review of Earth and Planetary Sciences, v. 14, p. 351-376

Folk, R. L., Land, L. S., 1975, MgrCa ratio and salinity: two controls on crystallization of dolomite. American Association of Petroleum Geologists Bulletin v. 59, p. 60-68.

Fortunato, K. S., and W. C. Ward, 1982, Upper Jurassic-Lower Cretaceous fan delta complex La Casita Formation of the Saltillo area, Coahuila, Mexico: Gulf Coast Association of Geological Societies Transactions, v. 32, p. 473-482.

Fortunato, K. S., 1982, Depositional Framework of the La Casita Formation (Upper Jurassic-Lowermost Cretaceous) Near Saltillo, Coahuila, Mexico: M. S. thesis, University of New Orleans, New Orleans, 198 p.

Foster, T. R., 2003, The Evution of a Lower Cretaceous Platform within a Divergent Margin Setting: The Cupido Formation, Northeastern Mexico: M. S. thesis, Austin, The University of Texas at Austin, p. 226.

Frakes, J. R., and Francis, M. N., 1988, A guide to Phanerozoic cold polar climates from highlatitude ice-rafting in the Cretaceous: Nature, v. 333, p. 547-549.Gianolla, P., De Zanche, V., and Mietto, P., 1998a, Triassic sequence stratigraphy in the Southern Alps (northern Italy): definition of sequences and basin evution, *in* De Graciansky, P.C., J. Hardenbol, t. Jacquin, and P. R. Vail, (ed.), Mesozoic and Cenozoic Sequence Stratigraphy of European Basins: Society of Economic Paleontologists and Mineralogists, Special Publication 60, p. 719-747.

Friedman, G. M., 1980, Dolomite is an evaporite mineral: evidence from the rock record and from sea-marginal ponds of the Red Sea. In: Zenger, E.H., Dunham, J.B., Ethington, R.L. (eds)., Concepts and Models of Dolomitization. Special Publication-Society of Economic Paleontologists and Mineralogists, v. 28, pp. 69-80.

Fullmer, S. M., 2005, Modeling reflux dolomitization: M.S. Thesis, Austin, Texas, The University of Texas at Austin, 97p.

Gao, G., and Land, L. S., 1991, Early Ordovician Cool Creak Dolomite, Middle Arbuckle Group, Slick Hills, SW Oklahoma, USA: Origin and modification; Journal of Sedimentary Petrology, v. 61, p. 161-173.

Gao, G., Land, L. S., and Elmore, R. D., 1995, Multiple episodes of dolomitization in the Arbuckle Group, Arbuckle Mountains, south-central Oklahoma; field, petrographic, and geochemical evidence. Journal of Sedimentary Research, Section A 65 (2), 321-331.

Ginsburg, R. N., 1971, Landward movement of carbonate mud: new model for regressive cycles in carbonates (abstract): American Association of Petroleum Geologists Bulletin, v.55, p. 340.

Ginsburg, R. N., 1974, Introduction to Comparative Sedimentology of Carbonates: American Association of Petroleum Geologists Bulletin, v. 58, p. 781-786.

Given, R. K., and Wilkinsn, B. H., 1987, Dolomite abundance and stratigraphic age-constarints on rates and mechanisms of Phanerozoic dolostone formation: Journal of Sedimentary Petrology, v. 57, p. 1068-1078.

Goldhammer, R. K., 2003, Cyclic sedimentology, in G. V. Middleton, (ed.), Encyclopedia of sediments and sedimentary rocks; Boston : Kluwer Academic Publishers, p. 173-185.

Goldhammer, R. K., P. J. Lehmann, R. G. Todd, J. L. Wilson, W. C. Ward, and C. R. Johnson, 1991a, Sequence stratigraphy and cyclostratigraphy of the Mesozoic of the Sierra Madre Oriental, northeast Mexico, a field guidebook: Gulf Coast Section, Society of Economic Paleontologists and Mineralogists, p. 85.

Goldhammer, R. K., 1999, Mesozoic sequence stratigraphy and paleogeographic evution of northeast Mexico, *in* T. F. Lawton, (ed.), Mesozoic Sedimentary and Tectonic History of North-Central Mexico: Boulder, Colorado, Geological Society of America Special Paper 340, p. 1-57.

Goldhammer, R. K., E. J. Oswald, and P. A. Dunn, 1991b, The hierarchy of stratigraphic forcing: and example from Middle Pennsylvanian shelf carbonates of the Paradox Basin, *in* W. Ross, (ed.), Sedimentary Modeling: Computer Simulations and Methods for Improved Parameter Definition, Kansas Geological Survey Special Publication 233, p. 361-413.

Goldhammer, R. K., Dunn, P. A., and Hardie, L. A., 1987, High-frequency glacio-eustatic sea-level oscillations with Milankovitch characteristics recorded in Middle Triassic platform carbonates in northern Italy, American Journal of Science, v. 287, p. 853-892.

Goldhammer, R. K., Dunn, P. A., and Hardie, L. A., 1990, Depositional cycles, composite sea-level changes, cycle stacking patterns, and the hierarchy of

stratigraphic forcing: Examples from Alpine Triassic platform carbonates: Geological Society of America, Bulletin, v. 102, p. 535-562.

Gorody, A. W., 1980, Dolomitization and paleohydraulic history of the Loer Ordovician Mascot Formation, Upper Know Group, in north central Tennessee (abstract): Geological Society of America Abstract with Programs, v. 12, Issue 7, p. 435.

Gradstein, R. M., Agterberg, F. P., Ogg, J. G., Hardenbol, J., Van Veen, P., Thierry, J., and Huang, Z., 1995, A Triassic, Jurassic, and Cretaceous time scale, *in* J. Hardenbol, (ed.), Geochronology, Time Scales and Global Stratigraphic Correlation: Society of Economic Paleontologists and Mineralogists Special Publication 54, p. 95-126.

Gradstein, R. M., and Ogg, J. G., 2004, Geologic time scale 2004 – why, how and what next!; Lethaia, v.37, p.175-181.

Gray, G. G., Pottorf, D. A., Yurewicz, D. A., Mahon, K. I., Pevear, D. R., and Chuchla, R. J., 2001, *in* C. Bartolini, (ed.), The western Gulf of Mexico Basin; Tectonics and sedimentary basins, and petroleum systems: American Association of Petroleum Geologists Memoir 75, p. 159-181.

Grotzinger, J. P., 1986, Cyclicity and paleoenvironmental dynamics, Rocknest platform, northwest Canada: Geological Society of America Bulletin, v. 97, p. 1208-1231.

Handschy, J. W., Keller, G. R., and Smith, K. J., 1987, The Ouachita system in northern Mexico: Tectonics, v. 6, p. 323-330.

Haq, B. U., Hardenbol, J., and Vail, P. R., 1987, Chronology of fluctuating sea levels since the Triassic: Science, v.235, p. 1156-1167.

Hardenbol, J., Jacquin, T., Farley, M. B., de Graciansky, P. C., and Vail, P. R., 1998, Mesozoic and Cenozoic sequence chronostratigraphic framework of European basins, *in* P. R. Vail, (ed.), Mesozoic and Cenozoic Sequence Stratigraphy of European Basins: Society of Economic Paleontologists and Mineralogists Special Publication 60.

Hardie, L. A., and Shinn, E. A., 1986, Carbonate depositional environments, modern and ancient, 3 tidal flats: Colorado School of Mines Quarterly, v. 81, p. 1-74.

Hardie, L. A., Dunn, P.A., and Goldhammer, R.K., 1991, Field and modeling studies of Cambrian carbonate cycles, Virginia Appalachians: a discussion, Journal of Sedimentary Petrology, v. 61, p. 636-646.

Hardie, L. A., 1977, Sedimentation on the Modern Carbonate Tidal Flats of Northwestern Andros Island, Bahamas: Studies in Geology No. 22: Baltimore, The Johns Hopkins University Press, 202 p.

Hardie, L. A., 1989, Cyclic platform carbonates in the Cambro-Ordovician of the central Appalachians, *in* K. R. Walker, (eds)., Cambro-Ordovician carbonate banks and siliciclastic basins of the United States Appalachains: International Geological Congress, 28th, Field Trip Guidebook T161: Washington, D.C., American Geophysical Union, p.45-76.

Hardie, L. A., and Shinn, E. A., 1986, Carbonate depositional environments, modern and ancient, 3 tidal flats: Colorado School of Mines Quarterly, v. 81, p. 1-74.

Hardie, L. A., Bossellini, A., and Goldhammer, R. K., 1986, Repeated Subaerial Exposure of Subtidal Carbonate Platforms, Triassic, northern Italy: Evidence for High Frequency Sea Level Oscillations on a 10^4 year Scale: Paleoceanography, v. 2, p.447-457.

Harris, L. D., 1973, Dolomitization model for the Upper Cambrian and Lower Ordovician carbonate rocks in the eastern U.S.: U. S. Geological Survey Journal of Research, v. 1, p. 63-78.

Harris, P. M., Kowalik, W. S. and Lomando, A. J., 1993, Structural control of carbonate platform configuration and depositional environment distribution; Caicos platform, B. W. I. and Chinchorro Bank, offshore Yucatan (Abstract): American Association of Petroleum Geologists, 1993 Annual Convention, p.114.

Hay, W. W., and Leslie, M.A., 1990, Could possible changes in global sea-water reservoir cause euscatic sea-level fluctuations? *in* R. Revelle, (ed.), sea-level change: National Research Council, studies in Gepphysics, p. 161-170.

Hinnov, L. A., 2000, New perspectives on orbitally forced stratigraphy: Annual Review of Earth and Planetary Sciences, v. 28, p. 419-475.

Hinnov, L. A., and Goldhammer, R.K., 1991, Spectral analysis of the Middle Triassic Latemar Limestone: Journal of Sedimentary Petrology, v. 61, p. 1173-1193.

Hooker, J. N., Marrett, R and Laubach, S., 2002, Timing of faults and extension fractures in the Sierra Madre Oriental, northeastern Mexico, *in* S. P. Dutton, S. C. Ruppel, and T. F. Hentz, (eds.): Gulf Coast Association of Geological Societies Transactions, v. 52, p. 421-428.

House, M. R., 1995, Orbital forcing timescales: an introduction, *in* A. S. Gale, (ed.), Orbital Forcing Timescales and Cyclostratigraphy: Geological Society of America Special Publication, v. 85, p. 1-18.

Hsu, K. J., Siegenthaler, C., 1969, Preliminary experiments on hydrodynamic movement induced by evaporation and their bearing on the dolomite problem: Sedimentology 12, p. 448-453.

Humphrey, W. E., 1949, Geology of the Sierra de los Muertos area, Mexico (with descriptions of Aptian Cephalopods from the La Peña Formation): American Association of Petroleum Geologists Bulletin, v. 60, p. 89-176.

Hunt, D., and Tucker, M.E., 1993, The middle Cretaceous Urgonian platform of southeastern France, *in* J. A. Simo, R. W. Scott, and J. P. Masse, (eds.), Cretaceous Carbonate Platforms: American Association of Petroleum Geologists, Memoir 56, p. 409-453.

Ice, R. G., 1981, The Cuesta del Cura Formation in north-central Mexico, *in* C. I. Smith, (ed.), Lower Cretaceous Stratigraphy and Structure, Northern Mexico: West Texas Geological Society Publication 81-74, p. 58-74.

Illing, L. V., Wells, A. J., Taylor, J. C. M., 1965, Penecontemporaneous dolomite in the Persian Gulf, *in* L. C. Pray, R. C. Murray (eds.), Dolomitization and Limestone Diagenesis: Special Publication Society of Economic Paleontologists and Mineralogists, v. 13, pp. 89-111.

Imlay, R. W., 1936, Geology of the western part of the Sierra de Parras: Geological Society of America Bulletin, v. 47, p. 1723-1744.

Imlay, R. W., 1944, Cretaceous formations of Central America and Mexico: American Association of Petroleum Geologists Bulletin, v. 29, p. 445-560.

Jacobs, D. K., and D. L. Sahagian, 1993, Climate induced fluctuations in sea level during non-glacial times: Nature, v. 361, p. 710-712.

Jacobs, D. K., and Sahagian, D. L., 1995, Milankovitch fluctuations in sea level and recent trends in sea-level change: Ice may not always be the answer, *in* B.U. Haq, (ed.), Sequence Stratigraphy and Depositional Response to Eustatic, Tectonic and Climatic Forcing: Dordrecht, The Netherlands, Kluwer, p. 329-366.

James, N. P., 1984, Shallowing-upward sequences in carbonates, *in* R. G. Walker, (ed.), Facies Models: Geoscience Canada Reprint Series 1, p. 213-228.

Kerans, C., 1995, Use of one- and two-dimensional cycle analysis in establishing high-frequency sequence frameworks, *in* L. J. Weber, (ed.), Milankovitch Sea Level Changes, Cycles and Reservoirs on Carbonate Platfroms in Greenhouse and Ice-house Worlds: Society of Economic Paleontologists and Mineralogists (Society for Sedimentary Geology) Short Course Notes no. 35, p. 1-20.

Kerans, C., and Lucia, F. J., 1989, Recognition of second, third, and fourth/fifth order scales of cyclicity in the El Paso Group and their relation to genesis and architecture of Ellenburger reservoirs, *in* B. K. Cunningham, and D. W. Cromwell, (eds.) , The Lower Paleozoic of west Texas and Southern New Mexico- Modern exploration concepts: Permian Basin Section, Society of Economic Paleontologists and Mineralogists Publication 89-31, p. 105-110.

Kerans, C., and Tinker, S. W., 1997, Sequence Stratigraphy and Characterization of Carbonate Reservoirs: Society of Economic Paleontologists and Mineralogists, Short Course Notes no. 40, 130 p.

Kocurko, M. J., 1979, Dolomitization by spray-zone brine seepage, San Andres, Colombia: Journal of Sedimentary Petrology, v. 49, p. 209-214.

Koerschner III, W. F., and Read, J. F., 1989, Field and modeling studies of Cambrian carbonate cycles, Virginia Appalachians: Journal of Sedimentary Petrology, v. 59, p. 654-687.

Kominz, M.A., and Bond, G.C., 1990, A new method of testing periodicity in cyclic sediments, applications to the Newark Supergroup: Earth and planetary Science Letters, v. 78, p. 233-244.

Kupecz, J. A., Montañez, I. P., and Gao, G., 1993, Recrystallization of dolomite with time, *in* K. Rezak, (eds.), Carbonate microfabrics: Frontiers in sedimentary geology, New York, Springer-Verlag, p. 187-194.

Kupecz, J. A., Land, L. S., 1994, Progressive recrystallization and stabilization of early-stage dolomite: lower Ordovician Ellenburger Group, west Texas. In: Purser, B., Tucker, M., Zenger, D. (eds)., Dolomites: A Volume in Honor of Dolomieu, Special Publication.-International Association of Sedimentology, v. 21, Blackwell Scientific Publications, Cambridge, pp. 255-279.

Land, L. S., 1980, The isotopic and trace element geochemistry of dolomite: the state of the art. In: Zenger, D.H., Dunham, J.B., Ethington, R.L.(eds)., Concepts and Models of Dolomitization: Special Publication-Society of Economic Paleontologists and Mineralogists v. 28, pp. 87-110.

Land, L. S., 1985, The origin of massive dolomite: Journal of Geological Education, v. 33, p. 112–125.

Lehmann, C., Osleger, D. A., and Montañez, I. P., 1998, Controls on cyclostratigraphy of Lower Cretaceous carbonates and evaporites, Cupido and Coahuila platforms, northeastern Mexico: Journal of Sedimentary Research, v. 68, p. 1109-1130.

Lehmann, C., Osleger, D. A., and Montañez, I. P., 2000, Sequence stratigraphy of Lower Cretaceous (Barremian-Albian) carbonate platforms of northeastern Mexico: regional and global correlations: Journal of Sedimentary Research, v. 70, p. 373-391.

Lehmann, C., Osleger, D. A., and Montañez, I. P., Sliter, W., Arnaud-Vanneau, A., and Banner, J., 1999, Evolution of Cupido and Coahuila carbonate platforms, Early Cretaceous, northeastern Mexico: Geological Society of America Bulletin, v. 111, p. 1010-1029.

Lehrmann, D. J., and Goldhammer, R. K., 1999, Secular variation in parasequence and facies stacking patterns of platform carbonates: A guide to application of stacking-patterns analysis in strata of diverse ages and settings, *in* P. M. Harris, (ed.), Advances in Carbonate Sequence Stratigraphy: Application to Reservoirs, Outcrops and Models: Society of Economic Paleontologists and Mineralogists Special Publication no. 63: Tulsa, Society of Economic Paleontologists and Mineralogists, p. 187-225.

Loucks, R. G., and Longman, M. W., 1982, Lower Cretaceous Ferry Lake Anhydrite, Fairway field, east Texas; product of shallow-subtidal deposition, *in* Depositional and Diagenetic Spectra of Evaporites-A Core Workshop: Society of Economic Paleontologists and Mineralogists, Core Workshop No. 3, p. 276-304.

Lucia, F. J., Major, R. P., 1994, Porosity evution through hypersaline reflux dolomitization, *in* B. Purser, M. Tucker, D. Zenger (eds)., Dolomites: A volume in Honor of Dolomieu, Special Publication.-International Association of Sedimentology v. 21. Blackwell Scientific Publications, Cambridge, p. 325-341.

Lumsden, D. N., 1989, Toward a normal marine dolomite model: Geological Society of America Abstracts with Programs, v. 21, p. 76.

Machel, H. G., Mountjoy, E. W., 1986, Chemistry and environments of dolomitization: a reappraisal. Earth Science Review. v. 23, p. 175-222.

Mackenzie, F. T. and Agegian, C. R., 1989, Biomineralization and tentative links to plate tectonics, *in* R. E. Crick (ed)., Origin, evution, and modern aspects of biomineralization in plants and animals, Origin, evution, and modern aspects of biomineralization in plants and animals, p.11-27.

Mackenzie, F. T., and Morse, J. W., 1992, Sedimentary carbonates through Phanerozoic time, in H. C. Haelgeson (ed)., The Robert M. Garrels memorial issue; Geochmica et Cosmochimica Acta, v., 56(8), p. 3281-3295.

Mackenzie, F. T., and Pigott, J. D., 1981, Phanerozoic ocean-atmosphere-sediment history; secular variations and tectonic control: International Association of Sedimentologists, v. 11, pp.114.

Mackenzie, J., 1981, Holocene dolomitzation of calcium carbonate sediments from the coastal sabkhas of Abu Dhabi, U.A.E., Journal of Geology, v.89, p. 185-198.

Marrett, R. and Aranda-García, M., 1999, Structure and Kinematic Development of the Sierra Madre Oriental Fold-Thrust Belt, Mexico, *in*: Stratigraphy and Structure of the Jurassic and Cretaceous Platform and Basin Systems of the Sierra Madre Oriental, Monterrey and Saltillo Areas, Northeastern Mexico, A Field Book and Related Papers: South Texas Geological Society, Special Publication for the Annual Meeting of the American Association of Petroleum Geologists and the Society of Economic Paleontologists and Mineralogists Society for Sedimentary Geology, San Antonio, pp. 69-98.

Marrett, R., Gale, J. F. W., and Gomez, L. A., *in review*, Spatial arrangement of fractures III- Correlation Analyses: Journal of Structural Geology.

Mazzullo, S. J., Teal, C. S., and Bischoff, W. D., 1997, Syndepositional, subtidal dolomitization model for the formation of some Paleozoic reservoirs in the Permian Basin (Abstract): American Association of Petroleum Geologists, v. 81, pp. 868.

McFarlan, E., and Menes, L. S., 1991, Lower Cretaceous, *in* A. Salvador (ed.), The Gulf of Mexico Basin: Boulder, Colorado, Geological Society of America, The Geology of North America, v. J, p. 181-204.

Meier, M. F., 1984, Contribution of small glaciers to global sea level: Science, v. 226, p. 1418-1421.

Mitchum, R. M., JR., and Van Wagoner, J. C., 1991, High-frequency sequences and their stacking patterns: sequence-stratigraphic evidence of high-

frequency eustatic cycles, *in* K. T. Biddle, and W. Schlager (eds.), The Record of Sea-Level Fluctuations: Sedimentary Geology, v. 70, p. 131–160.

Mixon, R. B., Murray, G. E., and Diax, T. G., 1959, Age and correlation of Huizachal Group (Mesozoic), State of Tamaulipas, Mexico: American Association of Petroleum Geologists Bulletin, v. 43, p. 757-771.

Monroy-Santiago, F., Laubach, S. E., and Marrett R., 2001, Preliminary Diagenetic and Stable Isotope Analyses of Fractures in the Cupido Formation, Sierra Madre Oriental, *in* R. Marrett (ed.), Genesis and Controls of Reservoir- Scale Carbonate Deformation, Monterrey Salient, Mexico: Field Trip Guidebook 28, Bureau of Economic Geology, The University of Texas at Austin, p. 83-107.

Montañez, I. P., and Read, J. F., 1992, Eustatic control on early dolomitization of cyclic peritidal carbonates: evidence from the Early Ordovician Upper Knox Group, Appalachians: Geological Society of America Bulletin, v. 104, p. 872-886.

Montañez, I. P., 1994, Late diagenetic dolomitization of Lower Ordovician, Upper Knox carbonates: a record of the hydrodynamic evolution of the south Appalachian Basin. American Association of Petroleum Geologists Bulletin v. 78 (8), p. 1210-1239.

Moore, C. H., 1989, Carbonate diagenesis and porosity: Development in Sedimentology 46: New York, Elsevier, 338 p.

Moore, C. H., 2001, Carbonate reservoirs: Developments in Sedimentology: Amsterdam, Elsevier Science, v. 55, p. 341–355.

Morrow, D. W., 1982, Diagenesis 2; Dolomite: Part 2. Dolomitization models and ancient dolostones: Geoscience Canada, v. 9 (2), p. 95-107.

Müller, S., Teitz, G., 1971, Dolomite replacing cement AB in biocalcarenites from Fuerteventura, Canary Islands, Spain. In: D. P. Bricker (ed)., Carbonate Cements. John Hopkins Press, Baltimore, 376 pp.

Oivanki, S. M., 1974, Paleodepositional environments in the Upper Jurassic Zuloaga Formation (Smackover), northeast Mexico: Gulf Coast Association of Geological Societies Transactions, v. 24, p. 258-278.

Ortega, O., 2002, Fracture-size scaling and stratigraphic controls on fracture intensity [unpublished PhD Dissertation]: Austin, University of Texas at Austin, 426 p.

Ortega, O., and Marrett, R., 2001, Stratigraphic controls on fracture intensity in Barremian-Aptian Carbonates, Northeastern Mexico, *in* R. Marrett (ed.), Genesis and Controls of Reservoir- Scale Carbonate Deformation, Monterrey Salient, Mexico: Field Trip Guidebook 28, Bureau of Economic Geology, The University of Texas at Austin, p.57-82.

Osleger, D. A., and Read, J. F., 1991, Relation of eustasy to stacking patterns of meter-scale carbonate cycles, Late Cambrian, U.S.A.: Journal of Sedimentary Petrology, v. 61, p. 1225-1252.

Osleger, D., 1991, Subtidal carbonate cycles: Implications for allocyclic vs. autocyclic controls: Geology, v. 19, p. 917-920.

Paillard, D., Labeyrie, L., and Yiou, P., 1996, Macintosh programs performs time-series analysis: Eos, Transactions, American Geophysical Union, v. 77, p. 379.

Papoulis, A., 1984, Probability, Random variables and stochastic processes. McGraw-Hill International Editions, Singapore, 576 pp.

Pardo-Igúzquiza, E., and Rodriguez-Tovar, F.J., 2004, POWGRAF2: a program for graphical correlation of spectral analysis in cyclostratigraphy; Computer and Geosciences, v. 30, p. 533-542.

Park, J., and Herbert, T. D., 1987, Hunting for paleoclimatic periodicities in a geologic time series with an uncertain time scale, Journal of Geophysical Research, v. 92, p. 14027-14040.

Patterson, R. K., 1972, Hydrology and carbonate diagenesis of a coastal sabkha along Arabian Gulf [unpublished PhD Dissertation]: Princeton, New Jersey, Princeton University, 473 p.

Patterson, R. J., Kinsman, D. J. J., 1982, Formation of diagenetic dolomite in coastal sabkhas along the Arabian Persian Gulf. American Association of Petroleum Geologists Bulletin v. 66, p. 28-43.

Pindell, J. L., 1985, Alleghenian reconstruction and subsequent evolution of the Gulf of Mexico, Bahamas, and Proto-Caribbean: Tectonics, v. 4, p. 1-39.

Posamentier, H. W., and G. P. Allen, 1999, Siliciclastic Sequence Stratigraphy-Concepts and Applications: Concepts in Sedimentology and Paleontology 7: Tulsa, Society of Economic Paleontologists and Mineralogists, 210 p.

Pratt, B., and James, N., 1986, The St. George Group (Lower Ordovician) of western New Founland: Tidal-flat island model for carbonate sedimentation in shallow eperic seas, Sedimentology, v. 33, p. 313-343.

Preto, N., and Hinnov, L. A., 2003, Unraveling the origin of carbonate platform cyclothems in the Upper Triassic Dürrentein Formation (Dolomites, Italy): Journal of sedimentary Research, v.73, p. 774-789.

Preto, N., Hinnov, L. A., Hardie, L. A., and De Zanche, V., 2001, Middle Triassic orbital signature recorded in the shallow-marine Latemar carbonate buildup (Dolomites, Italy): Geology, v. 29, p. 1123-1126.

Purser, B. H., 1973, Sedimentation around bathymetric highs in the southern Persian Gulf, *in* B. H. Purser, (ed.), The Persian Gulf: New York, Springer-Verlag, p. 157-177.

Read, J. F., 1995, Overview of carbonate platform sequences, cycle stratigraphy and reservoirs in greenhouse and ice-house worlds, *in* L. J. Weber, (ed.), Milankovitch Sea Level Changes, Cycles and Reservoirs on Carbonate Platforms in Greenhouse and Ice-House Worlds: Society of Economic Paleontologists and Mineralogists Short Course no. 35: Tulsa, Society of Economic Paleontologists and Mineralogists, p. 102.

Read, J. F., and Goldhammer, R. K., 1988, Use of Fischer plots to define third-order sea-level curves in Ordovician peritidal carbonates, Appalachians: Geology, v. 16, p. 895-899.

Revelle, R., (ed.), 1990, Sea-level change: National Research Council, Studies in Geophysics, Washington, D.C., National Academy Press, 234 p.

Rhoads, D. C., 1967, Biogenic reworking of intertidal and subtidal sediments in Barnstable Harbor and Buzzards Bay, Massachusetts: Journal of Geology, v. 75, p. 461-476.

Röhl, U., and Ogg, J. G., 1996, Aptian-Albian sea-level history from guyots in western Pacific: Paleoceanography, v. 11, p. 595-624.

Ross, M. A., 1981, Stratigraphy of the Tamaulipas Limestone, Lower Cretaceous, Mexico, *in* C. I. Smith, (ed.), Lower Cretaceous Stratigraphy and Structure, Northern Mexico, West Texas Geological Society Publication 81-74, p. 43-54.

Ross, M. I., and Scotese, C. R., 1988, A hierarchical tectonic model of the Gulf of Mexico and Caribbean region: Tectonophysics, v. 155, p. 139-168.

Ruddiman, W. F., and Wright, H. E., (eds.), 1987, North America and adjacent oceans during the last deglaciation: The geological Society of America, Boulder, CO, 501 p.

Sadler, P. M., 1994, The expected duration of upward-shallowing peritidal carbonate cycles and their terminal hiatuses: Geological Society of America, Bulletin, v. 106, p. 791-802.

Salvador, A., 1987, Late Triassic-Jurassic paleogeography and origin of Gulf of Mexico Basin: American Association of Petroleum Geologists Bulletin, v. 71, p. 419-451.

Satterley, A. K., 1996, Cyclic sedimentation in the Upper Triassic Dachstein Limestone, Austria: the role of patterns of sediment supply and tectonics in a platform-reef-basin system: Journal of Sedimentary Research, v. 66, p. 307-323.

Schlager, W., 1981, The paradox of drowned reefs and carbonate platforms: Geological Society of America, Bulletin, v. 92, p. 197-211.

Schlager, W., 1989, Drowning unconformities on carbonate platforms, Controls on Carbonate Platform and Basin Development: Society of Economic Paleontologists and Mineralogists Special Publication no. 44, p. 15-25.

Schwarzacher, W., 1993, Cyclostratigraphy and the Milankovitch Theory: Amsterdam, Elsevier, 225 p.

Schwarzacher, W., 2000, Repetitions and cycles in stratigraphy: Earth-Science Reviews, v. 50, p. 51-75.

Scotese, C. R., 1997, Paleogeographic Atlas, PALEOMAP Progress Report 90-0497, Arlington, Texas, Department of Geology, University of Texas at Arlington, p. 45.

Scott, R. W., 1990, Models and stratigraphy of mid-Cretaceous reef communities, Gulf of Mexico: Society of Economic Paleontologists and Mineralogists, Concepts in Sedimentology and Paleontology, v. 2, 102 p.

Shelton, K. L., So, C., Haeussler, G. T., Chi, S., and Lee, K., 1990, Geochemical studies of the Tongyoung gold-silver deposits, Republic of Korea; evidence of meteoric water dominance in a Te-bearing epithermal system: Economic Geology and the Bulletin of the Society of Economic Geologists, v. 85, p. 1114-1132.

Shinn, E. A., 1968, Burrowing in recent lime sediments of Florida and the Bahamas: Journal of Paleontology, v. 42, p. 879-894.

Shinn, E. A., Ginsburg, R. N., and Lloyd, R. M., 1965, Recent supratidal dolomite Andros island, Bahamas: Special Publication, Society of Economic Paleontologists and Mineralogists, p. 112-123.

Shinn, E. A., 1983, Tidal-flat environment: American Association of Petroleum Geologists Memoir 33, p. 173-310.

Sibley, D. F., 1991, Secular changes in the amount and texture of dolomite: Geology, v. 19, p. 151-154.

Sibley, D. F., Dedoes, R. E., and Bartlett, T. R., 1987, Kinetics of dolomitization: Geology, v. 15, p. 1112–1114.

Sibley, D. F., Gregg, J. M., 1987, Classification of dolomite rock textures, Journal of Sedimentary Petrology, v. 57, p. 967-975.

Skelton, P. W., 2003, The Cretaceous World, Cambridge University Press: The Open University, 360 p.

Sloan, L. C., and Huber, M., 2001, Eocene oceanic responses to the orbital forcing on precessional time scales: Paleocenaography, v. 19, p.101-111.

Smith, C. I., 1981, Review of the geologic setting, stratigraphy, and facies distribution of the Lower Cretaceous in northern Mexico, *in* C. I. Smith, (ed.), Lower Cretaceous Stratigraphy and Structure, Northern Mexico, West Texas Geological Society Publication 81-74, p. 1-27.

Smith, L. B., Eberli, G. P., and Sonnenfeld, M., 2004, Sequence-stratigraphic and Paleogeographic Distribution of Reservoir-quality Dolomite, Madison Formation, Wyoming and Montana, *in* G. M. Grammer, P. M. Harris, and G. P. Eberli, (eds.), Integration of outcrop and modern analogs in reservoir modeling: American Association of Petroleum Geologists Memoir 80, p. 67-92.

Smith, T. M., and Dorobeck, S. L., 1989, Meteoric alteration of early-formed dolomite during intermittent subaerial exposure: Mississippian Mission Canyon Formation, south-central Montana (abstract): Geological Society of America Abstracts with Programs, v. 20, p. A220

Stage, M., 1999, Signal analysis of cyclicity in Maastrichtian pelagic chalks from the Danish north sea: Earth and Planetary Science letters, v. 173, p. 75-90.

Stanton, R. J. J., 1966, The solution brecciation process: Geological Society of America Bulletin, v. 77, p. 843-848.

Strasser, A., 1988, Shallowing upward sequences in Purbeckian peritidal carbonates (Lower cretaceous, Swiss and French Jura Mountains): Sedimentology, v. 35, p. 369-383.

Strasser, A., Pittet, B., Hillgärtner, H., and Pasquier, J. B., 1999, Depositional sequences in shallow carbonate-dominated sedimentary systems: concepts for a high-resolution analysis: Sedimentary Geology, v. 128, p. 201-221.

Swennen, R., W. Viaene, and C. Cornelissen, 1990, Petrography and geochemistry of the Belle Roche breccia (Lower Visean, Belgium): evidence for brecciation by evaporite dissolution: Sedimentology, v. 37, p. 859-878.

Tardy, M., 1977, Essai sur la constitution de l'evution paleogeographique et structurale de la partie septentrionale du Mexique au cours du Mesozoique et du Cenozoique: Bulletin de la Societe Geologique de France, v. 19, p. 1297-1308.

Teal, C. S., Mazzullo, S. J., and Bischoff, W. D., 1998, Syndepositional marine dolomitization in shallow subtidal deposits, northern Belize (Abstract): Annual Meeting Expanded Abstracts: American Association of Petroleum Geologists, v. 1998, p. R11.

Tinker, S. W., 1985, Lithostratigraphy and Biostratigraphy of the Aptian La Peña Formation, Northeast Mexico and South Texas, and the Depositional Setting of the Aptian Pearsall-La Peña Formations, Texas Subsurface and Northeast Mexico: Why is there not another Fairway Field?: M. S. thesis, University of Michigan, Ann Arbor, 80 p.

Todd, R. G., and Mitchum, R. M. Jr., 1977, Seismic stratigraphy and global changes of sea level, Part 8: Identification of Upper Triassic, Jurassic, and Lower Cretaceous seismic sequences in Gulf of Mexico and offshore west Africa, *in* C. E. Payton, (ed.), Seismic Stratigraphy-Applications to Hydrocarbon Exploration, American Association of Petroleum Geologists Memoir 26, p. 145-163.

Vail, P. R., 1987, Seismic stratigraphy interpretation procedure, *in* A. W. Bally, (ed.), Atlas of Seismic Stratigraphy: American Association of Petroleum Geologists Studies in Geology 27, v. 1: Tulsa, p. 83-97.

Vail, P. R., Audemard, F., Bowman, S. A., Eisner, P. N. and Perez-Cruz, C., 1991, The stratigraphic signatures of tectonics, eustasy, and sedimentology- an overview, *in* A. Seilacher, (ed.), Cycles and Events in Stratigraphy: New York, Springer-Verlag, p. 617-659.

Vail, P. R., Hardenbol, J., and Todd, R. G., 1984, Jurassic unconformities, chronostratigraphy, and sea level changes from seismic stratigraphy and biostratigraphy, *in* J. S. Schlee, (ed.), Interregional Unconformities and

Hydrocarbon Accumulation: American Association of Petroleum Geologists Memoir 36, p. 129-144.

Van Wagoner, J. C., Mitchum, R. M. , Posamentier, H. W., and Vail, P. R., 1987, The key definitions of stratigraphy, *in* A. W. Bally, (ed.), Atlas of seismic stratigraphy, volume 1: American Association of Petroleum Geologists Studies in Geology 27: Tulsa, p. 11-14.

Vasconcelos, C., Mackenzie, J. A., Bernasconi, S., Grujic, D., Tien, A. J., 1995, Microbial mediation as a possible mechanism for natural dolomite formation at low temperatures: Nature, v. 377(6546), p. 220-222.

Wall, J. R., Murray, G. E., and Diaz, T. G., 1961, Geologic occurrence of intrusive gypsum and its effect on structural forms in Coahuila Marginal Folded Province of northeastern Mexico: American Association of Petroleum Geologists Bulletin, v. 45, p. 1504-1522.

Warren, J. K., 1999, Evaporites: Their Evolution and Economics, Blackwell Science, 438 pp.

Warren, J. K., and Kendall, C. G., 1985, Comparison of sequences formed in marine sabkha (subaerial) and salina (subaqueous) settings-modern and ancient: American Association of Petroleum Geologists Bulletin, v. 69, p. 1013-1023.

Warren, J. K., 2000, Dolomite*;* occurrence, evolution and economically important associations: Earth-Science Reviews, v. 52 (1-3), p. 1-81.

Weissert, H., and Lini, A., 1991, Ice age interludes during the time of Cretaceous greenhouse climate?, *in* D. W. Müller, J. A. Mckenzie, and h. Weissert, (ed.), Controversies in Modern Geology: New York, Academic Press, p. 173–191.

Wenk, H. R., Hu, M., and Frisia, S., 1993, Partially disordered dolomite: microstructural characterization of Abu Dhabi sabkha carbonates. American Mineralogists, v. 78, p.769-774.

Wigley, T. M. L., and Raper, S. C. B., 1987, Thermal expansion of seawater associated with global warming: Nature, v. 330, p. 127–131.

Wilkinson, B. H., and Algeo, T. J., 1989, Sedimentary carbonate record of calcium-magnesium cycling: American Journal of Science, v. 289, p. 1158-1194.

Wilkinson, B. H., and Given, R. K., 1986, Secular variation in abiotic marine carbonates; constraints on Phanerozoic atmospheric carbon dioxide

contents and oceanic Mg/Ca ratios: Journal of Geology, v.94 (3), p. 321-333.

Wilkinson, B. H., Owen, R. M., and Carroll, A. R., 1985, Submarine hydrothermal weathering, global eustasy, and carbonate polymorphism in Phanerozoic marine oolites: Society of Economic Paleontologists and Mineralogists, v. 55 (2), p. 171-183

Wilkinson, B. H., Diedrich, N. W., Drummond, C. N., and Rothman, E.D., 1998, Michigan hockey, meteoric precipitation, and rhythmicity of accumulation on peritidal carbonate platforms: Geological Society of America Bulletin, v. 110, p. 1075-1093.

Wilson, J. L., and Ward, W. C., 1993, Early Cretaceous carbonate platforms of northeastern and east-central Mexico, *in* J. P. Masse, (ed.), Cretaceous Carbonate platforms: American Association of Petroleum Geologists Memoir 56: Tulsa, Oklahoma, American Association of Petroleum Geologists, p. 35-50.

Wilson, J. L., 1969, Microfacies and sedimentary structures in "deeper water" lime mudstones, *in* G. M. Friedman, (ed.), Depositional Environments in Carbonate Rocks, Society of Economic Paleontologists and Mineralogists Special Publication 9, p. 4-17.

Wilson, J. L., 1975, Carbonate Facies in Geologic History: New York, Springer-Verlag, 471 p.

Wilson, J. L., 1990, Basement structural control on Mesozoic carbonate facies in northeastern Mexico- A review, *in* M. Tucker, J. L. Wilson, P. D. Crevello, J. F. Sarg, and J. F. Read, (ed.), Carbonate platforms, facies, sequences and evolution: International Association of Sedimentologits Special Publication 9, p. 235-255.

Wilson, J. L., 1999, Controls on the wandering path of the Cupido Reef trend in northeastern Mexico, *in* T. F. Lawton, (ed.), Mesozoic Sedimentary and Tectonic History of North-Central Mexico: Boulder, Colorado, Geological Society of America Special Paper 340, p. 135-143.

Wilson, J. L., and Selvius, D. B., 1984, Early Cretaceous in the Monterrey-Saltillo area of northern Mexico, *in* J. Finneran, (ed.), A Field Guide to Upper Jurassic and Lower Cretaceous Carbonate platform and Basin Systems, Monterrey-Saltillo Area, Northeast Mexico, Gulf Coast Section, Society of Economic Paleontologists and Mineralogists, p. 76.

Wilson, J. L., and Pialli, G., 1977, A Lower Cretaceous shelf margin in northern Mexico, *in* R. G. Loucks, (ed.), Cretaceous Carbonates of Texas and Mexico: Applications to Subsurface Exploration: University of Texas Bureau of Economic Geology Report of Investigations no. 89: Austin, The Bureau of Economic Geology, p. 286-294.

Wilson, J. L., and W. C. Ward, 1993, Early Cretaceous carbonate platforms of northeastern and east-central Mexico, *in* J. P. Masse, (ed.), Cretaceous Carbonate platforms: American Association of Petroleum Geologists Memoir 56: Tulsa, Oklahoma, American Association of Petroleum Geologists, p. 35-50.

Wilson, J. L., 1981, Lower Cretaceous stratigraphy in the Monterrey Saltillo area*, in* C.I. Smith, (ed.), Lower Cretaceous Stratigraphy and Structure, Northern Mexico: West Texas Geological Society, Publication 81-74, p. 78–84.

Wojcik, K. M., Goldstein, R. H., Walton, A. W., 1994. History of diagenetic fluids in a distant foreland area, Middle and Upper Pennsylvanian, Cherokee Basin, Kansas, USA: Fluid inclusion evidence. Geochim. Cosmochim. Acta 58 (3), p. 1175–1191.

Yang, W., Harmsen, F., Komniz, M. A., 1995, Depositional Cyclicity of the Middle and Late Devonian Lost Burro Formation, Death Valley, California: A possible record of Milankovitch climatic cycles: Journal of Sedimentary Research, v. B65, p.306-322.

Zühlke, R., 2004, Integrated cyclostratigraphy of a model Mesozoic carbonate platform- The Latamar (Middle Triassic, Italy), *in* B. D'Agreno, (ed.), Cyclostratigraphy: approaches and case histories: Society of Economic Paleontologists and Mineralogists Special publication No. 81, Tulsa, Oklahoma, p. 83-211.

Vita

Younis Khamis Altobi was born in Manah, Oman on September 8, 1977 to Khamis Juma Altobi and Alyia Said Al-Busaidi. He was raised in Manah and attended Manah Boys High School. He attended John Leggott Sixth Form College in Scunthorpe, England for 2 years to do A'levels in Mathematics, Chemistry, Physics and Geology. He was awarded international student of the year in 1998. He received a B.S. with honors in Geology from the University of Leeds in Leeds, England in July of 2001. He worked for Petroleum Development Oman (PDO) in Muscat Oman between June-December of 2001 applying sequence stratigraphic concepts to a giant hydrocarbon field for future development planning. In the Spring of 2002, he entered the graduate program in the Jackson school of Geosciences at the University of Texas at Austin to work with Bob Goldhammer. During graduate school, he worked as a graduate research assistance at the Bureau of Economic Geology. He interned for Occidental Oil and Gas and BP America in Houston during Summer and Fall 2004, respectively.

Permanent address: P. O. Box. 175 Manah
P.C. 619 Sultanate of Oman

This dissertation was typed by the author.